THE UNIVERSITY OF CHICAGO

GERM GRANULES PROMOTE SELF VERSUS NON-SELF RNA RECOGNITION TO PROTECT FERTILITY

A DISSERTATION SUBMITTED TO

THE FACULTY OF THE DIVISION OF THE BIOLOGICAL SCIENCES

AND THE PRITZKER SCHOOL OF MEDICINE

IN CANDIDACY FOR THE DEGREE OF

DOCTOR OF PHILOSOPHY

COMMITTEE ON DEVELOPMENT, REGENERATION, AND STEM CELL BIOLOGY

BY

OLIVIA J. GAYLORD

CHICAGO, ILLINOIS

AUGUST 2025

Copyright © 2025 by Olivia J. Gaylord

All Rights Reserved

TABLE OF CONTENTS

LIST OF FIGURES v

LIST OF TABLES viii

ACKNOWLEDGEMENTS ix

STATEMENT OF CONTRIBUTIONS x

ABSTRACT xi

CHAPTER 1: Introduction 1

1.1 Overview 1

1.2 Origins of RNA interference 1

1.3 Discovery of endogenous small RNAs: miRNAs and piRNAs 4

1.4 Argonaute family of proteins and small RNA biogenesis 7

1.5 The endogenous siRNA pathways 15

1.6 Small RNA sorting: matching small RNAs with specific Argonautes 20

1.7 Regulation of small RNA pathway activity 23

1.8 Small RNA pathway organization within germ granules 26

1.9 Germ granules and small RNA pathways protect fertility during temperature stress 35

1.10 Concluding remarks and dissertation outline 37

CHAPTER 2: RNA Helicase A promotes small RNA biogenesis and sorting in germ cells . 39

2.1 Abstract 39

2.2 Introduction 39

2.3 Results 42

2.4 Discussion 78

2.5 Methods 86

CHAPTER 3: Small RNA pathway competition drives tissue-specific differences in RNAi efficiency 100

3.1 Abstract 100

3.2 Introduction 100

3.3 Results 103

3.4 Discussion 127

3.5 Methods 130

CHAPTER 4: Germ granules coordinate RNA granule assembly to ensure germline recovery after stress 137

4.1 Abstract 137

4.2 Introduction 137

4.3 Results 140

4.4 Discussion 158

4.5 Methods 162

CHAPTER 5: Discussion: conclusions and future directions 167

APPENDIX: Mapping the interface between nuclear pores and germ granules 182

REFERENCES 191

LIST OF FIGURES

Figure 1.1: Small RNA pathways share processing machinery 10

Figure 1.2: Small RNA targeting rules 11

Figure 1.3: Expanded endo-siRNA pathways in *C. elegans* 17

Figure 1.4: Perinuclear germ granules surround the nuclear periphery of germ cells 28

Figure 1.5: Model for the small RNA functions in granule compartments 30

Figure 2.1: RHA-1 is required for germline RNAi and germline immortality 44

Figure 2.2: RHA-1 ATPase activity is required for optimal fertility 45

Figure 2.3: RHA-1 localizes to germ cell nuclei and germ granules 47

Figure 2.4: RHA-1 is expressed in the male germline and developing embryos 48

Figure 2.5: Total small RNA abundance is relatively unchanged in *rha-1* mutants 51

Figure 2.6: RHA-1 is required for the biogenesis of CSR-1 bound 22G-RNAs and 22G-RNA sorting 52

Figure 2.7: RHA-1 contributes to the generation of CSR-1 bound 22G-RNAs mapping to the 5' region of CSR-1 target mRNAs 55

Figure 2.8: RHA-1 and CSR-1 slicer activity promote 22G-RNA production from 5' region of mRNAs 56

Figure 2.9: RHA-1 localizes to the E compartment of germ granules 58

Figure 2.10: RHA-1 germ granule localization depends on CSR-1 and EGO-1 61

Figure 2.11: P compartments show reduced co-localization with D and E in *rha-1* mutants 63

Figure 2.12: CSR-1 target mRNAs are upregulated in *rha-1* mutants 67

Figure 2.13: Loss of RHA-1 results in similar mRNA expression changes as CSR-1 compromised animals 70

Figure 2.14: RHA-1 is required for optimal fertility and sperm differentiation 73

Figure 2.15: RHA-1 ATPase activity is required for optimal sperm differentiation 76

Figure 2.16: CSR-1 slicer activity is required for optimal male fertility 77

Figure 2.17: Model illustrating proposed function of RHA-1 in CSR-1 small RNA biogenesis and sorting 80

Figure 3.1: Sex-differences in germline RNAi efficacy 104

Figure 3.2: Germline small RNA pathways share gene silencing machinery 107

Figure 3.3: Loss of endo-siRNAs or piRNAs enhance RNAi efficiency 108

Figure 3.4: Sex-differences in RNAi efficacy 110

Figure 3.5: Germline-specific RNAi mutants recover RNAi function by loss of endo-siRNAs or piRNAs 113

Figure 3.6: Germline RNAi function recovered in mutants by loss of endo-siRNAs or piRNAs 115

Figure 3.7: CSR-1 germline RNAi function recovered by loss of piRNA pathway function 117

Figure 3.8: Endo-siRNA pathway primary and secondary siRNA steps limit RNAi function 118

Figure 3.9: Secondary siRNAs are increased against RNAi target in endo-siRNA mutant 121

Figure 3.10: Small RNAs in endo-siRNA mutants 122

Figure 3.11: RNAi inheritance of somatic gene requires functional germline RNAi 124

Figure 3.12: Efficiency of RNAi inheritance regulated by endo-siRNA and piRNA pathway function 126

Figure 4.1: Heat stress induced stress granule and P-body formation in germ cells 141

Figure 4.2: Germ granule compartments disrupted after heat stress 143

Figure 4.3: Stress granules and P-bodies form at germ granules after heat shock 146

Figure 4.4: Stress granules and P-bodies form throughout germline after heat shock 147

Figure 4.5: Stress granules form adjacent to germ granules after heat shock..... 148

Figure 4.6: Germ granules promote heat stress induced stress granule and P-body perinuclear formation..... 150

Figure 4.7: Germ granule assembly factors promote stress granule and P-body perinuclear formation after heat shock 152

Figure 4.8: Heat stress induced perinuclear stress granules and P-bodies form independently . 153

Figure 4.9: Germ granule assembly factors promote germ cell recovery after heat stress..... 156

Figure 4.10: Model illustrating germ granule compartments in response to heat stress..... 159

Figure 5.1: Two models for CSR-1 small RNA amplification on target mRNAs 173

Figure 5.2: ALG-3/4 26G-RNAs promote secondary siRNA production at mRNA 5' ends..... 177

Figure A.1: Nucleoporins NPP-6/7 regulate CSR-1 localization 184

Figure A.2: Nucleoporins regulate multiple germ granule compartments 185

Figure A.3: Nucleoporins impact NPC assembly and nuclear heterochromatin foci 187

LIST OF TABLES

Table 2.1: List of *C. elegans* strains used in this study..... 86

Table 3.1: RNAi inheritance of somatic gene *dpy-11*..... 125

Table 3.2: List of C. elegans strains used in this study..... 130

Table 4.1: List of *C. elegans* strains used in this study..... 162

Table A.1: List of *C. elegans* strains used in this study..... 189

ACKNOWLEDGEMENTS

I would like to thank my advisor, Heng-Chi Lee, for supporting my growth and development as a scientist. Heng-Chi's desire to investigate the less explored, more mysterious phenomena stood out to me early on. As a result of his enthusiasm, the diversity of projects within the lab sparked many thoughtful discussions. I also would like to thank current and past lab members Jordan Brown, Donglei Zhang, and Wenjun Chen. They each greatly contributed to my scientific and personal development, training me on different techniques, sharing in the discussion of our research questions, and all other support. I am especially grateful to Jordan for his rigorous computational work and in-depth discussions related to my research. I also appreciate the younger generation of scientists that I have mentored and worked alongside. Their unbridled enthusiasm and positive outlook were strong reminders of the simple joys and curiosities sparked by scientific exploration.

I also want to thank my thesis committee Rick Fehon, Sally Horne-Badovinac, and Jon Staley for their guidance throughout the different stages of my thesis work. Additionally, I would like to thank Paschalis Kratsios for training me on how to culture worms. His support and encouragement during my rotation hooked me on the fun fast-paced worm work. I also want to thank current and past members of the eighth floor of CLSC for creating a supportive research environment. Specifically, the Ruthenburg and Staley lab members for establishing numerous fun activities, including pie pandemonium, summer beach volleyball, and the adventurous Ruthenburg camping trips.

Finally, no number of words can express how grateful I am for my close friends and family who supported me throughout my time as a graduate student. I am especially grateful for my mom, dad, and brother for their endless encouragement, love, and support.

STATEMENT OF CONTRIBUTIONS

The work described in this dissertation includes several notable contributions from collaborators. The computational analyses for all high-throughput sequencing datasets described in Chapters 2 and 3 were performed by previous lab member Dr. Jordan Brown, and collaborator Dr. Wei-Sheng Wu from National Cheng Kung University. In addition to writing new scripts specific to the type of analysis my data required, these collaborators set up web-based analysis tools that allowed me to conduct downstream functional analyses without writing my own code. The work described in Chapter 4 was conducted with graduate rotation student Ari Basu under my mentorship. All other work was done by me under the supervision of Dr. Heng-Chi Lee.

ABSTRACT

Germ cells are uniquely capable of giving rise to an entirely new organism. This totipotency relies on their ability to assemble germ granules, RNA and protein condensates enriched with conserved RNA regulators. Among the conserved factors, small RNAs and their processing machinery play critical roles in germ cell identity, genome integrity, and gamete differentiation. To carry out these roles, several types of small RNAs function in RNA regulation to limit the expression of "non-self" genetic elements, like transposons, and regulate the timing and spatial expression of endogenous "self" mRNAs. How small RNAs distinguish "self" from "non-self" mRNAs during germ cell development remains poorly understood. While many steps of small RNA processing are spatially organized within germ granules, it is unclear how critical this organization is for the regulation and function of small RNA processes.

In this dissertation, I investigate the regulation of small RNA pathways within germ cells and how environmental changes challenge these processes. First, I identify RNA helicase RHA-1/DHX9 as a key factor that promotes specialized small RNA biogenesis and sorting. This small RNA sorting enables germ cells to distinguish "self" from "non-self" mRNAs. Next, I explore sex-dependent differences in the response to environmental double-stranded RNAs. I find small RNA pathway competition limits the RNA interference activity in male germ cells. Finally, I examine how environmental stress impacts germ granule organization. Following heat stress, I find germ granules partially disassemble but also promote stress granule and P-body assembly at the nuclear periphery. I show that like stress granules, germ granules ensure the recovery of germ cell viability after stress. Overall, these findings improve our understanding of how germ granules and small RNAs coordinate the regulation of diverse RNA sequences to protect germ cells from an array of environmental challenges for future generations.

CHAPTER 1

Introduction

1.1 Overview

Shortly following the landmark discovery that double-stranded RNA triggers effective and sequence-specific gene silencing, small RNAs emerged as the sequence determinants in guiding target RNA degradation. Coinciding with these studies, the finding of a conserved miRNA transcribed from the genome, led to the realization that miRNAs are common regulators of gene expression in plants and animals. Since these key breakthroughs, we have deepened our understanding of the widespread existence of small RNAs and their role as critical regulators of gene expression in diverse biological processes from development to immunity. Even with the extensive conservation of mechanisms related to the biogenesis and molecular actions of small RNAs, we still have limited understanding of how small RNAs distinguish “self” from “non-self” mRNAs and how small RNA activity is regulated.

In this introductory chapter, I will highlight the breakthrough findings that led to the discovery of small RNAs and elaborate on the diverse small RNA species that are crucial for development and genome integrity. I will define the small RNA network, and how small RNA sorting and small RNA pathway competition ensures accurate and balanced small RNA activity. Lastly, I will introduce germ granules and focus on their role in promoting the fidelity and spatial organization of distinct small RNA pathways in germ cells.

1.2 Origins of RNA interference

Before the discovery of small RNAs, the surprising phenomenon of antisense RNA inhibition, whereby an antisense RNA inhibits the activity of homologous endogenous genes, was

documented across several different model systems. First demonstrated in mouse cell lines, the introduction of transgenes with antisense transcription specifically inhibited the expression of the homologous endogenous genes (Izant & Weintraub, 1985). Later shown in *C. elegans*, similar introduction of antisense transgenic constructs effectively disrupted the expression of the homologous endogenous genes (Fire et al., 1991). Even before fully understanding the mechanism, antisense RNA inhibition was proposed as an easy method to uncover the functions of specific genes in cellular processes and development.

In related studies, with the goal to manipulate the expression of specific endogenous plant genes, post-transcriptional gene silencing (PTGS) was discovered. Similar to antisense RNA inhibition, several studies observed that stably expressed antisense transgenes resulted in the suppression of endogenous genes (C. J. S. Smith et al., 1988; van der Krol et al., 1988). In an effort to deepen the violet color of petunias by overexpressing a gene involved in pigmentation, the introduction of sense transgenes unexpectedly resulted in white petunias (Napoli, 1990). In this case, they observed reduced expression of both the endogenous genes and the transgenes, termed co-suppression. Follow up to these findings revealed that gene suppression occurred at the level of RNA degradation (Van Blokland et al., 1994). Together with a collection of research on plant RNA viruses and pathogen-derived resistance, these studies were instrumental in determining the role of PTGS as an anti-viral defense mechanism (H. A. Smith et al., 1994). Further, this collection of work predicted the existence of a cytoplasmic RNA- and homology-based regulatory system operating in host cells.

With growing evidence for RNA silencing, the proposed model was that antisense RNA hybridization with endogenous mRNAs resulted in double-stranded RNA (dsRNA) that either inhibited mRNA translation or guided mRNA degradation. This model was challenged by

findings in *C. elegans* where the introduction of either sense or antisense RNA both resulted in degradation of the homologous mRNA transcript (Guo & Kemphues, 1995). This finding that sense RNA also guides RNA silencing led to further questions regarding the determinants of RNA silencing. Was gene silencing triggered from single-stranded RNA (ssRNA) or dsRNA? In a seminal paper published by Fire and Mello, they determined that dsRNA, not ssRNA, triggers the potent and specific repression of endogenous gene expression (Fire et al., 1998). A phenomenon termed RNA interference (RNAi). Working in *C. elegans*, they compared the effects of injecting extensively purified ssRNAs, either sense or antisense, and dsRNA on the *unc-22* gene. Consistently, ssRNAs were significantly less effective than dsRNA, revealing dsRNA as the trigger of gene silencing. These findings indicated that earlier observations of RNA silencing in other model systems likely occurred through the formation of dsRNA.

The work by Fire and Mello provided the first explanation for previous observations in plants, implicating transgenes in the production of dsRNAs. Shortly following their findings, dsRNA-containing transgenes were shown to be the most potent trigger of PTGS in plants (Waterhouse et al., 1998). A major breakthrough came a year later, when small RNAs about 25-nucleotides in length were identified matching both sense and antisense strands of transgenes undergoing PTGS (Hamilton & Baulcombe, 1999). These small RNAs were absent in strains that were not undergoing PTGS, suggesting their specific role in transgene silencing. Moreover, the mixed population of sense and antisense small RNAs suggested that they were processed from the dsRNA triggers. Several studies uncovered the endonuclease Dicer that directly cleaves long dsRNA into smaller fragments about 21-23-nucleotides in length (Hammond et al., 2000; Zamore et al., 2000). These small RNAs then serve as sequence-specific guides to target

mRNAs. Altogether, these studies established a framework of RNA silencing, defining a new paradigm of gene regulation.

Due to the conservation of the RNAi mechanism in plants and animals, RNAi has developed into a powerful tool for investigating gene function. Gene function can be inferred by observing changes in cellular processes after gene silencing by dsRNA or short-hairpin RNA. RNAi is especially useful for uncovering the function of essential genes, providing a method to study their effects at different developmental timepoints and without permanently altering the genome. Additionally, the sequence-specificity and extensive conservation of RNAi has led to the development of RNAi therapies (Bumcrot et al., 2006; Jadhav et al., 2024). RNAi therapies offer a promising approach to treat diseases where aberrant RNA is directly implicated, diseases like Alzheimer's and amyotrophic lateral sclerosis (ALS) (Balendra & Isaacs, 2018; Kallweit et al., 2025; Raguseo et al., 2023). Considering these broad applications of RNAi, we still have limited understanding of why RNAi efficacy can vary depending on siRNA sequence and cell type.

1.3 Discovery of endogenous small RNAs: miRNAs and piRNAs

Preceding the seminal finding of RNAi by Fire and Mello, Ambros and Ruvkun discovered the first miRNA *lin-4*. During their investigation of heterochronic genes that control the temporal development pattern of all larval stages in *C. elegans*, they identified *lin-4* by the isolation of a null mutation that caused either precocious or delayed development (Chalfie et al., 1981; Horvitz & Sulston, 1980; R. C. Lee et al., 1993). More specifically, mutation to *lin-4* caused temporal transformations of cell fates, where cells either expressed fates that normally occur later in development, or reiterated fates specific to earlier developmental stages (Liu & Ambros, 1989).

Notably, a suppressor mutation in the *lin-14* gene was able to revert the *lin-4* null mutant phenotype (Ferguson et al., 1987). Additionally, null mutations in the *lin-14* gene displayed an opposite phenotype of the *lin-4* null mutant, suggesting that *lin-4* could negatively regulate *lin-14* (Ferguson et al., 1987). Surprisingly, the *lin-4* gene lacked conventional start and stop codons, and mutations to the predicted open reading frame had no impact on *lin-4* function (R. C. Lee et al., 1993). This suggested *lin-4* did not encode a protein. Instead, they found two small *lin-4* transcripts of 61- and 22-nucleotides in length. Separately, *lin-14* was shown to be post-transcriptionally downregulated, and this required only the 3' untranslated region (3'UTR) of the *lin-14* transcript (Ruvkun & Giusto, 1989). Adding these findings together, Ambros and Ruvkun determined the *lin-4* short transcripts were complementary to the repeated sequence in the 3'UTR of the *lin-14* gene (R. C. Lee et al., 1993; Wightman et al., 1993). Their work uncovered a remarkable and unexpected gene regulatory mechanism involving a small non-coding RNA, later termed miRNA.

The significance of the first discovered miRNA was likely undervalued due to the lack of conservation of the *lin-4* gene. This changed after the discovery in *C. elegans* of a second miRNA *let-7* with homologs in animals (Reinhart et al., 2000). *Let-7* was determined to control the late temporal transitions during development across species from flies to humans (Pasquinelli et al., 2000). The discovery of a highly conserved miRNA sparked an expansion in the research dedicated to the new class of small RNAs. These miRNAs were proposed to pair with 3'UTRs of target genes and function in translational repression (Ambros, 2000). We now appreciate that miRNAs constitute a large family of small ~21-nucleotide long RNAs that function as key post-transcriptional regulators of gene expression in all plants and animals. After hybridizing to target mRNAs, miRNAs regulate either mRNA translation or stability to control gene expression.

Overall, miRNAs perform crucial functions in a wide range of biological processes, including development, differentiation, proliferation, and apoptosis.

The third major class of small RNAs, called piRNAs, is mainly expressed in the germ cells of animals. They were first reported in *Drosophila* as small silencing RNAs that target genomic repeats and transposable elements in the male germline (A. A. Aravin et al., 2001). In later studies, high-throughput sequencing of small RNA species uncovered piRNAs and their remarkable sequence diversity and abundance in animal germ cells (A. Aravin et al., 2006; Brennecke et al., 2007a). Unlike other small RNA classes, piRNAs are processed from single-stranded RNA precursors transcribed from discrete genomic loci. While the sequences of piRNAs diverged rapidly in evolution, the genomic loci generating piRNAs are conserved in synteny in placental mammals (Özata et al., 2020). Work in mice, *C. elegans*, *Drosophila*, and zebrafish have demonstrated that piRNAs perform critical roles in male and female fertility (Batista et al., 2008; Carmell et al., 2007, 2007; Malone et al., 2009). Overall, piRNAs are primarily considered to facilitate germ cell development by silencing transposable elements, thereby guarding the genome from mutagenic sequences. However, new roles for piRNAs in endogenous gene regulation during spermatogenesis have also recently been uncovered (Cornes et al., 2022; P. H. Wu et al., 2020). These newly described piRNA roles in endogenous gene regulation during gamete development expand our historical thinking of piRNAs beyond transposon silencers.

So far, I have described the original findings leading to the discovery of the three main classes of small RNAs, RNAi-derived small interfering RNAs (siRNAs), miRNAs, and piRNAs. In the remainder of this introduction, I will mainly focus on the regulation and function of these small RNA pathways in *C. elegans*, the model system in which the major discoveries of siRNAs

and miRNAs were first established. Since the original findings, *C. elegans* has continued to be widely used to study small RNA-mediated gene silencing mechanisms and their biological roles. Also *C. elegans* are highly genetically tractable, allowing for easy genetic manipulations such as targeted mutations or gene editing. Lastly, the extensive conservation of small RNA processing factors and small RNA-based gene silencing mechanisms allows findings in *C. elegans* to be highly informative for studies in other systems, including mammals.

1.4 Argonaute family of proteins and small RNA biogenesis

Small RNAs are bound by the Argonaute family of proteins first identified genetically in plants. Argonaute protein family members are defined by the presence of PAZ (Piwi-Argonaute-Zwille), Mid, and PIWI domains (Bohmert et al., 1998). Within the Argonaute protein, specific binding pockets of the PAZ and Mid domains serve to anchor each end of the small RNA. With the small RNA as the guide, the Argonaute is directed to target mRNAs to carry out post-transcriptional gene regulation.

Argonaute proteins are phylogenetically subdivided into the Ago and Piwi subfamilies. In most animals, Ago proteins are ubiquitously expressed and bind to siRNAs or miRNAs. These Ago-small RNA complexes induce either translational repression or mRNA destabilization. Piwi proteins are expressed in the germline and associate with piRNAs as guides for target gene silencing. Many organisms encode multiple members of Ago and Piwi proteins. For example, humans encode eight Argonaute genes, while *C. elegans* encode over twenty (Carmell et al., 2002; Seroussi et al., 2023). In each organism, only a handful of Argonautes possess the catalytic residues within the PIWI domain that allow for endonuclease activity (Yigit et al., 2006). Argonaute endonuclease activity functions to slice target mRNAs, thereby directly

contributing to mRNA destabilization. While the features of these subfamilies generally hold true, the roles and expression patterns of each Argonaute gene is still being characterized. For example, more detailed studies have observed unique expression patterns of the three mouse Piwi proteins during male germ cell development and differentiation (Ernst et al., 2017). Additionally, these distinct Piwi proteins associate with different piRNA populations and therefore can regulate unique sets of genes. Together, this suggests distinct Argonaute proteins likely function in specific roles throughout development across their respective tissues.

Small RNA pathways share similar mechanisms of small RNA biogenesis and RNA regulation. Below, I briefly describe the key factors and small RNA processing steps for each small RNA pathway in *C. elegans*. Small RNA pathways form an extensive and interconnected gene regulatory network that is especially complex within the developing germline.

The RNAi pathway

During RNAi, the introduction of environmental or exogenous dsRNA results in potent silencing of homologous genes. These dsRNAs are processed into smaller segments of 21-23-nucleotides in length by the conserved RNase III enzyme Dicer (Bernstein et al., ; Zamore et al., 2000). In *C. elegans*, most of the small RNA effectors of RNAi were identified by two independent genetic screens. The first screen aimed to identify RNAi deficient mutants (Tabara et al., 1999a). This screen uncovered the Argonaute RDE-1 that binds the primary siRNAs processed by Dicer. In the second screen, factors required for transposon silencing were identified and termed mutator class genes (Collins et al., 1987). Notably, these two screens uncovered an overlapping set of factors, suggesting a natural role of RNAi may be to silence transposable elements. Additionally, mutations to this set of genes resulted in compromised fertility.

Upon further investigation, RDE-1 bound primary siRNAs were found to trigger the production of abundant secondary siRNAs against the target gene (Figure 1.1A). Secondary siRNAs are produced by an RNA-dependent RNA polymerase (RdRP) RRF-1, that uses the target mRNA as a template for small RNA synthesis (Sijen et al., 2001). The amplified siRNAs produced by RRF-1 are termed 22G-RNAs due to their 22-nucleotide length and bias for 5' guanosine. These 22G-RNAs are produced across the entire length of the target RNA outside of the original dsRNA trigger sequence. 22G-RNAs are associated with WAGO Argonautes that belong to the worm-specific Argonaute clade (W. Gu et al., 2009; Yigit et al., 2006). WAGO bound 22G-RNA targeting leads to the recruitment of downstream factors to carry out mRNA degradation. Based on the biogenesis process of RDE-1 and WAGO class small RNAs, these small RNAs target mRNAs with perfect sequence complementarity (Figure 1.2A). Notably, robust target gene silencing requires this two-step process where primary siRNAs triggering the production of secondary siRNAs. This mechanism likely amplifies and focuses the RNAi response. Primary siRNAs processed by Dicer from dsRNA contain an equal population of sense and antisense siRNAs. The production of secondary siRNAs ensures the enrichment of siRNAs that are antisense to the target mRNA sequence.

Gene silencing by RNAi can also be epigenetically inherited for generations after parental exposure to dsRNA. This process of RNAi inheritance occurs through nuclear Argonautes that bind 22G-RNAs downstream of RDE-1 targeting. RNAi against germline-expressed genes can be inherited for over five generations. In this case, the nuclear Argonaute HRDE-1 bound to 22G-RNAs associates with nascent mRNAs at the site of transcription (Buckley et al., 2012). HRDE-1 then directs the deposition of histone marks at the target gene locus, including heterochromatic H3K9me3 (S. G. Gu et al., 2012). Additionally, RNAi of

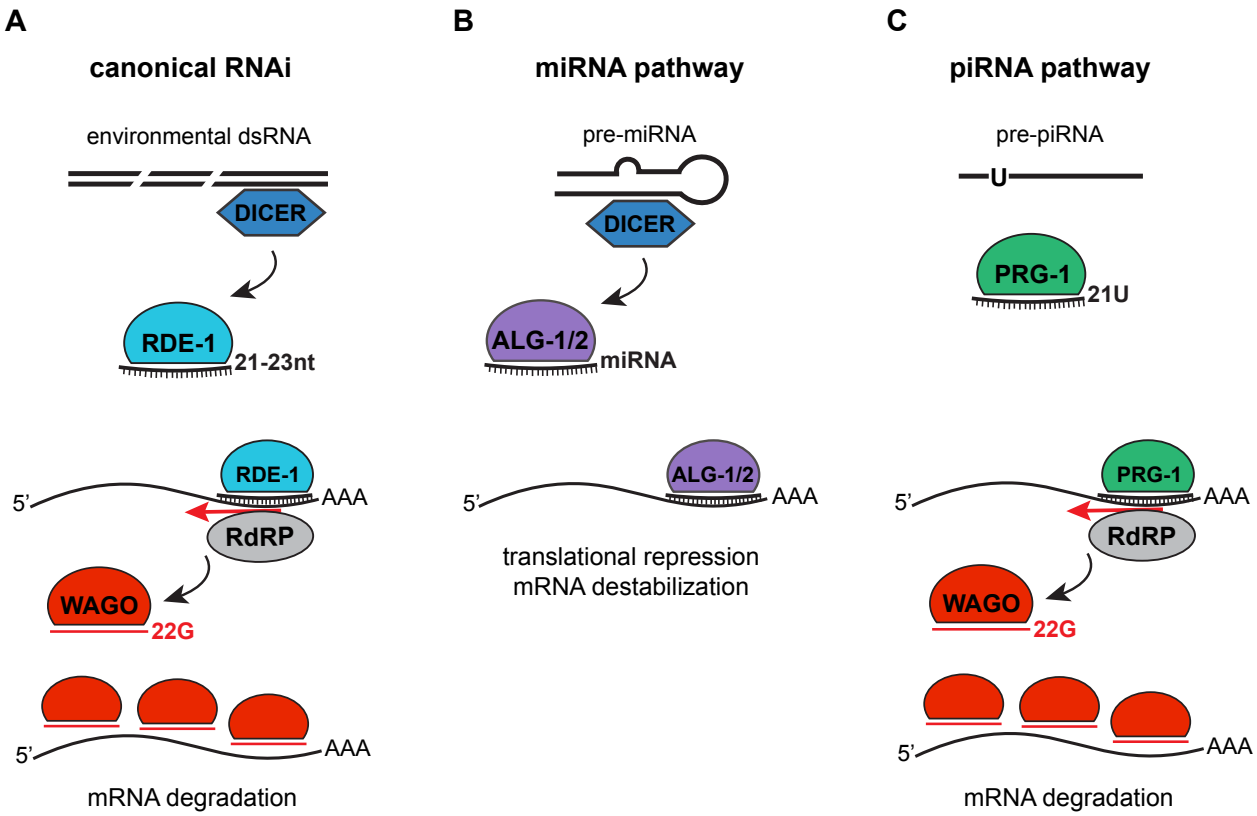

Figure 1.1: Small RNA pathways share processing machinery.
(**A**) For canonical RNAi, exogenous long dsRNA is processed by Dicer into 21-23-nucleotide small RNA duplexes that are loaded to Argonaute RDE-1. RDE-1 bound to primary siRNAs target mRNAs triggering secondary small RNA production by RNA-dependent RNA polymerase (RdRP). Secondary siRNAs (22G-RNAs) are loaded to WAGO Argonautes that recruit downstream factors to target mRNAs for degradation. (**B**) For the miRNA pathway, pre-miRNAs processed by Dicer are loaded to Argonautes ALG-1 and ALG-2. miRNAs can regulate target mRNAs by blocking translation or mRNA degradation. (**C**) For the piRNA pathway, single strand piRNA precursors are processed and loaded to Argonuate PRG-1. PRG-1 targeting also triggers secondary siRNA production.

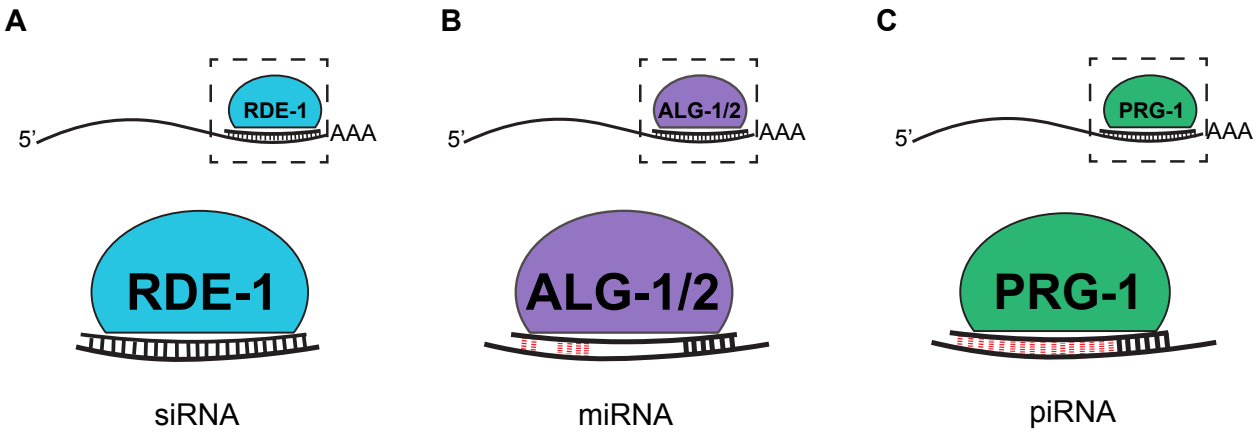

Figure 1.2: Small RNA targeting rules.
(**A**) siRNAs target mRNAs with perfect antisense sequence complementarity. (**B**) miRNA minimal requirements for targeting: perfect base pairing to targets in the seed sequence, nucleotides 2-8, and pairing beyond the seed region at the 3' end supports targeting. (**C**) Canonical piRNAs can target sequences with perfect complementarity, other piRNA rules are similar to miRNAs.

somatic-expressed genes can also be inherited but only for a single generation. In this case, RDE-1 triggered 22G-RNA production on target mRNAs are loaded to nuclear Argonaute NRDE-3 (Burton et al., 2011). Like HRDE-1, NRDE-3 directs the deposition of histone marks at the target gene locus. NRDE-3 activity in the inheriting embryo was shown to establish heterochromatic marks at the somatic gene locus (Burton et al., 2011). Within the field, the determinants of the epigenetic inheriting signal have been questioned. Specifically, whether the ingested dsRNAs, small RNAs, or chromatin marks are the signal transferred from parent to offspring. Also, the mechanism that determines the number of generations gene silencing is inherited is still largely unknown. How targets are sorted between HRDE-1 and NRDE-3 is also unclear but may involve their differences in tissue expression patterns. Overall, whether the activity of nuclear RNAi simply provides a heritable signal against threatening RNAs, or more broadly functions to regulate chromatin dynamics is an ongoing area of exploration.

The miRNA pathway

Due to their chemical and functional similarities, understanding the biogenesis and function of miRNAs has been facilitated by comparisons with siRNAs. Like siRNAs, miRNAs are processed by Dicer and loaded to miRNA Argonautes ALG-1 and ALG-2 (Figure 1.1B). However, a key difference is that miRNAs are transcribed from the genome as poly-adenylated primary miRNAs (pri-miRNAs) (Y. Lee et al., 2002). The pri-miRNA is processed in the nucleus by conserved RNase III endonuclease Drosha into a 60-70-nucleotide molecule that folds back on itself forming a hairpin loop structure known as the pre-miRNA (Y. Lee et al., 2003). The pre-miRNA is then exported from the nucleus and further processed by Dicer into a 20-25-nucleotide in length mature miRNA (Bernstein et al., 2001).

ALG-1/2 bound to miRNAs target sets of mRNAs and induce translational repression, mRNA deadenylation, and mRNA decapping (Tops et al., 2006). Unlike siRNAs, mature miRNAs can bind to imperfectly complementary mRNA sequences. Because of this somewhat flexible targeting, the complete sets of mRNAs targeted by miRNAs has proven more difficult to determine. Prediction models highlight the importance of the miRNA seed region, or the first 2-7 nucleotides of the 5' region of the miRNA, in target pairing (Figure 1.2B) (Lewis et al., 2003). The seed region is the most conserved portion of the metazoan miRNAs and miRNAs are grouped into families based on their seed sequences or structure. These miRNA families are involved in a wide range of processes including developmental timing and immune response. They also contribute to fundamental cellular processes like proliferation and apoptosis. More recently, a third miRNA binding Argonaute ALG-5 was described for its role in the transition of the *C. elegans* hermaphrodite germline from sperm production to oocyte production (K. C. Brown et al., 2017). While ALG-1 and ALG-2 associate with almost all miRNAs and perform general roles, ALG-5 was found to associate with a specific subset of miRNAs specifically expressed in the germline. The specific physiological roles, target mRNAs, and regulation of miRNA processing remains an active area of investigation.

The piRNA pathway

The piRNA pathway is widely considered as a defense system against invasive selfish nucleic acids because they induce robust silencing of transposons and repetitive elements. Deep sequencing of small RNAs in *C. elegans* uncovered the highly diverse population of piRNAs, also termed 21U-RNAs due to their characteristic 21-nucleotide length and 5' uridine bias (Ruby et al., 2006). The precursors of piRNAs are individually transcribed from genomic loci that are

mainly clustered on two gene-depleted regions of chromosome IV (Ruby et al., 2006). Consistent with their role as a genome defense system against transposable elements, piRNAs show no sequence conservation (H. C. Lee et al., 2012; Ruby et al., 2006). Interestingly, piRNAs show differences in expression between the male and female germlines (Billi et al., 2013). The distinct enrichment patterns suggest male and female piRNAs are under different evolutionary pressures.

The Argonaute PRG-1 associates with piRNAs and target mRNAs with partial sequence complementarity. Like RNAi-derived siRNAs, piRNAs direct the production of secondary siRNAs by the RdRP RRF-1 (Figure 1.1C). These amplified 22G-RNAs are similarly loaded to WAGO, where WAGO bound 22G-RNA targeting results in the recruitment of downstream factors that carry out mRNA destabilization (Das et al., 2008; H. C. Lee et al., 2012). The nuclear Argonaute HRDE-1 can also bind 22G-RNAs produced downstream of piRNA targeting and carry out transcriptional gene silencing (Ashe et al., 2012). Several studies have defined the piRNA targeting rules, similar to miRNAs, where the seed region and supplementary 3' pairing is important for gene silencing (Figure 1.2C) (Shen et al., 2018; D. Zhang et al., 2018). The permissive pairing rules allow piRNAs to detect and adapt to a wide array of threats and "non-self" genes like transposons. Strikingly, these predicted targeting rules suggest piRNAs can also target nearly all germline mRNAs. These findings suggest a protective mechanism exists to prevent piRNA silencing of endogenous genes. One proposed protection mechanism involves another class of endogenous small RNAs bound to the Argonaute CSR-1 described in a section below. Still, how "non-self" and "self" sequences are distinguished within germ cells is a major question in the field.

The piRNA pathway performs important roles in genome integrity and protects germline fertility. Many mutants of the piRNA and RNAi pathways exhibit a mortal germline phenotype

where homozygous mutants get progressively sterile over several generations (Simon et al., 2014). This phenotype was historically attributed to the accumulation of mutations during transposon mobilization in piRNA pathway mutants. However, recent evidence suggests piRNAs function in roles outside of transposon gene silencing. During spermatogenesis, piRNAs were shown to regulate endogenous gene expression (Cornes et al., 2022). This finding suggests piRNAs may contribute more broadly to gene regulation within germ cells. Future work is needed to investigate the expanding roles of the piRNA pathway during male and female germ cell development.

1.5 The endogenous siRNA pathways

Following the discovery of RNAi, questions remained as to whether RNAi performed a function within cells in the absence of exogenous or environmental exposure to dsRNAs. Early deep sequencing of small RNA species revealed distinct populations of 26-nucleotide and 22-nucleotide sequences with a 5' guanosine bias termed 26G-RNAs and 22G-RNAs, respectively (Ruby et al., 2006). These small RNAs are largely antisense to protein-coding genes and therefore are classified as endo-siRNAs. Below, I describe the 26G-RNA and 22G-RNA pathways that regulate endogenous genes during germline development.

The 26G-RNA pathway

26G-RNAs are synthesized by the RdRP RRF-3 that uses mRNA transcripts as templates. How target mRNAs are selected for RRF-3 production of 26G-RNAs is largely unknown. These 26G-RNAs, like miRNAs and RNAi triggered siRNAs, require Dicer for processing (Figure 1.3A). 26G-RNAs function as primary siRNAs and can trigger the production of secondary

siRNAs on targets. The amplified 22G-RNAs are loaded to WAGO Argonautes for target gene silencing. Within the germline, distinct populations of 26G-RNAs are produced during oogenesis and spermatogenesis.

In the oogenic germline, 26G-RNAs are bound by the ERGO-1 Argonaute and are highly abundant in embryos (T. Han et al., 2009). Although expressed during oogenesis, ERGO-1 class 26G-RNAs are thought to regulate zygotic targets throughout development. Many ERGO-1 26G-RNA targets include pseudogenes, long intergenic noncoding RNAs (lincRNAs), and recently duplicated genes, suggesting the role of these small RNAs is mainly to buffer the expression of non-coding or non-functional genes (Fischer et al., 2011). Mutants for *ergo-1* show only minor fertility defects, suggesting ERGO-1 class 26G-RNAs play a minor or redundant role in gene regulation during oocyte and embryo development.

In the male germline, 26G-RNAs are loaded to two redundant paralogs ALG-3 and ALG-4 (Conine et al., 2013b). ALG-3/4 are specifically expressed in the male germline and target spermatogenesis-enriched genes (Conine et al., 2010). By an unknown mechanism, ALG-3/4 class 26G-RNAs can both positively and negatively regulate target genes. How ALG-3/4 26G-RNA activity on target mRNAs is regulated is unclear. However, ALG-3/4 26G-RNA-mediated regulation of sperm genes is crucial for male fertility and sperm differentiation.

Endo-siRNAs, initially identified in *C. elegans*, were later found in *Drosophila* and mammals. These animals lack RdRPs and instead endo-siRNAs are derived from naturally formed dsRNAs processed by Dicer. Like ERGO-1 class 26G-RNAs in worms, endo-siRNAs in mouse oocytes have been shown to reduce the expression of pseudogenes (Tam et al., 2008). Similarly, the endo-siRNAs in *Drosophila* are also derived from convergent transcription, transposons, and pseudogenes that naturally form dsRNAs (Czech et al., 2008a). Together, these

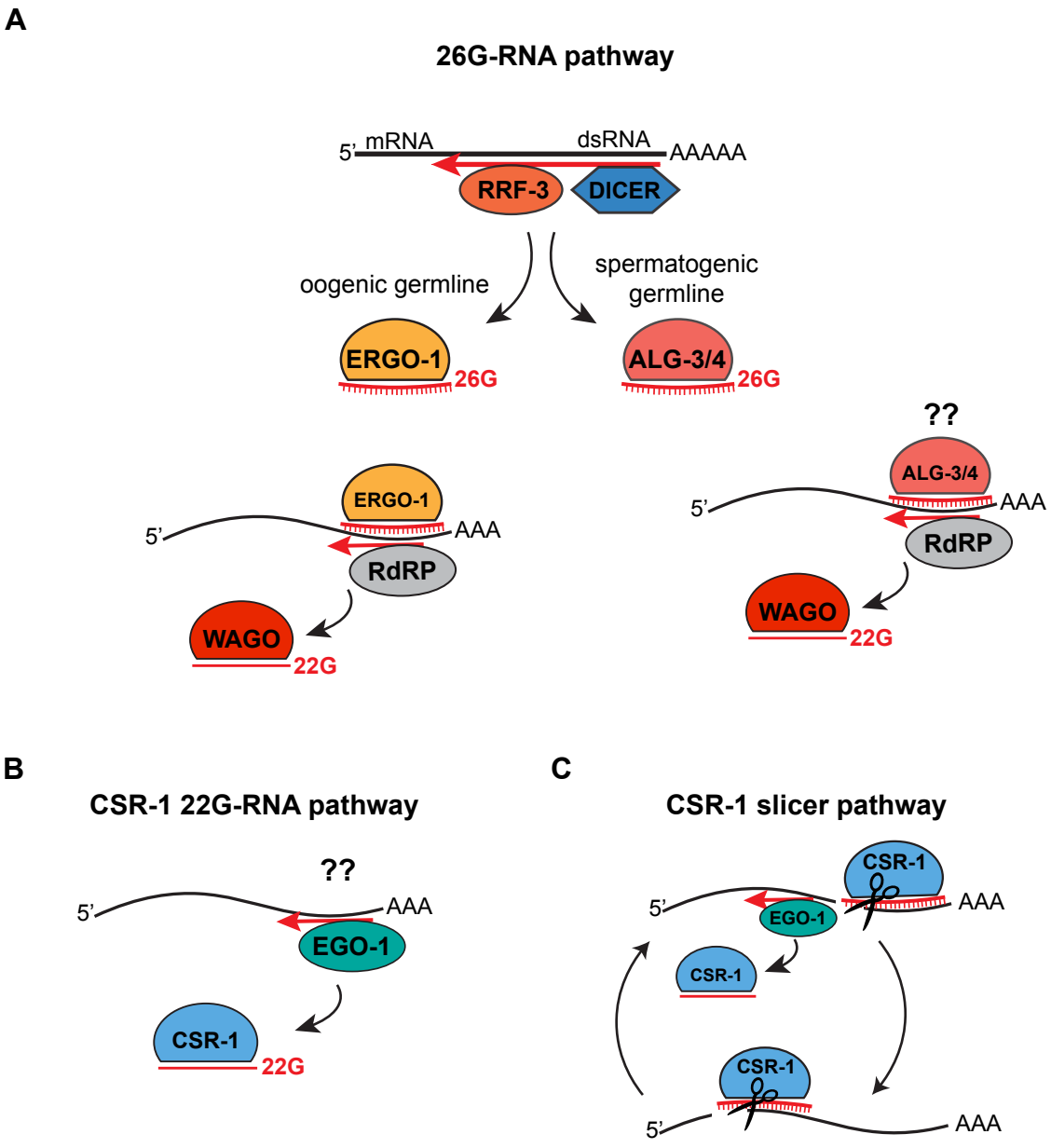

Figure 1.3: Expanded endo-siRNA pathways in *C. elegans*.
(**A**) For the 26G-RNA pathway, RdRP RRF-3 uses mRNA transcripts as templates for small RNA synthesis. Dicer processes this dsRNA intermediate into 26G-RNAs loaded to ERGO-1 in the oogenic germline and embryogenesis or ALG-3/4 in the spermatogenic germline. ERGO-1 class 26G-RNAs trigger secondary siRNA production. ALG-3/4 triggers secondary siRNAs on a subset of downregulated targets. How ALG-3/4 positively regulates targets is unknown. (**B**) CSR-1 small RNA production is initiated by an unknown signal. The RdRP EGO-1 synthesizes CSR-1 class 22G-RNAs. (**C**) In the CSR-1 slicer pathway, CSR-1 slices target mRNAs, EGO-1 synthesizes CSR-1 small RNAs from the new 3' end of target mRNAs. Multiple rounds facilitate CSR-1 small RNA amplification.

studies highlight broad and possibly conserved roles for endogenous RNA interference in regulating pseudogene expression and transposable elements.

WAGO versus CSR-1 22G-RNA pathways

Downstream of both RNAi and piRNA pathways, WAGO bound 22G-RNAs are largely considered to function as a defense against "non-self" genes or invading sequences. As described in an early section, primary siRNA and piRNA targeting directs the amplified production of secondary siRNAs, or 22G-RNAs, by the RdRP RRF-1. The 22G-RNAs loaded to WAGOs, HRDE-1, and NRDE-3 mediate post-transcriptional and transcriptional gene silencing. Since piRNAs bind with partial sequence complementarity and siRNAs derived from dsRNAs are both sense and antisense to target genes, this two-step siRNA mechanism allows for an amplified gene silencing response. Moreover, 22G-RNAs are produced against the entire target gene length, therefore expanding the region of the RNA targeted by small RNAs. Together, this mechanism generates robust targeting and gene silencing efficiency.

Although the amplification mechanism is not conserved in organisms that lack RdRPs, siRNA amplification appears to be a common strategy to defend against "non-self" RNAs like transposons. For example, in *Drosophila*, a ping-pong mechanism has been described as a positive feedback loop to amplify the piRNAs derived from transposable elements (Brennecke et al., 2007a; Gunawardane et al., 2007). This amplification requires Argonaute slicer activity to cleave transposon mRNAs resulting in phased populations of piRNAs. The ping-pong mechanism allows piRNA production to spread into downstream transcript regions, thereby allowing for the targeting of diverse sequences in proximity to the original threat. A ping-pong mechanism for piRNA amplification that requires Argonaute slicer activity has similarly been

reported in mouse germ cells during prenatal development (A. A. Aravin et al., 2008). While these mechanisms promote a robust response against mutagenic transposons, they also pose the problem of how transposons or "non-self" sequences are initially distinguished from host "self" genes.

In contrast to WAGO 22G-RNA pathways, the Argonaute CSR-1 (Chromosome Segregation and RNAi deficient) binds 22G-RNAs that are antisense to most endogenous germline-expressed mRNAs and are proposed to function in gene licensing. CSR-1 is expressed throughout germline development and associates with 22G-RNAs antisense to genes expressed during spermatogenesis, oogenesis, and embryogenesis (W. Gu et al., 2009). CSR-1 is the only essential Argonaute in *C. elegans* due to its role in chromosome segregation during early embryo cell divisions (Claycomb et al., 2009a). CSR-1 class 22G-RNAs are synthesized by the RdRP EGO-1 from mRNA transcripts that serve as templates (Figure 1.3B). Interestingly, studies found that *csr-1* mutants do not show large changes in CSR-1 target gene expression compared to wild type, suggesting CSR-1 does not function in gene silencing (Claycomb et al., 2009a). Instead, loss of CSR-1 activity results in wide scale changes to chromatin organization and ectopic expression of silent genes, suggesting CSR-1 22G-RNAs promote the distinction between "active" and "silenced" regions of chromatin (Cecere et al., 2014). Together with other studies, these findings suggested CSR-1 small RNAs do not inhibit the expression of their target genes and instead may license genes for expression.

Work from our lab and others, have revealed that CSR-1 small RNAs inhibit piRNA binding and WAGO small RNA production on target mRNAs (Shen et al., 2018; W. S. Wu et al., 2023). Additionally, artificially tethering of CSR-1 *in vivo* to an endogenous piRNA target gene protected the target gene from piRNA silencing (Cornes et al., 2022). Overall, a large body of

work has supported CSR-1 small RNAs as protectors of "self" gene expression. Still, how the CSR-1 pathway initially establishes "self" target mRNAs remains poorly understood.

More recently, CSR-1 22G-RNAs have been shown to fine-tune a subset of target mRNAs during both embryo development and in the young adult germline. These targets are characterized as having a high abundance of antisense CSR-1 22G-RNAs targeting the full length of the mRNA (Quarato et al., 2021; Singh et al., 2021). These studies also revealed that CSR-1 fine-tuned target mRNAs largely correspond to mRNAs no longer being translated or with lower translation efficiency. This suggested these CSR-1 22G-RNAs function to buffer the endogenous mRNA levels for a subset of targets. Additionally, CSR-1 target fine-tuning was shown to require CSR-1 slicer activity. CSR-1 slicer activity facilitates the amplified production of 22G-RNAs on target mRNA, and ultimately, downregulation of the target (Singh et al., 2021). The proposed model is that CSR-1 slicing of the target mRNA generates a new 3' end for EGO-1 small RNA synthesis. Sequential rounds of this process would result in amplified CSR-1 22G-RNA production and CSR-1 22G-RNA targeting across the full target gene length (Figure 1.3C). CSR-1 slicer activity is required for fertility and embryo viability, suggesting CSR-1 fine-tuning of target mRNAs is critical during germline development (Quarato et al., 2021). Although CSR-1 target fine-tuning is anti-correlated with translation efficiency, how CSR-1 specifically regulates this subset of targets while protecting all other targets from piRNA silencing remains unclear.

1.6 Small RNA sorting: matching small RNAs with specific Argonautes

To perform their wide array of roles, different classes of small RNAs must be generated in a precise manner and sorted into specific Argonaute complexes. Eukaryotic organisms often encode multiple Argonaute family proteins that function in distinct small RNA pathways. The

small RNAs associated with Argonautes function as the core of the RNA-induced silencing complex (RISC). The specific combination of the small RNA species with the Argonaute protein determines its biological function. Therefore, the accurate sorting of small RNAs to Argonautes is crucial for their roles in gene regulation. Several general factors contribute to the precision of small RNA sorting in animals. These factors include the identity of the small RNA terminal nucleotides and specific protein-protein interactions between effector components and biogenesis factors. Additionally, whether the siRNA is initially bound by the Argonaute as a dsRNA complex after Dicer processing, as is the case for miRNAs and siRNAs, may facilitate sorting specificity. Overall, our understanding of these sorting mechanisms is only partially understood.

In *Drosophila*, miRNA and RNAi pathway specific cofactors, including two distinct Dicer proteins, contribute to the precise sorting of miRNAs and siRNAs to AGO1 and AGO2, respectively. Dicer1, as well as a specific isoform of cofactor Loquacious, LOQS-PB, processes pre-miRNAs into miRNAs that preferentially associate with AGO1 (Förstemann et al., 2007; Saito et al., 2005). Dicer2, along with a distinct Loquacious isoform LOQS-PD, processes long dsRNAs into siRNAs that preferentially associate with AGO2 (Czech et al., 2009; Zhou et al., 2009). The initial specificity of Dicer1 and Dicer2 may result from differences in the structural and thermodynamic properties of the RNA duplexes they process. While miRNAs are processed from pre-miRNAs that are relatively short with incomplete base pairing, siRNAs are processed from long dsRNAs that are perfectly paired (Czech et al., 2009). Additionally, the specific protein interactions between the small RNA biogenesis factors, Dicer and Loquacious, with distinct Argonaute proteins, AGO1 and AGO2, may further ensure proper sorting. Interestingly, mammals and *C. elegans* have a single Dicer, and therefore must rely on other mechanisms for precise sorting.

Another mechanism for sorting specificity comes from structural studies revealing that two Argonaute domains associate with the small RNA 5' and 3' ends. The PAZ domain associates with the 3' end of the small RNA while the Mid domain anchors the 5' end (Frank et al., 2010; J.-J. Song et al., 2003). Particularly, the Mid domain of miRNA associated Argonautes shows evidence for nucleotide-specific interactions that ensure a bias for small RNAs with a 5' terminal U nucleotides. In line with this finding, miRNAs from plants, flies, worms, and humans show a strong bias for 5' Us (Hu et al., 2009; Lau et al., 2001; Mi et al., 2008). Additionally, the structure of the small RNA duplex may contribute to Argonaute binding preference after Dicer processing. For example, miRNA duplexes contain mismatches, while siRNA duplexes are perfectly paired (Steiner et al., 2007). This may help siRNAs and miRNAs sort to distinct Argonautes in *C. elegans*. Overall, the mechanisms of small RNA sorting in *C. elegans* have not been explored in as much detail compared to *Drosophila.*

While siRNAs and miRNAs possess potential structural differences that ensure Argonaute specificity, the endo-siRNA class 22G-RNAs in *C. elegans* potentially present a tougher sorting challenge. The proper sorting of 22G-RNAs between WAGOs and CSR-1 Argonaute is essential for marking "non-self" and "self" genes. Moreover, WAGO and CSR-1 class 22G-RNAs guide different types of gene regulation, gene silencing and licensing, respectively. The dependence of CSR-1 class 22G-RNAs on EGO-1 may help specify small RNA sorting. However, EGO-1, like RRF-1, can also produce WAGO class 22G-RNAs complicating this model of EGO-1 providing specificity (Claycomb et al., 2009a; W. Gu et al., 2009). One recent study identified RNA helicase HRDE-2 as required for nuclear Argonaute HRDE-1 22G-RNA binding specificity (S. Chen & Phillips, 2024). In the absence of HRDE-2, HRDE-1 aberrantly bound to 22G-RNAs normally sorted to CSR-1. In this background, CSR-1

still bound a portion of normal 22G-RNAs, suggesting HRDE-1 and CSR-1 compete over small RNA binding in the absence of HRDE-2. Because of this 22G-RNA mis-sorting, heterochromatin marks were deposited on CSR-1 target genes. This study revealed specific effector components may contribute to the specificity in 22G-RNA sorting to the correct Argonaute. Still, how the molecularly indistinguishable 22G-RNAs are sorted between WAGO and CSR-1 remains largely unknown.

1.7 Regulation of small RNA pathway activity

As small RNAs contribute to a myriad of biological processes, precise control over small RNA levels and their interactions with target mRNAs is crucial for proper cellular function. If small RNA activity is too high or if small RNAs bind unintended targets, this could disrupt cellular homeostasis and negatively impact developmental programs. Studies have found the activity of small RNA pathways is regulated by competition between pathways for limited cofactors and negative feedback within small RNA pathways. Below, I describe evidence for the competition model and negative feedback loops that balance the activity and gene expression regulation by various small RNA pathways.

The competition model

One proposed mechanism by which small RNA pathway activity is controlled or held at a balance is by competition between small RNA pathways for limited shared components. Because distinct small RNA pathways share common biogenesis factors, like Dicer and RdRPs, competition for limited resources between distinct small RNA pathways occurs at the level of primary and secondary siRNA production.

In *C. elegans*, a single Dicer, DCR-1, functions in multiple distinct silencing mechanisms: (1) siRNAs triggered by exogenous dsRNAs, (2) endo-siRNAs derived from endogenous genes, and (3) developmental regulatory miRNAs (Duchaine et al., 2006). Strong evidence for pathway competition comes from the disruption of the production or stability of endogenous siRNAs. Mutation to factors required for endo-siRNA production exhibit an enhanced response to exogenous dsRNA, or enhanced RNAi (Zhuang & Hunter, 2011). These endo-siRNA mutants also show increased miRNA activity (Zhuang & Hunter, 2012). In the other direction, animals exposed to exogenous dsRNA show decreased endo-siRNA and miRNA activity (Zhuang & Hunter, 2012). These findings reveal competition between small RNA pathways for limited resources and suggest small RNA activity is held in balance under normal growth conditions.

Several small RNA pathways share a common two step mechanism for gene silencing, where primary siRNA targeting triggers amplified secondary siRNA production by RdRPs. These secondary siRNAs are loaded to WAGO Argonautes that recruit mRNA degradation factors to the target mRNAs. Distinct small RNA pathways are also proposed to be in competition for these key effectors of gene silencing. In support of this, gene silencing by RNAi is permanently inherited in the absence of PRG-1 and piRNA function, indicative of overly robust WAGO 22G-RNA production (Shukla et al., 2021). This finding suggests piRNA activity limits RNAi activity in gene silencing and inheritance of gene silencing. Conversely, mutants that exhibit enhanced piRNA silencing are defective in RNAi inheritance (Shi et al., 2025). These findings reveal competition between piRNA and siRNA pathways for secondary siRNA production and gene silencing machinery.

Regulation of small RNA activity by negative feedback loops

Another mechanism regulating small RNA activity occurs through negative feedback loops. In an example from *C. elegans*, a group of CSR-1 fine-tuned targets are genes involved in small RNA biogenesis (Singh et al., 2021). These findings revealed CSR-1 negatively regulates the mRNAs for a subset of factors required for biogenesis of its own small RNAs. Thus, this loop would turn down the activity of CSR-1 small RNA production. Another negative feedback loop was shown for miRNA levels in human cell lines. This study found that the miRNA *let-7* can target the 3'UTR of Dicer transcripts and downregulate Dicer protein levels (Tokumaru et al., 2008). This in turn leads to downregulation of miRNA levels including the *let-7* miRNA. Similarly shown in plants, two miRNAs, miR168 and miR162, direct the cleavage of *AGO1* and *DCL1* transcripts reducing Argonaute and Dicer protein levels (Vaucheret et al., 2004; Xie et al., 2003). This regulation is another example of a negative feedback loop to control total miRNA levels.

Other mechanisms that regulate small RNA activity include modifications to the small RNAs that change their stability and turnover, as well as modifications to Argonaute proteins and other small RNA biogenesis factors that regulate their stability and localization within cells (Billi et al., 2012; Johnston & Hutvagner, 2011; van Wolfswinkel et al., 2009). Although not an exhaustive list of the mechanisms in place to regulate the activity of small RNAs, the work described here highlight several pathways that limit small RNA activity. These mechanisms are likely in place to ensure the small RNA network can respond to new threats and adapt to changing environmental conditions while preventing off target silencing.

1.8 Small RNA pathway organization within germ granules

Cells spatially organize molecular components to facilitate essential biological processes and guide proper development. The spatial organization of RNA within the cell can both support and result from precise gene regulatory control. One form of spatial organization within cells occurs through RNA granules. Early observations of insect germ cells stained with RNA dyes revealed cytoplasmic aggregates without a surrounding membrane, now generally termed germ granules. Germ granules are phase-separated organelles that concentrate RNA and protein complexes (Brangwynne et al., 2009). Since they were first observed, we now appreciate that germ granules are common features of animal germ cells and contain conserved protein components like Vasa family helicases and PIWI Argonaute proteins (Eddy, 1976; Strome & Wood, 1982). Seminal studies of *Drosophila* germ plasm uncovered germ granules as crucial regulators of germline development and germ cell fate. Together, two key studies demonstrated that the germ plasm was both necessary and sufficient to guide germline development and specify germ cell fate (Illmensee & Mahowald, 1974; Okada et al., 1974). Since these finding, not all animal germ granules have been found to be sufficient for germ cell fate specification. However, in our current understanding, germ granules consistently perform critical functions in animal germ cell development and differentiation.

For several organisms, such as *C. elegans*, *Drosophila*, *Xenopus*, and zebrafish, germ granules are present continuously throughout development and have been shown to cluster around germ cell nuclei (Ikenishi et al., 1996; Knaut et al., 2000; Mahowald, 1971; Strome & Wood, 1982). Based on their association with nuclei, these germ granules are referred to as perinuclear granules. In *C. elegans*, electron micrographs and fluorescence microscopy revealed the close association of perinuclear granules with nuclear pores, the major sites of mRNA export

(Figure 1.4) (Pitt et al., 2000). These perinuclear granules are enriched with RNA regulatory and small RNA processing machinery, as well as developmentally regulated mRNAs like *nanos-2* (Kobayashi et al., 1996; Subramaniam & Seydoux, 1999). Because of their enrichment of RNA regulatory components and their position outside of nuclear pores, perinuclear granules have been proposed to function as centers of post-transcriptional gene regulation. Whether specific steps of RNA regulation occur within germ granules, or germ granules simply function as sites of RNA sorting remains an active area of investigation.

Small RNA pathway activity within germ granules

Major insights into the assembly, composition, and function of germ granules have emerged from rigorous studies performed in *C. elegans*. In *C. elegans*, germ granules are called P granules for their concentration in the P (posterior) and progenitor germ lineage (Strome & Wood, 1982). To understand the role of P granules during development, many studies characterize the protein components and mRNAs enriched within P granules. From these studies, P granules were determined to contain over ninety proteins associated with RNA binding, degradation, small RNA processing, and translational control (Phillips & Updike, 2022). The characterization of P granule associated mRNAs within embryos uncovered several interesting trends. First, hundreds of lowly translated mRNAs are enriched within P granules (C.-Y. S. Lee et al., 2020). Second, the 3'UTRs of mRNAs are sufficient for P granule localization (Parker et al., 2020). These studies also demonstrated that germ granules are not required for translation inhibition, but rather function to concentrate developmentally regulated mRNAs in the germ lineage for proper germline development (C.-Y. S. Lee et al., 2020; Parker et al., 2020).

Along with concentrating mRNAs in the germ lineage, P granules facilitate germline-specific small RNA surveillance. More recent studies investigating the organization of small

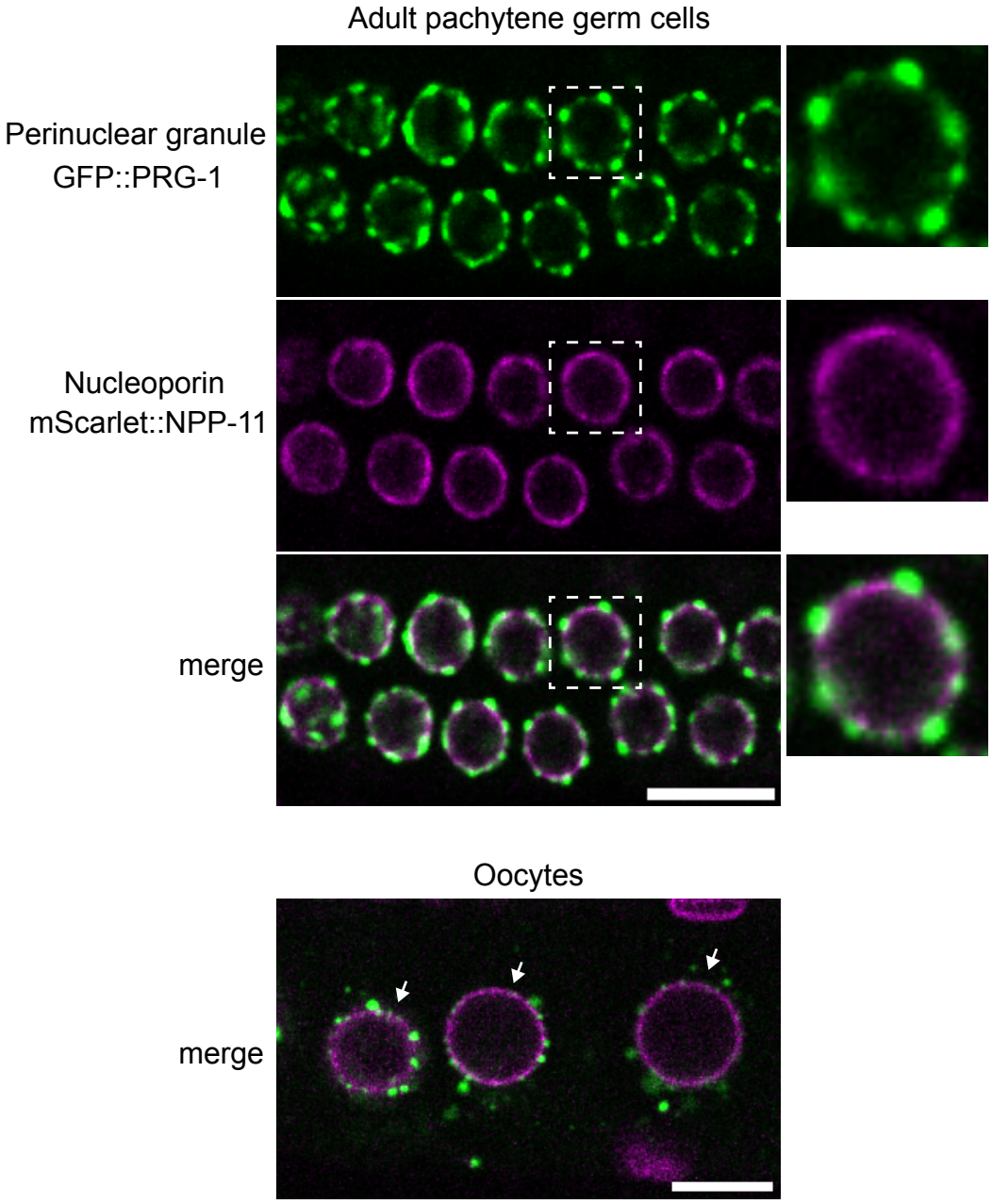

Figure 1.4: Perinuclear germ granules surround the nuclear periphery of germ cells. Live-fluorescent images of the adult C. elegans pachytene germ cells and oocytes co-expressing germ granule marker GFP::PRG-1 and nuclear pore marker mScarlet::NPP-11. Dashed white boxes outline the enlarged nucleus shown to the right. Arrows point to oocyte nuclei. Scale bars = 10 μm.

RNA pathway components within germ granules demonstrated that they are composed of spatially separated condensates (Ishidate et al., 2018; Manage et al., 2020; Phillips et al., 2012; Wan et al., 2018). These granule sub-compartments are enriched for different subsets of small RNA pathway components and are associated with distinct functional roles (Huang et al., 2025). Most of the defined sub-compartments also have distinct assembly factors that when mutated disrupt only the localization of factors within that sub-compartment. The phenotypes observed in the absence of these assembly factors are often used to infer the function of specific compartments. However, the assembly of sub-compartments are not completely independent.

Loss of certain assembly factors can also lead to the loss of separation between individual compartments or mixing of sub-compartments. This complex compartmentalization has prompted further research into whether this organization promotes mRNA sorting into distinct small RNA pathways, and whether key steps of post-transcriptional gene regulation occur within these compartments. The currently defined germ granule compartments of the adult germline and their respective roles in small RNA processing are discussed below.

P granule

As described, the P granule is the best studied germ granule compartment long proposed to function in small RNA-guided mRNA surveillance. At the nuclear periphery, P granules are estimated to associate with 75% of nuclear pores per nucleus and are considered the principal sites of mRNA export (Pitt et al., 2000; Sheth et al., 2010). Inhibition of mRNA transcription rapidly results in the reduction of P granule size, consistent with P granules concentrating newly exported mRNAs (W. Chen et al., 2020; Sheth et al., 2010). Additionally, tethering a reporter mRNA to P granule factor PGL-1 leads to reporter mRNA repression, dependent on P granule

assembly and WAGO-1 (Aoki et al., 2021). Together, these studies suggested P granules are hubs of mRNA surveillance and that mRNA localization within P granules is sufficient for gene silencing. In line with this role, P granules are enriched with the major effectors of the piRNA pathway, PRG-1 and WAGO-1 that together target "non-self" mRNAs for gene silencing (Figure 1.5).

The assembly of P granules requires a handful of factors that includes Vasa-homolog RNA helicase GLH-1, LOTUS domain proteins MIP-1 and MIP-2, and RNA binding protein PGL-1 (Kawasaki et al., 2004; Price et al., 2021; Spike et al., 2008). Work from our lab demonstrated that defects in P granule formation by mutation to major assembly factors like GLH-1 did not greatly impact the population of piRNAs and secondary small RNAs. Instead, loss of P granules resulted in the activation of many piRNA targets as well as aberrant silencing of endogenous genes (W. Chen et al., 2022). From this work and other related studies, P granules are proposed to promote the small RNA-based distinction between "self" and "non-self" mRNAs.

D and E granules

The D granule is a sub-compartment of germ granules positioned closest to the nuclear pores and therefore closest the newly exported mRNAs. CSR-1 class 22G-RNAs are enriched within the D compartment (Figure 1.5). Since CSR-1 class small RNAs target most germline-expressed endogenous genes, CSR-1 is positioned to interact with "self" genes prior to P granule factors. The E granule is situated just outside of and partially overlapped with the D granule relative to the nucleus. The E granule contains EGO-1, the RNA-dependent RNA polymerase required for CSR-1 class 22G-RNA synthesis (Figure 1.5). This suggests CSR-1 recognition of "self"

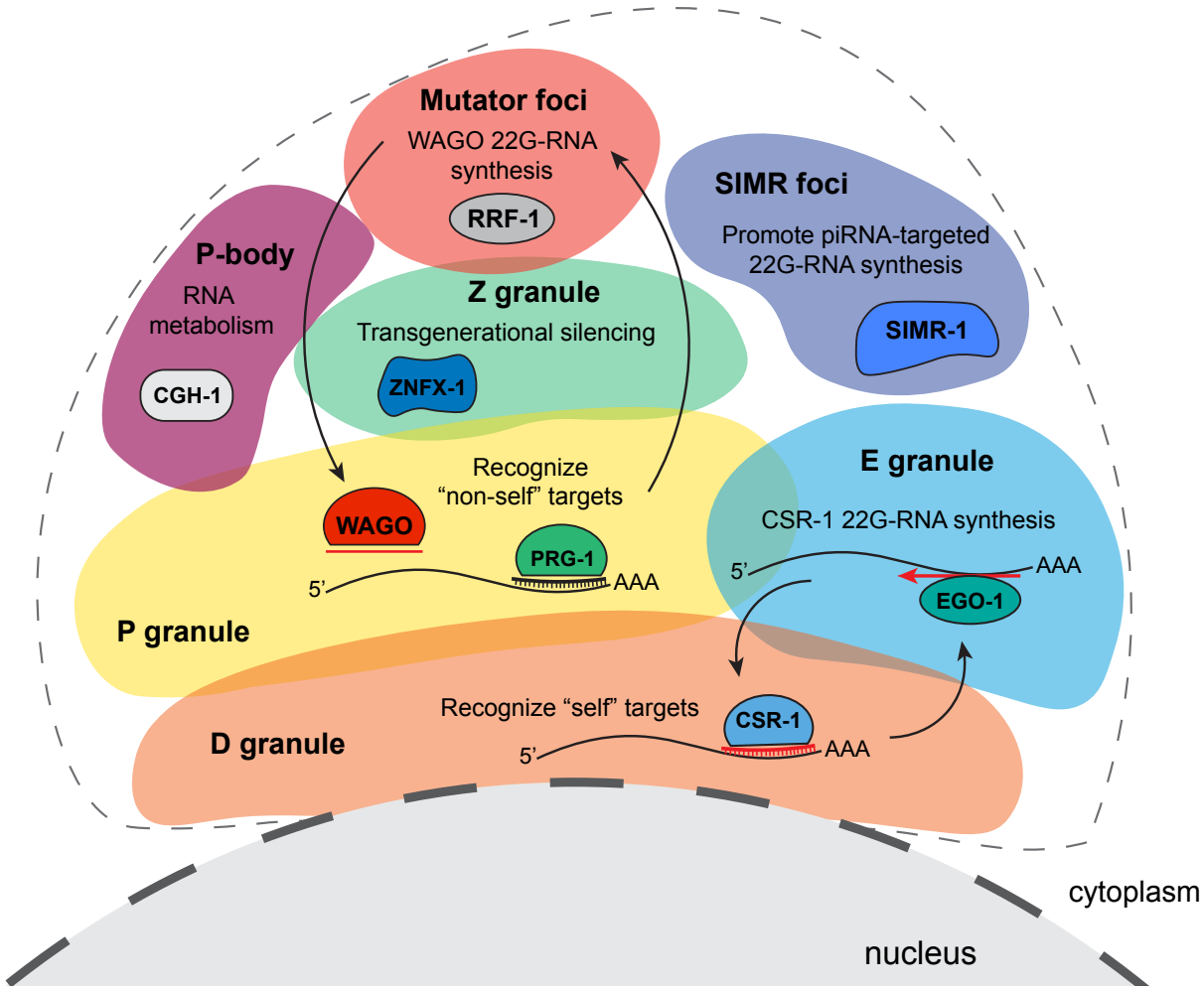

Figure 1.5: Model for the small RNA functions in granule compartments.
mRNAs exit through nuclear pores, which may or may not be associates with germ granules. CSR-1 22G-RNAs in the D granule are closest to the nuclear pores and may interact with "self" mRNAs before PRG-1. CSR-1 targeting may promote mRNA transport to the cytoplasm or amplified CSR-1 small RNA synthesis by EGO-1 in the E granule. In the P granule, PRG-1 can bind to "non-self" targets. These targets are proposed to be shuttled to the Mutator foci for WAGO class 22G-RNA amplification by RRF-1. Z granules promote the transgenerational inheritance of RNAi- and piRNA-mediated gene silencing mediated by ZNFX-1. SIMR foci assembled by SIMR-1 promote 22G-RNA production against piRNA targeted genes. The P-body assembled by CGH-1 associates with the outer layer of germ granules at developmental timepoints for mRNA storage and decay.

mRNAs in the D granule may facilitate further CSR-1 class small RNA synthesis within the E granule by EGO-1. Alternatively, CSR-1 targeting in the D granule may facilitate “self” mRNA transport out of the germ granule and into the cytoplasm for translation. Consistent with this role, DDX19, a DEAD-box RNA helicase involved in mRNA export from the nucleus and mRNA translation is also enriched within the D granule (Lu et al., 2025). Taken together, the D granule may facilitate “self” gene recognition and mRNA transport to the cytoplasm, bypassing the P granule.

Formation of the D granule was shown to require two nuclear pore proteins, and loss of either these proteins or DDX19 disrupted the organization of other germ granule compartments, including the P granule (Lu et al., 2025). This demonstrates the interdependence of germ granule compartment assembly, and suggests a hierarchical assembly directed by the D granule assembly factors. In contrast, loss of the E granule assembly factors, ELLI-1 and EGC-1, only impacts E granule formation, as the other compartments showed normal assembly (X. Chen et al., 2024). In the absence of the E granule, EGO-1 continues to synthesize CSR-1 class small RNAs, but these small RNAs are restricted to the extreme 3’ ends of mRNAs. The amplified CSR-1 small RNAs from the 5’ regions of target mRNAs failed to be produced or stabilized (X. Chen et al., 2024). Together, this suggested the E granule may function as the site of CSR-1 small RNA production from the 5’ ends of mRNAs. Overall, the D and E granules may facilitate the recognition, transport, and regulation of endogenous “self” mRNAs.

Mutator foci, Z granule, and SIMR foci

Mutator foci are enriched with a class of genes originally identified in the genetic screen for factors that derepressed transposable elements in the germline (Collins et al., 1987). This set of

factors was found to highly overlap with genes identified in the genetic screen for factors defective in canonical RNAi (Tabara et al., 1999a). Together, this suggested factors within the Mutator foci facilitate RNAi and transposon silencing. Notably, the RNA-dependent RNA polymerase RRF-1 that synthesizes WAGO class 22G-RNAs is enriched within the Mutator foci (Figure 1.5). Based on the phenotypes of Mutator class genes and the role of RRF-1, the Mutator foci are considered as the principal site of WAGO class small RNA amplification. Production of these WAGO 22G-RNAs is necessary for both piRNA- and RNAi-mediated gene silencing. The factors required for Mutator foci assembly are well-described and primarily require disordered protein MUT-16 for assembly (Phillips et al., 2012).

Interestingly, high-resolution imaging revealed that the Z granule compartment is positioned between the P granule and mutator foci (Wan et al., 2018). The Z granule factors include RNA helicase ZNFX-1 and Argonaute WAGO-4, factors required for RNAi inheritance and transgenerational epigenetic inheritance (Ouyang et al., 2022; Xu et al., 2018). There currently is no known assembly factor for Z granules. Instead, Z granule formation appears highly dependent on P granule assembly (W. Chen et al., 2022). Overall, the Z granule is proposed to function in marking mRNAs for heritable silencing, as loss of ZNFX-1 and WAGO-4 result in RNAi inheritance defects.

SIMR foci are adjacent to the Z granule and Mutator foci (Figure 1.5). The SIMR foci are named after the tudor domain protein SIMR-1 that forms these foci. Loss of SIMR-1 results in loss of WAGO class small RNAs against piRNA-targeted mRNAs (Manage et al., 2020). This suggests that SIMR foci function downstream of the piRNA pathway. Also enriched within SIMR foci, HRDE-2 was recently shown to promote small RNA loading to nuclear Argonaute HRDE-1 that functions downstream of RNAi and piRNA targeting (S. Chen & Phillips, 2024).

Through a series of genetic mutants that blocked small RNA loading to HRDE-1, unloaded HRDE-1 was shown to localize to SIMR foci, suggesting SIMR foci are the sites of HRDE-1 small RNA loading (S. Chen & Phillips, 2024). This work highlighted that static images of germ granules fail to capture the dynamic shuttling of proteins between germ granule compartments and other subcellular localizations. Further investigations with mutations that block specific steps within small RNA pathways may improve our understanding of where specific RNA regulatory processes occur within granules.

Altogether, the Mutator foci, Z granule, and SIMR foci are proposed to amplify "non-self" signals after initial targeting by RNAi primary small RNAs and piRNAs.

P-bodies

Processing-bodies (P-bodies) were first observed in mouse cells as cytoplasmic foci of the 5' to 3' exonuclease, XRN-1 (Bashkirov et al., 1997). In somatic cells, P-bodies are observed as discrete foci in the cytoplasm. Based on the enrichment of XRN-1 and other RNA decay machinery within P-bodies, they were initially thought to function as distinct sites of RNA decay. However, mRNA decay continued in the absence of condensed P-bodies (Eulalio et al., 2007). Moreover, P-bodies contain miRNA-mediated translational repression machinery and non-sense mediated decay inhibitors, suggesting P-bodies perform broader roles in translation regulation and RNA metabolism (Hubstenberger et al., 2017).

In *C. elegans* embryos, P-bodies were observed in close association with germ granules suggesting these distinct condensates interact during embryo development (Gallo et al., 2008). Recently in the adult germline, P-bodies were also observed in close association with germ granules at the nuclear periphery of germ cells (Du et al., 2023). Moreover, P-body factors, like

CGH-1/DDX6, were found to specifically interact with P and Z granule factors (Figure 1.5). Notably, loss of CGH-1 resulted in disrupted germ granule organization, where the P and Z granule factors collapsed into one condensate (Du et al., 2023). Loss of CGH-1 also disrupted RNAi-mediated transgenerational inheritance. Together, these findings demonstrated that interactions between P-bodies and germ granules may function to coordinate RNA regulation.

Interestingly, germ granules, P-bodies, and stress granules share an overlapping set of molecular components and similarly associate with lowly translated RNAs. Whether these three types of RNA granules coordinate RNA regulation within cells under normal or stress conditions is poorly understood. As indicated in the name, stress granules were originally observed by microscopy as cytoplasmic condensation of heat shock proteins under stress, which dissolved upon removal from stress (Nover et al., 1983). Stress granules also form when translation initiation is inhibited (Kedersha et al., 1999). Overall, stress granules are proposed to store and regulate translationally repressed mRNA, allowing gene expression to be reprogrammed during stress. Consistent with this role, stress granule defective cells show decreased recovery following stress (Yang et al., 2014). Future studies to uncover whether distinct types of RNA granules work together to coordinate RNA regulation will improve our understanding of whether RNAs are sorted between RNA granules in a directional and controlled manner.

1.9 Germ granules and small RNA pathways protect fertility during temperature stress

Widely observed across studies, mutations of germ granule components and small RNA pathway factors result in common defects in germline development that lead to infertility. Two common phenotypes of these mutants include temperature-sensitive male fertility defects and the mortal germline phenotype.

The loss of germ granule components and small RNA factors consistently lead to the upregulation of spermatogenic genes during oogenesis. As a hermaphroditic species, *C. elegans* produce and set aside sperm during the L4 larval stage, then as young adults, switch to making oocytes within the same gonad. The increased spermatogenic mRNAs in the adult gonad suggests a failure to stop transcription or post-transcriptionally regulate these mRNAs during the switch to oocyte production. This phenotype is observed during loss of P granules, and in mutants of the Mutator foci, SIMR foci, nuclear RNAi pathway, piRNA binding Argonaute PRG-1, and gene licensing factor CSR-1 (Campbell & Updike, 2015; Cornes et al., 2022; Ni et al., 2016; Rogers & Phillips, 2020). These findings highlight that various small RNA pathways contribute to the regulation of spermatogenic genes during germ cell development. Moreover, many of these mutants display corresponding defects in male fertility, particularly in elevated temperature. Normal growth temperature of *C. elegans* in lab conditions is 16 to 25 °C. The sperm defects for many of these mutants are more robust at 25 °C compared to 20 °C. This temperature-sensitivity suggests small RNAs may perform a greater role in gene regulation during higher temperatures, potentially due to the accelerated growth at high temperatures. Although PRG-1 and CSR-1 are mainly thought to function in opposing roles for "non-self" and "self" gene regulation, both *prg-1* and *csr-1* mutants display defects in sperm differentiation and male fertility (Conine et al., 2013b; Cornes et al., 2022). Overall, this highlights how multiple small RNA pathways function during gametogenesis to coordinate proper germ cell development.

Mutations to germ granule and small RNA pathway components also lead to germline mortality, where the germline deteriorates over generations until completely sterile. This is especially apparent when strains are grown in elevated temperature (25 °C). This phenotype has

been associated with defects in chromatin and gene regulation that affects chromosome structure as well as epigenetic inheritance (Ahmed & Hodgkin, 2000). Components from each germ granule sub-compartment display the germline mortality phenotype. Studies on DDX19, PRG-1, MUT-16, ELLI-1, ZNFX-1, and SIMR-1 show these factors are important for the maintenance of germline immortality (X. Chen et al., 2024; Ishidate et al., 2018; Lu et al., 2025; Manage et al., 2020; Simon et al., 2014). Why mutations to small RNA factors that perform unique gene regulatory roles consistently result in germline mortality remains an open question. However, these studies underscore the crucial roles for small RNA pathway factors in germline maintenance, especially during heat stress.

1.10 Concluding remarks and dissertation outline

Since the seminal discoveries of miRNAs and siRNAs, we have expanded our understanding of the molecular mechanisms governing small RNA biogenesis and small RNA-guided gene expression regulation. We have also deepened our insight into the diverse and crucial roles small RNAs perform throughout development. However, how small RNAs are sorted to the correct Argonaute proteins and how small RNAs distinguish “self” from “non-self” mRNAs remains poorly understood. These features are key for precise control over gene expression and ultimately proper development. As many small RNA processing components are enriched within distinct germ granule compartments, whether this organization is critical for small RNA-guided RNA regulation is still largely unclear. More broadly, whether distinct small RNA pathways and RNA granules coordinate gene regulation within a given tissue, particularly when under stress, remains an active area of investigation.

In this dissertation, I will investigate the regulation and germ granule organization of germline small RNA pathways under normal and stress conditions. In Chapter 2, I will describe a mechanism that promotes small RNA sorting between CSR-1 and WAGO Argonautes, thereby ensuring proper "self" and "non-self" target gene regulation. In Chapter 3, I will demonstrate that small RNA pathway competition underlies the differences in RNAi efficacy between male and female germ cells. In Chapter 4, I investigate the coordination of germ granules, stress granules, and P-bodies during heat stress, and show that germ granules ensure germ cell recovery. In the appendix, I explore the relationship between germ granule compartments, nuclear pore complexes, and chromatin organization, since loss of specific nucleoporins has been shown to result in distinct small RNA-mediated gene silencing defects. Collectively, my work provides a mechanism for small RNA sorting and expands our knowledge of how diverse small RNAs coordinate the regulation of threatening RNAs and endogenous mRNAs to protect germ cells from varying environmental challenges.

CHAPTER 2

RNA Helicase A promotes small RNA biogenesis and sorting in germ cells

2.1 Abstract

In germ cells, small RNAs protect genome integrity by silencing invading elements such as viruses and transposons. The broad silencing capacity of small RNAs raises the question of how germ cells avoid silencing their own mRNAs. In C. elegans, WAGO Argonautes silence transposon mRNAs, while CSR-1 Argonautes protect endogenous mRNAs from aberrant silencing and fine-tune their expression. Here, we identify the conserved RNA helicase RHA-1/DHX9 as a key factor that enables germ cells to distinguish endogenous RNAs from transposon mRNAs. We find that RHA-1 promotes the biogenesis of CSR-1 bound small RNAs and prevents their mis-sorting to WAGO-1. The enrichment of RHA-1 at perinuclear germ granules depends on EGO-1, which synthesizes CSR-1 small RNAs. Lastly, we show loss of RHA-1 impairs CSR-1 mediated mRNA fine-tuning and compromises fertility. Together, our study highlights the role of RHA-1 in small RNA sorting to safeguard endogenous gene expression and germ cell function.

2.2 Introduction

In animals, small RNAs are bound by the conserved family of Argonaute proteins to form complexes that can induce RNA silencing by binding complementary mRNA sequences leading to mRNA degradation, translational repression, or transcriptional silencing (Ghildiyal & Zamore, 2009; Okamura & Lai, 2008). Within germ cells, several classes of small RNAs, including micro-RNAs (miRNAs), short-interfering RNAs (siRNAs), and piwi-interacting RNAs (piRNAs) are produced by different biogenesis factors and bound by distinct Argonaute

members (Hutvagner & Simard, 2008). Together these small RNA classes perform crucial roles in genome integrity, germ cell development and differentiation, and overall germline fertility (Ghildiyal & Zamore, 2009). PiRNAs and siRNAs perform well-established roles in defending the genome from mutagenic invading RNAs including viral RNAs and transposons (Brennecke et al., 2007b; Carmell et al., 2007; Das et al., 2008; Tabara et al., 1999b). Outside of this role in genome defense, more recent work uncovered that piRNAs and endogenous siRNAs also regulate endogenous protein-coding mRNAs during sperm development in mice, fruit flies, and worms (Cornes et al., 2022; Iki et al., 2023; P. H. Wu et al., 2020). These expanded gene regulatory roles complicate our understanding of how small RNA classes establish and maintain their mRNA target specificity to facilitate multiple biological processes during germ cell development.

In *C. elegans*, the most abundant class of small RNAs are endogenous siRNAs termed 22G-RNAs. This class of small RNAs is bound by a group of worm-specific Argonautes termed WAGOs and Argonaute CSR-1 (Yigit et al., 2006). These 22G-RNAs are produced directly from mRNA transcripts that serve as templates for RNA-dependent RNA polymerases (RdRPs) EGO-1 and RRF-1 (Gent et al., 2009; Maniar & Fire, 2011; Smardon et al., 2000). The production of CSR-1 22G-RNAs requires EGO-1, whereas WAGO-1 22G-RNAs can be produced by either EGO-1 or RRF-1. WAGO-1 and CSR-1 bound 22G-RNAs target distinct sets of mRNAs and induce different gene regulatory outcomes. While WAGO-1 bound 22G-RNAs primarily function downstream of piRNAs and siRNAs to robustly silence transposons and viral RNAs, CSR-1 bound 22G-RNAs protect endogenous protein-coding mRNAs from piRNA silencing (Batista et al., 2008; H. C. Lee et al., 2012; Seth et al., 2013; G. Wang & Reinke, 2008). Together, this system allows for robust defense against invading mutagenic RNAs, while

preventing aberrant silencing of endogenous genes. Disruption to this small RNA system often results in germ cell development and differentiation defects, especially in combination with environmental stress like elevated temperature (Seroussi et al., 2023).

In addition to mRNA protection, more recent work discovered that CSR-1 also fine-tunes or decreases the mRNA levels for a subset of endogenous mRNA targets during embryo and adult germ cell development (Gerson-Gurwitz et al., 2016; Quarato et al., 2021; Singh et al., 2021). This subset of mRNAs are termed CSR-1 slicer targets because they require CSR-1 slicer activity for mRNA fine-tuning. CSR-1 slicer activity performs a critical role in gene regulation as CSR-1 slicer mutants display robust defects in fertility and embryo viability nearly identical to *csr-1* knockout animals (Gerson-Gurwitz et al., 2016; Quarato et al., 2021). Notably, WAGOs do not possess the critical catalytic residues for slicer activity, marking a key difference in CSR-1 and WAGO-1 gene regulatory pathways (Yigit et al., 2006). Given that CSR-1 and WAGO-1 perform distinct regulatory roles in germ cells but share the RdRP EGO-1 for producing their associated 22G-RNAs, how 22G-RNAs are correctly sorted to CSR-1 or WAGO-1 remains an important area of investigation.

Here, we demonstrate that the conserved RNA Helicase A (RHA-1) promotes 22G-RNA biogenesis and sorting to CSR-1. Loss of RHA-1 leads to reduced CSR-1 bound 22G-RNAs and increased WAGO-1 bound 22G-RNAs derived from endogenous protein-coding mRNAs. These small RNA defects correspond to increased mRNA levels of CSR-1 target genes and spermatogenesis-enriched genes, suggesting disruption of CSR-1 target fine-tuning and germline gene regulation. Consistent with a role in CSR-1 small RNA synthesis, we found RHA-1 localizes to perinuclear germ granules within the E compartment where EGO-1 is also enriched. Moreover, RHA-1 localization to germ granules depends on both EGO-1 and CSR-1.

Furthermore, we found that RHA-1 is a critical regulator of germ cell development as its loss leads to defects in sperm activation, fertility, and germline immortality.

2.3 Results

RHA-1 ATPase activity promotes RNAi and fertility in germ cells

Previous reports identified *rha-1/dhx-9*, a conserved member of the DExH family of RNA helicases, as required for various processes of genome integrity, including RNAi-mediated gene silencing in fruit flies, human cells, and worms (Cugusi et al., 2016; Fu & Yuan, 2013; Robb & Rana, 2007; Walstrom et al., 2005). Since these reports, how RHA-1 contributes to genome integrity remains unknown. In follow up, we aimed to confirm whether RHA-1 is required for RNAi by feeding animals bacteria expressing-dsRNA against germline genes *pos-1* and *mex-3*, and somatic genes *dpy-13* and *unc-22*. For germline genes, wild-type animals showed entirely unhatched embryos, indicative of successful RNAi knockdown of *pos-1* and *mex-3* genes. In contrast, *rha-1(tm329)* mutants showed nearly all hatched embryos, indicating RHA-1 is required for RNAi against germline genes (Figure 2.1A). Nonetheless, both wild type and *rha-1(tm329)* mutants showed successful RNAi knockdown of somatic genes *dpy-13* and *unc-22*, based on the visible phenotypes of shortened dumpy bodies and uncoordinated twitching, respectively (Figure 2.1B). Together, this data demonstrates RHA-1 is only required for RNAi function in germ cells but not somatic cells. This places RHA-1 amongst a small set of genes including CSR-1 and EGO-1 that are similarly required for RNAi only in germ cells (Claycomb et al., 2009b; Smardon et al., 2000).

In addition, these germ cell-only RNAi factors have been shown to play critical roles in germline fertility and immortality, especially at elevated growth temperature (25 °C)

(Charlesworth et al., 2021; Smardon et al., 2000). A previous report observed reduced fertility in *rha-1(tm329)* mutants, particularly in elevated temperature (Walstrom et al., 2005). However, it was later discovered an unlinked mutation in the gene *haf-6* in the strain background may have increased the penetrance of the reported phenotypes (Walstrom et al., 2014). After outcrossing the *haf-6* mutation from the background, we examined the fertility of the *rha-1(tm329)* mutant animals. We observed a moderate reduction in fertility in *rha-1(tm329)* mutants at normal growth temperature (20 °C) (Figure 2.2A). When grown at 25 °C, *rha-1(tm329)* mutants exhibited a progressive decline in fertility and were sterile by the second generation (Figure 2.1C). These results suggest RHA-1 promotes fertility and germline immortality, consistent with a role in germline small RNA pathways.

Next, we investigated whether RHA-1 ATPase activity contributes to RHA-1 function in RNAi and fertility. To this aim, we generated two RHA-1 ATPase activity mutants by substituting critical amino acids in the conserved ATP binding and ATP hydrolysis domains of DExH family helicases (Fairman-Williams et al., 2010; Prabu et al., 2015). In the background of endogenously tagged GFP::RHA-1, we used CRISPR Cas9-mediated gene editing to substitute the critical lysine residue in the GKT motif required for ATP binding with glutamine, generating an ATP binding mutant *gfp::rha-1(K410Q)*. Additionally, we substituted the key glutamic acid residue of the ATP hydrolysis domain with alanine, generating an ATP hydrolysis mutant *gfp::rha-1(E505A)*. First, we examined whether RHA-1 ATPase activity regulates RNAi as observed for *rha-1(tm329)* mutants. In both RHA-1 ATP binding and ATP hydrolysis mutants, RNAi of germline gene *pos-1* or *mex-3* was much less effective in comparison to control animals (Figure 2.1D). Like *rha-1(tm329)* mutants, RHA-1 ATP binding and ATP hydrolysis mutants

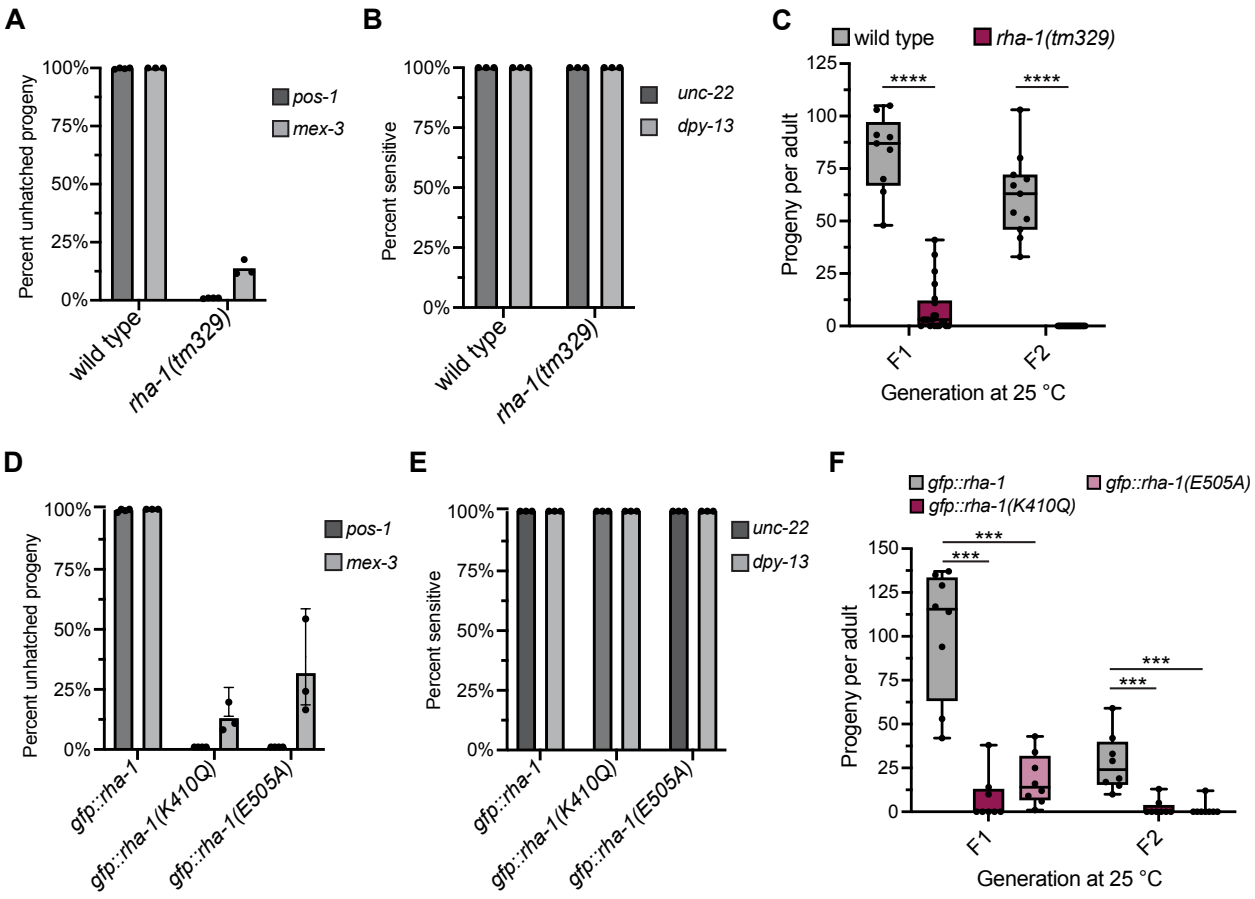

Figure 2.1: RHA-1 is required for germline RNAi and germline immortality.
(**A** and **D**) Quantification of unhatched embryos of the indicated animals after feeding RNAi targeting *pos-1* and *mex-3*. Data are presented as mean values + / - SD of three biologically independent samples. (**B** and **E**) Quantification of twitching or dumpy short body phenotypes of the indicated animals after feeding RNAi targeting *unc-22* and *dpy-13* respectively. Percent sensitive indicates ratio of worms with the successful target knockdown phenotypes. Data are presented as mean values + / - SD of three biologically independent samples. (**C** and **F**) Brood sizes of the indicated animals grown at 25 °C for one (F1) or two (F2) generations. Single L3 stage animals were transferred to individual plates at each generation and number of progeny per worm was measured. N = 8-12 animals. For the boxplots, the line indicates the median value, the box indicates the first and third quartiles, and the whiskers indicate the min and max values. Two-tailed p values were calculated using Mann-Whitney-Wilcoxon test. ***, p<0.001; ****, p<0.0001.

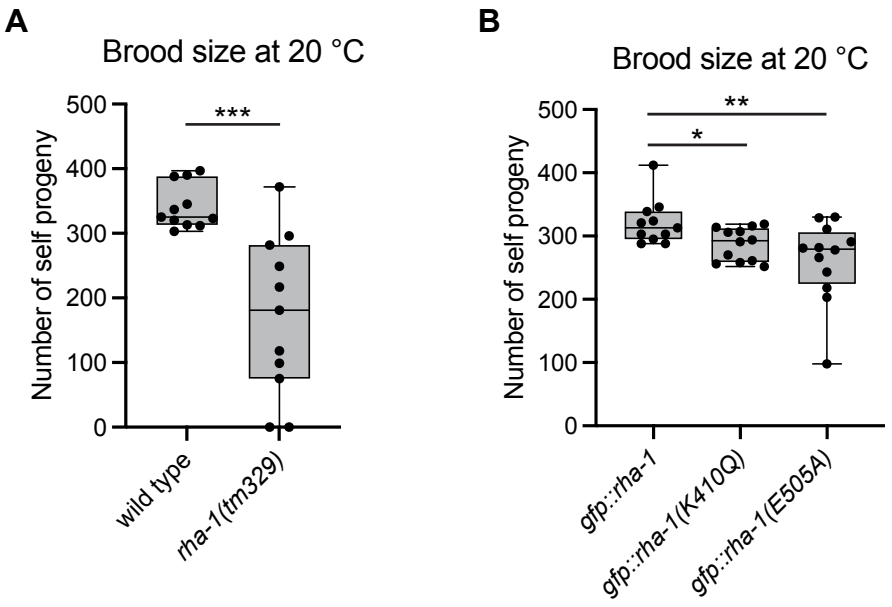

Figure 2.2: RHA-1 ATPase activity is required for optimal fertility.
(**A** and **B**) Brood sizes of the indicated animals grown at 20 °C. *N* = 11-12 animals. For the boxplots, the line indicates the median value, the box indicates the first and third quartiles, and the whiskers indicate the min and max values. Two-tailed p values were calculated using Mann-Whitney-Wilcoxon test. *, $p<0.05$; **, $p<0.01$; ***, $p<0.001$.

were fully sensitive to RNAi of somatic genes *dpy-13* and *unc-22* (Figure 2.1E). These data suggest RHA-1 ATPase activity contributes to RHA-1 function in germline RNAi.

Next, we investigated whether RHA-1 ATPase activity regulates germline fertility, and immortality. At 20 °C, RHA-1 ATP binding and ATP hydrolysis mutants showed a modest reduction in fertility (Figure 2.2B). At 25 °C, RHA-1 ATP binding and ATP hydrolysis mutants exhibited progressively reduced fertility and reached near sterility by the second generation (Figure 2.1F). Thus, loss of RHA-1 ATPase activity impacts germline fertility and immortality comparable to the complete loss of RHA-1, indicating RHA-1 ATPase activity is critical for these processes.

RHA-1 localizes to germ cell nuclei and germ granules

Based on our findings that RHA-1 performs a role in germline RNAi and fertility, we investigated RHA-1 localization. To this aim, we introduced a GFP tag at the N-terminus of endogenous RHA-1 using CRISPR Cas9-mediated gene editing. We find RHA-1 is expressed in somatic and germ cells throughout development, including the spermatogenic germline of L4 hermaphrodites and males, the oogenic germline of adult hermaphrodites, and developing embryos (Figure 2.3A and Figure 2.4, A and B). In germ cells, comparing RHA-1 localization to nuclear pore protein NPP-7, we find RHA-1 localizes both inside and outside of nuclei in puncta that resemble germ granules (Figure 2.3A).

Germ granules are RNA-rich biomolecular condensates that contain small RNA factors and RNA processing machinery (Eddy, 1976; Strome & Wood, 1982; Updike & Strome, 2010).To determine whether RHA-1 localizes to germ granules, we examined RHA-1 localization relative to PGL-1-marked germ granules. We find RHA-1 granules are in proximity

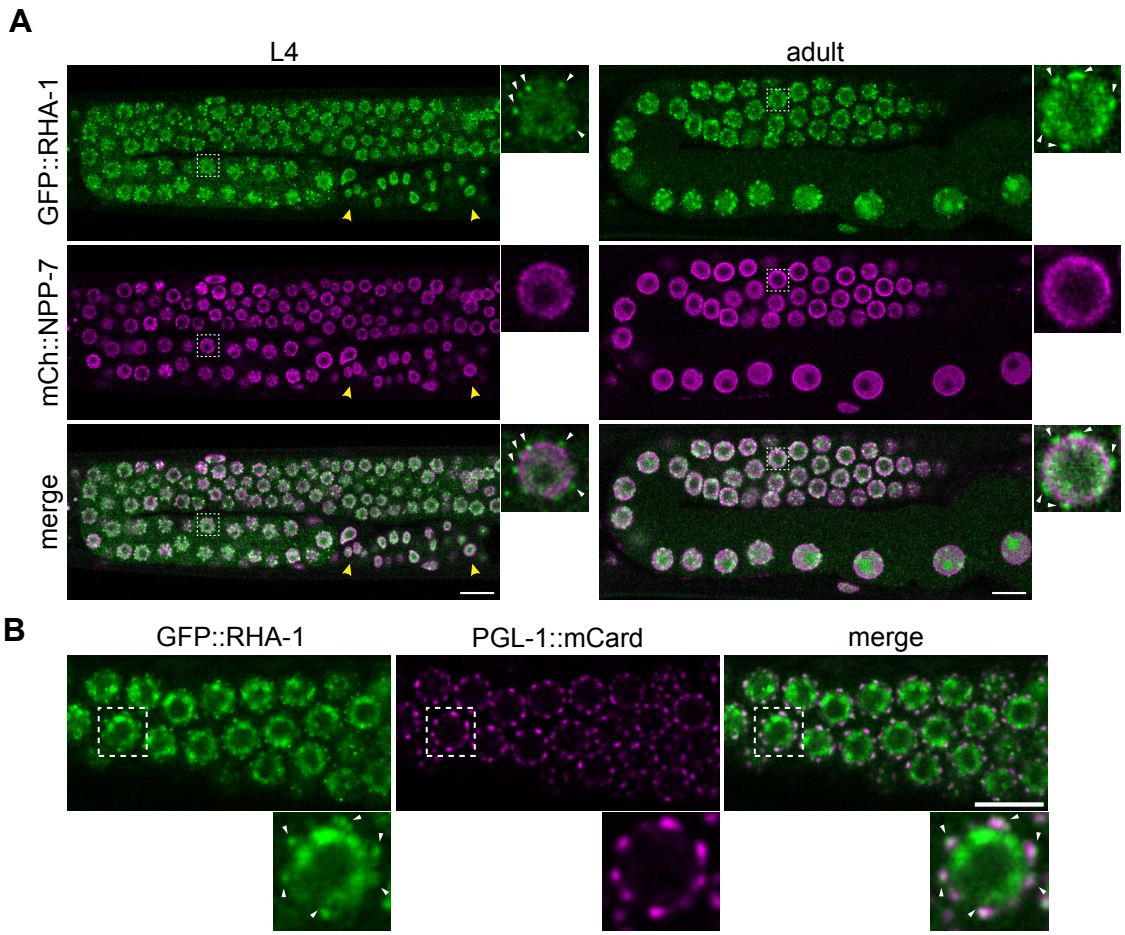

Figure 2.3: RHA-1 localizes to germ cell nuclei and germ granules.
(**A**) Representative live-fluorescent images of animals expressing GFP::RHA-1 and mCherry:NPP-7 (nuclear pore marker). L4 germline (left) and adult germline (right). Boxes with dashed outline show the single cropped and enlarged nucleus. Between the yellow arrowheads are somatic cell nuclei outside of the germline. (**B**) Representative live-fluorescent images of adult pachytene region germ cells in animals expressing GFP::RHA-1 and PGL-1::mCardinal (P compartment marker). (**A** and **B**) Boxes with dashed outline show the single cropped and enlarged nucleus. White arrowheads point to the RHA-1 granules at the nuclear periphery outside of the germ cell nucleus. Scale bars = 10 µm.

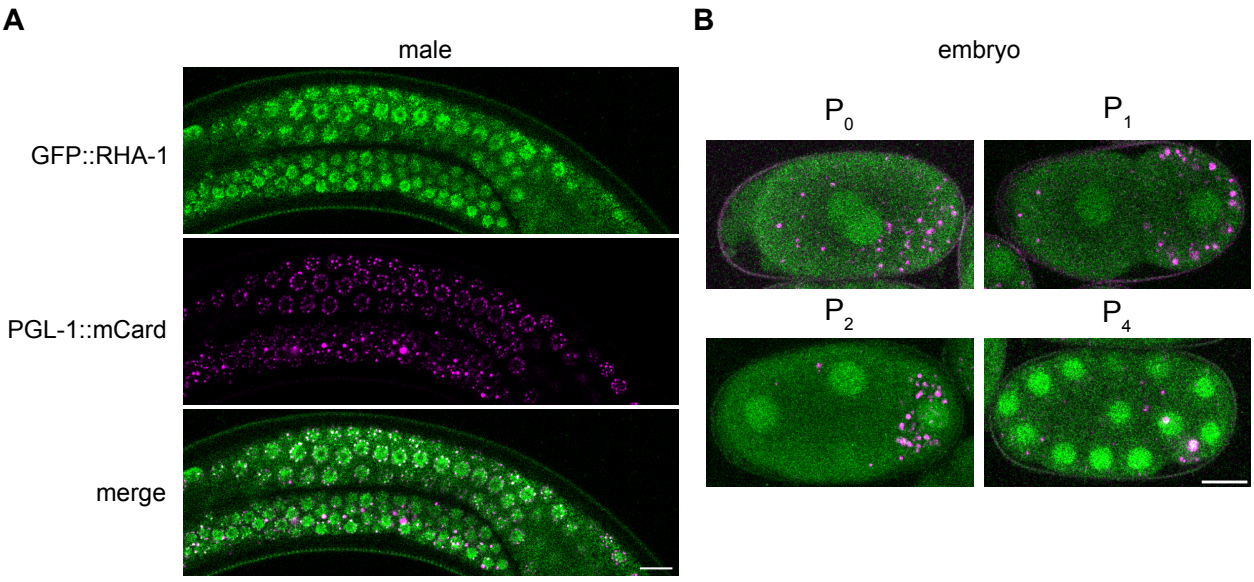

Figure 2.4: RHA-1 is expressed in the male germline and developing embryos.
(**A**) Representative live-fluorescent images of animals expressing GFP::RHA-1 and PGL-1::mCardinal (P compartment marker) in the young adult male germline. (**B**) Representative live-fluorescent images of animals expressing GFP::RHA-1 and PGL-1::mCardinal (P compartment marker) in the four labeled stages of developing embryos. Scale bars = 10 µm.

but not fully overlapped with PGL-1-marked granules surrounding germ cell nuclei (Figure 2.3B). This result suggests RHA-1 and PGL-1 localize to distinct sub-compartments of germ granules (see additional details below). Nonetheless, our observation identifies RHA-1 as a germ granule factor throughout germ cell development.

RHA-1 promotes 22G-RNA production and sorting from CSR-1 target genes

Given several germ cell-only RNAi factors, including EGO-1 and CSR-1, contribute to 22G-RNA production, this raised the possibility that RHA-1 is also involved in 22G-RNA production. We performed deep sequencing of the small RNA species isolated from young adult wild type and *rha-1(tm329)* mutants grown at normal growth temperature (20 °C). We first assessed the overall abundance of the major classes of small RNAs including piRNAs, miRNAs, and 22G-RNAs. In result, neither piRNAs nor miRNAs showed a notable change in abundance in *rha-1(tm329)* mutants compared to wild type across replicates (Figure 2.5, A and B). Additionally, the abundance of 22G-RNAs mapping to WAGO and CSR-1 target genes showed no uniform change in *rha-1(tm329)* mutants compared to wild type (Figure 2.6A and Figure 2.5C).

22G-RNAs are produced by RdRPs directly from mRNA targets and processive RNA helicases such as DRH-3 and ZNFX-1 facilitate the spread of 22G-RNA production across the entire length of the mRNA targets (W. Gu et al., 2009; Ishidate et al., 2018). Given RHA-1 is similarly a processive RNA helicase, we analyzed the 22G-RNA distribution on WAGO and CSR-1 target genes. For WAGO target genes, the 22G-RNA distributions were similar for *rha-1(tm329)* mutants and wild type (Figure 2.6B and Figure 2.5D). Strikingly, the 22G-RNA distributions on CSR-1 target genes showed an increase in production from the 3’ end with a

drop off in production at the 5' end of gene lengths in *rha-1(tm329)* mutants compared to wild type (Figure 2.6C and Figure 2.5E). These findings suggest RHA-1 contributes to the production of 22G-RNAs derived across the full length of CSR-1 target mRNAs. Consistent with a role for helicase activity in this 22G-RNA production, we find RHA-1 ATP binding and ATP hydrolysis mutants show a similar change to the 22G-RNA distribution on CSR-1 target genes as *rha-1(tm329)* mutant animals (Figure 2.6D). These data indicate RHA-1 helicase activity facilitates 22G-RNA production across the full length of CSR-1 target mRNAs.

Since 22G-RNAs are bound by CSR-1 and WAGOs, we asked whether the changes in 22G-RNA distribution on CSR-1 target genes in *rha-1(tm329)* mutants reflect changes to CSR-1 bound 22G-RNAs. To examine this, we immunoprecipitated either CSR-1 or WAGO-1 and sequenced the bound small RNAs with the expected outcome that CSR-1 22G-RNAs would report the same changes observed in total small RNAs, while WAGO-1 22G-RNAs would report no change. Instead, we found changes in the abundance of both CSR-1 and WAGO-1 bound 22G-RNAs derived from CSR-1 target genes. For CSR-1 bound 22G-RNAs, we find reduced overall abundance mapping to CSR-1 target genes (Figure 2.6E). Strikingly, for WAGO-1 bound 22G-RNAs, we find increased abundance mapping to CSR-1 target genes (Figure 2.6F). These observations suggest that RHA-1 promotes CSR-1 22G-RNA biogenesis and prevents the aberrant binding of CSR-1 target derived 22G-RNAs by WAGO-1.

Although WAGO-1 aberrantly binds small RNAs mapping to CSR-1 target genes in *rha-1(tm329)* mutants, WAGO-1 bound 22G-RNAs mapping to WAGO target genes showed no change in abundance from wild type (Figure 2.6F). Additionally, CSR-1 bound 22G-RNAs mapping to WAGO target genes showed no change in abundance for *rha-1(tm329)* mutants

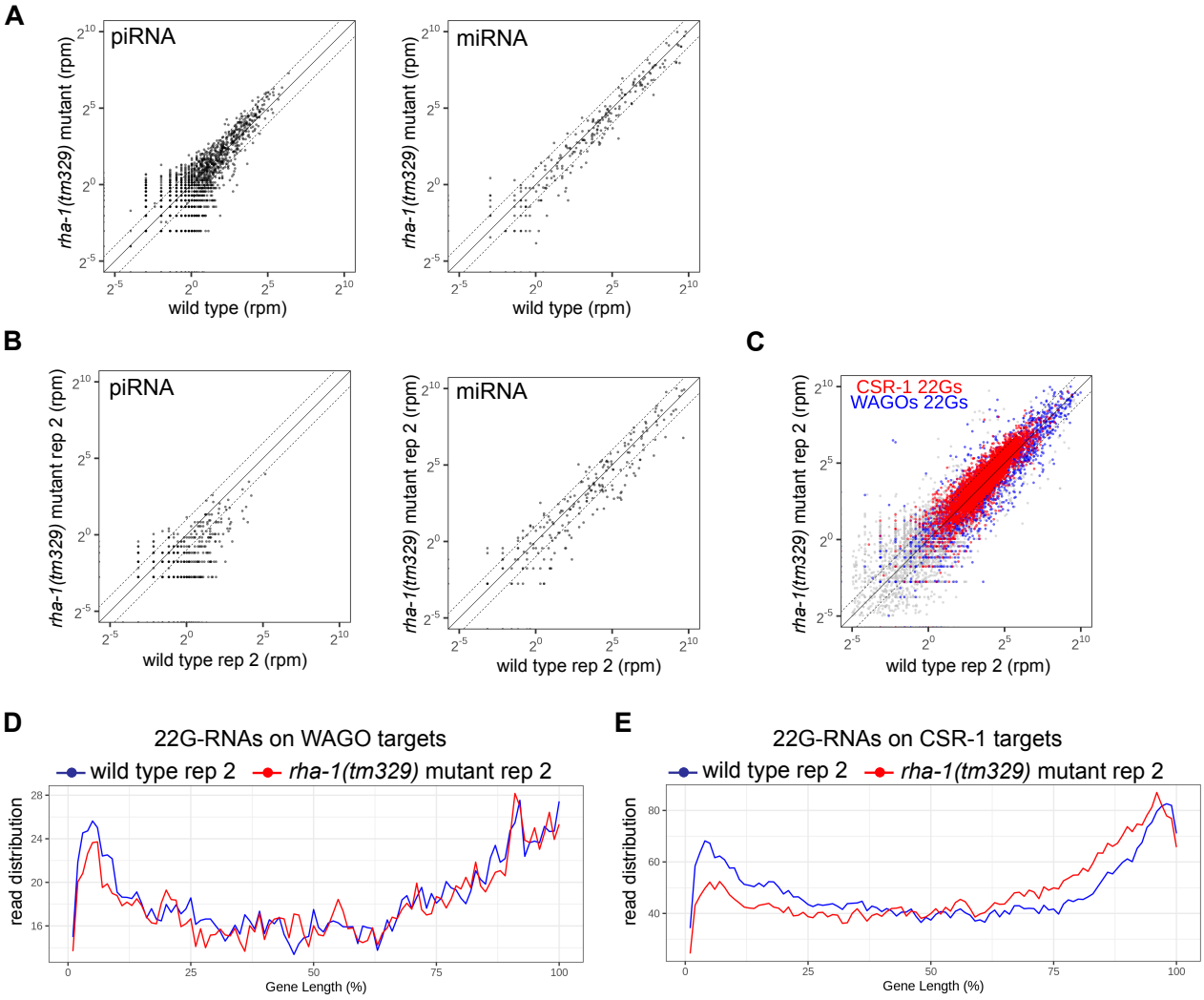

Figure 2.5: Total small RNA abundance is relatively unchanged in *rha-1* mutants.
(**A**) Scatterplots showing the abundance of piRNAs (left) or miRNAs (right) in wild-type worms compared to *rha-1(tm329)* mutant worms for replicate 1. (**B**) Scatterplots showing the abundance of piRNAs (left), miRNAs (middle), or all 22G-RNAs (right) mapped to each CSR-1 target (red) and WAGO target (blue) in wild-type worms compared to *rha-1(tm329)* mutant worms for replicate 2. (**C** and **D**) Metagene traces show the distribution of normalized 22G-RNAs (sRNA-seq) in arbitrary units mapping to WAGO (**C**) or CSR-1 (**D**) target genes by percentage of WAGO or CSR-1 target gene length. Reads from wild type (blue) and *rha-1(tm329)* mutant (red) for replicate 2. For all scatterplots the three diagonal lines indicate a two-fold increase (top), no change (middle), or a two-fold depletion (bottom) in indicated *rha-1* mutant animals.

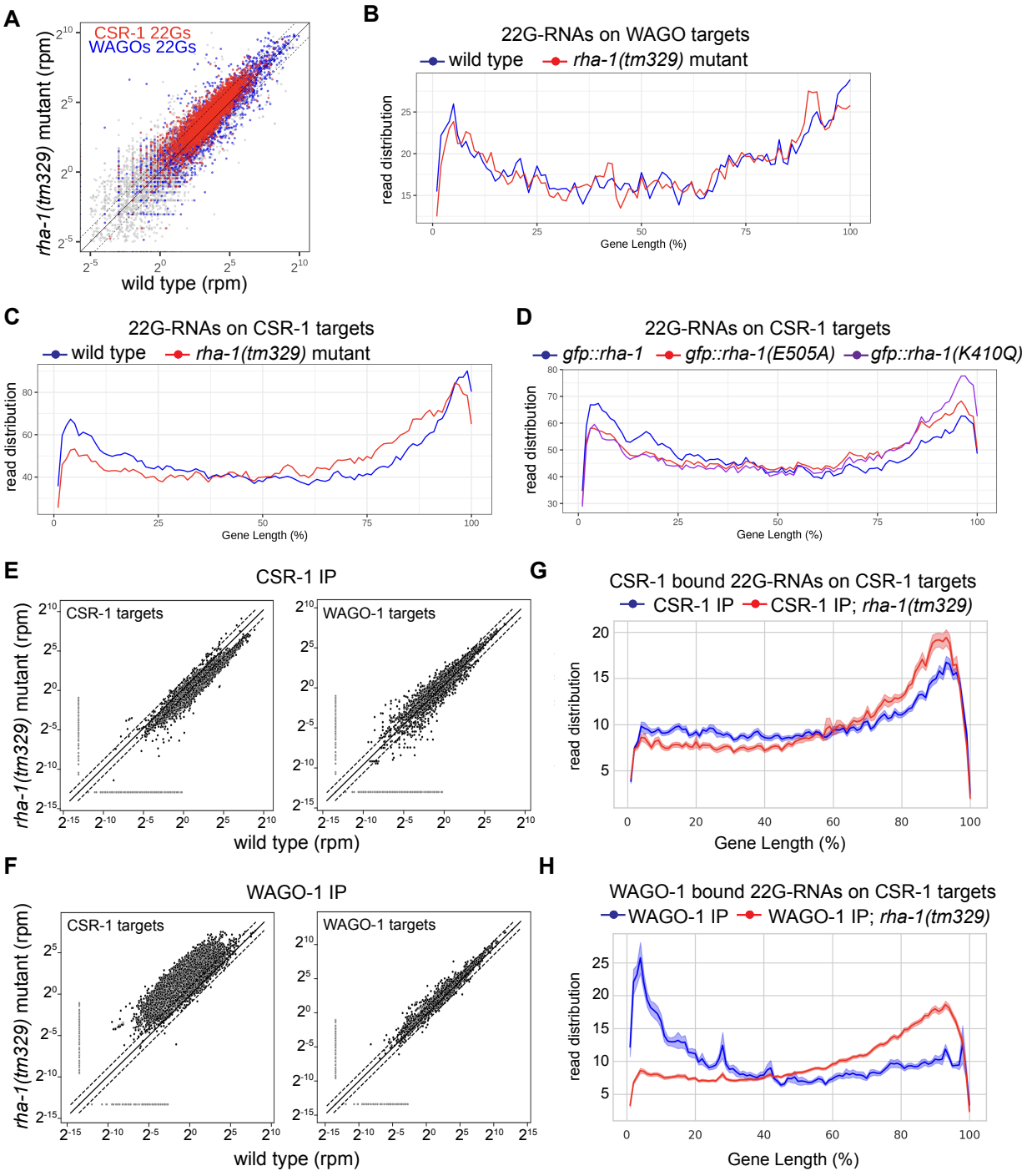

Figure 2.6: RHA-1 is required for the biogenesis of CSR-1 bound 22G-RNAs and 22G-RNA sorting.

(**A**) Scatterplot showing the abundance of all 22G-RNAs mapped to each CSR-1 target (red) and WAGO target (blue) in wild-type worms compared to *rha-1(tm329)* mutant worms. The three diagonal lines indicate a two-fold increase (top), no change (middle), or a two-fold depletion (bottom) in *rha-1(tm329)* mutant. (**B** and **C**) Metagene traces show the distribution of normalized

Figure 2.6 continued
22G-RNAs (sRNA-seq) mapping to WAGO (**B**) or CSR-1 (**C**) target genes by percentage of WAGO or CSR-1 target gene length. Reads from wild type (blue) and *rha-1(tm329)* mutant (red). (**D**) Metagene traces show the distribution of normalized 22G-RNAs (sRNA-seq) mapping to CSR-1 target genes by percentage of CSR-1 target gene length. Reads from control *gfp::rha-1* (blue), *gfp::rha-1(E505A)* (red), and *gfp::rha-1(K410Q)* (purple) animals. (**E** and **F**) Scatterplots showing the abundance of CSR-1 bound 22G-RNAs (CSR-1 IP-sRNA-seq) (**E**) or WAGO-1 bound 22G-RNAs (WAGO-1 IP-sRNA-seq) (**F**) mapped to each CSR-1 target (left) and WAGO target (right) in wild-type worms compared to *rha-1(tm329)* mutant worms. The three diagonal lines indicate a two-fold increase (top), no change (middle), or a two-fold depletion (bottom) in *rha-1(tm329)* mutant. (**G** and **H**) Metagene traces show the read counts distribution of normalized CSR-1 bound 22G-RNAs (IP-sRNA-seq) (**G**) or WAGO-1 bound 22G-RNAs (WAGO-1 IP-sRNA-seq) (**H**) mapping to CSR-1 target genes by percentage of CSR-1 target gene length. Traces show the mean read counts +/- one standard error. Reads from wild type IPs (blue) and *rha-1(tm329)* mutant IP samples (red).

compared to wild type (Figure 2.6E). These results suggest that RHA-1 does not regulate the biogenesis or sorting of 22G-RNAs derived from WAGO target genes.

The distributions of CSR-1 and WAGO-1 bound 22G-RNAs on CSR-1 target genes showed decreased abundance of small RNAs derived from the 5' end of mRNAs in *rha-1(tm329)* mutants compared to wild type, consistent with our results from total small RNAs (Figure 2.6, G and H). Inspection of the CSR-1 bound 22G-RNAs mapping to several individual CSR-1 target genes showed CSR-1 22G-RNAs greatly reduced from the 5' region of genes in *rha-1(tm329)* mutants compared to wild type (Figure 2.7A). For these CSR-1 target genes, the incorrectly sorted WAGO-1 bound 22G-RNAs in *rha-1(tm329)* mutants are also reduced at the 5' end of genes (Figure 2.7A). In contrast, WAGO-1 and CSR-1 bound 22G-RNAs mapping to several WAGO target genes showed relatively no change in *rha-1(tm329)* mutants compared to wild type (f Figure 2.7B). This further supports our findings that RHA-1 regulates 22G-RNA biogenesis and sorting from CSR-1 target mRNAs, but not WAGO target mRNAs.

We next aimed to gain insight into how RHA-1 contributes to CSR-1 22G-RNA distribution. Notably, both *rha-1(tm329)* and CSR-1 slicer mutants show similar changes to the CSR-1 bound 22G-RNA distribution on CSR-1 target gene lengths, where 22G-RNA production from the 5' end of mRNAs is greatly reduced (Figure 2.8, A and B). Given that CSR-1-mediated cleavage of target mRNAs is proposed to initiate 22G-RNA synthesis from the new cleaved 3′ ends, sequential CSR-1 slicing events are thought to drive the production of 22G-RNAs by EGO-1 from the 3' end toward the 5′ end across the full length of target mRNAs (Singh et al., 2021). Like *rha-1* mutants, CSR-1 slicer mutants showed no change in total abundance of 22G-RNAs mapped to CSR-1 targets but showed a slight decrease in abundance of CSR-1 bound 22G-RNAs mapped to CSR-1 targets (Figure 2.8, C and D). This hints that small RNAs may also

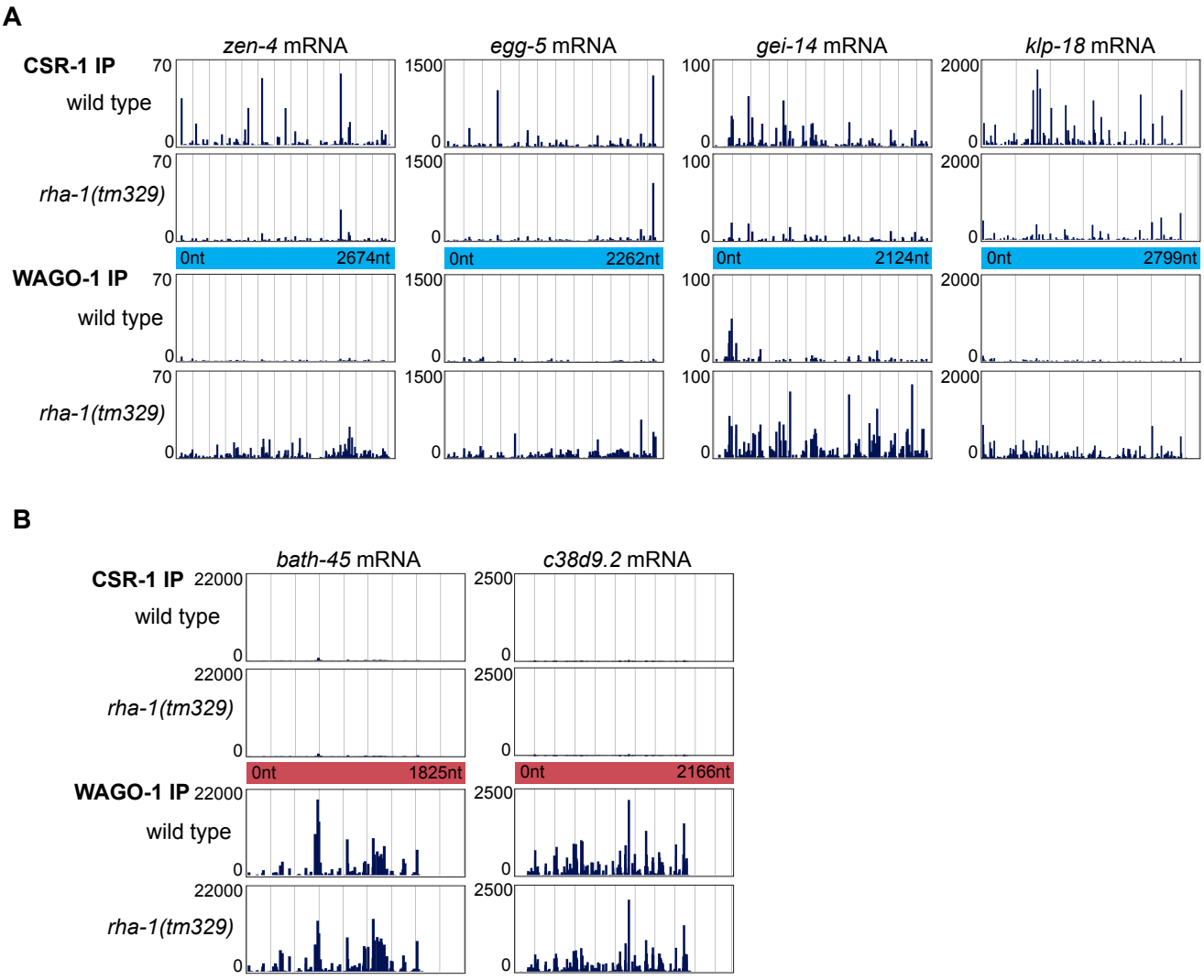

Figure 2.7: RHA-1 contributes to the generation of CSR-1 bound 22G-RNAs mapping to the 5' region of CSR-1 target mRNAs.

(**A** and **B**) Examples of normalized antisense 22G-RNAs bound by either CSR-1 or WAGO-1 in the wild type or *rha-1(tm329)* mutant samples mapping to the indicated CSR-1 target mRNAs (**A**) or WAGO-1 target mRNAs (**B**).

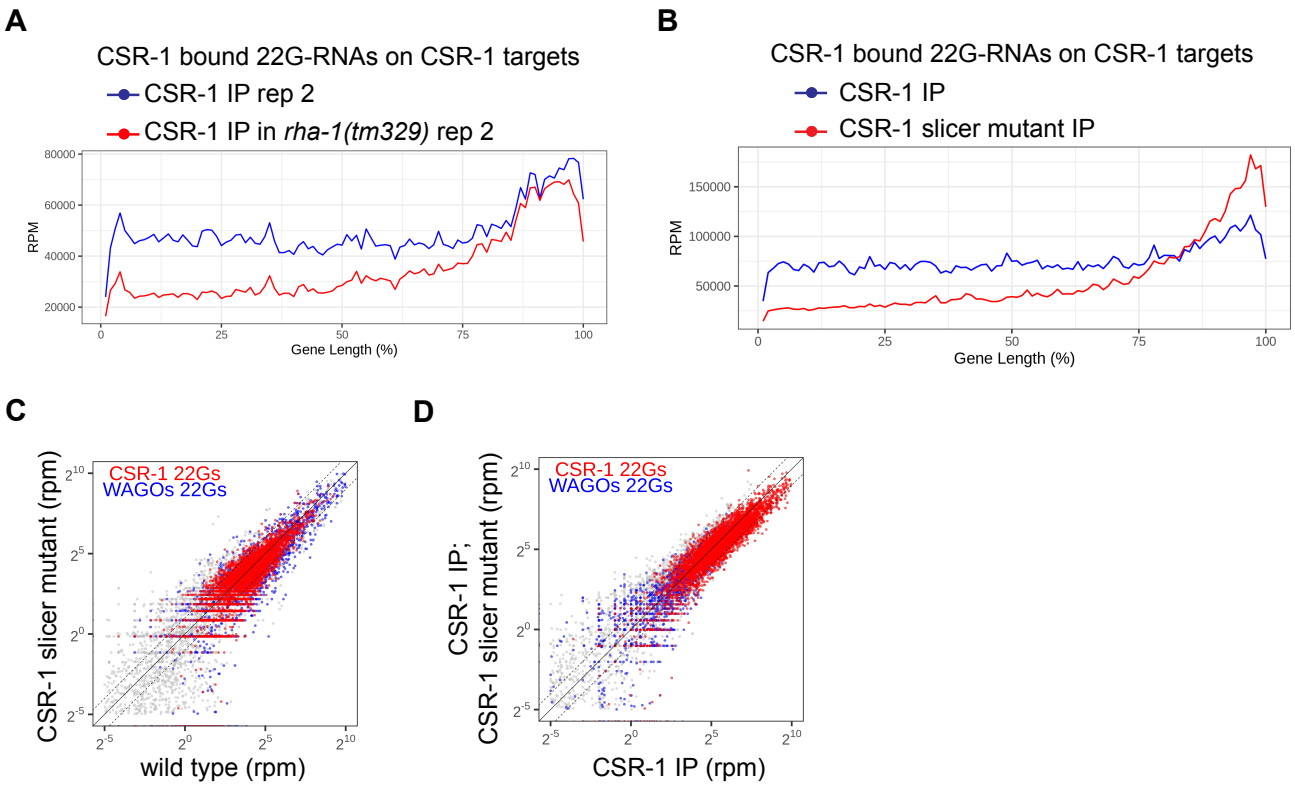

Figure 2.8: RHA-1 and CSR-1 slicer activity promote 22G-RNA production from 5' region of mRNAs.

(**A**) Metagene traces show the distribution of normalized CSR-1 bound 22G-RNAs (IP-sRNA-seq) in reads per million (RPM) mapping to CSR-1 target genes by percentage of CSR-1 target gene length. Reads from wild type (blue) and *rha-1(tm329)* mutant (red). (**B**) Metagene traces show the distribution of normalized CSR-1 bound 22G-RNAs (IP-sRNA-seq) in reads per million (RPM) mapping to CSR-1 target genes by percentage of CSR-1 target gene length. Reads from wild type (blue) and CSR-1 slicer mutant (red). (**C** and **D**) Scatterplots showing the abundance of all 22G-RNAs mapped to each CSR-1 target (red) and WAGO target (blue) in wild-type worms compared to CSR-1 slicer mutant worms from total small RNAs (sRNA-seq) (**C**) or CSR-1 bound 22G-RNAs (IP-sRNA-seq) (**D**). The three diagonal lines indicate a two-fold increase (top), no change (middle), or a two-fold depletion (bottom) in CSR-1 slicer mutant animals. (**B** to **D**) Data re-analyzed from published data sets in (Singh et al. 2021).

be mis-sorted in CSR-1 slicer mutants. Together, these data suggest both RHA-1 and CSR-1 slicer activity are critical for 22G-RNA production from the 5' region of target mRNAs. Our analyses raise the possibility that RHA-1 may promote CSR-1 slicer activity or facilitate sequential rounds of CSR-1-mediated cleavage and 22G-RNA synthesis on target mRNAs.

Overall, these data lead us to propose that RHA-1 promotes 22G-RNA biogenesis from the 5' region of CSR-1 target mRNAs and 22G-RNA sorting to CSR-1.

RHA-1 localizes to the E compartment of germ granules

Germ granules exhibit a complex organization of spatially distinct sub-compartments. These sub-compartments are enriched for distinct sets of small RNA components and generally linked to specific pathway functions (Huang et al., 2025; Phillips & Updike, 2022; Uebel et al., 2023; Wan et al., 2018). Specifically, the RdRP EGO-1, which is responsible for CSR-1 22G-RNA biogenesis, is largely enriched in the E compartment, while CSR-1 and WAGO-1 are enriched in D and P compartments, respectively (Figure 2.9A). Based on our results that RHA-1 promotes CSR-1 22G-RNA biogenesis, we wondered whether RHA-1 localizes within the E compartment of germ granules. Thus, we examined RHA-1 localization compared to EGO-1 and found RHA-1 granules highly overlap with EGO-1 (Figure 2.9B). In addition, we observed that RHA-1 exhibited higher levels of co-localization with E compartment factor ELLI-1, than with P compartment factor PGL-1 (Figure 2.9, C and D).

The E compartment of germ granules specifically requires the assembly factor ELLI-1 for formation (X. Chen et al., 2024). To examine whether RHA-1 requires the E compartment for localization to germ granules, we examined RHA-1 localization in *elli-1(uoc35)* mutants. Strikingly, in *elli-1(uoc35)* mutants, RHA-1 germ granule localization is completely disrupted,

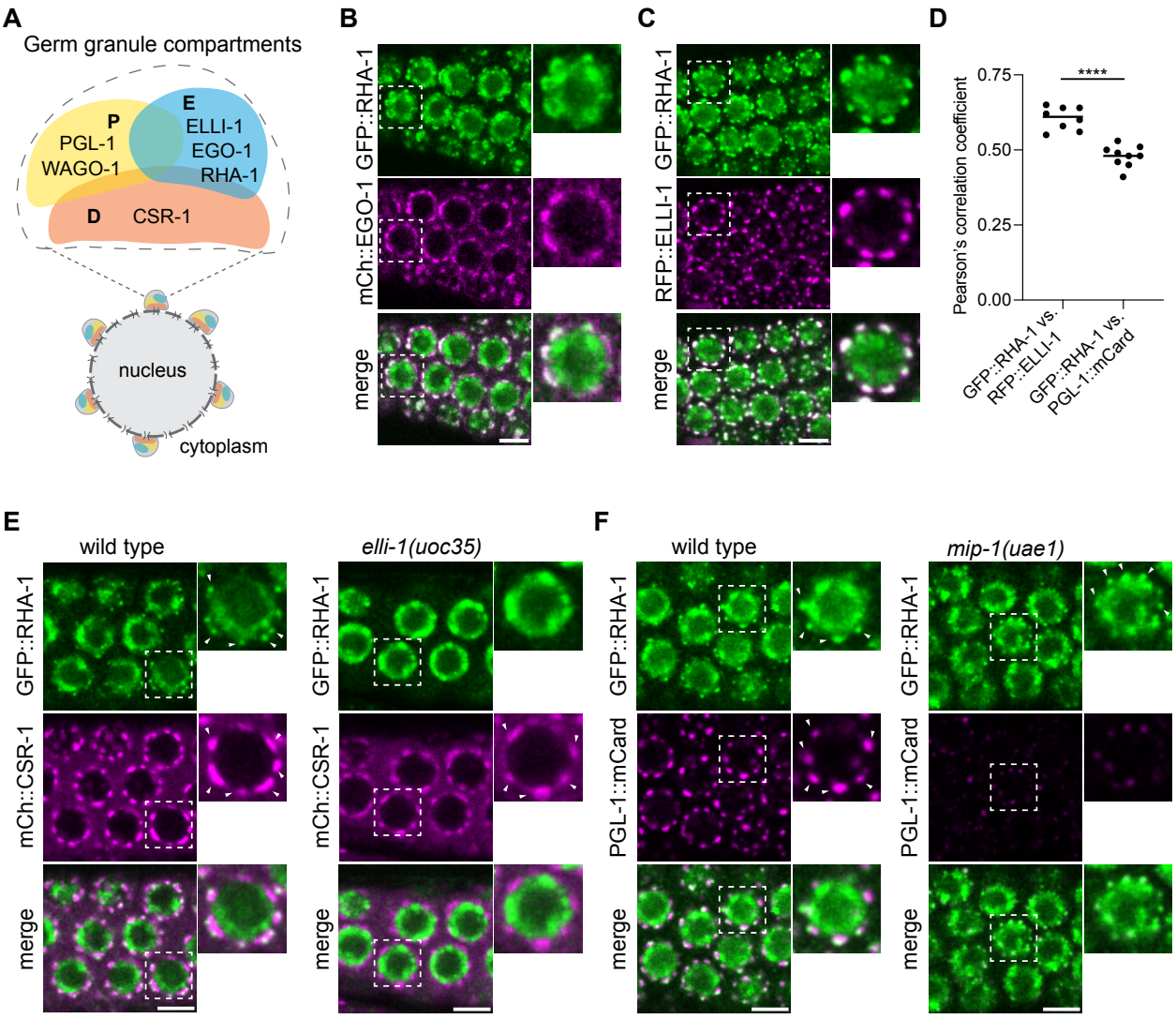

Figure 2.9: RHA-1 localizes to the E compartment of germ granules.
(**A**) Cartoon depicting germ granule sub-compartment spatial organization and factors that localize to these sub-compartments. (**B** and **C**) Representative live-fluorescent images of adult germ cells in the pachytene region in animals expressing GFP::RHA-1 and mCherry::EGO-1 (E compartment marker) (**B**) or RFP::ELLI-1 (E compartment marker) (**C**). (**D**) Quantification of colocalization between the indicated fluorescent proteins of pachytene germ cells. Each data point represents the Pearson's R-value showing the degree of colocalization between two fluorescence channels indicated. The solid black line indicates the mean value. Each data point represents independent gonad images. *N* = 8-9 gonads. Two-tailed p values were calculated using Mann-Whitney-Wilcoxon test. ****, p<0.0001. (**E**) Representative live-fluorescent images of pachytene germ cells show the localization of GFP::RHA-1 and mCherry::CSR-1 (D compartment marker) in wild-type (left) or *elli-1(uoc35)* mutant animals (right). White arrowheads point to the RHA-1 or CSR-1 granules at the nuclear periphery outside of the germ

Figure 2.9 continued
cell nucleus. (**F**) Representative live-fluorescent images of pachytene germ cells show the localization of GFP::RHA-1 and PGL-1::mCardinal (P compartment marker) in wild-type (left) or *mip-1(uae1)* mutant animals (right). White arrowheads point to the RHA-1 or PGL-1 granules at the nuclear periphery outside of the germ cell nucleus. For all images, boxes with dashed outline show the single cropped and enlarged nucleus. Scale bars = 5 μm.

while D compartment factor CSR-1 germ granule localization is maintained (Figure 2.9E). In contrast, loss of the P compartment assembly factor MIP-1 strongly disrupted P compartment factor PGL-1 germ granule localization but not RHA-1 granule localization (Figure 2.9F). Together, these findings identify RHA-1 as an E compartment factor within germ granules (Figure 2.9A). Intriguingly, loss of E compartment assembly was recently shown to disrupt EGO-1 22G-RNA production specifically from the 5' region of mRNAs (X. Chen et al., 2024). Together, these results suggest that RHA-1 and EGO-1 enriched within the E compartment facilitate 22G-RNA production from the 5' region of CSR-1 target mRNAs.

RHA-1 localization to the E compartment depends on CSR-1 and EGO-1

The organization of small RNA factors within germ granule compartments is proposed to facilitate the fidelity of gene regulation by small RNAs (W. Chen et al., 2022; Ouyang et al., 2019; Wan et al., 2018). Given the observed changes in 22G-RNA biogenesis and sorting in *rha-1* mutants, we wondered whether loss of RHA-1 leads to disrupted germ granule compartment formation or organization. We focused on the P, D, and E sub-compartments of germ granules since WAGO-1, CSR-1, and EGO-1 localize to these compartments respectively. Fluorescence imaging of PGL-1-marked P compartments and EGO-1- and ELLI-1-marked E compartments revealed a slight increase to granule size in *rha-1(tm329)* mutants compared to wild type (Figure 2.10, A to D). For WAGO-1-marked P compartments and CSR-1-marked D compartments, we observed no change to granule size (Figure 2.10, A and B). These results suggest RHA-1 does not greatly impact the formation of these compartments.

Next, we examined whether loss of RHA-1 leads to changes in germ granule compartment organization. Typically, the D compartment localizes closest to the nuclear

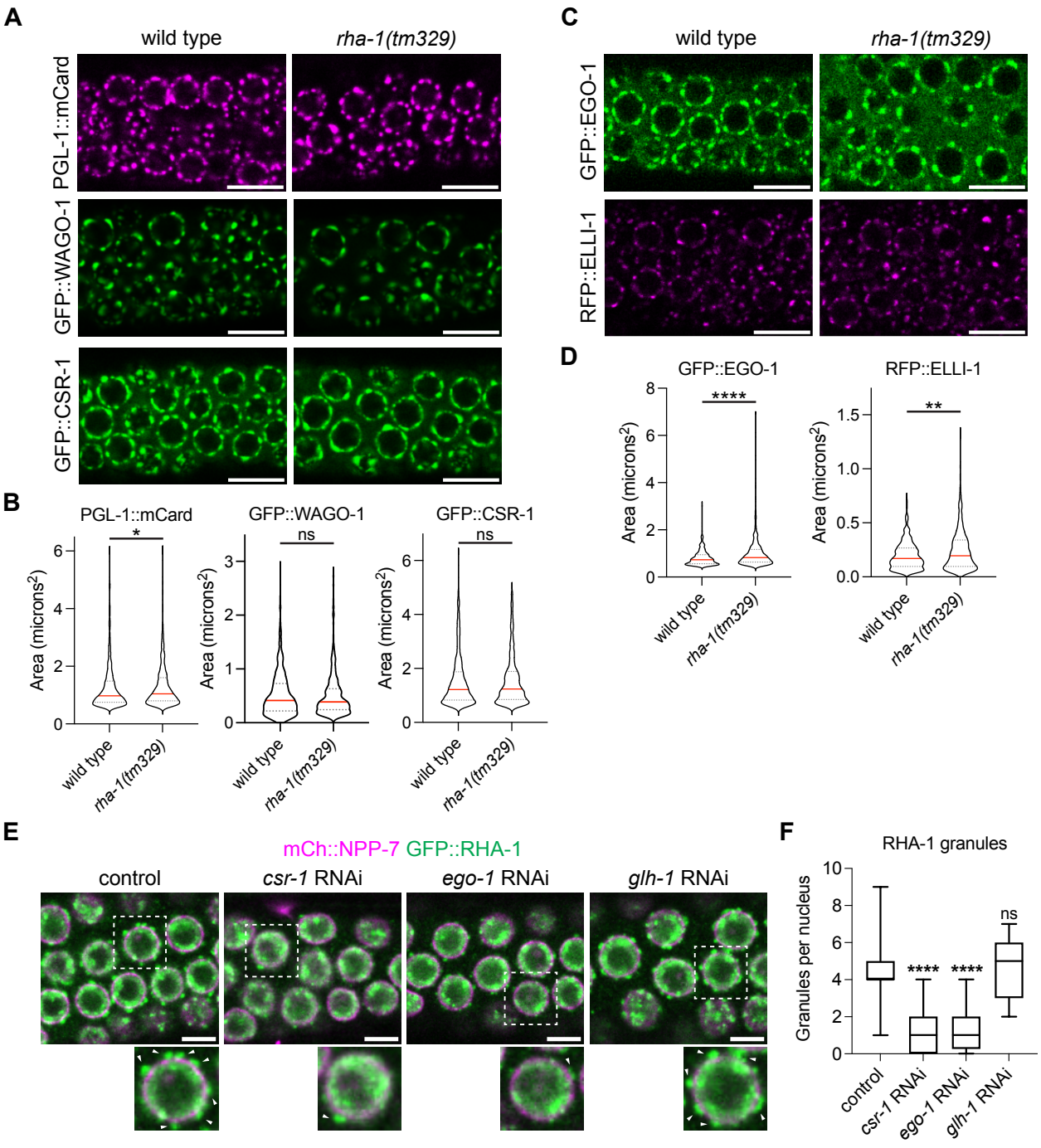

Figure 2.10: RHA-1 germ granule localization depends on CSR-1 and EGO-1.
(**A** and **C**) Representative live-fluorescent images of pachytene germ cells show the localization of the indicated germ granule markers in wild-type and *rha-1(tm329)* mutant animals. (**A**) PGL-1::mCard and GFP::WAGO-1 are P compartment markers, and GFP::CSR-1 is the D compartment marker. (**C**) GFP::EGO-1 and RFP::ELLI-1 are E compartment markers. Scale bars = 10 µm. (**B** and **D**) Violin plots depicting granule size (µm^2) quantified from experiment in part

Figure 2.10 continued
(**A** and **C**) for *N* = 8-10 independent germlines for wild-type and *rha-1(tm329)* mutant animals. Red line marks the median value. Two-tailed p values were calculated using Mann-Whitney-Wilcoxon test. *, p<0.05; **, p<0.01; ***, p<0.001. ns, no significance. (**E**) Representative live-fluorescent merged images of pachytene germ cells in animals expressing GFP::RHA-1 (green) and mCherry:NPP-7 (nuclear pore marker) (magenta) in control or RNAi knockdown of the indicated genes. Boxes with dashed outline show the single cropped and enlarged nucleus. White arrowheads point to RHA-1 granules. Scale bars = 5 μm. (**F**) Boxplots show the number of GFP::RHA-1 granules per germ cell nuclei from the experiment in (**E**). *N* = 8-10 gonads and number of granules per nucleus was quantified for 10 nuclei per gonad. For the boxplots, the line indicates the median value, the box indicates the first and third quartiles, and the whiskers indicate the min and max values. Two-tailed p values were calculated using Mann-Whitney-Wilcoxon test. ****, p<0.001. ns, no significance.

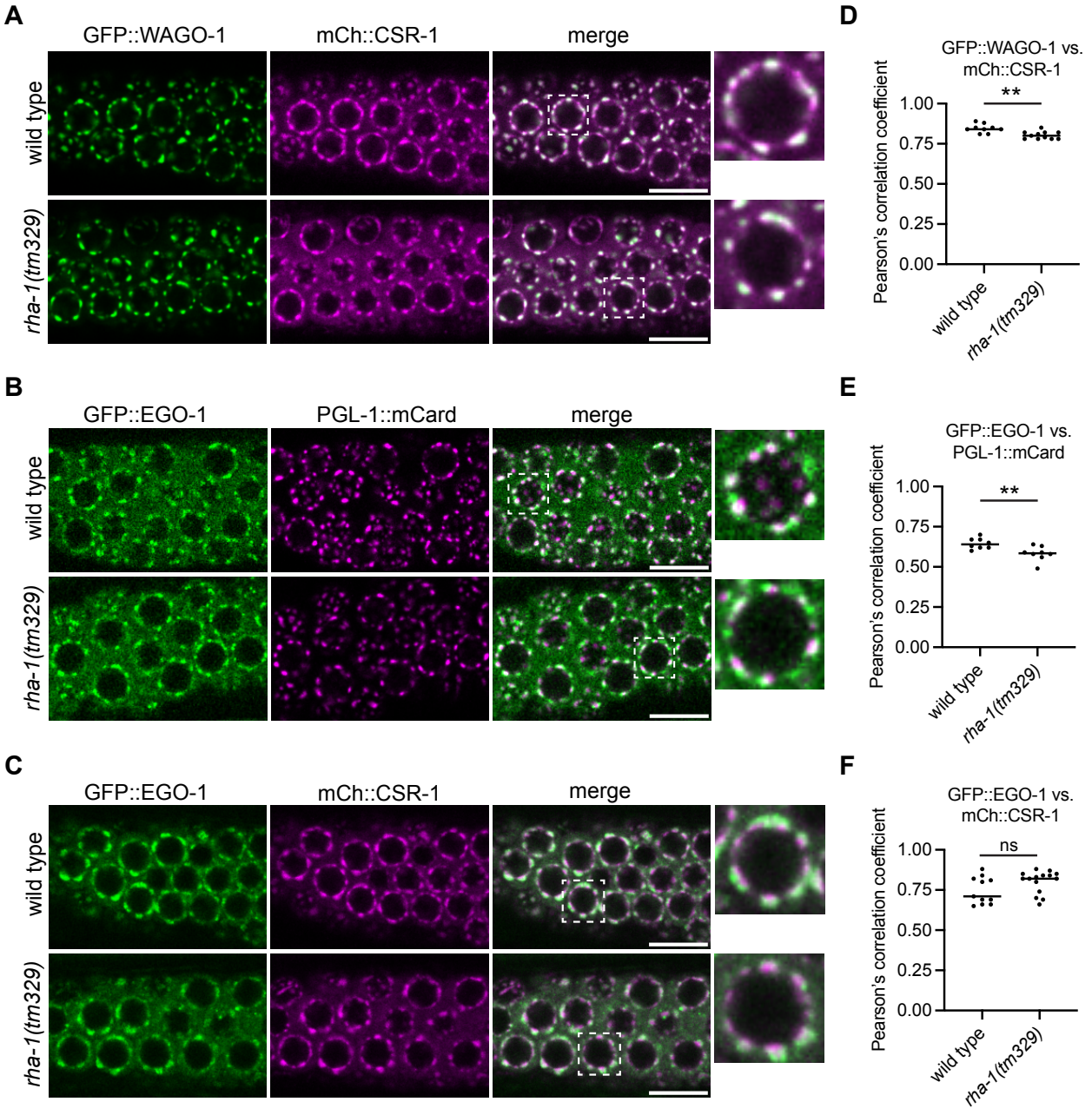

Figure 2.11: P compartments show reduced co-localization with D and E in *rha-1* mutants. (**A** to **C**) Representative live-fluorescent images of germ cells show localization of indicated germ granule markers in wild-type and *rha-1(tm329)* mutant animals. Co-marked strains for comparison of the P to D compartment (GFP::WAGO-1 to mCh::CSR-1) (**A**) or E to P compartment (GFP::EGO-1 to PGL-1::mCard) (**B**) or E to D compartment (GFP::EGO-1 to mCh::CSR-1) (**C**). Boxes with dashed outline show single cropped and enlarged nucleus. Scale bars = 10 µm. (**D** to **F**) Quantification of co-localization between the indicated fluorescent proteins of pachytene germ cells. Each data point represents the Pearson's R-value showing the degree of co-localization between two fluorescence channels. Solid black line indicates the mean

Figure 2.11 continued
value. Each data point represents independent gonad. *N* = 8-15 gonads. Two-tailed p values were calculated using Mann-Whitney-Wilcoxon test. **, $p<0.01$; ns, no significance.

envelope with the P and E compartments positioned adjacent to each other just outside of the D compartment (Figure 2.9A). These compartments also partially overlap indicative of factor interaction between sub-compartments. We compared the relative positions of these compartments by pair-wise comparisons in co-marked strains. Overall, the relative positions of the D, P, and E compartments showed similar organization in *rha-1(tm329)* mutants as wild type (Figure 2.11, A to C). We measured a decrease in co-localization between the P and D compartments and P and E compartments in *rha-1(tm329)* mutants compared to wild type (Figure 2.11, D and E). Co-localization between D and E compartments showed no change (Figure 2.11F). We also noted that the increase in granule sizes for PGL-1 and EGO-1 in *rha-1(tm329)* mutants were not always apparent in these co-marked backgrounds (Figure 2.11, A to C). This data suggests loss of RHA-1 leads to minor changes in germ granule compartment organization.

Following from our findings that RHA-1 does not greatly disrupt germ granule formation or organization, we hypothesized RHA-1 may function in CSR-1 22G-RNA biogenesis downstream of CSR-1 or EGO-1 activity. To test whether RHA-1 localization depends on CSR-1 or EGO-1, we performed RNAi knockdown of *csr-1* or *ego-1*, then evaluated RHA-1 localization compared to nuclear pore marker NPP-7. As a result of both *csr-1* or *ego-1* knockdown, RHA-1 germ granule localization was largely disrupted and formed a reduced number of germ granules per nucleus (Figure 2.10, E and F). In contrast, knockdown of *glh-1*, a factor well known for its role in P granule assembly, resulted in no change to RHA-1 germ granule localization or granule number per nucleus (Figure 2.10, E and F) (W. Chen et al., 2022; Spike et al., 2008). These results indicate RHA-1 localization to germ granules depends on CSR-1 and EGO-1, but not P granule factor GLH-1. Moreover, these results indicate RHA-1 germ

granule recruitment downstream of CSR-1 or EGO-1 may contribute to RHA-1 specificity in small RNA biogenesis on CSR-1 target mRNAs.

CSR-1 target genes are upregulated in *rha-1* mutants

Since small RNAs regulate target gene expression, we next examined whether *rha-1(tm329)* mutants exhibit changes in gene expression, particularly for CSR-1 target genes. To this aim, we generated mRNA high-throughput sequencing libraries from young adult wild type and *rha-1(tm329)* mutants grown at 20 °C and evaluated mRNA level fold changes. We proposed two potential outcomes based on our small RNA results. First, incorrect sorting of 22G-RNAs to WAGO-1 could lead to WAGO-1-mediated RNA silencing, and as a result, CSR-1 target mRNA levels would be reduced in *rha-1(tm329)* mutants compared to wild type. Alternatively, reduction in CSR-1 bound 22G-RNAs could lead to loss of CSR-1-mediated mRNA fine-tuning, and as a result, CSR-1 target mRNA levels would be increased in *rha-1(tm329)* mutants. The mRNA sequencing results displayed an increase in mRNA fold change for CSR-1 targets in *rha-1(tm329)* mutants. In contrast, WAGO target genes showed relatively no change (Figure 2.12A). Additionally, we evaluated CSR-1 top slicer target genes defined in a previous report as genes with 2-fold or more decrease in CSR-1 IP-associated 22G-RNAs in the CSR-1 slicer mutant, and 2-fold or more increase in mRNA level in the CSR-1 slicer mutant compared to wild type (Singh et al., 2021). The CSR-1 top slicer targets showed an increase in mRNA fold change in *rha-1(tm329)* mutants compared to wild type at a higher fold than all CSR-1 targets (Figure 2.12A). This data suggests that loss of RHA-1 mainly disrupts CSR-1-mediated mRNA fine-tuning. Additionally, in *rha-1(tm329)* mutants the gained WAGO-1 bound 22G-RNAs mapping to CSR-1 target genes do not aberrantly silence these targets.

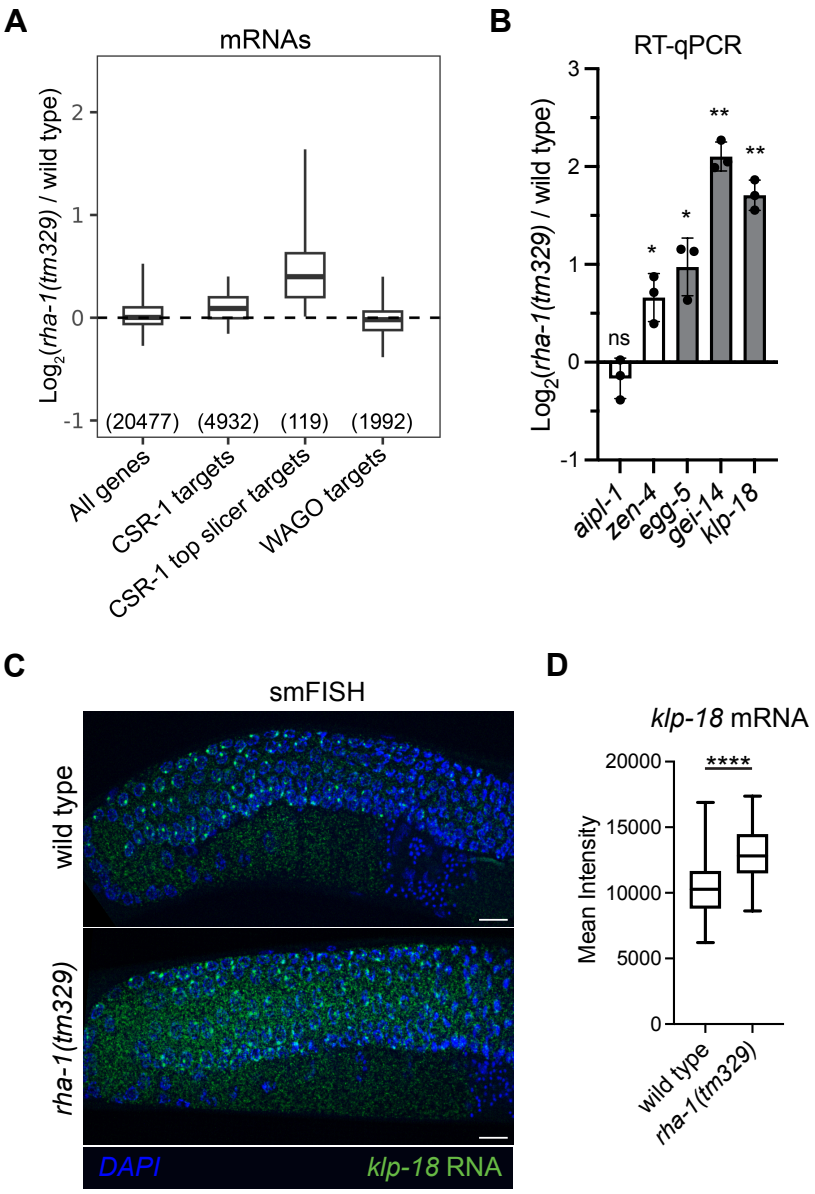

Figure 2.12: CSR-1 target mRNAs are upregulated in *rha-1* mutants.
(**A**) Boxplot showing $\log_2$ fold change in mRNA abundance for adult stage *rha-1(tm329)* mutants compared to wild-type animals (two biological replicates). For the boxplot, the line indicates the median value, the box indicates the first and third quartiles, and the whiskers indicate the 5th and 95th percentiles, excluding outliers. The sample size n (genes) is indicated in parentheses. (**B**) Bar graph showing $\log_2$ fold change in mRNA expression (RT-qPCR) of the indicated genes in wild-type compared to *rha-1(tm329)* mutant young adult animals. White bars are CSR-1 targets and gray bars indicate CSR-1 top slicer targets. Data are represented as mean and standard deviation for three biological replicates. Two-tailed p values were calculated from ΔCt values using Mann-Whitney-Wilcoxon test. *, $p<0.05$; **, $p<0.01$. ns, no significance. (**C**) Representative images of *klp-18* mRNA smFISH in wild type and *rha-1(tm329)* mutant adult

Figure 2.12 continued
germlines. DAPI stain (blue) and *klp-18* mRNA (green). Scale bars = 10 µm. (**D**) Boxplot depicting smFISH quantification of *klp-18* mRNA in wild type and *rha-1(tm329)* mutant adult germlines. *N* = 10-12 independent animals. For the boxplot, the line indicates the median value, the box indicates the first and third quartiles, and the whiskers indicate the minimum and maximum. Two-tailed p values were calculated using Mann-Whitney-Wilcoxon test. ****, $p<0.0001$.

Given loss of RHA-1 largely impacts CSR-1 bound small RNAs and regulation of target genes, we compared the genes that exhibit mRNA level changes in *rha-1(tm329)* mutants to those in CSR-1 compromised mutants. We performed DESeq2 analysis to identify significantly upregulated and downregulated mRNAs in *rha-1(tm329)* mutants, CSR-1 slicer mutants, and CSR-1 depleted animals (Gerson-Gurwitz et al., 2016; Shen et al., 2018). Of the genes that exhibit significantly upregulated mRNA levels in *rha-1(tm329)* mutants (DESeq2 adjusted p value of ≤0.05), 63.1% are shared with those in CSR-1 slicer mutants, CSR-1 depleted animals, or both (Figure 2.13A). In contrast, none of the significantly downregulated mRNAs in *rha-1(tm329)* mutants are in common with either CSR-1 slicer mutants or CSR-1 depleted animals (Figure 2.13B). Taken together, this data suggests RHA-1 activity is important for fine-tuning the mRNA level of CSR-1 target genes, like CSR-1 slicer activity.

To validate our mRNA sequencing results, we evaluated mRNA level fold change by RT-qPCR for several CSR-1 and CSR-1 top slicer target genes. CSR-1 target genes *aipl-1* and *zen-4* showed a slight decrease or increase in mRNA expression respectively (Figure 2.12B). CSR-1 top slicer target genes *egg-5*, *gei-14*, and *klp-18*, all showed a nearly 2-fold or more increase mRNA expression (Figure 2.12B). Additionally, we performed single molecule fluorescence in situ hybridization (smFISH) for CSR-1 top slicer target *klp-18* mRNA in young adults. We observed an increase in *klp-18* mRNA signal throughout the adult syncytial germline in *rha-1(tm329)* mutants compared to wild type (Figure 2.12, C and D). We also performed smFISH for *klp-18* in CSR-1 depleted animals utilizing a CSR-1 degron strain (Quarato et al., 2021). Like *rha-1(tm329)* mutants, CSR-1 depleted animals displayed an increase in *klp-18* mRNA signal throughout the adult germline compared to control animals (Figure 2.13, C and D).

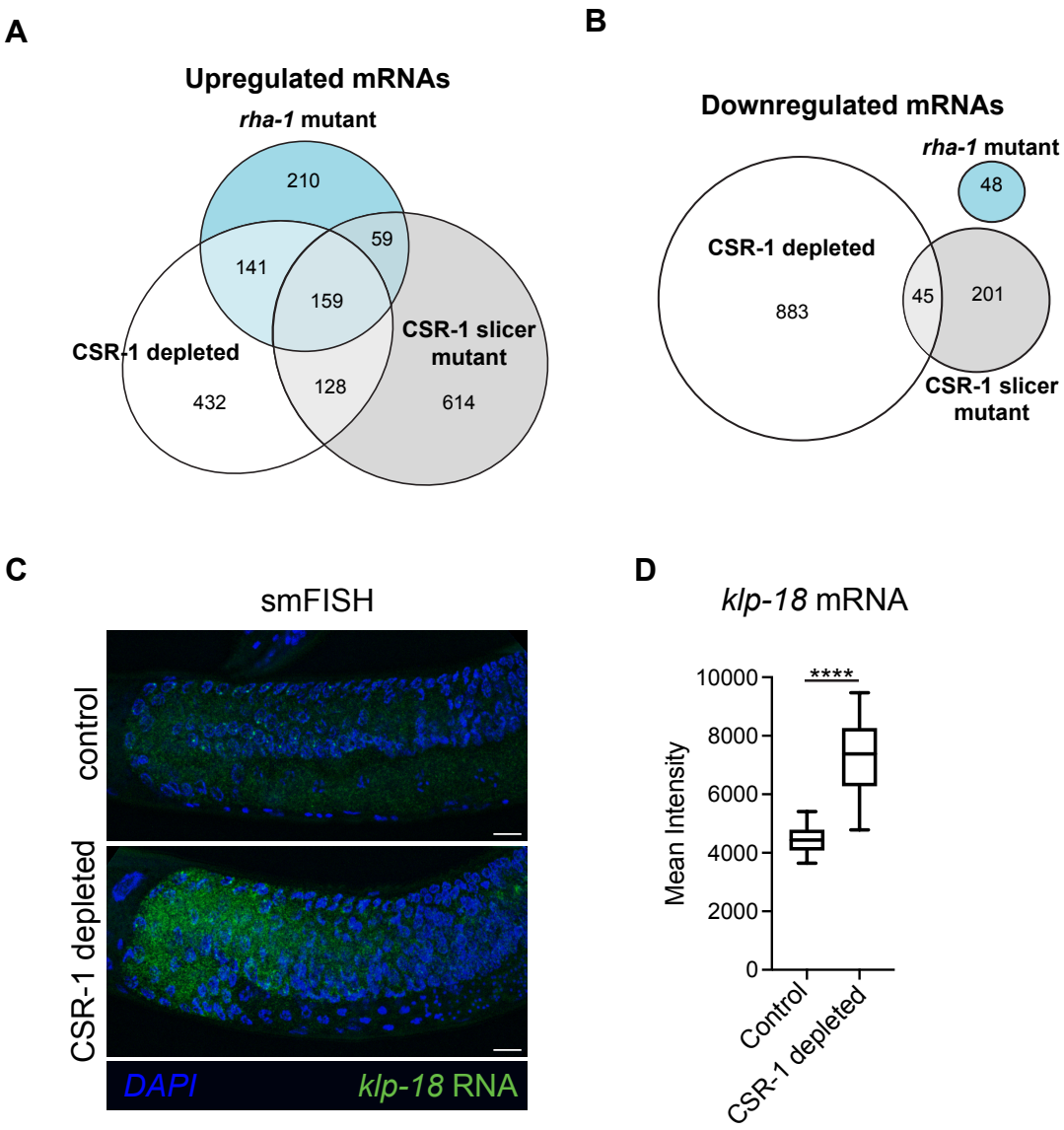

Figure 2.13: Loss of RHA-1 results in similar mRNA expression changes as CSR-1 compromised animals.

(**A** and **B**) Proportional Venn diagrams show the overlap in number of shared significantly upregulated (**A**) or downregulated (**B**) mRNAs in *rha-1(329)* mutant (blue) CSR-1 depleted (white) and CSR-1 slicer mutant (gray) animals. Differentially regulated genes computed from two biological replicates, DESeq2 adjusted p value of ≤0.05. Data analyzed from published mRNA-seq data sets for CSR-1 depleted (Shen et *al.*, 2018) and CSR-1 slicer mutants (Gerson-Gurwitz et *al.*, 2016). (**C**) Representative images of *klp-18* mRNA smFISH in adult germlines of control (no auxin) and CSR-1 depleted by auxin-induced degradation. DAPI stain (blue) and *klp-18* mRNA (green). Scale bars = 10 µm. (**D**) Boxplot depicting smFISH quantification of *klp-18* mRNA in control and CSR-1 depleted adult germlines. *N* = 10-12 independent animals. For the boxplot, the line indicates the median value, the box indicates the first and third quartiles, and the

Figure 2.13 continued
whiskers indicate the minimum and maximum. Two-tailed p values were calculated using Mann-Whitney-Wilcoxon test. ****, $p<0.0001$.

Overall, we find loss of RHA-1 leads to increased mRNA levels of CSR-1 target genes, especially CSR-1 slicer target genes, suggesting RHA-1 promotes CSR-1 target mRNA fine-tuning.

RHA-1 safeguards male fertility and sperm differentiation

CSR-1 small RNAs target germline-expressed genes throughout development, including mRNAs enriched during spermatogenesis and oogenesis (Claycomb et al., 2009b; Nguyen & Phillips, 2021). At the earlier L4 stage, germ cells actively undergo spermatogenesis, and by the adult stage, germ cells switch to oocyte production. Interestingly, for young adult animals grown at 20 °C we found increased mRNA levels for spermatogenesis-enriched genes in *rha-1(tm329)* mutants compared to wild type, while oogenesis-enriched genes show relatively no change (Figure 2.14A). Since spermatogenic genes are no longer transcribed in adults, the increase in spermatogenic mRNAs in *rha-1(tm329)* mutant animals likely results from a defect in post-transcriptional mRNA degradation. In follow up, we performed smFISH for spermatogenic gene *gipc-1* mRNA in L4 stage animals grown at 20 °C. We found increased levels of *gipc-1* mRNA in *rha-1(tm329)* mutant germlines compared to wild type (Figure 2.14B). This data indicates RHA-1 promotes downregulation of spermatogenic mRNAs in germ cells actively undergoing spermatogenesis

Since *rha-1(tm329)* mutants showed elevated spermatogenic mRNA levels, we investigated whether RHA-1 contributes to male fertility, female fertility, or both. For this, we utilized *rha-1(tm329); fog-2(q71)* double mutant animals. This background generates a population of animals producing only female germ cells and males producing normal male germ cells. Therefore, all offspring of this background result from mating, not self-fertilization. At 20

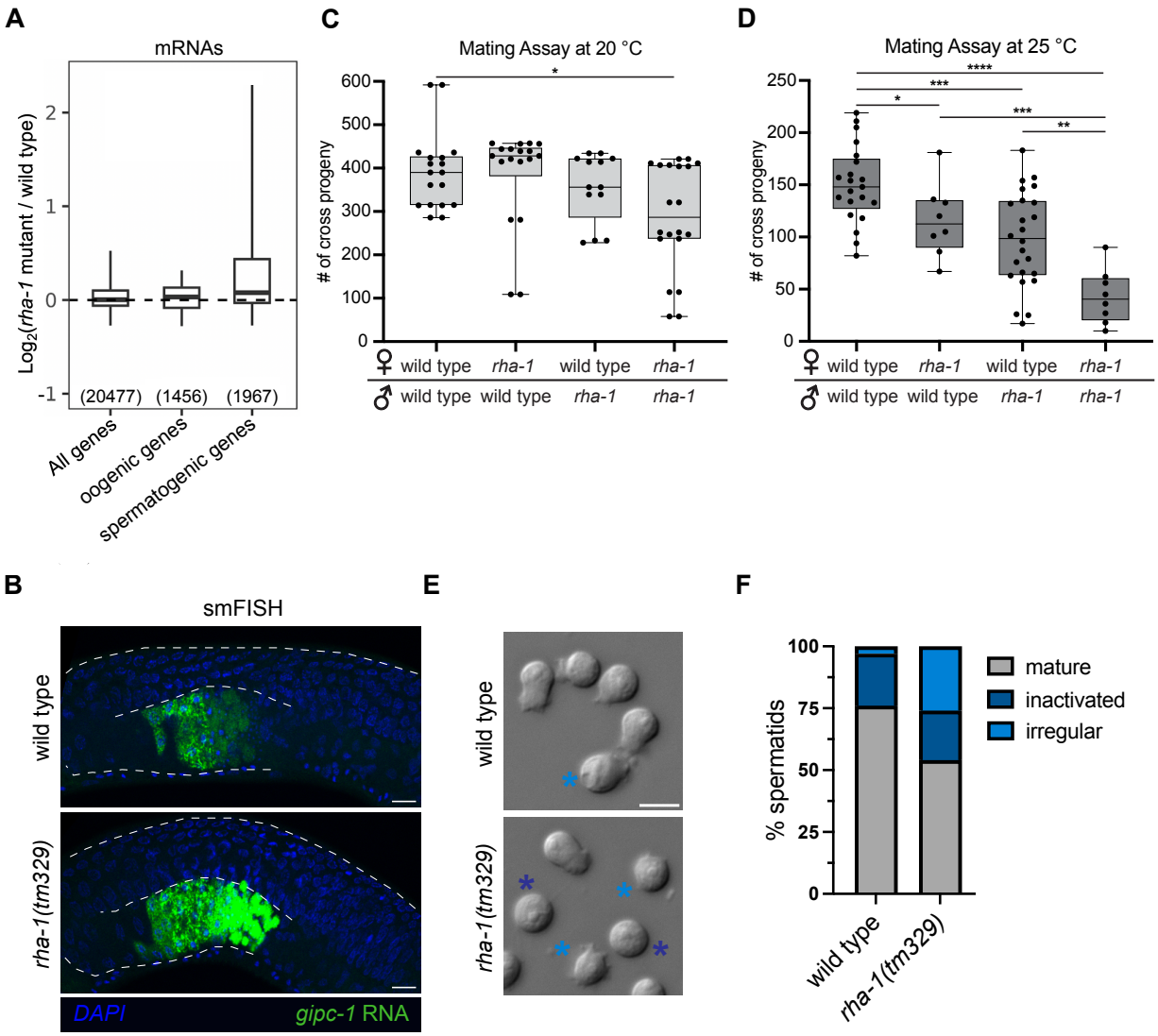

Figure 2.14: RHA-1 is required for optimal fertility and sperm differentiation.
(**A**) Boxplot showing $\log_2$ fold change in mRNA abundance for adult stage *rha-1(tm329)* mutants compared to wild-type animals (two biological replicates). For the boxplot, the line indicates the median value, the box indicates the first and third quartiles, and the whiskers indicate the 5th and 95th percentiles, excluding outliers. The sample size n (genes) is indicated in parentheses. (**B**) Representative images of *gipc-1* mRNA smFISH in L4 stage wild type and *rha-1(tm329)* mutant animals. DAPI stain (blue) and *gipc-1* mRNA (green). Dashed line marks the border of the germline. Scale bar = 10 µm. (**C** and **D**) Brood sizes from pair-wise mating between *fog-2(q71)* (wild type) and *rha-1(tm329); fog-2(q71)* mutant (*rha-1*) obligate females and males at (**C**) 20 °C or (**D**) 25 °C. Data points correspond to the number of alive F1 cross progeny from individual obligate females. For the boxplots, the line indicates the median value, the box indicates the first and third quartiles, and the whiskers indicate the minimum and maximum. Two-tailed p values were calculated using Mann-Whitney-Wilcoxon test. *, $p<0.05$;

Figure 2.14 continued
, p<0.01; ***, p<0.001; ****, p<0.0001. (E**) Representative images of *in vitro* activated sperm by pronase treatment from wild type (top) and *rha-1(tm329)* mutant (bottom) animals. Dark blue asterisks mark inactivated round spermatids. Light blue asterisk mark irregular sperm. Scale bar = 5 μm. (**F**) Stacked bar graph showing percentage of activated mature, inactivated, and irregular spermatids from *in vitro* sperm activation assay for wild type and *rha-1(tm329)* mutant males where 10 adult male animals were dissected. Number of spermatids scored equals 833 for wild type and 857 for *rha-1(tm329)* mutant animals.

°C, mating between *rha-1(tm329); fog-2(q71)* mutant males and females resulted in a significant decrease in cross progeny (Figure 2.14C). At 25 °C, mating of either *rha-1(tm329); fog-2(q71)* mutant females or males to *fog-2(q71)* animals resulted in a reduced number of cross progeny (Figure 2.14D). Moreover, mating of *rha-1(tm329); fog-2(q71)* mutant females to *rha-1(tm329); fog-2(q71)* mutant males resulted in the smallest brood sizes (Figure 2.14D). These mating results suggest RHA-1 promotes the fertility of both female and male germ cells.

To investigate the cause of reduced male fertility observed in *rha-1* mutants, we examined sperm quality and function. During spermiogenesis, immature round spermatids differentiate into mature motile sperm with pseudopods. We isolated spermatids from *rha-1(tm329)* mutant and wild type males grown at 25 °C, and after inducing spermiogenesis *in vitro* by pronase treatment, we scored sperm for normal pseudopod formation, irregular pseudopod formation, or inactivated round spermatids (Shakes & Ward, 1989). Most spermatids collected from wild type males developed normal pseudopods, with 24% combined irregular pseudopod formation or inactivated round spermatids (Figure 2.14, E and F). Notably, just over half of spermatids collected from *rha-1(tm329)* mutant males developed normal pseudopods, with 46% combined irregular pseudopod formation or inactivated round spermatids (Figure 2.14, E and F). Additionally, we found about half of the spermatids isolated from RHA-1 ATP binding and ATP hydrolysis mutant males were inactivated or formed irregular pseudopods, double that of the control male spermatids (Figure 2.15, A and B). Together, this data indicate RHA-1 is required for optimal male fertility and sperm differentiation.

Like RHA-1, CSR-1 has been shown to regulate male fertility and spermiogenesis (Conine et al., 2013a). Additionally, knockdown of *csr-1* results in increased expression of spermatogenesis-enriched genes measured by mRNA-sequencing (Campbell & Updike, 2015).

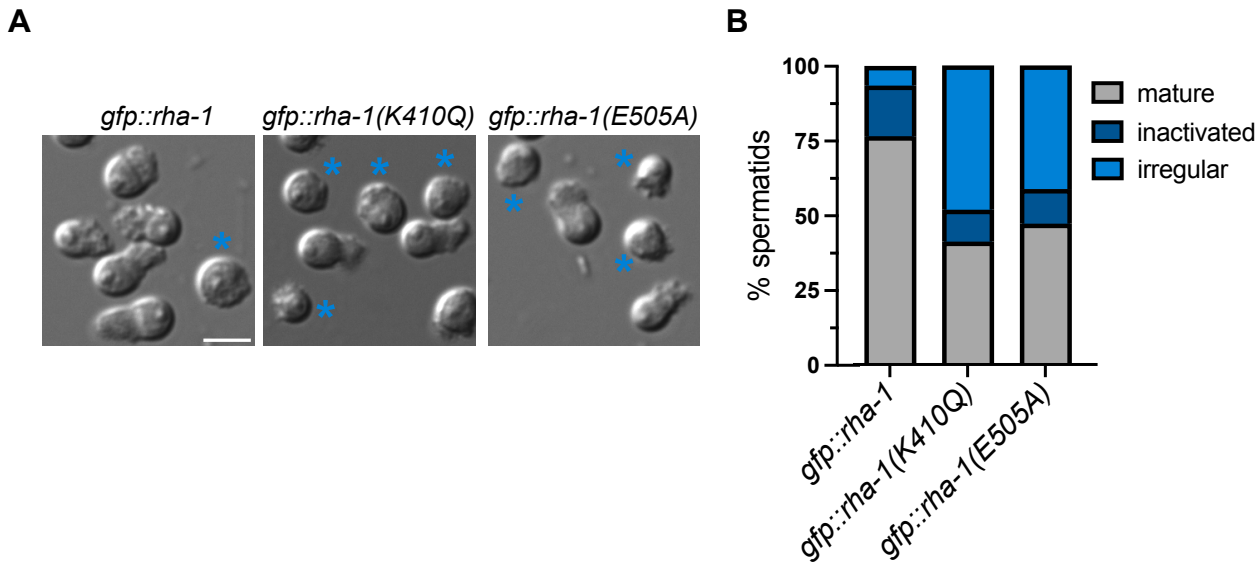

Figure 2.15: RHA-1 ATPase activity is required for optimal sperm differentiation.
(**A**) Representative images of *in vitro* activated sperm by pronase treatment from the indicated strains. Light blue asterisk mark irregular sperm. Scale bar = 5 µm. (**B**) Stacked bar graph showing percentage of activated mature, inactivated, and irregular spermatids from *in vitro* sperm activation assay for the indicated strains. Ten adult male animals were dissected for each strain. More than 1000 spermatids were scored per strain.

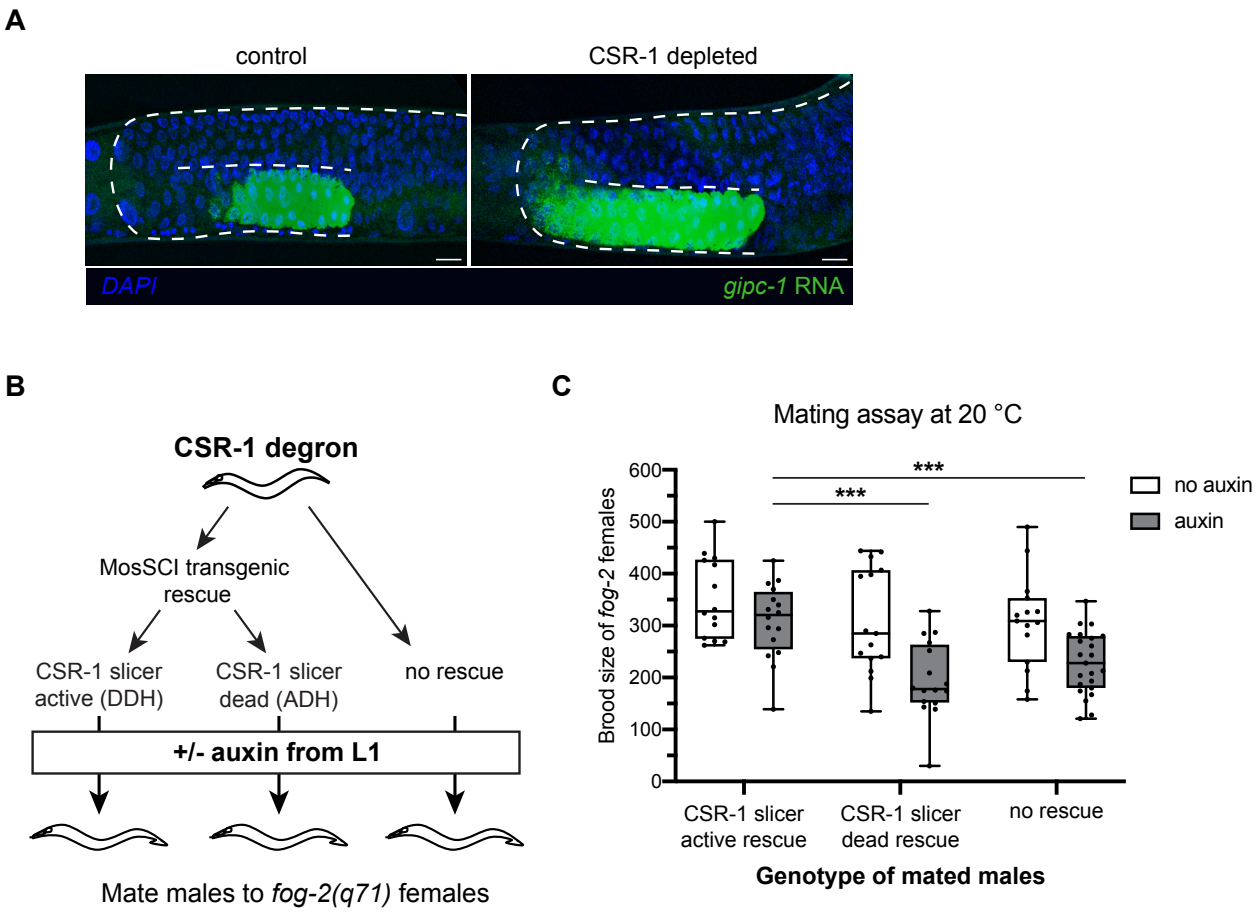

Figure 2.16: CSR-1 slicer activity is required for optimal male fertility.
(**A**) Representative images of *gipc-1* mRNA smFISH in L4 stage control and CSR-1 depleted animals. DAPI stain (blue) and *gipc-1* mRNA (green). Dashed line marks the border of the germline. Scale bar = 10 µm. (**B**) Schematic showing the strains and experimental setup for male mating assay. (**C**) Brood sizes from *fog-2(q71)* females mated to males of the indicated strains grown without auxin (white boxplots) as controls or with auxin (gray boxplots) to deplete endogenous CSR-1. *N* = 14-20 independent animals mated. For the boxplots, the line indicates the median value, the box indicates the first and third quartiles, and the whiskers indicate the minimum and maximum. Two-tailed p values were calculated using Mann-Whitney-Wilcoxon test. ***, p<0.001.

By smFISH, we also observed a strong increase in spermatogenic gene *gipc-1* mRNA level in L4 germlines of CSR-1 depleted compared to control animals (Figure 2.16A). We next wondered whether CSR-1 slicer activity contributes to CSR-1 function in male fertility. To test this, we utilized CSR-1 degron strains with transgenic rescue by either wild-type slicer active CSR-1 or slicer dead CSR-1, or no transgenic rescue (Quarato et al., 2021). Males for these three strains were grown without auxin for controls, or with auxin to deplete endogenous CSR-1 and mated to *fog-2(q71)* mutant obligate females at 20 °C (Figure 2.16B). Control males grown without auxin showed similar brood sizes for all three strains (Figure 2.16C). For males grown with auxin, brood sizes were significantly reduced for both CSR-1 slicer dead males and no rescue males compared to CSR-1 slicer active males (Figure 2.16C). This data indicates that like RHA-1, CSR-1 slicer activity also ensures optimal male fertility.

Overall, our data demonstrate loss of RHA-1 leads to elevated spermatogenic mRNA levels. This defect in mRNA regulation likely contributes to decreased male and female fertility observed in *rha-1* mutant animals. Additionally, our data hint at a critical gene regulatory role for RHA-1 ATPase and CSR-1 slicer activity during male germ cell development and differentiation.

2.4 Discussion

A poorly understood aspect of small RNA networks is how each small RNA class establishes and regulates the correct mRNA targets. Here we identify a role for the conserved RNA helicase RHA-1 in regulating small RNA biogenesis and small RNA sorting to ensure proper gene expression in germ cells. More specifically, we find RHA-1 contributes to 22G-RNA production and sorting from CSR-1 target genes. Consistent with this role, RHA-1

localizes to E compartment of germ granules where factors that function in CSR-1 22G-RNA biogenesis are also located. Overall, the small RNA gene regulatory defects observed in *rha-1* mutants disrupt fertility, germline immortality, and sperm function, especially in elevated temperatures.

Model for RHA-1 role in CSR-1 small RNA biogenesis and mRNA fine-tuning

An unresolved question is how CSR-1 performs opposing regulatory roles in mRNA fine-tuning and mRNA protection. One distinction between these two roles is that CSR-1 slicer activity mainly impacts CSR-1-mediated mRNA fine-tuning (Singh et al., 2021). CSR-1 slicer activity allows for amplified 22G-RNA production across the full length of target mRNAs but is dispensable for small RNA production at the 3' ends. We find RHA-1 is similarly required for robust CSR-1 small RNA production from the 5' regions of target mRNAs but dispensable for production at the 3' ends (Figure 2.17). Consistent with reduced abundance of CSR-1 22G-RNA targeting the full length of mRNAs, loss of RHA-1 leads to notable defects in mRNA fine-tuning.

CSR-1 slicer activity is proposed to slice mRNA targets generating a new 3' mRNA end that serves as a template for EGO-1 22G-RNA synthesis. Sequential rounds of CSR-1 target slicing and small RNA synthesis by EGO-1 leads to the production of abundant 22G-RNAs derived from the full mRNA length. Our results suggest RHA-1 promotes sequential rounds of 22G-RNA production. Considering RHA-1 is a DExH RNA helicase where its ATPase activity allows processive translocation along RNA from the 3' to 5' direction (Fairman-Williams et al., 2010), one model is that RHA-1 may promote mRNA accessibility for CSR-1 or EGO-1 during small RNA biogenesis (Figure 2.17). By remodeling these RNA-protein complexes, RHA-1 may

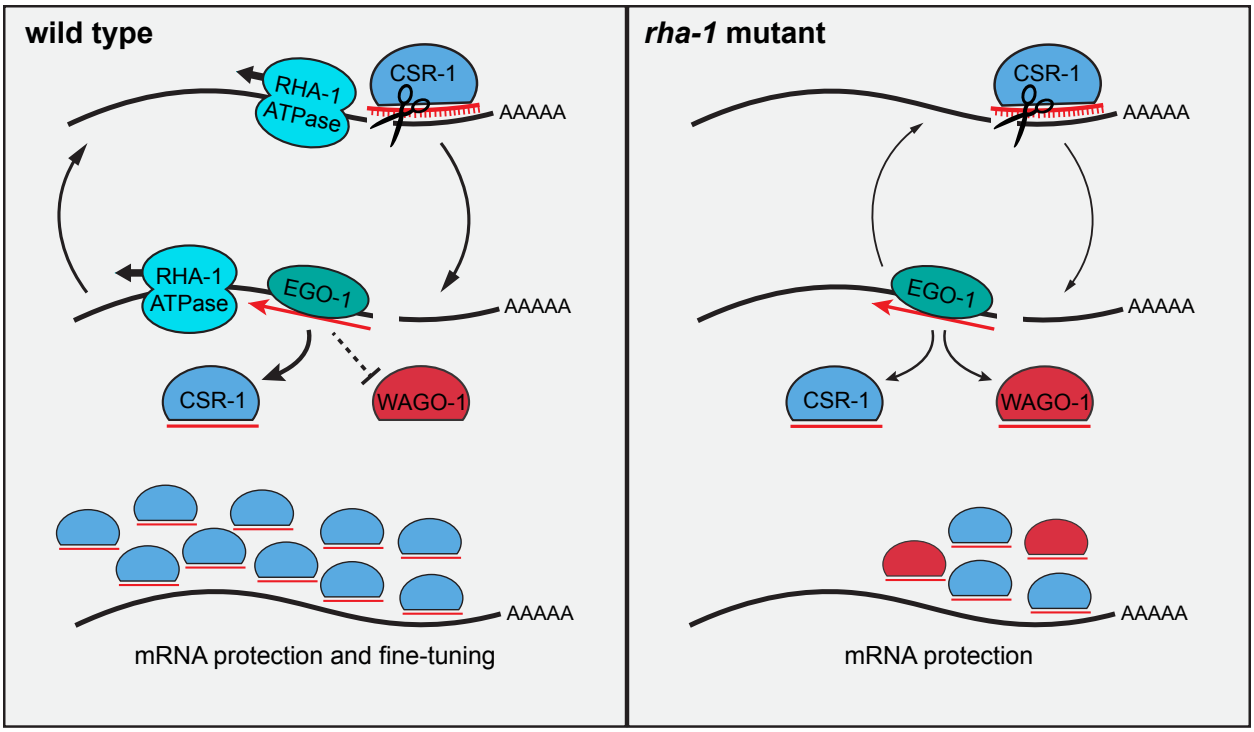

Figure 2.17: Model illustrating proposed function of RHA-1 in CSR-1 small RNA biogenesis and sorting.

Model showing the proposed cycle of small RNA biogenesis on CSR-1 target mRNAs. (Left) RHA-1 ATPase activity may remodel RNP complexes on CSR-1 target mRNAs to facilitate multiple rounds of small RNA synthesis by EGO-1 and CSR-1 slicing. RHA-1 activity may promote the efficiency and mRNA availability during this cycle and facilitate small RNA sorting to CSR-1 over WAGO-1. CSR-1 targets are protected from WAGO-1 silencing and those targets with high abundance of CSR-1 bound small RNAs derived from the full mRNA length are fine-tuned by CSR-1. (Right) In *rha-1* mutants, the abundance of CSR-1 bound small RNAs is reduced from the 5' region of mRNA lengths. Additionally, WAGO-1 aberrantly binds small RNAs derived from CSR-1 targets. Cycles of CSR-1 small RNA production are less efficient. CSR-1 target mRNAs maintain protection from WAGO-1 silencing but fail to be fine-tuned.

facilitate consecutive rounds of CSR-1 mRNA slicing and EGO-1 small RNA synthesis. Alternatively, given that RHA-1's germ granule localization requires both CSR-1 and EGO-1, we propose that RHA-1 may promote small RNA loading to CSR-1 while inhibiting loading to WAGO-1 after 22G-RNA synthesis by EGO-1 (Figure 2.17). Because WAGO-1 does not possess slicer activity, in the absence of RHA-1, mis-sorted WAGO-1 bound 22G-RNAs could similarly disrupt the amplification of small RNAs derived from the 5' regions of CSR-1 target mRNAs.

While 22G-RNAs produced from CSR-1 targets are aberrantly sorted to WAGO-1 in *rha-1* mutants, we do not find evidence for gain of WAGO-1-mediated silencing of these targets. Given that we find 3' CSR-1 22G-RNA targeting is intact in *rha-1* mutants, one model is that the residual level of CSR-1 bound 22G-RNAs is sufficient to protect endogenous protein-coding genes from piRNA and WAGO-1-mediated silencing (Figure 2.17). Additionally, these aberrant WAGO-1 22G-RNAs may not be effective in recruiting mRNA degradation factors needed for robust RNA silencing. Since piRNAs and WAGO-1 22G-RNAs normally target about 2000 genes in the germline, 22G-RNA mis-sorting in the absence of RHA-1, results in approximately 3-fold increase to total WAGO target genes. This increase in target genes potentially weakens WAGO-1 recruitment of downstream factors needed for mRNA degradation.

Intriguingly, another conserved RNA helicase ZNFX-1 promotes amplified production of small RNAs at the 3' ends of WAGO and CSR-1 target mRNAs (Ishidate et al., 2018). ZNFX-1 helicase is processive on RNA substrates in the 5' to 3' direction, opposite of RHA-1, potentially explaining how these helicases promote small RNA production on the opposite ends of mRNAs (Fairman-Williams et al., 2010). This role for ZNFX-1 in balancing small RNA production across target mRNA lengths is proposed to contribute to the stability of epigenetic inheritance

across generations (Ishidate et al., 2018; Ouyang et al., 2022). Together our findings suggest that in addition to WAGO versus CSR-1 targeting, the site of small RNA production along mRNA target lengths may impact whether a given mRNA is protected or degraded following small RNA targeting. Our study along with others provide valuable insight into the diverse roles for RNA helicases in small RNA-mediated gene regulation.

Spatial organization of CSR-1 and EGO-1 localization

Another outstanding question in the field is where within germ cells CSR-1 small RNAs are produced and function in gene regulation. While germ granule factors are enriched within specific sub-compartments, these proteins rapidly exchange between granule and cytoplasmic localization (Huang et al., 2025). CSR-1 and EGO-1 localize to the cytoplasm and are also enriched in distinct germ granule sub-compartments, D and E respectively. Notably, the D compartment is closest to the nucleus just outside of nuclear pores, where CSR-1 is positioned to potentially interact with newly exported mRNAs prior to piRNAs and WAGO-1 located in the P compartment. Because CSR-1 and EGO-1 localize both within germ granules and the cytoplasm, where CSR-1 targeting, slicing, and EGO-1-dependent small RNA production occurs is still under investigation.

In support of EGO-1 small RNA production occurring in the cytoplasm, 22G-RNAs produced from CSR-1 targets exhibit a three-nucleotide periodicity in phase with ribosomal protected fragments (Shen et al., 2018). This suggests either 22G-RNA production or CSR-1 slicing of mRNA targets occurs in the cytoplasm on transcripts undergoing translation. Additionally, the abundance of small RNAs mapping to mRNAs anti-correlates with translation efficiency (Singh et al., 2021). The model follows that efficiently and highly translated mRNAs

are inaccessible to both EGO-1 dependent small RNA synthesis and CSR-1 binding, while poorly translated mRNAs with less active ribosomes are more accessible. Potentially in conflict with this model, specific loss of the E compartment and EGO-1 granule localization by mutations to either ELLI-1 or EGC-1, disrupts EGO-1-dependent small RNA production on 5' regions of mRNA target lengths (X. Chen et al., 2024). This suggests EGO-1 must localize to the E compartment at some point in the 22G-RNA production cycle for 22G-RNA synthesis to occur from the 5' ends of mRNA targets. Our study provides insights that could reconcile these two models.

We identify RHA-1 as an additional E compartment factor required for CSR-1 22G-RNA production on the 5' regions of target mRNAs. Unlike ELLI-1 and EGC-1, loss of RHA-1 does not greatly compromise CSR-1 or EGO-1 germ granule formation. Instead, RHA-1 germ granule localization depends on both CSR-1 and EGO-1, suggesting RHA-1 function in CSR-1 small RNA biogenesis and sorting occurs downstream of initial CSR-1 and EGO-1 activity. Additionally, this recruitment likely contributes to the specificity of RHA-1 function in CSR-1 small RNA production. Taken together, our study supports a hybrid model in which CSR-1 mRNA slicing occurs in the cytoplasm, followed by 22G-RNA synthesis and sorting to CSR-1 at the E compartment. This model explains how CSR-1 loading specificity is achieved and why both cytoplasmic translation and the E granule compartment contribute to CSR-1 small RNA synthesis at the 5' ends of target mRNAs.

Germline-specific RNAi factors

We and others have identified factors required for exogenous RNAi only in the germline but not somatic cells. Since the core components of RNAi are conserved and shared across

tissues, these germline-specific factors are likely a result of competition over cofactors shared between different small RNA pathways (Zhuang & Hunter, 2012). In line with this cofactor competition model, both loss of CSR-1 and RHA-1 result in the mis-sorting of 22G-RNAs produced from CSR-1 target mRNAs. Previously reported, CSR-1 depletion results in 22G-RNA mis-sorting to WAGO-9 (Shen et al., 2018). Here we found loss of RHA-1 results in 22G-RNA mis-sorting to WAGO-1. This disruption of normal 22G-RNA production and sorting potentially dilutes WAGO targeting across an increased number of genes. This may decrease the availability of 22G-RNA production machinery or free WAGOs to bind the newly synthesized small RNAs. Based on this competition model, CSR-1 small RNA pathway factors like RHA-1, CSR-1, and ELLI-1 indirectly impact the function of germline RNAi.

Small RNA roles in male fertility

In *C. elegans*, several Argonaute proteins have been shown to regulate male germ cell differentiation and function, including CSR-1 and PRG-1 (Conine et al., 2013a; Cornes et al., 2022). In most animals, endo-siRNAs and piRNAs are dynamically produced throughout male germline development and essential for spermatogenesis (Banisch et al., 2012; R. Song et al., 2011). In male germ cells of mice and fruit flies, groups of endo-siRNAs and piRNAs function to silence endogenous protein coding genes, performing roles outside of genome defense (Iki et al., 2023; P. H. Wu et al., 2020). In our study, we find RHA-1 ATPase and CSR-1 slicer activity also contribute to male fertility, likely through the regulation of spermatogenesis-enriched genes. Together, these studies hint at the evolutionary conserved roles of endogenous gene regulation by small RNAs in male germ cell development and function.

Since murine and human orthologs of RHA-1 are essential genes, whether they function similarly in male fertility as we have shown for *C. elegans* remains unknown (C. G. Lee et al., 1998; T. Wang et al., 2015). Intriguingly, in a proteomics study, the RHA-1 murine ortholog DHX9 was found enriched in the chromatoid bodies (CBs) of male germ cells (Meikar et al., 2014). CBs are RNA-rich biomolecular condensates, like germ granules, that contain many small RNA pathway and RNA processing factors. The localization of DHX9 to CBs of male germ cells along with small RNA factors, suggests DHX9 may function similarly in male fertility and small RNA regulation as we show here for RHA-1. Overall, these findings leave open the possibility that RHA-1 performs a conserved role in small RNA regulation within male germ cells. Since multiple small RNA classes are present in the male germ cells of most animals, future work investigating the function of these small RNAs may provide valuable insight into the complex processes required for sperm development and germ cell fertility.

2.5 Methods

Caenorhabditis elegans maintenance

Animals were grown on standard nematode growth media (NGM) plates seeded with the Escherichia coli OP50 strain at 20 °C or temperatures where indicated.

Table 2.1: List of *C. elegans* strains used in this study.

Strain	Genotype	Gene(s)	Description	Origin
N2	*C. elegans wild isolate (Bristol)*		Reference C. elegans. Variety Bristol.	CGC
KMW1	*haf-6(ne335) I; rha-1(tm329) II*	*haf-6; rha-1*		CGC
HCL226	*rha-1(tm329) II*	*rha-1*	KMW1 strain from CGC outcrossed with N2	This study
HCL207	*rha-1(uoc39[gfp::rha-1]) II*	*rha-1*	GFP knockin by CRISPR-Cas9 to RHA-1 transcription start site at endogenous locus	This study
HCL209	*rha-1(uoc40[gfp::rha-1[K410Q]]) II*	*rha-1*	GFP::RHA-1 CRISPR-Cas9 amino acid substitution K410Q for ATP binding mutant	This study
HCL210	*rha-1(uoc41[gfp::rha-1[E505A]]) II*	*rha-1*	GFP::RHA-1 CRISPR-Cas9 amino acid substitution E505A for ATP hydrolysis mutant	This study
HCL105	*csr-1(uoc[gfp::csr-1]) IV*	*csr-1*	GFP knockin by CRISPR-Cas9 at start site of CSR-1 isoform b, tags both CSR-1A and CSR-1B isoforms	W Chen et al. 2020
JMC219	*wago-1(tor113[GFP::3xFLAG::wago-1]) I*	*wago-1*		CGC
HCL378	*wago-1(tor113[GFP::3xFLAG::wago-1]) I; rha-1(tm329) II*	*wago-1; rha-1*	JMC219 crossed to HCL226	This study

Table 2.1 continued

SHG1936	*ego-1(ust356[mCherry::ego-1]) I*	*ego-1*		CGC
HCL384	*ego-1(ust356[mCherry::ego-1]) I; rha-1(uoc39[gfp::rha-1]) II*	*ego-1; rha-1*	HCL207 crossed to SHG1936	This study
SHG1941	*ustIS268[mex-5p::tagrfp::elli-1::tbb-2_3'UTR] I*	*elli-1*		X Chen et al. 2024
HCL386	*ustIS268[mex-5p::tagrfp::elli-1::tbb-2_3'UTR] I; rha-1(uoc39[gfp::rha-1]) II*	*elli-1; rha-1*	HCL207 crossed to SHG1941	This study
HCL387	*ustIS268[mex-5p::tagrfp::elli-1::tbb-2_3'UTR] I; rha-1(tm329) II*	*elli-1; rha-1*	HCL226 crossed to SHG1941	This study
HCL190	*npp-7(uoc21[mCherry::npp-7]) I*	*npp-7*	mCherry knockin by CRISPR-Cas9 to NPP-7 endogenous locus	JS Brown et al. 2023
HCL214	*rha-1(tm329) II; csr-1(uoc[gfp::csr-1]) IV*	*rha-1; csr-1*	HCL226 crossed to HCL105	This study
HCL333	*npp-7(uoc21[mCherry::npp-7]) I; rha-1(uoc39[gfp::rha-1]) II*	*npp-7; rha-1*	HCL207 crossed to HCL190	This study
YY1492	*mut-16(cmp3[mut-16::gfp::flag + loxP] I; znfx-1(gg634[HA::tagRFP::znfx-1]) II; pgl-1(gg640[pgl-1::3xflag::mCardinal]) IV*	*mut-16; znfx-1; pgl-1*		CGC
HCL336	*pgl-1(gg640[pgl-1::3xflag::mCardinal]) IV*	*pgl-1*	Outcrossed from YY1492	This study
HCL334	*rha-1(uoc39[gfp::rha-1]) II; pgl-1(gg640[pgl-1::3xflag::mCardinal]) IV*	*rha-1; pgl-1*	HCL207 crossed to pgl-1(gg640[pgl-1::3xflag::mCardinal]) originally from YY1492	This study
HCL335	*rha-1(uoc39[gfp::rha-1]) II; csr-1(gc029[degron::mCherry::3xflag::ha::csr-1]) IV*	*rha-1; csr-1*	HCL207 crossed to MHE69	This study
HCL155	*ego-1(uoc34[3xflag::gfp::ego-1]) I*	*ego-1*	3xflag::GFP knockin by CRISPR-Cas9 to EGO-1	This study
HCL337	*ego-1(uoc34[3xflag::gfp::ego-1]) I; rha-1(tm329) II*	*ego-1; rha-1*	HCL226 crossed to HCL155	This study
HCL338	*rha-1(tm329) II; pgl-1(gg640[pgl-1::3xflag::mCardinal]) IV*	*rha-1; pgl-1*	HCL226 crossed to HCL366	This study

Table 2.1 continued

HCL339	*ego-1(uoc34[3xflag::gfp::ego-1]) I; pgl-1(gg640[pgl-1::3xflag::mCardinal]) IV*	*ego-1; pgl-1*	HCL155 crossed to pgl-1(gg640[pgl-1::3xflag::mCardinal]) originally from YY1492	This study
HCL388	*ego-1(uoc34[3xflag::gfp::ego-1]) I; rha-1(tm329) II; pgl-1(gg640[pgl-1::3xflag::mCardinal]) IV*	*ego-1; rha-1; pgl-1*	HCL339 crossed to HCL337	This study
HCL340	*ego-1(uoc34[3xflag::gfp::ego-1]) I; csr-1(gc029[degron::mCherry::3xflag::ha::csr-1]) IV*	*ego-1; csr-1*	HCL155 crossed to MHE69	This study
HCL341	*rha-1(uoc39[gfp::rha-1]) II; csr-1(gc029[degron::mCherry::3xflag::ha::csr-1]) IV; elli-1(uoc35) IV*	*rha-1; csr-1; elli-1*	CRISPR-Cas9 *elli-1* deletion strain made in HCL335	This study
HCL379	*ego-1(uoc34[3xflag::gfp::ego-1]) I; rha-1(tm329) II; csr-1(gc029[degron::mCherry::3xflag::ha::csr-1]) IV*	*ego-1; rha-1; csr-1*	HCL226 crossed to HCL340	This study
HCL376	*wago-1(tor113[GFP::3xFLAG::wago-1]) I; csr-1(gc029[degron::mCherry::3xflag::ha::csr-1]) IV*	*wago-1; csr-1*	JMC219 crossed to MHE69	This study
HCL389	*wago-1(tor113[GFP::3xFLAG::wago-1]) I; rha-1(tm329) II; csr-1(gc029[degron::mCherry::3xflag::ha::csr-1]) IV*	*wago-1; rha-1; csr-1*	HCL376 crossed to HCL378	This study
GKC1	*mip-1(uae1) III*	*mip-1*		CGC
HCL381	*rha-1(uoc24[gfp::rha-1]) II; mip-1(uae1) III; pgl-1(gg640[pgl-1::3xflag::mCardinal]) IV*	*rha-1; mip-1; pgl-1*	HCL334 crossed to GKC1	This study
CB4108	*fog-2(q71) V*	*fog-2*		CGC
HCL212	*rha-1(tm329) II; fog-2(q71) V*	*rha-1; fog-2*	HCL226 crossed to CB4108	This study

Table 2.1 continued

MHE69	*ieSi64 [gld-1p::TIR1::mRuby::gld-1 3'UTR + Cbr-unc-119(+)] II; csr-1(gc029[degron::mCherry::3xflag::ha::csr-1]) IV*	*csr-1*	Degron knock in by CRISPR-Cas9 in MHE54 and cross with CA1352 (CGC).	P Quarato et al. 2020
MHE113	*ieSi64 [gld-1p::TIR1::mRuby::gld-1 3'UTR + Cbr-unc-119(+)] II; csr-1(gc029[degron::mCherry::3xflag::ha::csr-1]) ; gcSi1 [mex-5p::csr1[D769A]::GFP::tbb-2 3'UTR + Cbr-unc-119(+)] IV*	*csr-1*	Single copy insertion of mex-5p::csr1[D769A]::GFP::tbb-2 3'UTR in chromosome IV generated by MosSCI on strain EG6703 (CGC). Resulting MosSCI strain crossed with MHE69 to generate MHE113.	P Quarato et al. 2020
MHE114	*ieSi64 [gld-1p::TIR1::mRuby::gld-1 3'UTR + Cbr-unc-119(+)] II; csr-1(gc029[degron::mCherry::3xflag::ha::csr-1]) ; gcSi1 [mex-5p ::csr1::GFP::tbb-2 3'UTR + Cbr-unc-119(+)] IV*	*csr-1*	Single copy insertion of mex-5p::csr1::GFP::tbb-2 3'UTR in chromosome IV generated by MosSCI on strain EG6703 (CGC). Resulting MosSCI strain crossed with MHE69 to generate MHE114.	P Quarato et al. 2020

Generation of CRISPR-Cas9 lines

Cas9/sgRNA constructs

We used the online tool CHOPCHOP to design sgRNAs. The sgRNAs were cloned into pDD162 by overlapping PCR using the plasmid PDD162 (Dickinson et al. 2013) as the PCR template and the appropriate primers with 20 base pair overlap. Overlapping PCR products were inserted into linearized PDD162 vector after SpeI/BsrBI digest by seamless ligation cloning extract (SLiCE) method (Zhang & Glotzer, 2015).

Donor constructs

To generate the GFP::RHA-1 donor construct, 500 bp upstream and 500 bp downstream of the *rha-1* TSS, and the GFP coding sequences were amplified by PCR using N2 genomic DNA or

plasmids containing GFP as templates. PCR fragments were inserted into linearized pUC19 digested with HindIII/KpnI and ligated by SLiCE. To generate amino acid substitutions for RHA-1(K410Q) and RHA-1(E505A), single-strand oligodeoxynucleotides (ssODNs) were used as donor templates designed with the single amino acid substitution, silent mutations to the sgRNA site to prevent recutting, and silent mutations to insert new restriction enzyme cut site for easy genotyping.

Cas9 mediated large gene deletions

To generate *elli-1* mutant alleles *(uoc35)* and *(uoc36)* two crRNAs approximately 1000 nucleotides apart with the 5' crRNA targeting near the start codon were injected at the same time following the protocol detailed in (Ghanta et al., 2021).

RNA interference

RNAi was performed by feeding animals with *E. coli* HT115 (DE3) strains expressing the appropriate dsRNA. RNAi bacterial strains were obtained from the Ahringer *C. elegans* RNAi Collection (Source BioScience). Bacterial cultures were grown in Luria broth supplemented with 100 μg/mL ampicillin and 50 μg/mL tetracycline overnight at 37°C. Cultures were seeded on NGM plates containing 100 μg/mL ampicillin, 50 μg/mL tetracycline, and 1 mM IPTG and incubated at room temperature for 24 hours. HT115 (DE3) expressing empty RNAi vector L4440 was used for control.

RNAi of germline genes

For RNAi of *pos-1* and *mex-3* genes, five L1 worms were moved to RNAi and control L4440 plates and performed in triplicate. Three days later, adult worms were removed from plates. The

following day unhatched embryos and hatched progeny were counted for each plate. Plots show percentage of unhatched embryos over sum of unhatched embryos and hatched progeny.

RNAi of somatic genes

For RNAi of *unc-22* and *dpy-13* genes, twenty-five L1 worms were transferred to RNAi and control L4440 plates, performed in triplicate. Three days later, adult worms were scored for phenotypes. For RNAi of *unc-22*, worms were scored for body muscle twitching. For RNAi of *dpy-13*, worms were scored for a dumpy and shortened body.

RNAi for RHA-1 granule counts

For RHA-1 granule counts, twenty L1 worms were transferred to RNAi and control L4440 plates, performed in triplicate. Three days later, the germlines of young adult animals were imaged following the confocal live imaging method (see details below). Number of GFP::RHA-1 granules were counted per germ cell nucleus as distinct puncta localized outside of mCh::NPP-7 signal at the nuclear periphery.

Mating assay with auxin-induced CSR-1 degradation

The degron-tagged CSR-1 strains (no rescue, transgenic rescue of wild-type CSR-1, and transgenic rescue of catalytic dead CSR-1) were self-crossed with males of the same genotype to maintain males in their population. Populations of L1 worms were transferred to NGM plates containing 500 µM auxin, 0.5% ethanol plates or 0.5% ethanol control plates. After 48 h, male worms were transferred to NGM cross plates containing 500 µM auxin, 0.5% ethanol plates or 0.5% ethanol control plates with obligate *fog-2* females. After 48h of mating, single *fog-2* females were transferred to NGM plates and hatched progeny was counted for brood size. For

strains grown on auxin, CSR-1 depletion was confirmed by live imaging. Transgenic rescue strains were confirmed for transgene expression by live fluorescence imaging.

Brood size and mating assay

Brood size

Individual L4 worms were transferred to fresh NGM plates and grown at 20 °C. Worms were transferred daily to fresh NGM plates to allow for easy quantification of progeny until no more eggs were laid. Progeny were counted 48 hours after transferring the parent and number of progeny per individual hermaphrodite was totaled.

Germline mortality assay

First, *rha-1(tm329)* mutants and RHA-1 ATPase mutants were outcrossed two times with wild type males to generate newly homozygous mutant strains. Ten adult worms for these mutant strains along with wild type or control *gfp::rha-1* strains were moved to 25 °C designated as the P0 generation. Ten L3 progeny from these worms were transferred to a new plate designated the F1 generation. This was performed for each subsequent generation. To test fertility of a given generation, twelve L3 worms for each generation were singled to new plates for brood size measurements.

Mating assay

For 20 °C mating assay, L3 males were isolated and grown at 20 °C. The next day single males were transferred to cross plate with single L4 obligate females and grown at 20 °C. After 24h, individual females were transferred to fresh NGM plate and resulting brood size was measured as described above. For 25 °C mating assay, L3 males were isolated and grown at 25 °C. The next day six males were transferred to cross plate with six L4 obligate females and grown at 25

°C. The increased number of worms per mating plate here was to ensure worms mated as we found reduced male mating behavior at 25 °C for both wild type and mutant males. After 24h, individual females were transferred to fresh NGM plate and resulting brood size was measured as described above.

Sperm activation assay

L4 males were isolated and kept overnight at 25 °C for 24 hours. Spermatids were isolated from 12 males washed and dissected on slides in sperm medium (50mM HEPES pH7.8, 50mM NaCl, 25mM KCl, 5mM $CaCl_2$, and 1mM $MgSO_4$) activated with 20μg/mL pronase E. Spermatids were imaged 30 min after dissection and scored by three categories: spermatids with normal pseudopods (wild type), spermatids with irregular pseudopods (irregular), and round spermatids with no pseudopods (inactivated).

Confocal live imaging

Tagged fluorescent proteins were visualized in living nematodes by mounting young adult animals on 2% agarose pads with M9 buffer (22 mM KH_2PO4, 42 mM Na_2HPO4, and 86 mM NaCl) with 20 mM levamisole. Fluorescent images used for localization studies were captured using a Zeiss LSM800 confocal microscope with a Plan-Apochromat 40×/1.4 Oil objective.

Quantitative real-time PCR

1 μg of total RNA was reverse transcribed with SuperScript IV Reverse Transcriptase (Invitrogen) in 1 × reaction buffer, 2 U SUPERase-In RNase Inhibitor (Invitrogen), 0.5 mM dNTPs, and 2.5 μM random hexamers. Each real-time PCR reaction consisted of 3 μL of cDNA,

1 μM forward gene-specific primer and 1 μM reverse gene-specific primer. The amplification was performed using iTaq Universal SYBR Green Supermix (Bio-Rad) on the Bio-Rad CFX96 Touch Real-Time PCR Detection System. The experiments were repeated for a total of three technical replicates. tba-1 expression was used as a housekeeping gene.

Total small RNA-seq library preparation

Total RNA was extracted using the standard method with TRIzol reagent (Invitrogen) from whole animals of ~100,000 synchronized young adults grown at 20 °C. Small (<200 nt) RNAs were enriched with mirVana miRNA Isolation Kit (Ambion). In brief, 80 μL (200–300 μg) of total RNA, 400 μL of mirVana lysis/binding buffer and 48 μL of mirVana homogenate buffer were mixed well and incubated at room temperature for 5 min. Then, 176 μL of 100% ethanol was added and samples were spun at 2500×g for 4 min at room temperature to pellet large (>200 nt) RNAs. The supernatant was transferred to a new tube and small (<200 nt) RNAs were precipitated with pre-cooled isopropanol at -80 °C. Small RNAs were pelleted at 20,000×g at 4 °C for 30 min, washed once with 70% pre-cooled ethanol, and dissolved with nuclease-free water. Ten micrograms of small RNAs were fractionated on a 15% PAGE/7M urea gel, and RNA from 17 nt to 40 nt was excised from the gel. RNA was extracted by soaking the gel in 2 gel volumes of NaCl TE buffer (0.3 M NaCl, 10 mM Tris-HCl, 1 mM EDTA pH 7.5) overnight. The supernatant was collected through a gel filtration column. RNA was precipitated with isopropanol, washed once with 70% ethanol, and resuspended with 15 μL nuclease-free water. RNA samples were treated with RppH to convert 22G-RNA 5′ triphosphates to monophosphates in 1 × reaction buffer, 10 U RppH (New England Biolabs), and 20 U SUPERase-In RNase Inhibitor (Invitrogen) for 3 h at 37 °C, followed by 5 min at 65 °C to inactivate RppH. RNA was

then concentrated with the RNA Clean and Concentrator-5 Kit (Zymo Research). Small RNA libraries were prepared according to the manufacturer's protocol of the NEBNext Multiplex Small RNA Sample Prep Set for Illumina-Library Preparation (New England Biolabs). NEBNext Multiplex Oligos for Illumina Index Primers were used for library preparation (New England Biolabs). Libraries were sequenced using an Illumina HiSeq4000 to obtain single-end 50 nt sequences at the University of Chicago Genomic Facility.

Immunoprecipitation – small RNA-seq

A total of 100,000 synchronized young adult animals were used for immunoprecipitation. Synchronized animals were washed with M9 buffer three times before frozen in liquid nitrogen and stored at -80 °C. Worm pellets were resuspended in equal volumes of immunoprecipitation buffer (20 mM Tris-HCl pH 7.5, 150 mM NaCl, 2.5 mM $MgCl_2$, 0.5% NP-40, 80 U/mL RNase Inhibitor (Thermo Fisher Scientific), 1 mM dithiothreitol, and protease inhibitor cocktail without EDTA (Promega)), and grinded in a stainless steel dounce tissue grinder until cuticles of most worms were broken down. Lysates were clarified by spinning down at 15,000 rpm, 4 °C, for 15 min. Supernatants were incubated with the GFP-Trap magnetic agarose beads (ChromoTek) at 4 °C for 1 h. Beads were washed with wash buffer (20 mM Tris-HCl pH 7.5, 150 mM NaCl, 2.5 mM $MgCl_2$, 0.5% NP-40, and 1 mM dithiothreitol) six times, and then resuspended in TBS buffer for RNA extraction. Total RNA was extracted using the standard method with TRIzol reagent (Invitrogen). Small RNA libraries were prepared as described above and sequenced using Illumina NovaSeq 6000 to obtain single-end 50 nt sequences at the University of Chicago Genomic Facility.

Poly A RNA-seq library preparation

Total RNA was extracted using the standard method with TRIzol reagent (Invitrogen) from whole animals of ~100,000 synchronized young adults. The Promega PolyATtract mRNA Isolation Systems was used to isolate the polyA mRNA fraction following the small-scale isolation protocol provided by Promega, starting with 100 µg total RNA. Next, RNA libraries were prepared with NEBNext Ultra II Directional RNA Library Prep Kit for Illumina (New England Biolabs) starting with 10ng of total polyA mRNA per sample. NEBNext Multiplex Oligos for Illumina Index Primers were used for library preparation (New England Biolabs). RNA libraries were sequenced using an Illumina NovaSeq to obtain paired-end 50 nt sequences at the University of Chicago Genomic Facility.

Single-molecule fluorescent in-situ hybridization (smFISH)

Whole worm smFISH was performed on staged L4 or young adult worms. Two technical replicates were performed for each genotype and condition. 100 staged worms were picked into M9 buffer in 1.5mL microcentrifuge tubes and washed with M9 three times. Worms were then fixed in 4% formaldehyde for 45 min at room temperature. Samples were then washed with PBS and dehydrated with 70% ethanol at 4 °C for two overnights. Gonads were re-hydrated with PBS and washed once with FISH wash buffer (2× SSC, 10% formamide) at 37 °C. FISH probes were suspended in Hybridization Buffer (10% formamide, 2 mM vanadyl ribonucleoside complex, 20 mg/mL BSA, 10 mg/mL dextran sulfate, 2 mg/mL *E. coli* tRNA) 1:50. smFISH probes were created by Biosearch Technologies to target *klp-18* mRNA or *gipc-1* mRNA. The *klp-18* mRNA and *gipc-1* mRNA probes were conjugated to Quasar670 (Custom probe, Biosearch Technologies Cat. No. SMF-1065-5). Samples were hybridized overnight at 37 °C in dark.

Samples were washed with FISH wash buffer, stained with DAPI, and mounted onto 25 mm × 75 mm × 1 mm plain glass slides with ProLong Diamond Antifade Mountant. Samples were imaged on a Zeiss LSM800 Confocal Microscope at ×40 magnification using a Plan-Apochromat ×40/1.4 Oil Objective.

Image processing and analysis

Image processing and quantification of fluorescent puncta were performed using ImageJ. Single slice images of gonads were used for quantification. ROIs were selected, and areas of ROIs were measured. For measurement of granule sizes, the same threshold and lower limit was applied across all germline images for control and mutants to eliminate background signal. Then the area in μm^2 was measured per granule. Granule area was measured for at least 10 gonads with the same ROI of about 10-12 pachytene nuclei per gonad. For quantitative co-localization analysis, all image manipulations were performed with ImageJ using the Coloc 2 plugin. Images of 8–10 gonads were collected and quantified. For smFISH (Quasar670), a rolling ball background subtraction was used across all images set manually and uniformly across all samples. Images from 20–30 gonads were collected. Signal from the RNA probes was quantified by measuring mean fluorescent intensity in the same ROI for each gonad. Data were compared by two-tailed p values calculated using Mann-Whitney-Wilcoxon test.

Sequencing data analysis

RNA-seq

Fastq reads were trimmed of adaptors using cutadapt (Martin, 2011). Trimmed reads were aligned to the C.elegans genome build WS230 using bowtie2 ver 2.3.0 (Langmead & Salzberg,

2012). After alignment, reads were overlapped with genomic features (protein-coding genes, pseudogenes, transposons) using bedtools intersect (Quinlan & Hall, 2010). Reads per kilobase million (RPKM) values were then calculated for each individual feature by summing the total reads mapping to that feature, multiplied by 1e6, and divided by the product of the kilobase length of the feature and the total number of reads mapping to protein-coding genes. Protein-coding genes were used to normalize by sequencing depth because mRNA libraries were prepared by polyA tail selection. RPKM values were then used in all downstream analyses using custom R scripts, which rely on packages ggplot2, reshape2, ggpubr, dplyr (Wickham, 2007). Differential expression analysis was performed using DESeq2 with an adjusted p value ≤ 0.05 (Love et al., 2014).

Small RNA-seq

Fastq reads were trimmed using custom perl scripts. Trimmed reads were aligned to the *C. elegans* genome build WS230 using bowtie ver 1.2.1.1 with options -v 0 -best -strata. After alignment, reads that were between 17–40 nucleotides in length were overlapped with genomic features (rRNAs, tRNAs, snoRNAs, miRNAs, piRNAs, protein-coding genes, pseudogenes, transposons) using bedtools intersect. Sense and antisense read mapping to individual miRNAs, piRNAs, protein-coding genes, pseudogenes, RNA/DNA transposons, simple repeats, and satellites were totaled and normalized to reads per million (RPM) by multiplying be 1e6 and dividing read counts by total mapped reads, minus reads mapping to structural RNAs (rRNAs, tRNAs, snoRNAs). Reads mapping to multiple loci were penalized by dividing the read count by the number of loci they perfectly aligned to. Reads mapping to miRNAs and piRNAs were only considered if they matched the sense annotation without any overlap. 22G-RNAs were defined as

21 to 23 nucleotide long reads with a 5′G that aligned to protein-coding genes, pseudogenes, or transposons. RPM values were then used in all downstream analyses using custom R scripts using R version 4.0.0, which rely on packages ggplot2, reshape2, ggpubr, dplyr.

Metagene analysis

Metagene profiles across gene lengths were calculated by computing the depth at each genomic position using 21–23 nucleotide long small RNA reads with a 5′G using bedtools genomecov. A custom R script was then used to divide genes into 100 bins and sum the normalized depth within each bin. Groups of genes were then plotted using the sum of the normalized depth at each bin with units in reads per million (RPM). The read distribution metagene normalizes the RPM metagene by dividing the sum of reads for each gene per bin by the total read count of the entire gene. From this, every gene contributes one unit so the area under each trace is the same between the compared samples. The metagene for IP-small RNA-seq data presents the read count mean plus or minus one standard deviation plotted for groups of gene sets.

CHAPTER 3

Small RNA pathway competition drives tissue-specific differences in RNAi efficiency

3.1 Abstract

Within the germline, RNA interference (RNAi) pathways coordinate gene expression and small RNA-based inheritance. Depending on the sex of the germline, RNAi pathways regulate unique sets of genes to ensure optimal germ cell development and fertility. Notably, female and male germlines differ in the capacity to silence genes by canonical RNAi triggered by environmental exposure to double-stranded RNAs. While female germ cells robustly silence genes by RNAi, male germ cells fail to trigger silencing. The underlying mechanism for male germline resistance to RNAi remains poorly understood. Here, we investigate the impact of small RNA pathway competition on germline RNAi efficiency in both sexes. We demonstrate loss to either endo-siRNA or piRNA pathway function improves RNAi efficiency in both female and male germlines. Enhanced RNAi coincides with increased secondary siRNA production. Overall, our study provides insights into how small RNA pathway competition limits the RNAi capacity in female and male germ cells.

3.2 Introduction

RNA interference (RNAi) is an evolutionary conserved gene silencing mechanism that protects host genomes from mutagenic sequences like viruses and transposons. During RNAi, double-stranded RNA (dsRNA) molecules are processed into 21-23 nucleotide small interfering RNAs (siRNAs) by the Dicer family of endoribonucleases (Bernstein et al., 2001a; Fire et al., 1998; Ketting et al., 2001). These small RNAs are bound by Argonaute proteins and serve as guides to complementary RNA targets where they form RNA-induced silencing complexes (Yigit et al.,

2006). In *C. elegans*, RNAi is systemic and heritable. Following environmental exposure to dsRNA, gene silencing spreads across most tissues and in certain cases can last for multiple generations (Grishok et al., 2000). Because of this, feeding worms bacteria expressing dsRNA yields a powerful tool for candidate-based RNAi screens in this organism (Fraser et al., 2000; Kamath et al., 2003). Notably, several tissues fail to trigger gene silencing by RNAi, including neuronal and male germ cells (Marré et al., 2016; Timmons et al., 2001). The reason neuronal cells fail to perform systemic RNAi is because they lack expression of the dsRNA importer, SID-1, responsible for the spread of dsRNA across tissues (Calixto et al., 2010). The underlying molecular mechanisms leading RNAi resistance in male germ cells remains poorly understood.

As part of the RNAi mechanism in *C. elegans*, primary small RNAs trigger the amplified production of secondary siRNAs (Sijen et al., 2001; Smardon et al., 2000). These amplified secondary siRNAs are required for robust gene silencing and RNAi inheritance. Primary siRNAs include those produced from environmentally supplied dsRNA, or endogenous small RNAs such as endo-siRNAs and piRNAs (Billi et al., 2014). These primary small RNAs recruit RNA-dependent RNA polymerases (RdRPs) to target mRNAs that serve as templates for the synthesis of secondary siRNAs termed 22G-RNAs. Secondary siRNAs are bound by WAGO Argonautes that recruit effector proteins to mRNA targets to either block mRNA translation or perform mRNA degradation (Seroussi et al., 2023). Additionally, secondary siRNAs can be bound by nuclear Argonaute proteins, HRDE-1 and NRDE-3, to carry out transcriptional gene silencing and RNAi inheritance (Burton et al., 2011; Spracklin et al., 2017). These factors guide heterochromatin modifications at target gene sites, leading to inherited gene silencing for one or more generations.

Small RNA pathways share similar small RNA biogenesis components. Because of this, distinct small RNA pathways are proposed to compete over shared factors required for gene silencing (Houri-Ze'evi et al., 2016; Zhuang & Hunter, 2012). This includes Dicer protein, which is essential to produce canonical RNAi triggered siRNAs, microRNAs, and endo-siRNAs (Duchaine et al., 2006; Ketting et al., 2001). As a result of small RNA pathway competition, mutants defective in the production of endo-siRNAs are more sensitive to environmental dsRNAs, and conversely, canonical RNAi mutants produce more endo-siRNAs (R. C. Lee et al., 2006; Simmer et al., 2002). Interestingly, compared to female germ cells, male germ cells express an expanded set of piRNAs and class of endo-siRNAs termed 26G-RNAs (Bezler et al., 2019; Conine et al., 2010; G. Wang & Reinke, 2008). This suggests male germ cell small RNA pathways may have increased competition for shared small RNA processing factors. Whether small RNA pathway competition underlies the differences observed in RNAi function between male and female germ cells is so far unexplored.

In this study, we examine the role of small RNA pathway competition in sex-dependent germline RNAi efficiency. We find loss of either endo-siRNA or piRNA pathway function improves gene silencing by canonical RNAi in male and female germ cells. These identified genetic backgrounds with improved RNAi efficiency can be used as a tool to perform loss of function studies that uncover novel gene functions during germ cell development. Additionally, we find several germline-specific RNAi factors are required to maintain sensitivity to environmental dsRNAs and promote RNAi inheritance. Overall, our work highlights the impact of competition among small RNA pathways on sex-dependent differences in germline RNAi.

3.3 Results

Female and male germ cells show different capacities for RNAi

Several studies have provided evidence that germline RNAi silencing may differ between *C. elegans* hermaphrodites and males. These studies found male germlines exhibited reduced sensitivity to RNAi by dsRNA feeding (Bezler et al., 2019; Marré et al., 2016). In contrast, hermaphrodites and males were similarly sensitive to somatic RNAi silencing. Together, this suggested only germline tissue showed sex-dependent differences in RNAi capacity. To follow up on these findings, we tested germline RNAi silencing for a set of GFP reporter genes in hermaphrodites and males (Figure 3.1A). These GFP reporters included constitutive germline-expressed gene GFP::H2B, oogenic-specific germline gene GFP::OMA-1, and spermatogenic-specific germline gene GFP::ALG-3 (Figure 3.1A). First for hermaphrodites, we tested germline RNAi silencing for constitutive germline and oogenic GFP reporters. As expected, robust germline RNAi silencing occurred for both GFP reporters in all Day 1 adult hermaphrodites (Figure 3.1B). Silencing occurred whether dsRNA feeding started from L1 or L4 stage animals. In contrast, Day 1 adult males displayed no germline RNAi silencing for either constitutive germline or spermatogenic GFP reporters (Figure 3.1C). Even after longer exposure time to dsRNA, Day 3 adult males still displayed no germline RNAi silencing. Together, this data suggests that male germlines exhibit differences in RNAi silencing efficiency compared to female germlines, even after longer duration of dsRNA exposure.

We next asked whether sperm producing tissue is generally RNAi resistant. Like males, L4 stage hermaphrodite germlines are also actively undergoing spermatogenesis. We tested RNAi silencing efficiency in L4 hermaphrodite germlines for both constitutive and spermatogenic GFP reporters in animals fed dsRNA from the L1 stage. We observed no

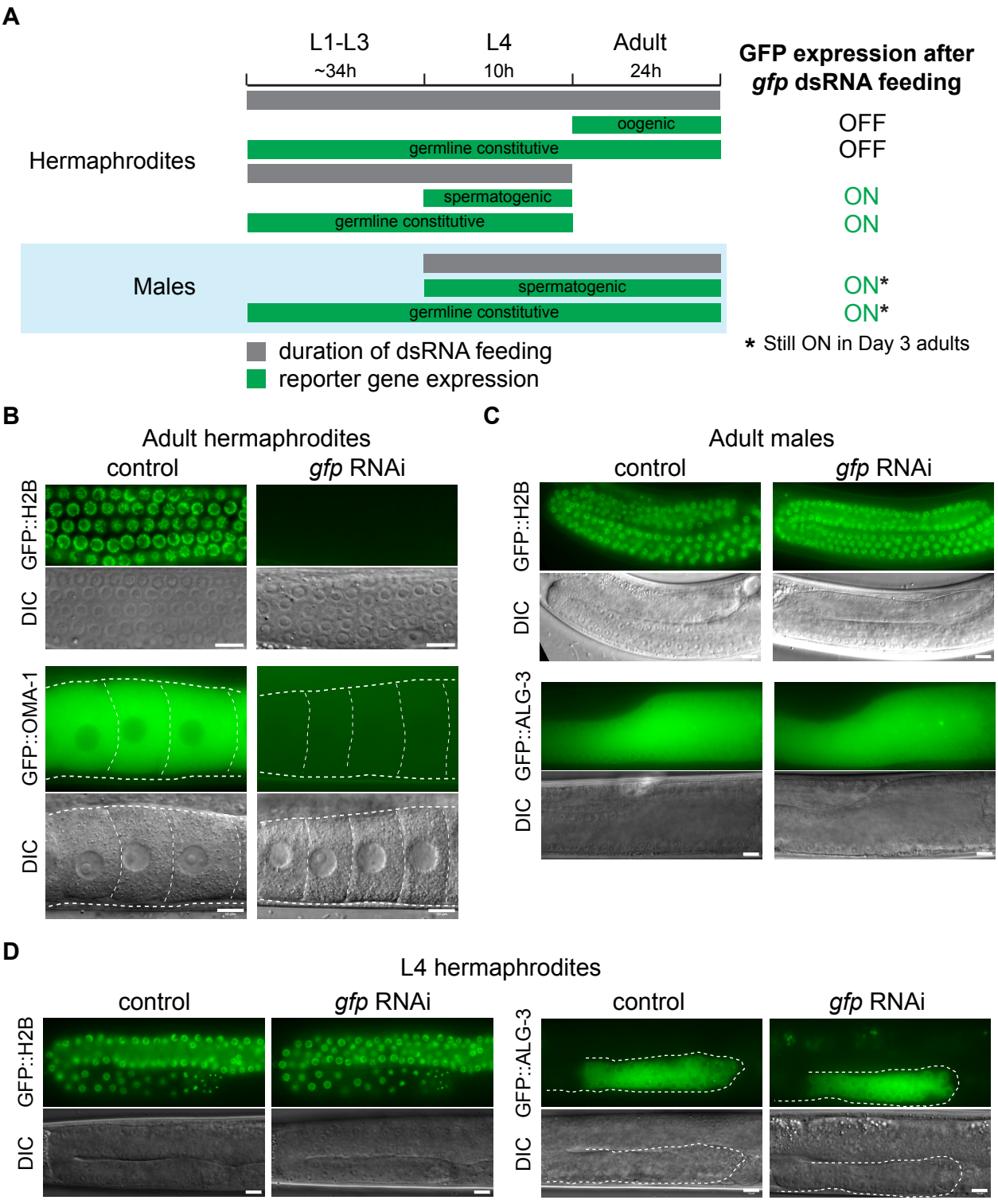

Figure 3.1: Sex-differences in germline RNAi efficacy.
(**A**) Experimental overview of germline RNAi feeding timeline, GFP reporter expression, and summary of RNAi silencing results in hermaphrodites and males. (**B**) Representative live-fluorescent images of adult hermaphrodite female germ cells for the indicated GFP reporters in

Figure 3.1 continued
control and *gfp* RNAi conditions. White dashed lines outline individual oocytes. (**C**) Representative live-fluorescent images of adult male germ cells for the indicated GFP reporters in control and *gfp* RNAi conditions. (**D**) Representative live-fluorescent images of L4 hermaphrodite male germ cells for the indicated GFP reporters in control and *gfp* RNAi conditions. White dashed lines outline the L4 spermatogenic gonad. DIC, differential interference contrast. Scale bars = 10 μm.

germline RNAi silencing for either GFP reporter in L4 germlines (Figure 3.1D). Taken together, our data suggest that developing male germ cells are largely resistant to RNAi.

Reduced small RNA pathway competition improves RNAi efficiency

Male and female germ cells are known to produce and express different sets of small RNAs, including piRNAs and endo-siRNAs, that contribute to gene regulation and germ cell development. For piRNAs, hermaphrodite gonads express about 4000 different piRNAs compared to 5400 in male gonads (Marré et al., 2016). In male germ cells, endo-siRNAs termed 26G-RNAs target about 1400 genes (Conine et al., 2010). In female germ cells, 26G-RNAs only target about 100 genes (Seroussi et al., 2023). We wondered whether these differences in piRNA and endo-siRNA pathways between male and female germlines contribute to the sex-dependent differences in RNAi efficiency. The greater number of male piRNAs and endo-siRNAs could increase the competition for cofactors between germline small RNA pathways (Figure 3.2).

To test this, we first examined whether loss of endo-siRNA or piRNA pathway function improves germline RNAi efficiency in adult hermaphrodites. Several germline genes, including *par-1* and *par-3* have been shown to display reduced RNAi efficiency when animals are fed dsRNA for a shortened time (Kamath et al., 2000). Successful RNAi silencing of these *par* genes in adult germlines results in the laying of dead embryos. This short-exposure RNAi assay allows us to measure backgrounds that improve RNAi efficiency, since wild-type animals display minimal RNAi silencing of *par-1* and *par-3* genes in this assay (Figure 3.3A). Next, we examined the RNAi efficiency in endo-siRNA *rrf-3(pk1426)* mutants that fail to produce 26G-RNAs, and piRNA-binding Argonaute *prg-1(uoc34)* mutants (Batista et al., 2008; Simmer et al., 2002). We found both *rrf-3(pk1426)* and *prg-1(uoc34)* mutants showed increased RNAi

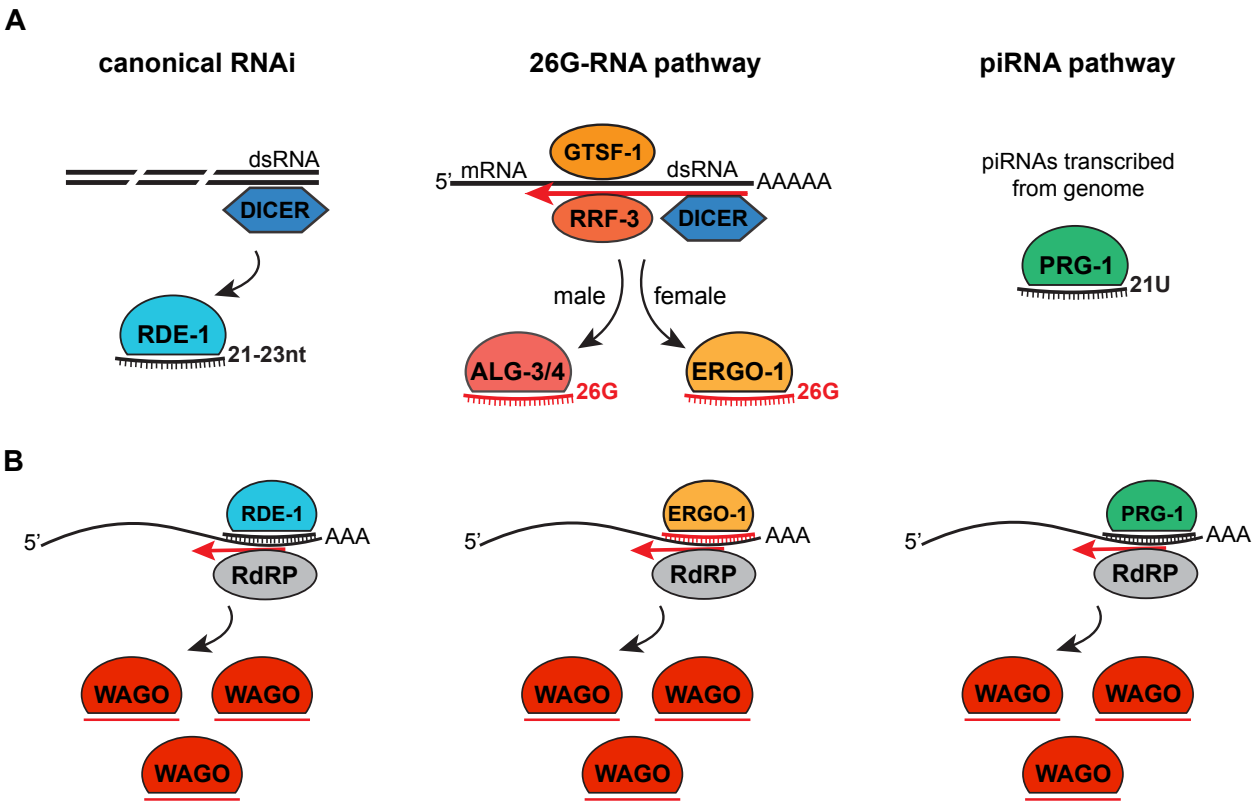

Figure 3.2: Germline small RNA pathways share gene silencing machinery.
(**A**) Cartoon illustrating key biogenesis factors required for primary siRNA production for the indicated germline small RNA pathways. (**B**) Cartoon illustrating the shared gene silencing mechanism and machinery for secondary siRNA production triggered by the Argonaute and primary siRNA complexes. All pathways utilize RNA-dependent RNA polymerase (RdRP) for secondary siRNA synthesis. Secondary siRNAs are loaded to WAGO Argonautes.

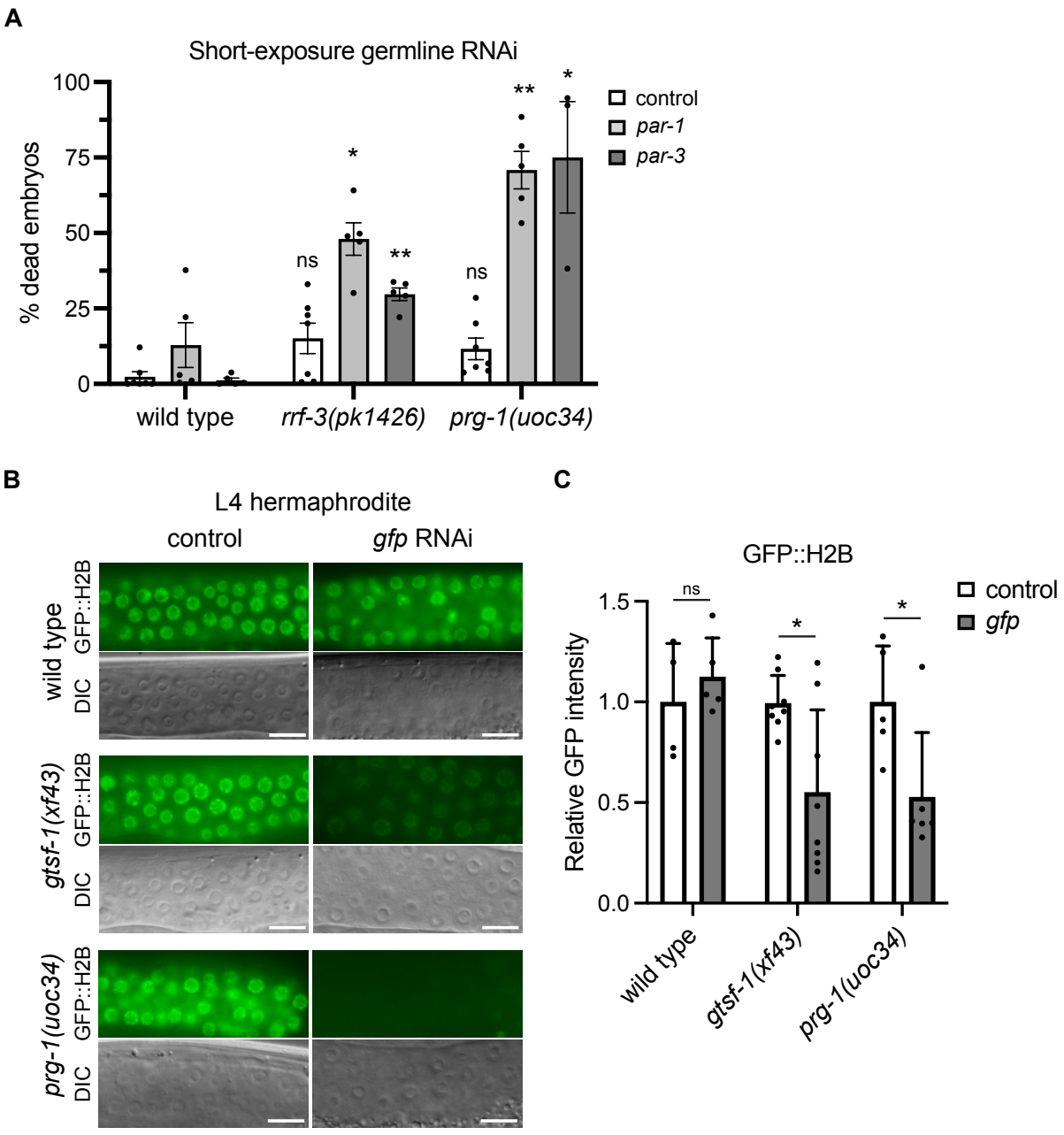

Figure 3.3: Loss of endo-siRNAs or piRNAs enhance RNAi efficiency.
(**A**) Bar graph displays results from short-exposure germline RNAi assay for the indicated strains. Conditions are control, *par-1* and *par-3* RNAi. % dead embryos is a measurement of RNAi efficiency. Each data point represents repeated experiments. (**B**) Representative live-fluorescent images of L4 hermaphrodite male germ cells for the indicated GFP reporter in the mutant backgrounds in control and *gfp* RNAi conditions. DIC, differential interference contrast. Scale bars = 10 µm. (**C**) Bar graph showing the relative GFP mean fluorescent intensity of GFP::H2B signal for control and gfp RNAi conditions in the indicated mutant backgrounds. Each point represents measurement from one germline. *N* = 4-8 germlines. Bar graphs show the

Figure 3.3 continued
mean +/- one standard deviation. Two-tailed p values were calculated using Mann-Whitney-Wilcoxon test. *, $p<0.05$; **, $p<0.01$; ns, no significance.

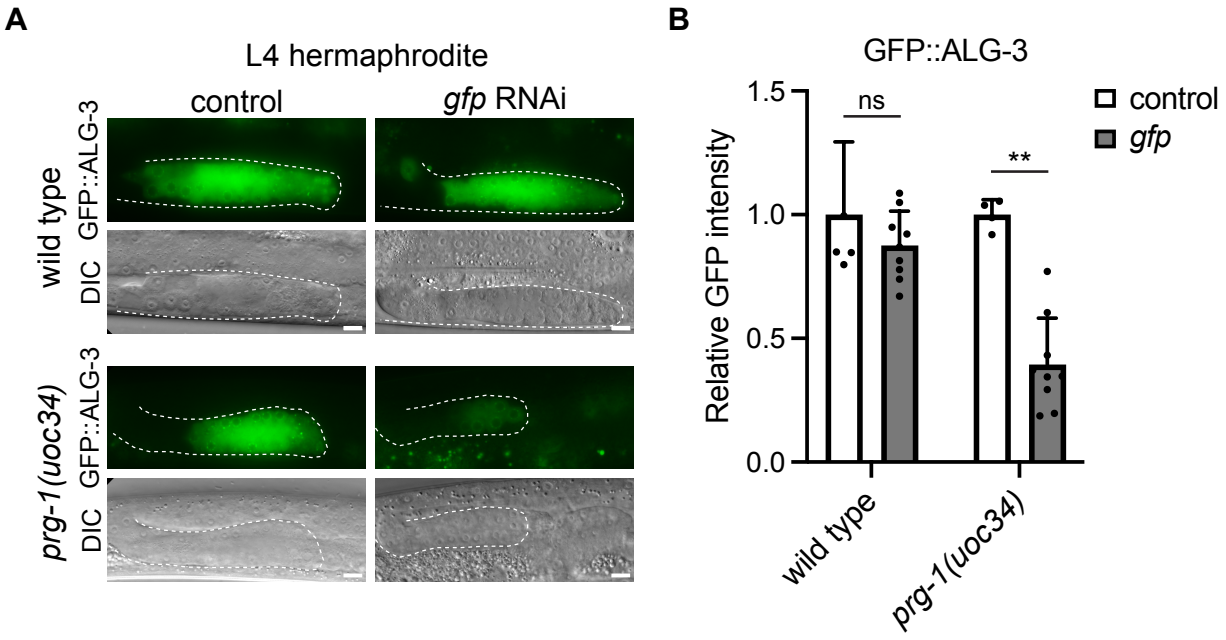

Figure 3.4: Sex-differences in RNAi efficacy.
(**A**) Representative live-fluorescent images of L4 hermaphrodite male germ cells for the indicated GFP reporter in the mutant backgrounds in control and *gfp* RNAi conditions. White dashed lines outline the L4 spermatogenic gonad. (**B**) Bar graph showing the relative GFP mean fluorescent intensity of GFP::ALG-3 signal for control and gfp RNAi conditions in the indicated mutant background. Each point represents measurement from one germline. N = 4-8 germlines. Bar graphs show the mean +/- one standard deviation. Two-tailed p values were calculated using Mann-Whitney-Wilcoxon test. **, p<0.01; ns, no significance.

silencing of *par-1* and *par-3* genes compared to wild type (Figure 3.3A). Our results suggest loss of endo-siRNA or piRNA pathway function enhances germline RNAi efficiency in adult hermaphrodites.

Next, we wondered whether loss of endo-siRNA or piRNA pathway function improves germline RNAi efficiency in male germ cells. For this, we tested germline RNAi of the constitutive germline-expressed GFP reporter in L4 hermaphrodites undergoing spermatogenesis. As shown before, L4 hermaphrodites failed to silence the GFP reporter by RNAi (Figure 3.3B-C). In contrast, endo-siRNA *gtsf-1(xf43)* mutants that fail to produce 26G-RNAs, and piRNA-binding Argonaute *prg-1(uoc34)* mutants showed improved RNAi efficiency in male germ cells (Figure 3.3B-C). Additionally, we tested whether improved germline RNAi efficiency applied to the spermatogenic GFP reporter. Indeed, *prg-1(uoc34)* mutant L4 hermaphrodites showed increased RNAi efficiency compared to wild type (Figure 3.4A-B). Our results suggest loss of endo-siRNA or piRNA pathway function improves germline RNAi efficiency in male germ cells.

Overall, we found loss of either endo-siRNA or piRNA function improved germline RNAi efficiency for both female and male germ cells.

Germline-specific RNAi factors balance the small RNA network

Although RNAi factors are expressed in widespread tissues, *C. elegans* germ cells require additional factors for RNAi function compared to somatic cells (X. Chen et al., 2024; Claycomb et al., 2009b; Gaylord et al., 2025; Phillips et al., 2014). We wondered whether these germline-specific RNAi factors are required due to small RNA pathway competition. To test this hypothesis, we first examined the germline and somatic RNAi efficiency for several reported

germline-specific RNAi factors. These factors included conserved DExH-box family RNA helicase RHA-1, redundant DEAD-box RNA helicase paralogs MUT-14/ SMUT-1, and nematode-specific disordered protein ELLI-1 (Andralojc et al., 2017; Phillips et al., 2014; Walstrom et al., 2005). As reported, *rha-1*, *elli-1*, and *mut-14; smut-1* mutants displayed low germline RNAi efficiency compared to wild type (Figure 3.5A). In contrast, these mutants showed complete sensitivity to somatic RNAi (Figure 3.5B). Our findings support previous reports that *rha-1*, *elli-1*, and *mut-14; smut-1* mutants exhibit defects in germline RNAi only.

Next, we tested whether loss of either endo-siRNA or piRNA pathway function improves the germline RNAi efficiency of *rha-1*, *elli-1*, and *mut-14; smut-1* mutants. To test this, we performed RNAi against *cdk-1* that when successfully knocked down results in embryos that fail to undergo cell division. As a result of successful *cdk-1* RNAi, wild type, endo siRNA *rrf-3* mutant, and piRNA *prg-1* mutant embryos failed to undergo cell division (Figure 3.5C-D). In contrast, a majority of *rha-1*, *elli-1*, and *mut-14/ smut-1* mutant animals continued to produce multicellular embryos during *cdk-1* RNAi, indicating failed RNAi (Figure 3.5C-D). Next, we examined *cdk-1* RNAi efficiency in *rha-1*, *elli-1*, and *mut-14/ smut-1* mutants in the background of either the endo siRNA or piRNA pathway mutant. We were unable to test *elli-1; rrf-3* mutants because this background was immediately sterile. However, loss of piRNA pathway function improved *cdk-1* RNAi efficiency in *elli-1* mutants (Figure 3.5C-D). Similarly, we found loss of either endo-siRNA or piRNA pathway function improved *cdk-1* RNAi efficiency in *rha-1* mutants (Figure 3.5C-D). In contrast, loss of endo-siRNA or piRNA pathway function failed to improve *cdk-1* RNAi efficiency in *mut-14/ smut-1* mutants (Figure 3.5C-D). These results were consistent for RNAi against other germline genes, where *rha-1* and *elli-1* mutant germline RNAi defects were suppressed by loss of endo-siRNA or piRNA pathway function (Figure 3.6A-B).

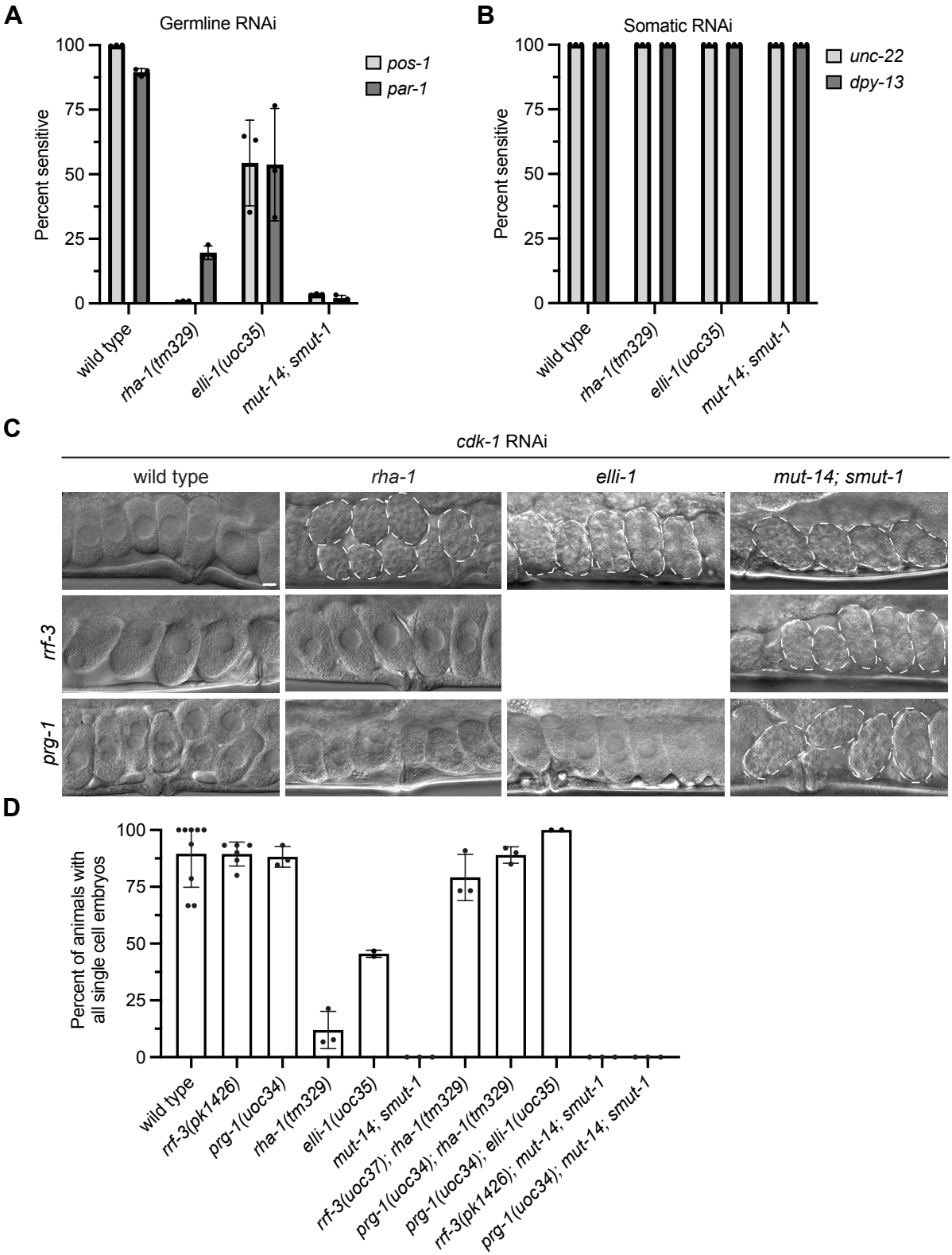

Figure 3.5: Germline-specific RNAi mutants recover RNAi function by loss of endo-siRNAs or piRNAs.

(**A** and **B**) Bar graphs showing RNAi sensitivity for germline genes *pos-1* and *par-1* (**A**) or

Figure 3.5 continued
somatic genes *unc-22* and *dpy-13* (**B**) in the indicated mutant backgrounds. Experiments were performed in triplicate. (**C**) Representative DIC, differential interference contrast, images of adult hermaphrodite embryos from *cdk-1* RNAi conditions in the indicated mutant backgrounds. Animals with the genotype *elli-1; rrf-3* double mutants are sterile and therefore no homozygous double mutant strain can be maintained. White dashed lines outline multicellular embryos indicative of RNAi resistance. Scale bars = 10 μm. (**D**) Bar graph displays quantification of *cdk-1* RNAi experiment shown in (**C**) where each point represents the mean percentage of animals with all single cell embryos for N = 25 animals. Bar graphs show the mean +/- one standard deviation.

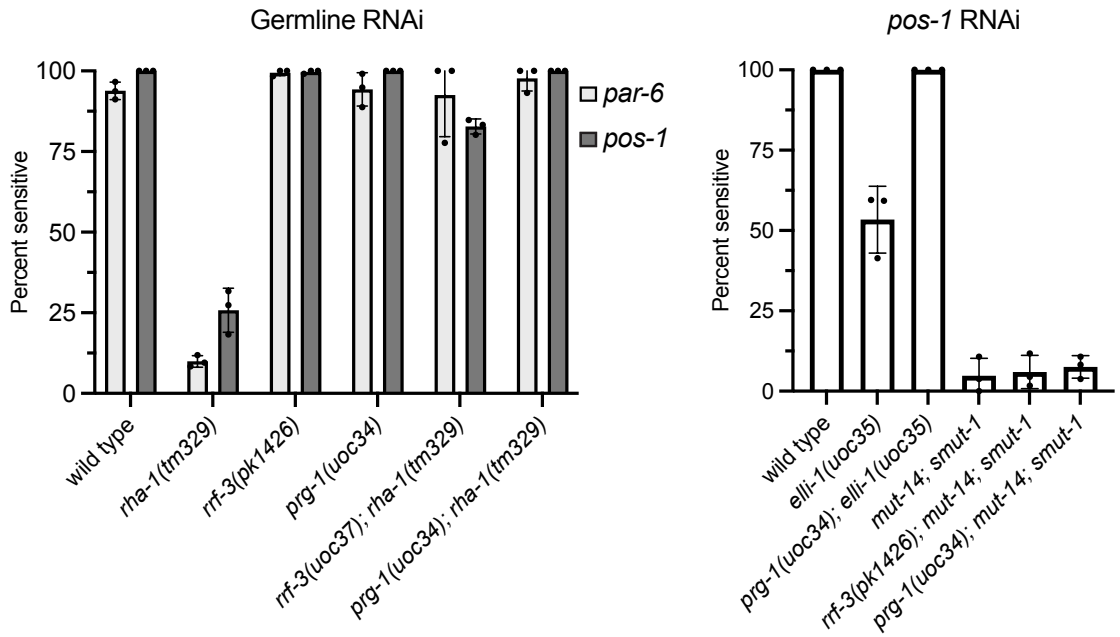

Figure 3.6: Germline RNAi function recovered in mutants by loss of endo-siRNAs or piRNAs.

(**A** and **B**) Bar graphs showing RNAi sensitivity for germline genes *pos-1* and *par-6* in the indicated mutant backgrounds. Experiments were performed in triplicate. Bar graphs show the mean +/- one standard deviation.

Robust gene silencing by RNAi requires the production of secondary siRNAs against the target gene. These secondary siRNAs are bound by WAGO Argonautes. Previously, MUT-14/ SMUT-1 helicases have been shown to function directly in WAGO siRNA production (Phillips et al., 2014). This likely explains why loss of endo-siRNA and piRNA pathway function fails to suppress the *mut-14; smut-1* mutant germline RNAi defect. In contrast, we and others previously found RHA-1 and ELLI-1 mainly promote Argonaute CSR-1 small RNA production (X. Chen et al., 2024; Gaylord et al., 2025). CSR-1 small RNAs promote germline gene expression while fine-tuning a subset of germline genes (Singh et al., 2021; Wedeles et al., 2013). Like RHA-1 and ELLI-1, CSR-1 is also required for germline RNAi only (Figure 3.7A-B). Additionally, we and others have found in the absence of RHA-1 and CSR-1, WAGOs aberrantly bind small RNAs normally sorted to CSR-1 (Gaylord et al., 2025; Shen et al., 2018; W. S. Wu et al., 2023). As a result, WAGOs and secondary siRNA machinery are diluted across several thousand more target genes reducing sensitivity to RNAi. In support of this, loss of piRNA pathway function suppressed the germline RNAi defect in CSR-1 compromised animals (Figure 3.7A-B). Interestingly, loss of endo-siRNA pathway function failed to suppress the germline RNAi defect in CSR-1 compromised animals (Figure 3.7A-B). These results may reflect the greater number of target genes downstream of piRNAs compared to endo-siRNAs in adult germlines. Loss of piRNAs would free up a greater proportion of WAGO siRNA production machinery.

In addition to shared WAGO siRNA machinery, the endo-siRNA and RNAi pathways share cofactors required for primary siRNA production. We wondered whether loss of endo-siRNA pathway function improved RNAi efficiency because of shared primary or secondary factors, or both. To test this, we examined germline RNAi efficiency in *rha-1* mutants in combination with loss of GTSF-1. Loss of GTSF-1 eliminates competition for both primary and

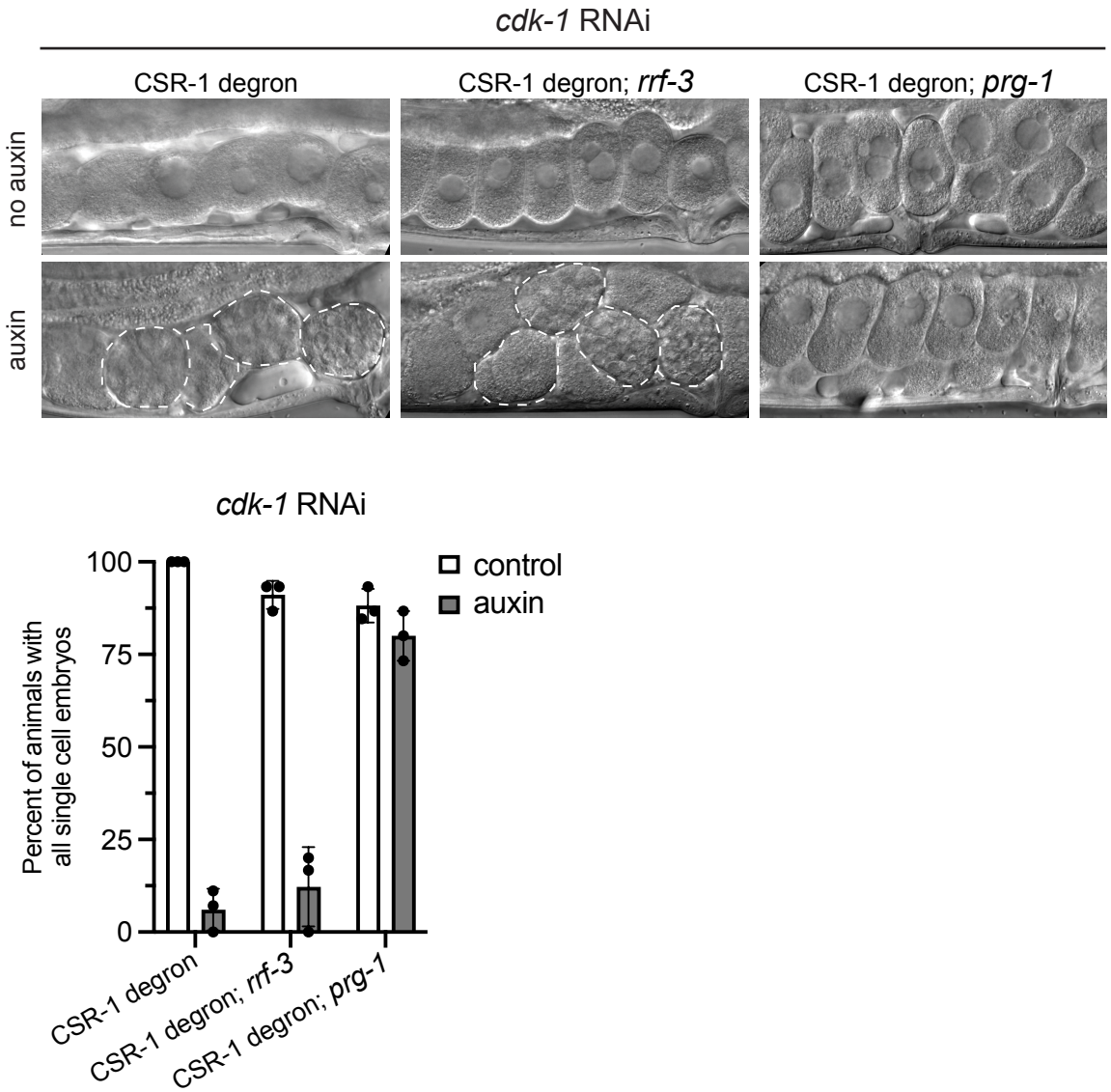

Figure 3.7: CSR-1 germline RNAi function recovered by loss of piRNA pathway function. (**A**) Representative DIC, differential interference contrast, images of adult hermaphrodite embryos from *cdk-1* RNAi conditions in the CSR-1 degron and indicated mutant backgrounds, with and without auxin for CSR-1 depletion. White dashed lines outline multicellular embryos indicative of RNAi resistance. Scale bars = 10 µm. (**B**) Bar graph displays quantification of *cdk-1* RNAi experiment shown in (**A**) where each point represents the mean percentage of animals with all single cell embryos for N = 25 animals. Bar graphs show the mean +/- one standard deviation.

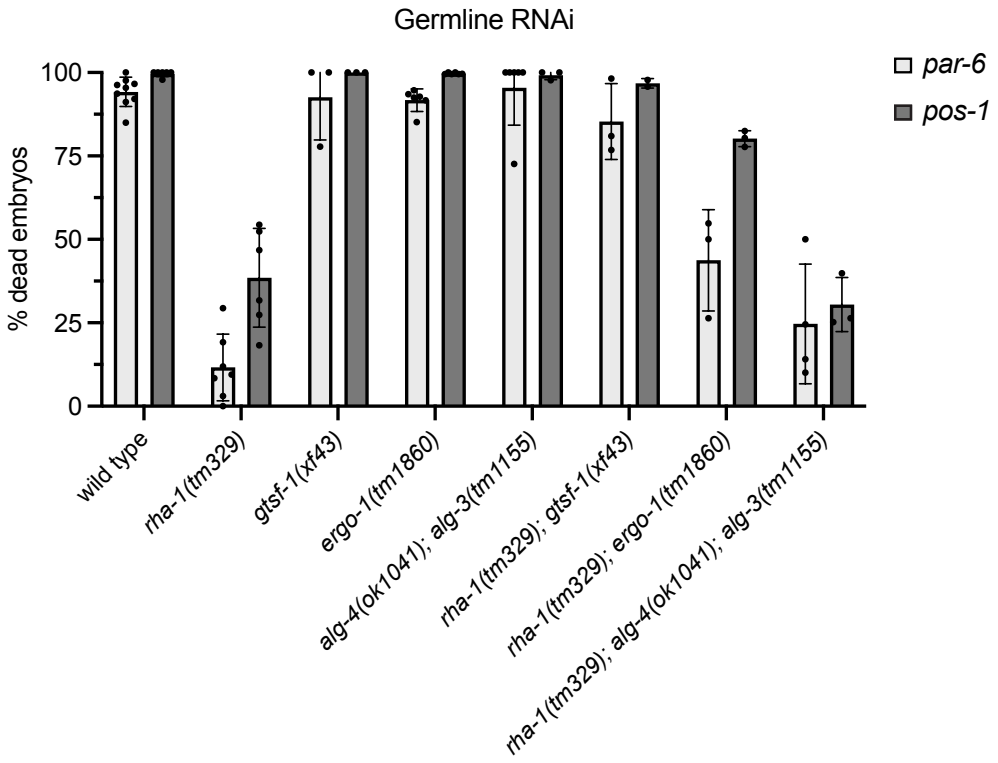

Figure 3.8: Endo-siRNA pathway primary and secondary siRNA steps limit RNAi function. Bar graphs showing RNAi sensitivity for germline genes *pos-1* and *par-6* in the indicated mutant backgrounds. Experiments were performed in triplicate. Bar graphs show the mean +/- one standard deviation.

secondary siRNA factors (Almeida et al., 2018). Compared to *rha-1* mutant animals, *rha-1; gtsf-1* mutant animals displayed improved germline RNAi efficiency comparable to wild-type animals (Figure 3.8). Next, we examined germline RNAi efficiency in *rha-1* mutants in combination with loss of Argonautes ERGO-1 or ALG-3/4 that both bind 26G-RNA endo-siRNAs (Billi et al., 2014). Loss of these Argonautes only eliminates competition for secondary siRNA production. In this background, *rha-1; ergo-1* and *rha-1; alg-3/4* mutants displayed partially improved germline RNAi efficiency compared to *rha-1* mutant animals, but reduced germline RNAi efficiency compared to wild-type animals (Figure 3.8). Together, these results suggest RNAi competes with the endo-siRNA pathway for machinery involved in both primary and secondary siRNA production.

Overall, we provide evidence that germline-specific RNAi factors are required to maintain the balance of competition between germline small RNA pathways for shared small RNA biogenesis factors.

Germline small RNA pathways compete for amplified siRNA production

Because we found both endo-siRNA and piRNA mutants displayed enhanced germline RNAi efficiency, we aimed to gain molecular insight into the small RNAs produced in these backgrounds. We focused on the endo-siRNA mutant, because endo-siRNAs compete with RNAi for both primary and secondary siRNA biogenesis factors. To this aim, we plated synchronized L1 stage wild type and endo-siRNA *rrf-3* mutant hermaphrodites on either control empty vector or *par-6* RNAi food. Successful *par-6* RNAi in adult germlines results in laying of dead embryos. Once these animals reached adults, we isolated RNA and generated two types of small RNA high-throughput sequencing libraries per condition. The two library preparations

utilized the molecular differences in 5'-phosphate of primary and secondary siRNAs (Pak & Fire, 2007). Primary siRNAs have 5'-monophosphate ends while secondary siRNAs have a 5'-triphosphate end. The first library preparation only ligates primary siRNAs that have have 5'-monophosphate ends. For the second library preparation, addition of RNA 5' pyrophosphohydrolase (RppH) removes the pyrophosphate from the 5' ends of secondary siRNAs. As a result, these libraries contain both primary and secondary siRNAs.

From this sequencing, we analyzed the normalized primary and total siRNAs mapping to the *par-6* gene in animals fed dsRNA against *par-6*. For primary siRNAs, we find *rrf-3* mutants produced similar levels of primary siRNA as wild type (Figure 3.9A). Secondary siRNAs, termed 22G-RNAs, are 22 nucleotides long with a 5'G nucleotide bias. We determined from the total siRNA libraries that *rrf-3* mutants produced nearly 33% more 22G-RNAs targeting *par-6* compared to wild type (Figure 3.9B). These results suggest loss of endo-siRNA pathway function improves RNAi-triggered secondary siRNA production more than primary siRNA production.

Next, we performed the same experiment in the *rha-1* mutant background where animals are defective in germline RNAi and *rrf-3; rha-1* mutant background that recovers germline RNAi efficiency. For both *rha-1* and *rrf-3; rha-1* mutants, we found primary siRNAs targeting the *par-6* gene were slightly reduced compared to wild type and *rrf-3* mutants (Figure 3.9A). From total siRNAs, we found secondary siRNAs targeting the *par-6* gene were slightly decreased in *rha-1* mutant animals (Figure 3.9B). In contrast, secondary siRNAs were produced to higher levels in *rrf-3; rha-1* mutants compared to wild type and *rrf-3* mutants (Figure 3.9B). These results further suggest RNAi efficiency is improved by increased secondary siRNA production in the absence of the endo-siRNA pathway. Additionally, loss of the endo-siRNA

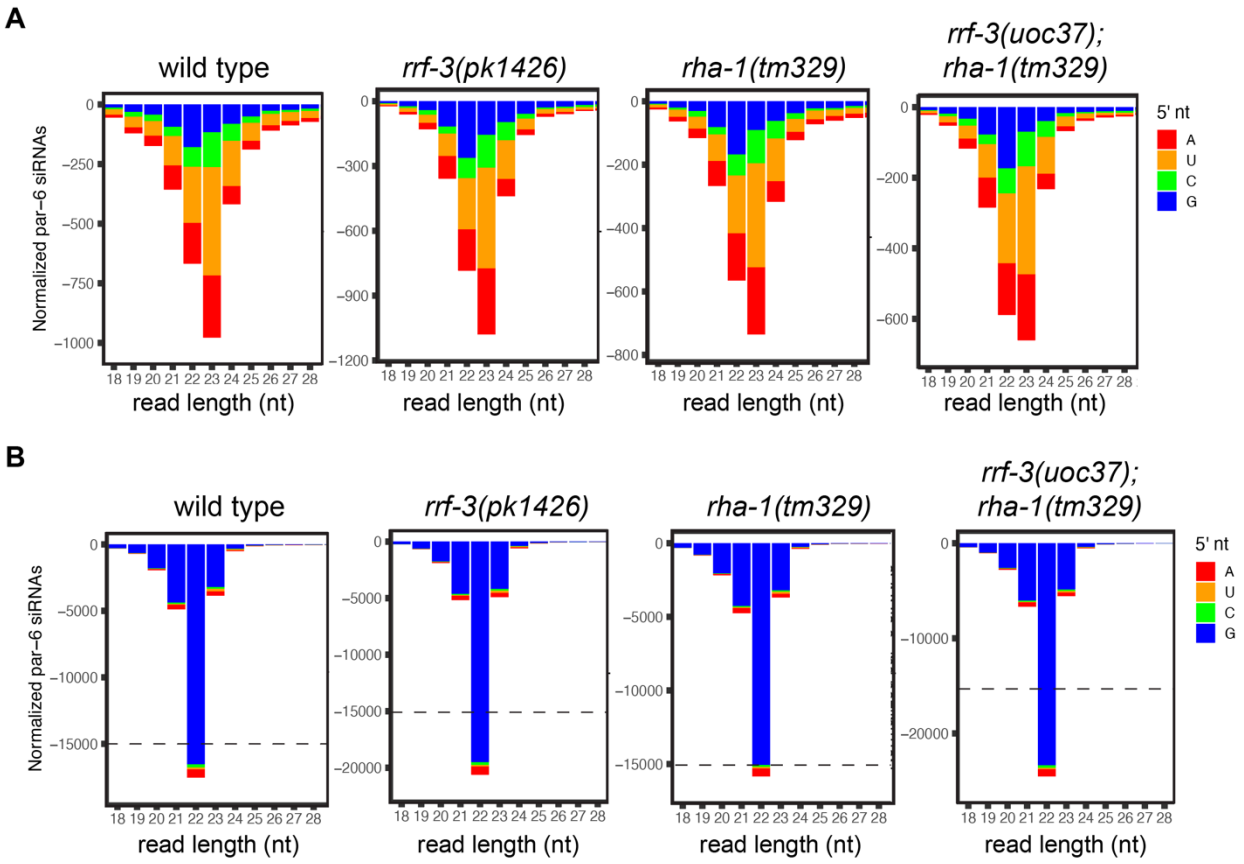

Figure 3.9: Secondary siRNAs are increased against RNAi target in endo-siRNA mutant. (**A**) Normalized abundance of primary siRNAs antisense to RNAi target gene *par-6* for the indicated mutant backgrounds. Plots show abundance of primary siRNAs for each length. Color indicates the identity of the 5' nucleotide. (**B**) Normalized abundance of primary and secondary siRNAs antisense to RNAi target gene *par-6* for the indicated mutant backgrounds. Plots show abundance of primary and secondary siRNAs for each length. Secondary siRNAs are 22 nucleotide 5'-G RNAs. Color indicates the identity of the 5' nucleotide. Since y-axis is at a different scale for each plot, black dashed line marks 15000 normalized antisense siRNAs y-axis position for each plot.

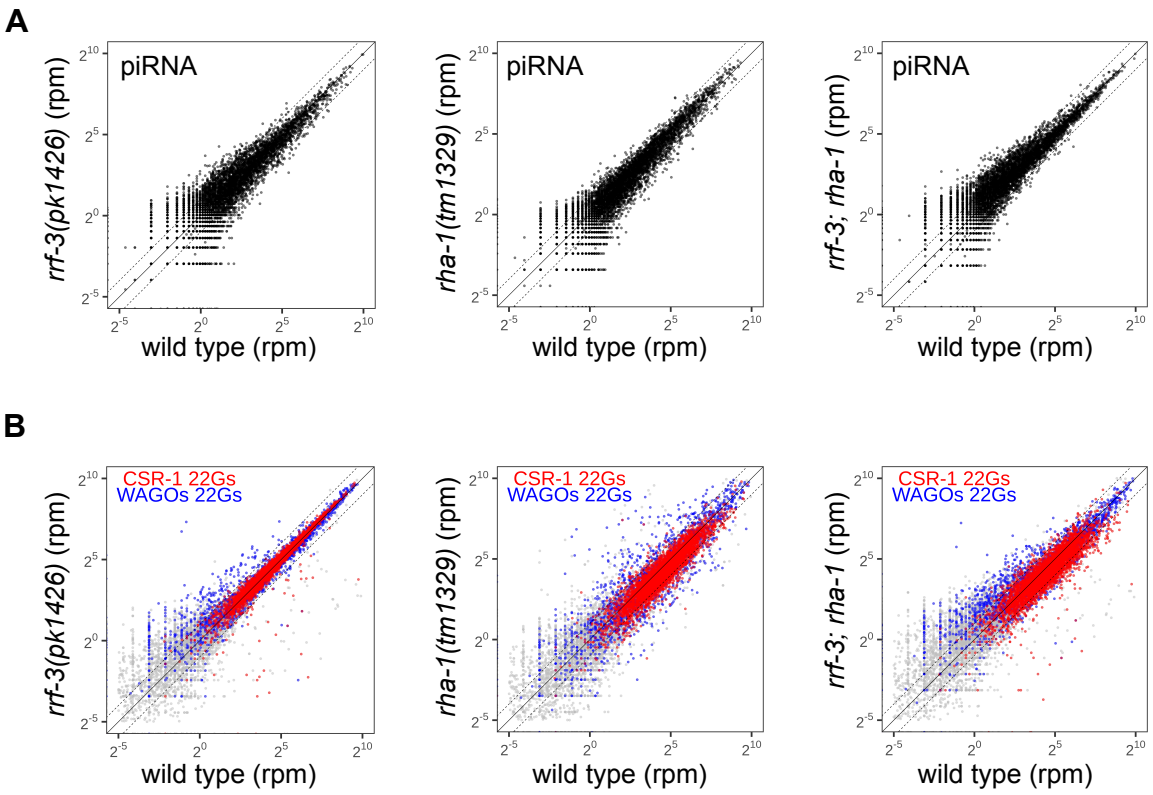

Figure 3.10: Small RNAs in endo-siRNA mutants.
(**A**) Scatterplots show the abundance of piRNAs in reads per million (rpm) for wild type compared to the indicated mutant. Results analyzed from primary siRNA sequencing libraries (no RppH). (**B**) Scatterplots show the abundance of secondary siRNAs 22G-RNAs mapping to indicated pathway target genes in reads per million (rpm) for wild type compared to the indicated mutant. CSR-1 22G-RNAs in red, WAGO 22G-RNAs in blue. Results analyzed from primary and secondary siRNA sequencing libraries (RppH). For all scatterplots the three diagonal lines indicate a two-fold increase (top), no change (middle), or a two-fold depletion (bottom) in indicated mutant animals.

pathway function did not result in changes to the abundance of piRNAs (Figure 3.10A). Instead, loss of the endo-siRNA pathway function only impacted the level of secondary siRNAs against target genes (Figure 3.10B). This further indicated germline small RNA pathways may compete over secondary small RNA production machinery.

Germline-specific RNAi factors regulate RNAi inheritance

Another feature of RNAi is the ability to trigger gene silencing for multiple generations, known as transgenerational inheritance. RNAi mediated silencing of germline genes can be inherited for over four generations while RNAi of somatic genes can be inherited for only a single generation (Burton et al., 2011; Spracklin et al., 2017). These differences in the duration of transgenerational inheritance suggested RNAi of germline and somatic genes may be regulated differently. HRDE-1, a key mediator of RNAi inheritance for germline genes, binds secondary siRNAs and functions in transcriptional gene silencing (Spracklin et al., 2017). We confirmed HRDE-1 is not required for RNAi inheritance for somatic gene *dpy-11* (Figure 3.11 and Table 3.1). Instead, RNAi inheritance of somatic genes has been reported to require NRDE-3, a WAGO Argonaute expressed in the nuclei of adult germ cells, embryos and somatic tissue (Burton et al., 2011). Because NRDE-3 is expressed in the germline and soma, we next tested whether RNAi inheritance of somatic genes requires functional germline RNAi. We found that animals capable of RNAi only in the germline were able to partially inherit RNAi against somatic gene *dpy-11* evident by a shortened body in 40 out of 130 animals in the inheriting generation (Figure 3.11 and Table 3.1). Taken together, our data suggests RNAi inheritance of somatic genes requires functional RNAi in germ cells, but distinct factors mediate the inheritance of germline genes.

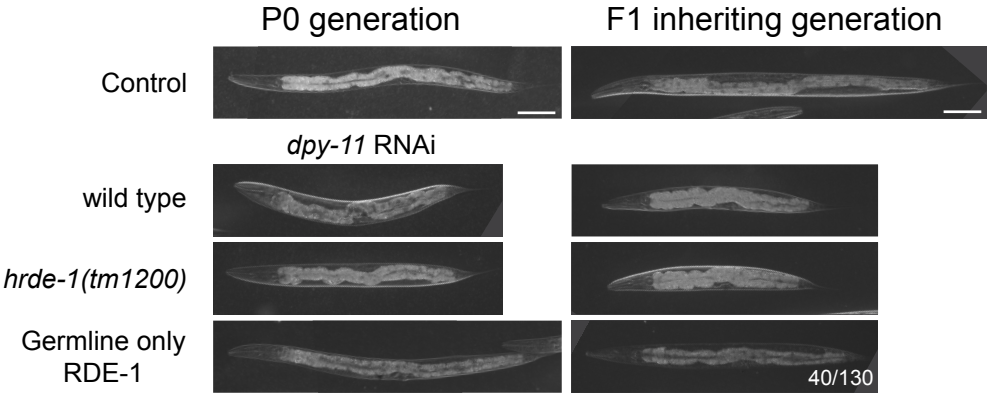

Figure 3.11: RNAi inheritance of somatic gene requires functional germline RNAi. Representative light microscopy DIC images of L3 stage worms for controls fed L4440 empty vector RNAi food in the P0 generation and F1 generation. For experimental condition, P0 animals were grown on *dpy-11* RNAi food. F1 progeny were grown in the absence of *dpy-11* dsRNA. Fer germline only RDE-1 F1 inheriting generation, image represents 40 out of 130 animals. Experiment details quantified in Table 3.1. Scale bar = 100 µm.

Strain	RNAi generation	
	P0	F1
wild type	100% (150/150)	100% (150/150)
rha-1(tm329)	100% (150/150)	0% (0/150)
elli-1(uoc35)	100% (150/150)	47% (72/152)
hrde-1(tm1200)	100% (150/150)	100% (150/150)
Germline only RDE-1	0% (0/150)	31% (40/130)
set-25; met-2	100% (150/150)	0% (0/150)
rrf-3(pk1426)	100% (150/150)	100% (150/150)
prg-1(uoc34)	100% (150/150)	100% (150/150)
rrf-3(uoc37); rha-1(tm329)	100% (150/150)	100% (150/150)
prg-1(uoc34); rha-1(tm329)	100% (150/150)	100% (150/150)

Table 3.1: RNAi inheritance of somatic gene *dpy-11*.
Percentages indicate percent of worms scored for shortened body. Numbers show the number of animals scored for shortened bodies over the total number of animals scored. P0 generation worms fed *dpy-11* dsRNA. F1 generation grown in the absence of *dpy-11* dsRNA.

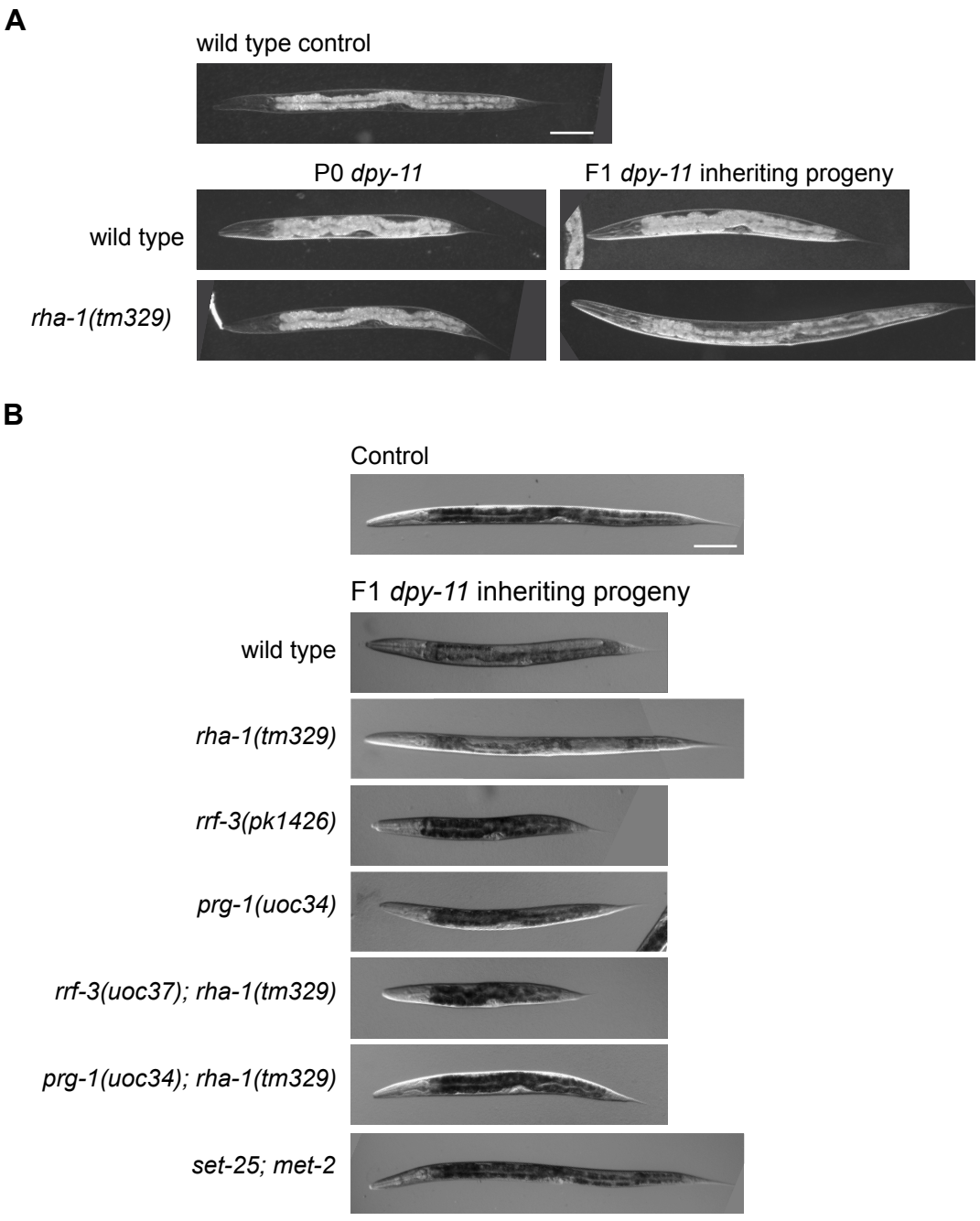

Figure 3.12: Efficiency of RNAi inheritance regulated by endo-siRNA and piRNA pathway function.

(**A**) Representative light microscopy DIC images of L3 stage worms for controls in the P0 and F1 generations. For the experimental condition, P0 animals were grown on *dpy-11* RNAi food. F1 inheriting progeny were grown in the absence of *dpy-11* dsRNA. (**B**) Representative light microscopy DIC images of L3 stage worms for F1 generation. For experimental condition, P0 animals were grown on *dpy-11* RNAi food. F1 inheriting progeny were grown in the absence of *dpy-11* dsRNA. Experiment details quantified in Table 3.1. Scale bar = 100 μm.

Based on our result that RNAi inheritance of somatic genes requires functional germline RNAi, we wondered whether germline-specific RNAi factors, like RHA-1 and ELLI-1, were also required. We found both RHA-1 and ELLI-1 were important for RNAi inheritance of somatic gene *dpy-11*, where mutant animals displayed normal body lengths in the inheriting generation (Figure 3.12A and Table 3.1). As we observed for germline RNAi, we next asked whether loss of endo-siRNA or piRNA pathway function in the background of *rha-1* mutants improves the efficiency of RNAi inheritance. Indeed, we find loss of endo-siRNA or piRNA pathway function in *rha-1* mutant animals resulted in improved somatic RNAi inheritance (Figure 3.12B and Table 3.1). Together, we find germline-specific RNAi factors are also involved in RNAi inheritance of somatic genes. Notably, although RNAi silencing of germline and somatic genes are inherited for a different number of generations, both require histone H3K9 methyltransferases SET-25 and MET-2 (Figure 3.12B and Table 3.1). Overall, our data suggests that RNAi inheritance of germline and somatic genes require a partially overlapping set of germline RNAi factors.

3.4 Discussion

While sex-differences in germline RNAi function have been reported, the mechanism for these differences remained poorly understood. Here, we demonstrate that increased small RNA pathway competition in male germ cells disrupts RNAi function. Notably, endo-siRNA and piRNA pathways each target over a thousand more mRNAs in male germ cells compared to female germ cells, highlighting the increased activity of these pathways in male germ cells (Bezler et al., 2019). In line with this, we uncover that loss of endo-siRNA and piRNA pathway function allowed for RNAi-mediated gene silencing in male germlines. Loss of these two

pathways also enhances RNAi function in female germ cells, suggesting small RNA pathway competition also limits RNAi function in female germ cells. Overall, our findings uncover a mechanism whereby increased competition between distinct small RNA pathways within male germ cells underlies sex-differences in germline RNAi function.

RNAi is a highly conserved mechanism of gene silencing, and RNAi factors are expressed across a wide range of tissues. In *C. elegans*, environmental exposure to dsRNA results in gene silencing throughout widespread tissues (Fire et al., 1998; Kamath et al., 2000). However, unlike female germ cells, male germ cells fail to trigger gene silencing in response to environmental dsRNAs. A previous study found male and female germ cells produced similar primary siRNAs during RNAi against a GFP reporter gene (Bezler et al., 2019). However, male germ cells were found to produce reduced levels of secondary siRNAs against the RNAi target. Before our work, it remained unclear whether small RNA pathway competition over shared secondary siRNA factors limited the RNAi capacity in male germ cells. Our work expands on this result, showing piRNA and endo-siRNA mutants enhance germline RNAi sensitivity and improved RNAi efficiency in male germ cells. Taken together, our findings suggest male germ cells are normally insensitive to systemic RNAi due to small RNA pathway competition for secondary siRNA production.

We and others have identified factors required for RNAi function in the germline but not somatic cells. Since the core components of RNAi are conserved and shared across tissues, these germline-specific factors are likely a result of competition over cofactors shared between distinct small RNA pathways. In line with this cofactor competition model, loss of endo-siRNA and piRNA pathway function suppressed the germline RNAi defects in *rha-1* and *elli-1* mutants. Additionally, loss of piRNA pathway function but not endo-siRNA function suppressed the

germline RNAi defects in CSR-1 compromised animals. Our results suggest loss of the endo-siRNA and piRNA pathways enhance germline RNAi to different degrees. Potentially, differences in the number of gene targets between the endo-siRNA pathway (~100) and the piRNA pathway (~2000) contribute to differences in the degree of germline RNAi enhancement of the mutants (Seroussi et al., 2023). Under the competition model, loss of piRNA pathway function frees up more secondary siRNA production machinery for RNAi compared to loss of endo-siRNA pathway function.

Somatic and germline RNAi differ in their ability to be inherited across generations. RNAi of somatic genes can be inherited for one generation, while RNAi of germline genes can be inherited for more than four generations (Burton et al., 2011). Here we find somatic RNAi inheritance requires functional germline RNAi as well as germline-specific RNAi factors. Understanding how RNAi inheritance of somatic and germline genes is differentially regulated will require future experiments.

Overall, our work establishes genetic backgrounds capable of systemic RNAi in male germ cells, allowing future studies to utilize RNAi to uncover novel gene functions in male germ cells.

3.5 Methods

Caenorhabditis elegans maintenance

Animals were grown on standard nematode growth media (NGM) plates seeded with the Escherichia coli OP50 strain at 20 °C. A complete list of strains used in this study are provided in

Table 3.2: List of C. elegans strains used in this study.

Strain	Genotype	Gene(s)	Description	Origin
N2	*C. elegans wild isolate (Bristol)*		Reference C. elegans. Variety Bristol.	CGC
HCL110	*oma-1::GFP I*	*oma-1*		
JMC205	*alg-3(tor141[GFP::3xFLAG::alg-3]) IV*	*alg-3*		CGC
DZ270	*pie-1p::gfp::H2B II*	*H2B*		
WM300	*alg-4(ok1041) III; alg-3(tm1155) IV*	*alg-4, alg-3*		CGC
WM158	*ergo-1(tm1860) V*	*ergo-1*		CGC
HCL226	*rha-1(tm329) II*	*rha-1*	KMW1 outcrossed with N2	
HCL276	*prg-1(uoc34) I*	*prg-1*	CRISPR-Cas9 large deletion null allele	
NL2099	*rrf-3(pk1426) II*	*rrf-3*		CGC
RFK607	*gtsf-1(xf43) IV*	*gtsf-1*		CGC
HCL341	*rha-1(uoc24[gfp::rha-1]) II; csr-1(gc029[degron::mCherry::3xflag::ha::csr-1]) IV; elli-1(uoc35) IVelli-1(uoc35) IV*	*elli-1*	Large deletion null mutant	This study
USC414	*mut-14 smut-1 V*	*mut-14, smut-1*		Carolyn Phillips lab
HCL394	*prg-1(uoc34) I; rha-1(tm329) II*	*prg-1, rha-1*		This study
HCL395	*rrf-3(uoc37) rha-1(tm329) II*	*rrf-3, rha-1*		This study
HCL396	*prg-1(uoc34) I; elli-1(uoc35) IV*	*prg-1, elli-1*		This study
HCL397	*prg-1(uoc34) I; mut-14 smut-1 V*	*prg-1, mut-14, smut-1*		This study

Table 3.2 continued

HCL398	*rha-1(tm329) II; alg-4(ok1041) III; alg-3(tm1155) IV*	*rha-1, alg-4, alg-3*		This study
HCL399	*rha-1(tm329) II; ergo-1(tm1860) V*	*rha-1, ergo-1*		This study
DCL569	*mkcSi13 [sun-1p::rde-1::sun-1 3'UTR + unc-119(+)] II; rde-1(mkc36) V*	*rde-1*	Germline rescue of the rde-1(mkc36) indel mutation, allowing germline-specific RNAi.	Zou L, et al. 2019
HCL393	*hrde-1(tm1200)*	*hrde-1*		
GW638	*met-2 (n4256) set-25 (n5021) III.*	*met-2, set-25*		CGC
MHE69	*ieSi64 [gld-1p::TIR1::mRuby::gld-1 3'UTR + Cbr-unc-119(+)] II; csr-1(gc029[degron::mCherry::3xflag::ha::csr-1]) IV*	*csr-1*	Degron knock in by CRISPR-Cas9 in MHE54 and cross with CA1352 (CGC).	P Quarato et al. 2020

RNA interference

RNAi was performed by feeding animals with *E. coli* HT115 (DE3) strains expressing the appropriate dsRNA. RNAi bacterial strains were obtained from the Ahringer *C. elegans* RNAi Collection (Source BioScience). Bacterial cultures were grown in Luria broth supplemented with 100 μg/mL ampicillin and 50 μg/mL tetracycline overnight at 37°C. Cultures were seeded on NGM plates containing 100 μg/mL ampicillin, 50 μg/mL tetracycline, and 1 mM IPTG and incubated at room temperature for 24 hours. HT115 (DE3) expressing empty RNAi vector L4440 was used for control. RNAi conditions were seeded in duplicate and fifty L1 stage animals were transferred to each plate unless stage was specified. For L4 stage hermaphrodite RNAi experiments, L1 stage animals were seeded on RNAi plates and 48 hours later worms were evaluated and imaged for GFP expression using a fluorescence compound microscope. For young adult animals, L1 stage animals were seeded on RNAi plates and 3 days later worms were

evaluated and imaged for GFP expression using a fluorescence compound microscope. For male animals, either L1 or L4 staged animals were placed on RNAi plates and evaluated 24 hours after L4 stage for GFP expression using a fluorescence compound microscope. Male animals were observed every 24 hours for an additional 3 days. For neuronal RNAi, L1 stage animals were transferred to RNAi plates and imaged 72 hours later for GFP expression.

Image processing and analysis

Image processing and quantification of GFP signal as mean fluorescent intensity were performed using ImageJ. Single slice images of gonads and ROIs were used for quantification. Images of 7–10 gonads were collected and quantified. Data were compared by two-tailed p values were calculated using Mann-Whitney-Wilcoxon test.

Short-exposure RNAi assay

For each strain, five L4 stage animals were plated per RNAi plate, control, *par-1* and *par-3* RNAi. Experiment was performed in triplicate. After 24 hours, all young adult animals were removed from the RNAi and control plates. Total number of embryos per plate were counted. The next day the total number of hatched animals were counted per plate. Results were plotted as % dead embryos equal to the total number of embryos laid minus number of hatched animals over the total number of embryos laid as a percentage. Percentage of dead embryos indicates successful RNAi knockdown.

RNAi of germline genes

For RNAi of *cdk-1*, twenty-five L3 stage animals were transferred to control or *cdk-1* RNAi plates in triplicate. Two days later, live animals were examined in compound microscope for single cell or multicellular embryos. Animals containing all single cell embryos were counted as successful RNAi.

For RNAi of *pos-1*, *par-1* or *par-6* genes, five L1 worms were moved to RNAi and control L4440 plates and performed in triplicate. Three days later, adult worms were removed from plates. The following day unhatched embryos and hatched progeny were counted for each plate. Plots show percentage of unhatched embryos over sum of unhatched embryos and hatched progeny.

RNAi of somatic genes

For RNAi of *unc-22* and *dpy-13* genes, twenty-five L1 worms were transferred to RNAi and control L4440 plates, performed in triplicate. Three days later, adult worms were scored for phenotypes. For RNAi of *unc-22*, worms were scored for body muscle twitching. For RNAi of *dpy-13*, worms were scored for a dumpy and shortened body.

Germline RNAi with auxin-induced CSR-1 degradation

For the degron-tagged CSR-1 strains, L3 staged worms were transferred to RNAi NGM plates containing 500 µM auxin, 0.5% ethanol plates or 0.5% ethanol control plates. Experiment was performed as written above for *cdk-1* RNAi.

RNAi inheritance of somatic gene

For RNAi inheritance of *dpy-11* gene, 50 P0 L1 stage animals were seeded per plate on control or *dpy-11* RNAi food. Experiment was set up in duplicate. After 48 hours, P0 animals were scored for shortened bodies, and 3 representative worms were imaged. After 48 more hours, P0 animals now full of embryos were bleached and rinsed in M9 three times following standard *C. elegans* population bleach protocol. Isolated and washed embryos were hatched allowed to hatch in M9 overnight on rotator. Fifty F1 L1 worms of the RNAi inheriting generation were seeded on OP50 seeded NGM plates. After 48 hours, F1 animals were scored for shortened bodies, and 3 representative F1 worms were imaged.

Primary and total small RNA-seq library preparation

Total RNA was extracted using the standard method with TRIzol reagent (Invitrogen) from whole animals of ~100,000 synchronized young adults grown from L1 on either L4440 control or par-6 RNAi seeded plates. Small (<200 nt) RNAs were enriched with mirVana miRNA Isolation Kit (Ambion). In brief, 80 μL (200–300 μg) of total RNA, 400 μL of mirVana lysis/binding buffer and 48 μL of mirVana homogenate buffer were mixed well and incubated at room temperature for 5 min. Then, 176 μL of 100% ethanol was added and samples were spun at 2500×g for 4 min at room temperature to pellet large (>200 nt) RNAs. The supernatant was transferred to a new tube and small (<200 nt) RNAs were precipitated with pre-cooled isopropanol at -80 °C. Small RNAs were pelleted at 20,000×g at 4 °C for 30 min, washed once with 70% pre-cooled ethanol, and dissolved with nuclease-free water. Ten micrograms of small RNAs were fractionated on a 15% PAGE/7M urea gel, and RNA from 17 nt to 40 nt was excised from the gel. RNA was extracted by soaking the gel in 2 gel volumes of NaCl TE buffer (0.3 M

NaCl, 10 mM Tris-HCl, 1 mM EDTA pH 7.5) overnight. The supernatant was collected through a gel filtration column. RNA was precipitated with isopropanol, washed once with 70% ethanol, and resuspended with 15 μL nuclease-free water. For total small RNA libraries, samples were treated with RppH to convert 22G-RNA 5′ triphosphates to monophosphates in 1 × reaction buffer, 10 U RppH (New England Biolabs), and 20 U SUPERase-In RNase Inhibitor (Invitrogen) for 3 h at 37 °C, followed by 5 min at 65 °C to inactivate RppH. Libraries generated for primary small RNAs skipped this RppH step. RNA was then concentrated with the RNA Clean and Concentrator-5 Kit (Zymo Research). Small RNA libraries were prepared according to the manufacturer's protocol of the NEBNext Multiplex Small RNA Sample Prep Set for Illumina-Library Preparation (New England Biolabs). NEBNext Multiplex Oligos for Illumina Index Primers were used for library preparation (New England Biolabs). Libraries were sequenced using an Illumina HiSeq4000 to obtain single-end 50 nt sequences at the University of Chicago Genomic Facility.

Small RNA-seq data analysis

Fastq reads were trimmed using custom perl scripts. Trimmed reads were aligned to the *C. elegans* genome build WS230 using bowtie ver 1.2.1.159 with options -v 0 -best -strata. After alignment, reads that were between 17–40 nucleotides in length were overlapped with genomic features (rRNAs, tRNAs, snoRNAs, miRNAs, piRNAs, protein-coding genes, pseudogenes, transposons) using bedtools intersect. Sense and antisense read mapping to individual miRNAs, piRNAs, protein-coding genes, pseudogenes, RNA/DNA transposons, simple repeats, and satellites were totaled and normalized to reads per million (RPM) by multiplying be 1e6 and dividing read counts by total mapped reads, minus reads mapping to structural RNAs (rRNAs,

tRNAs, snoRNAs) because this sense reads likely represent degraded products. Reads mapping to multiple loci were penalized by dividing the read count by the number of loci they perfectly aligned to. Reads mapping to miRNAs and piRNAs were only considered if they matched the sense annotation without any overlap. In other words, piRNA and miRNA reads that contained overhangs were not considered mature piRNAs or miRNAs respectively. 22G-RNAs were defined as 21 to 23 nucleotide long reads with a 5′G that aligned to protein-coding genes, pseudogenes, or transposons. RPM values were then used in all downstream analyses using custom R scripts using R version 4.0.060, which rely on packages ggplot2, reshape2, ggpubr, dplyr.

CHAPTER 4

Germ granules coordinate RNA granule assembly to ensure germline recovery after stress

4.1 Abstract

Germ granules are specialized membraneless RNA and protein complexes that play a crucial role in germline development and inheritance. Germ granules are enriched with components that function in RNA metabolism and small RNA processing. Notably, exposure to environmental stressors, like heat and starvation, disrupts small RNA-mediated gene regulation and inheritance without permanently compromising fertility. How germ cells recover fertility after environmental stress with disrupted germline small RNA pathway function remains unknown. Here, we investigate the impact of heat stress on germ granule integrity within adult germ cells. We find heat stress largely disrupts germ granule organization, including the complete dispersal of several small RNA components that mediate epigenetic inheritance. Further, germ granule assembly factors promote stress granule and P-body formation, ensuring recovery of fertility after heat stress. Overall, our work highlights a coordinated role for germ granules, stress granules, and P-bodies to safeguard germline recovery after stress.

4.2 Introduction

Germ granules are specialized RNA-protein condensates crucial for germ cell development and function (Eddy, 1976; Phillips & Updike, 2022; Strome & Wood, 1982; Trcek & Lehmann, 2019). Germ granules are present in the germ cells of most animals, including worms, flies, zebrafish, and mice (Dodson & Kennedy, 2020; Kemph & Lynch, 2022; Pamula & Lehmann, 2024; Phillips & Updike, 2022). Germ granules are enriched with conserved factors important for complex RNA regulatory processes, suggesting a fundamental role for germ granules in germ

cell development. Included in the set of conserved germ granule factors are proteins involved in small RNA processing, such as Argonaute family proteins (Banisch et al., 2012; Pamula & Lehmann, 2024). Small RNAs bound by Argonaute proteins regulate germline genes by inducing mRNA degradation, translational repression, or transcriptional gene silencing (Banisch et al., 2012). Further, small RNAs can establish gene silencing that persists across several generations (Lev et al., 2019; Spracklin et al., 2017). Recently, work in *C. elegans* found that exposure to environmental stress, like heat and starvation, disrupts small RNA function in gene regulation and terminates small RNA-based inheritance (Houri-Zeevi et al., 2021). How the stress response leads to disrupted small RNA function in gene regulation and inheritance remains an open question.

In *C. elegans*, extensive work has uncovered the complex organization of germ granules into several distinct sub-compartments enriched with unique sets of factors (X. Chen et al., 2024; Huang et al., 2025; Phillips & Updike, 2022). Several examples of these sub-compartments include P granules, Mutator foci, and Z granules that each carry out distinct biological functions (Phillips & Updike, 2022). The P granule functions in piRNA-mediated genome integrity (Batista et al., 2008; G. Wang & Reinke, 2008). The Mutator foci function in RNA interference (Phillips et al., 2012). The Z granule promotes small RNA-based inheritance (Ishidate et al., 2018). This germ granule sub-compartment organization into biological functions has been shown to support the fidelity of these small RNA processes. For example, disruption of germ granule assembly and organization by loss of either Vasa-homolog RNA helicase GLH-1 or LOTUS domain protein MIP-1 leads to defects in small RNA-based inheritance and gene regulation (W. Chen et al., 2022; Cipriani et al., 2021). Intriguingly, environmental heat stress has also been shown to disrupt germ granule assembly. In particular, heat stress leads to nearly

complete loss of PGL-1-marked P granules and MUT-16-marked Mutator foci (Uebel et al., 2018; Watkins & Schisa, 2021). So far, whether the impact of environmental stress on germ granule integrity leads to disrupted small RNA function remains poorly understood.

When exposed to stressful conditions, cells activate the integrated stress response pathway, leading to translation inhibition of most mRNAs and the assembly of stress granules (Decker & Parker, 2012; Ivanov et al., 2019). Stress granules are cytoplasmic RNA-protein condensates that rapidly form in response to stress stimulus and disassemble after removal of the stress stimulus. Stress granules are proposed to exert a protective role on cells during exposure to stress, primarily by pausing translation (Ivanov et al., 2019). Important nucleators of stress granules include conserved Ras GTPase-activating protein binding protein 1 and 2 (mammalian G3BP1 and G3BP2), or GTBP-1 in *C. elegans* (Abbatemarco et al., 2021; Alam & Kennedy, 2019; Riggs et al., 2020). In addition to stress granules, P-bodies are distinct cytoplasmic RNA-protein condensates crucial for the cellular stress response. P-bodies function mainly in mRNA decay and regulation (Ivanov et al., 2019; Riggs et al., 2020). A core component and nucleator of P-bodies is the DEAD box RNA helicase Dhh1 in yeast, or CGH-1 in *C. elegans* (Mugler et al., 2016; Navarro et al., 2001). Notably, P-bodies assemble under normal conditions without stress and have been shown to interact with germ granules in *C. elegans* embryos and adult germ cells (Du et al., 2023; Gallo et al., 2008). Considering these distinct RNA granules perform critical roles in RNA regulation, whether they interact to coordinate the stress response in germ cells remains an active area of investigation.

Here, we examine the impact of heat stress on RNA granule organization in germ cells. We establish that stress granules and P-bodies form at the germ cell perinucleus in response to stress. In contrast, most germ granule compartments are reduced in size after exposure to stress.

We demonstrate germ granule assembly factors GLH-1 and MIP-1 are required for the formation of perinuclear stress granules and P-bodies. Moreover, germ granule assembly factors are critical for recovery of germline fertility after environmental stress. Overall, our work highlights a critical integrative and protective role for germ granules during stress to coordinate perinuclear stress granule and P-body assembly.

4.3 Results

Heat stress induces perinuclear stress granules and P-bodies in germ cells

Various types of stress stimuli, including heat, oxidative, and osmotic stresses, have been shown to trigger formation of stress granules in the germline (Abbatemarco et al., 2021; Huelgas-Morales et al., 2016; Kuo et al., 2020). For our study, we utilized the stress stimulus of heat shock for the induction of a rapid and robust stress response. First, we examined the localization of conserved stress granule component GTBP-1 after exposure to heat shock (37 °C, 15 min). In the young adult germline of control animals, GTBP-1 is localized evenly throughout the germline cytoplasm (Figure 4.1A). When animals were exposed to heat shock, GTBP-1 assembled into granules throughout the germline (Figure 4.1A). Notably, GTBP-1 formed granules surrounding the germ cell nuclei resembling germ granules (Figure 4.1B). Upon examination of a second stress granule component PQN-59, we similarly found PQN-59 perinuclear granule formation after heat shock, although these granules were less robust compared to GTBP-1 granules (Figure 4.1B).

Stress granules share several components with P-bodies, and P-body assembly has also been shown to be induced during stress conditions (Stoecklin & Kedersha, 2013). Therefore, we next examined the localization of conserved P-body component CGH-1 after exposure to heat

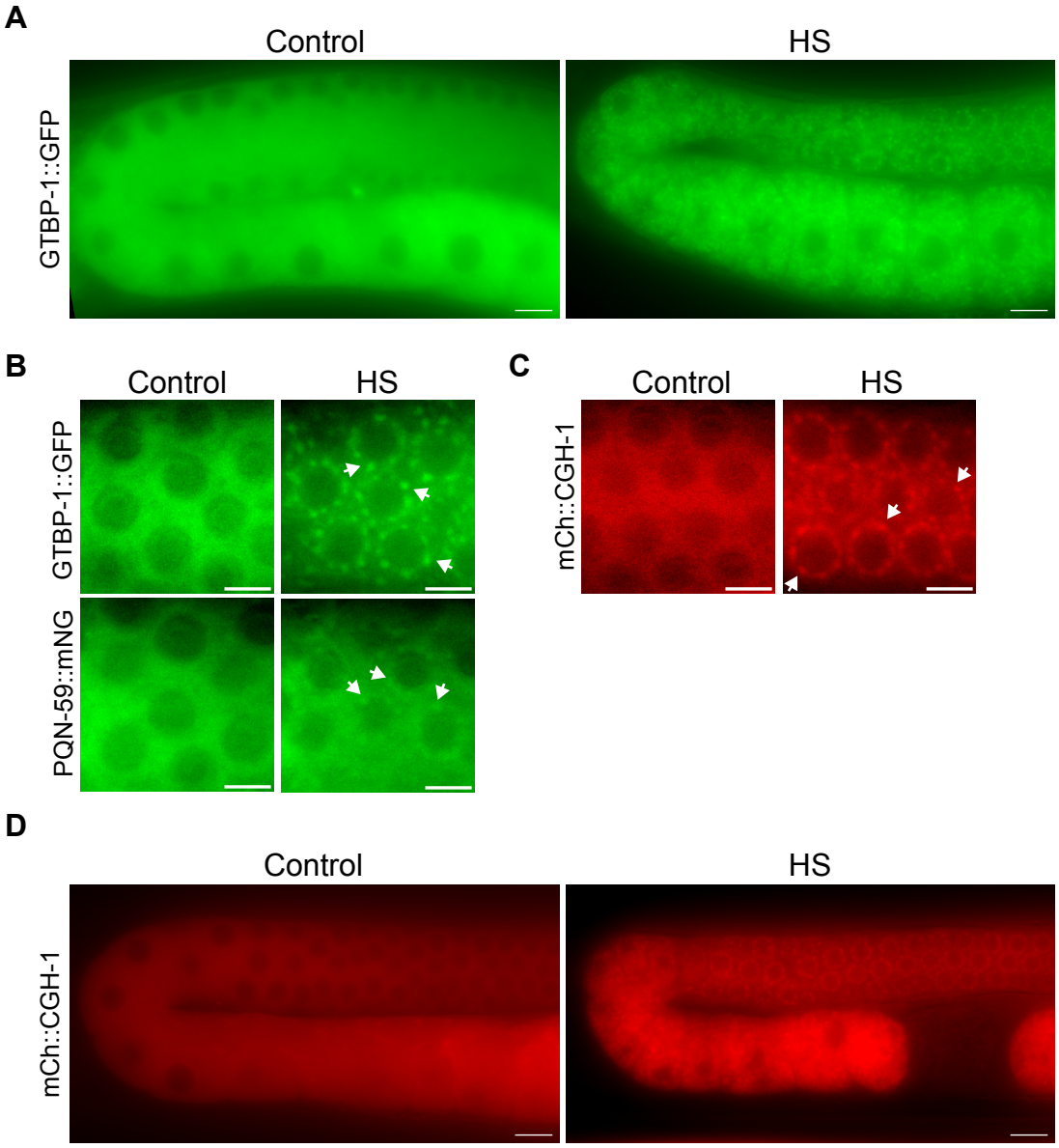

Figure 4.1: Heat stress induced stress granule and P-body formation in germ cells.
(**A**) Representative live-fluorescent images of young adult germlines expressing stress granule marker GTBP-1::GFP. Control germlines of animals grown at 20 °C (left) or animals exposed to heat shock (HS) (37 °C, 15 min) (right). (**B**) Representative live-fluorescent images of young adult pachytene germ cells expressing indicated stress granule markers for the indicated conditions. (**C**) Representative live-fluorescent images of young adult pachytene germ cells expressing P-body marker mCherry::CGH-1 for the indicated conditions. (**D**) Representative live-fluorescent images of young adult germlines expressing P-body marker mCherry::CGH-1 for the indicated conditions. Scale bars = 10 µm for (**A** and **D**) and 5 µm for (**B** and **C**). White arrows point out several examples of granules formed after heat shock.

shock. In the young adult germ cells of control animals, CGH-1 localized evenly throughout the cytoplasm (Figure 4.1C). When animals were exposed to heat shock, CGH-1 assembled into granules surrounding the perinucleus of germ cells (Figure 4.1C). Previously, CGH-1 in normal growth conditions was shown to assemble at the outer layer of germ granules closer to the cytoplasm (Du et al., 2023). However, in our experiments, we did not observe CGH-1 marked perinuclear granules within the germline (Figure 4.1D). We wondered whether P-body assembly at germ granules under normal growth conditions may be stage dependent. For our experiments, we examined young adult animals staged one day after the distinct L4 stage. Upon evaluation of other growth timepoints, we found CGH-1 germ granule localization in germ cells from L4 stage animals, as well as older adults than those used for our experiments.

Overall, we find heat shock induced both stress granule and P-body assembly at the perinucleus of young adult germ cells. Notably, the position of their assembly resembled the site of perinuclear germ granules.

Germ granule compartments are largely disrupted after heat stress

Under normal conditions, germ granules assemble surrounding the perinucleus of germ cells. Germ granules within *C. elegans* are composed of multiple spatially distinct sub-compartments enriched with distinct sets of components (Figure 4.2A). These sub-compartments generally perform different biological functions, many related to small RNA processing (Huang et al., 2025; Phillips & Updike, 2022). Previous studies have demonstrated germ granule factors PGL-1 and MUT-16 lose germ granule enrichment following environmental stress (Uebel et al., 2018; Watkins & Schisa, 2021). In follow up, we wondered whether stress impacts the localization of

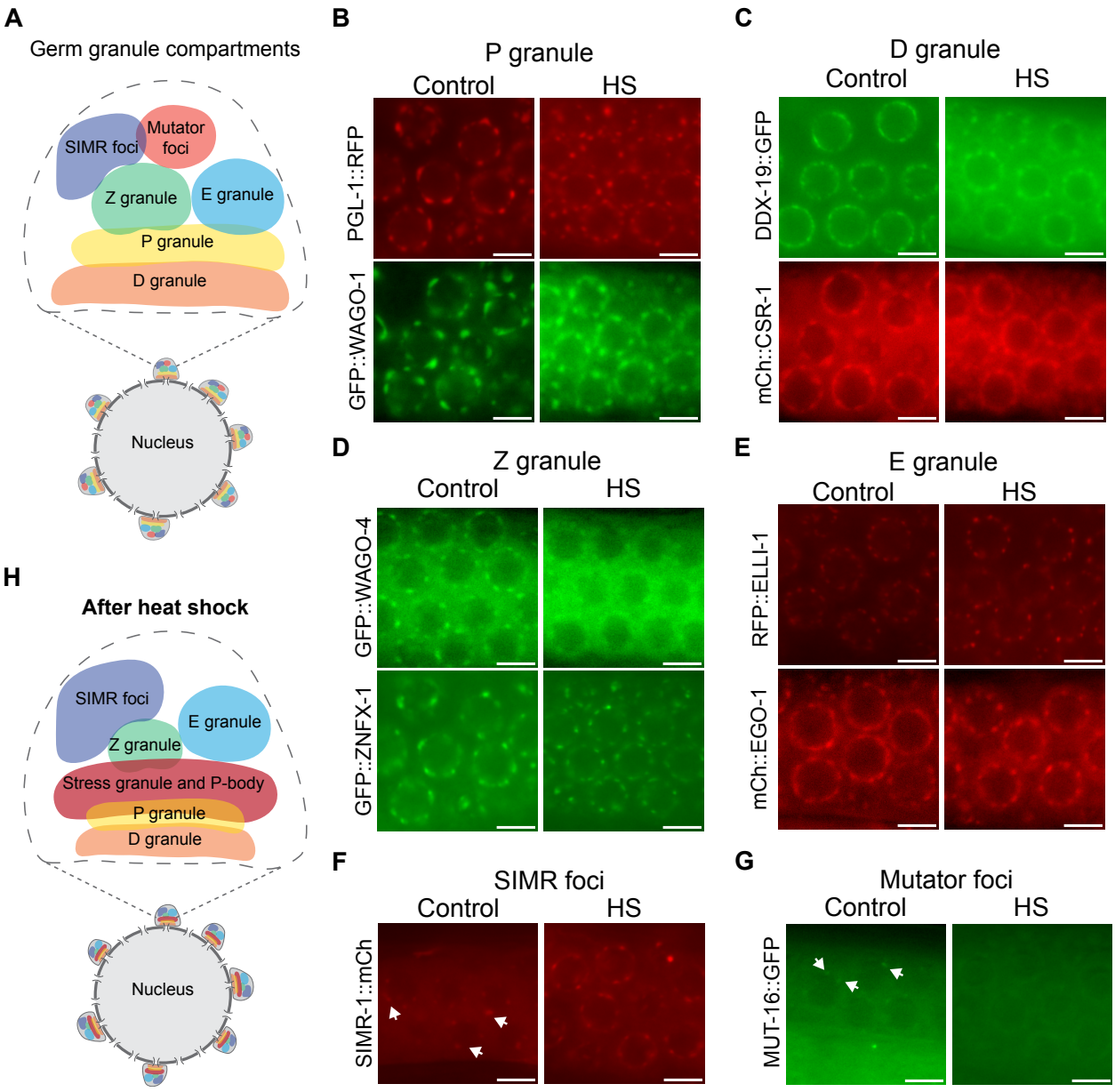

Figure 4.2: Germ granule compartments disrupted after heat stress.
(**A**) Cartoon model illustrating germ granule compartment organization for young adult pachytene germ cells in normal growth conditions. (**B-G**) Representative live-fluorescent images of young adult pachytene germ cells expressing indicated granule compartment or foci markers labeled. Control germlines of animals grown at 20 °C (left) or animals exposed to heat shock (HS) (37 °C, 15 min) (right). Scale bars = 5 µm. (**H**) Cartoon model illustrating germ granule compartment organization after heat shock based on our experimental findings. White arrows point to foci.

specific factors to germ granules, or more broadly impacts germ granule organization. To this aim, we examined the localization of factors from each sub-compartment of germ granules following exposure to heat shock. In result, for P, D, and Z granule compartment markers, we observed reduced granule size and increased cytoplasmic signal in heat shock compared to control animals (Figure 4.2B-D). This suggests components of the P, D and Z compartments largely lose germ granule enrichment after exposure to heat stress. In contrast to these compartments, E compartment markers showed relatively no change in granule localization after heat shock compared to control animals (Figure 4.2E). Together, these findings demonstrate that germ granule sub-compartments are differentially impacted by heat stress.

Next, we examined two distinct germ granule foci, SIMR and Mutator, that under normal conditions are reduced in number per nucleus compared to the other germ granule sub-compartments. First, for SIMR-1 marked SIMR foci, we observed an increase in number of foci per nucleus in animals exposed to heat shock compared to control (Figure 4.2F). In contrast, for MUT-16 marked Mutator foci, we observed complete loss of foci in animals exposed to heat shock compared to control (Figure 4.2G). Our results for MUT-16 matched the previously published findings (Uebel et al., 2018). These findings reveal that germ granule foci exhibit distinct dynamics after heat stress.

Overall, in our examination of germ granule sub-compartments after exposure to heat stress, we find loss of germ granule enrichment for several compartments, including complete loss of the Mutator foci (Figure 4.2H). Together, these results suggest that germ granules largely disassemble following heat stress. However, several compartments maintain normal or increased assembly after stress.

Stress granules and P-bodies form at the site of germ granules

Following stress, we have observed the induction of stress granule and P-body assembly and germ granule disassembly at the germ cell perinucleus. We wondered whether these RNA granules associated together or formed distinct granules at the nuclear periphery. To this aim, we exposed animals to heat shock expressing markers for both stress granules and P granules, GTBP-1 and WAGO-1, respectively. First in the germ cells of control animals, P granules surround the perinucleus, while the stress granule factor localized throughout the cytoplasm (Figure 4.3A and 4.4A). After exposure to heat shock, we observed reduction in P granule size and the assembly of stress granules at the site of remaining P granules (Figure 4.3A and 4.4A). Consistent with these observations, co-localization analysis measured strong correlation between the P-granule and stress granule markers after exposure to heat shock (Figure 4.3B). To further support these results, we examined the localization of another set of stress granule and P granule markers, TIAR-1 and PGL-1, respectively (Huelgas-Morales et al., 2016). We similarly observed overlap of TIAR-1 marked stress granules at the sites of P-granules in heat shock exposed animals (Figure 4.5A-B). Closer inspection of an individual nucleus from heat shocked animals showed that stress granules are positioned partially overlapped and just outside of P granules (Figure 4.3A). These results demonstrate stress granules assemble at similar sites as germ granules but at a spatially distinct compartment.

Next, we examined whether stress granules and P-bodies form at similar perinuclear sites after heat shock in animals expressing markers for both stress granules and P-bodies, GTBP-1 and CGH-1, respectively. First in control animals, both stress granule and P-body markers localize throughout the cytoplasm (Figure 4.3C and 4.4B). After heat shock, both stress granules and P-bodies assemble at similar sites surrounding the germ cell nuclei (Figure 4.3C and 4.4B).

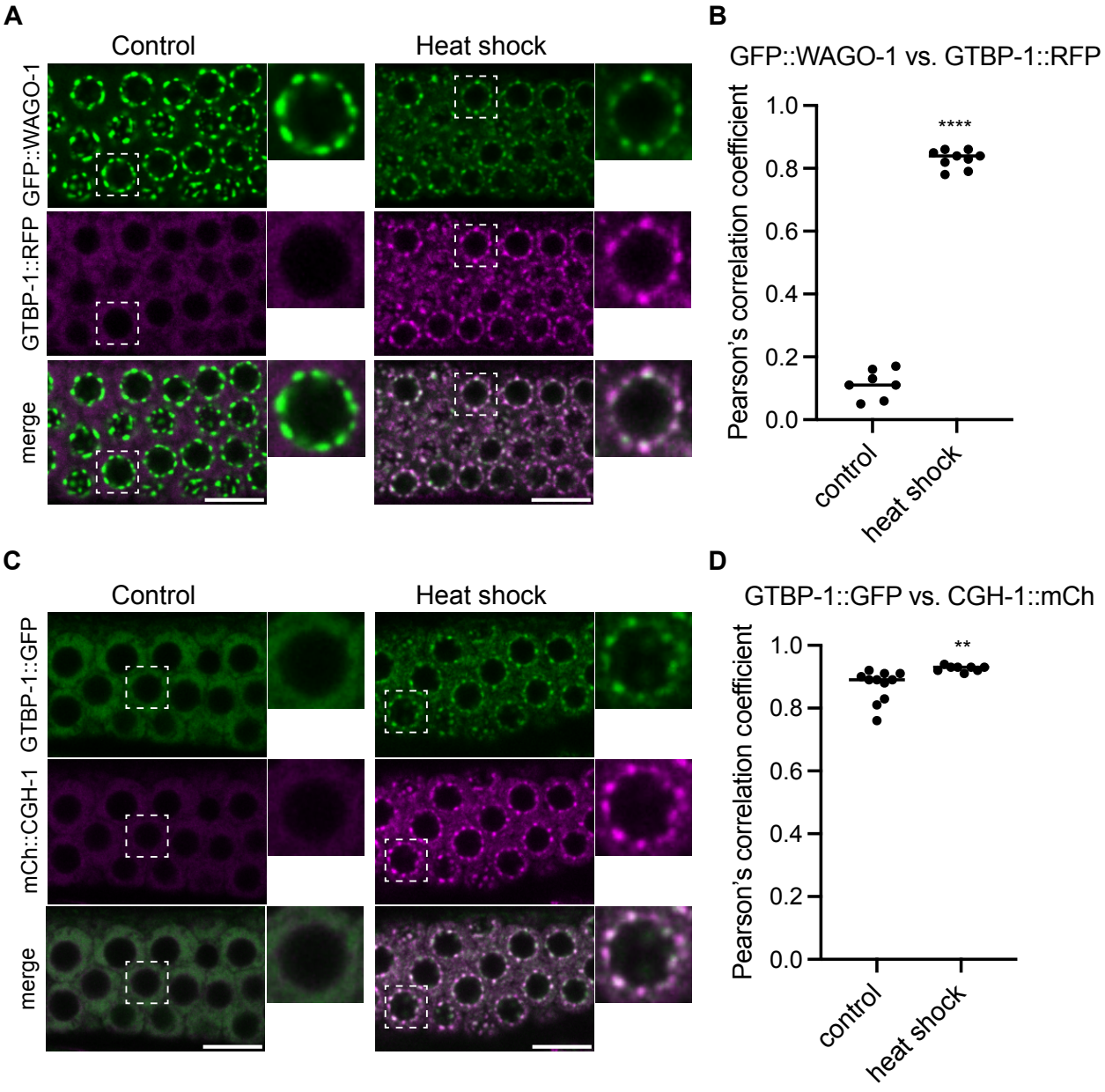

Figure 4.3: Stress granules and P-bodies form at germ granules after heat shock.
(**A**) Representative live-fluorescent images of germ cells co-expressing P granule marker GFP::WAGO-1 and stress granule marker GTBP-1::RFP for the indicated conditions. (**B** and **D**) Quantification of co-localization between the indicated fluorescent proteins. Each data point represents the Pearson's R-value showing the degree of co-localization between two fluorescence channels. The solid black line indicates the mean value. Each data point represents independent gonad images. *N* = 7-10 gonads. Two-tailed p values were calculated using Mann-Whitney-Wilcoxon test. **, p<0.01; ****, p<0.0001. (**C**) Representative live-fluorescent images of germ cells co-expressing stress granule marker GTBP-1::GFP and P-body marker mCh::CGH-1 for the indicated conditions. For all images scale bars = 10 μm. Dashed white boxes outline the individual germ cell shown in the enlarged images.

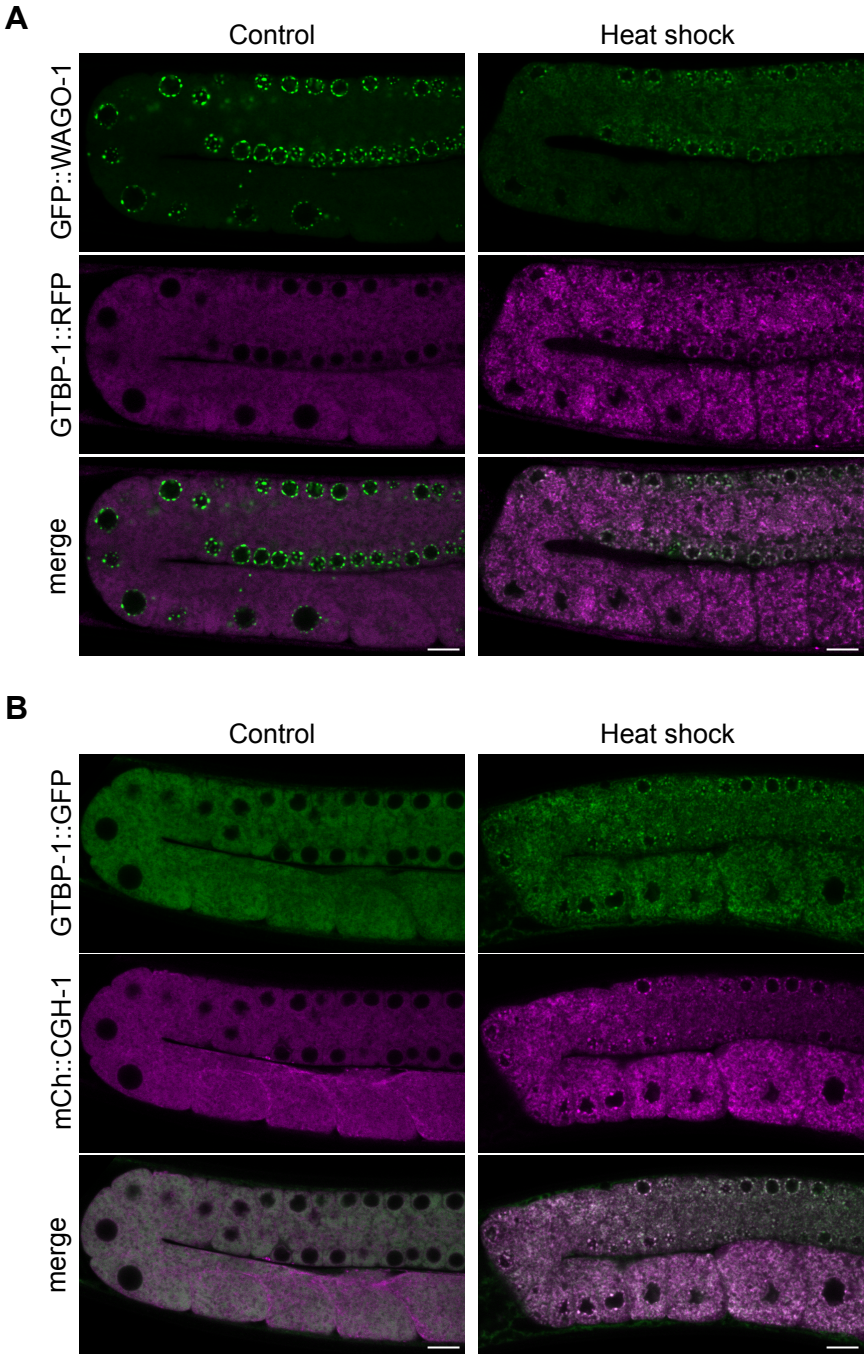

Figure 4.4: Stress granules and P-bodies form throughout germline after heat shock.
(**A**) Representative live-fluorescent images of young adult germlines expressing both P granule marker GFP::WAGO-1 and stress granule marker GTBP-1::RFP for the indicated conditions. (**B**) Representative live-fluorescent images of young adult germlines expressing both stress granule marker GTBP-1::GFP and P-body marker mCh::CGH-1 for the indicated conditions. Scale bars = 10 µm.

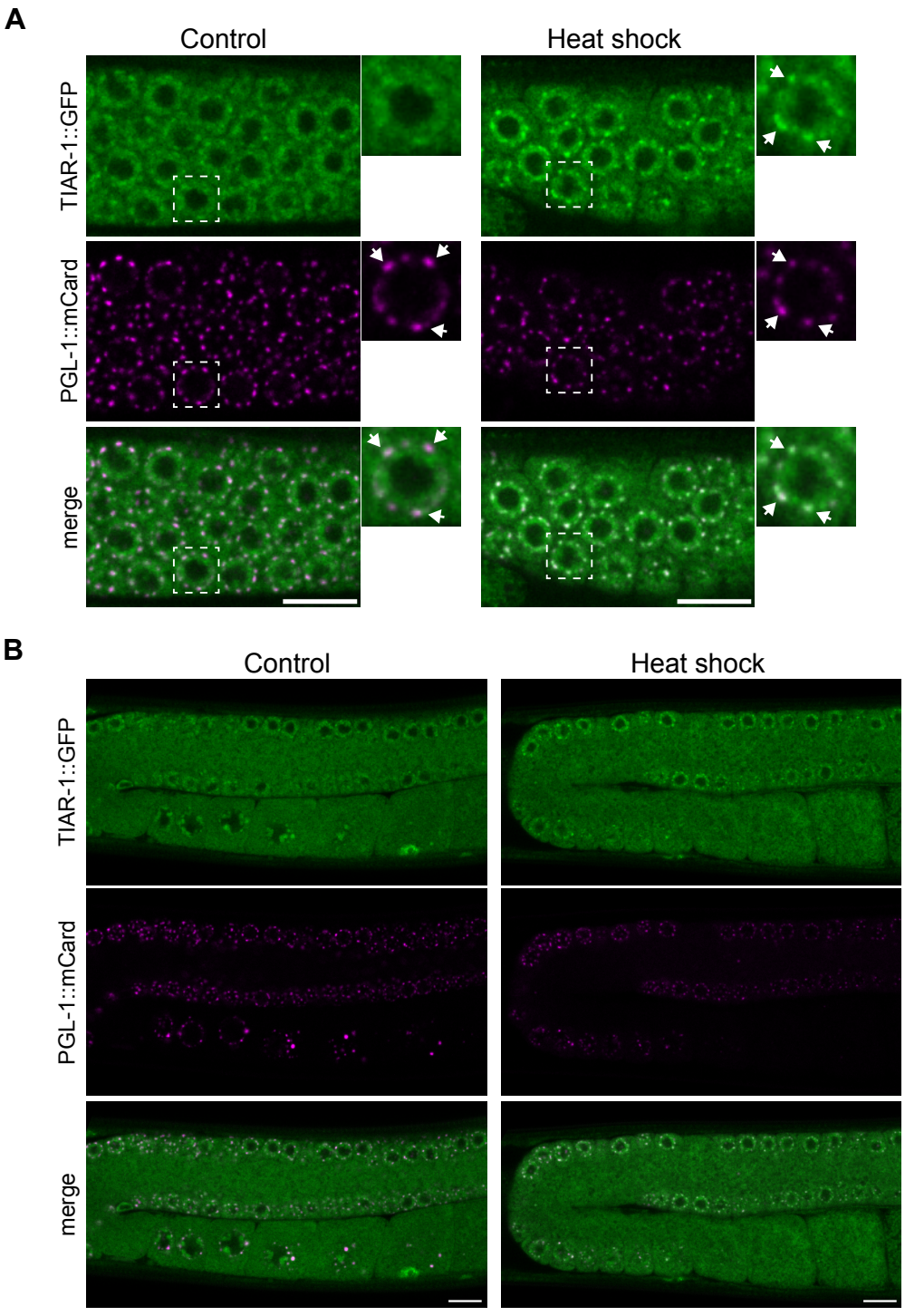

Figure 4.5: Stress granules form adjacent to germ granules after heat shock.
(**A** and **B**) Representative live-fluorescent images of young adult pachytene germ cells (**A**) or entire germline (**B**) in animals co-expressing stress granule TIAR-1::RFP and P granule PGL-1::mCardinal markers for the indicated conditions. Dashed white boxes outline the nucleus shown enlarged to the right. Arrows point to granules. Scale bars = 10 µm.

Consistent with these observations, co-localization analysis showed strong correlation between stress granule and P-body markers in both control and heat shock conditions (Figure 4.3D). Moreover, the stress granule and P-body markers showed slightly higher co-localization compared to the stress granule and P-granule markers. However, again stress granules and P-bodies did not show perfect overlap, suggesting they form distinct granules. Together, our findings indicate that following heat stress, closely associated stress granules and P-bodies form at the site of germ granules.

Germ granules promote perinuclear stress granule and P-body assembly

Based on our results that stress granules and P-bodies assemble near germ granules after heat stress, we hypothesized that germ granule assembly may be important for their formation at the perinucleus. Alternatively, stress granules and P-bodies may form at the germ cell perinucleus independent of germ granule assembly. To test this, we performed RNAi knockdown of germ granule assembly factors GLH-1 and MIP-1. Loss of these germ granule factors results in well-characterized defects in germ granule assembly and function (W. Chen et al., 2022; Cipriani et al., 2021; Marnik et al., 2019). We performed these knockdowns in animals expressing both stress granule and P-body markers in control and heat shock conditions. In control knockdown animals, we observed the expected induction of perinuclear stress granule and P-bodies after exposure to heat shock (Figure 4.6A). In both *glh-1* and *mip-1* knockdown animals, we observed greatly reduced formation of perinuclear stress granules and P-bodies after exposure to heat shock (Figure 4.6A). Quantification of the number of stress granules and P-bodies formed per germ cell nucleus showed reduced number of heat-induced stress granules and P-bodies in *glh-1* and *mip-1* knockdown animals compared to control knockdown animals (Figure 4.6B). These

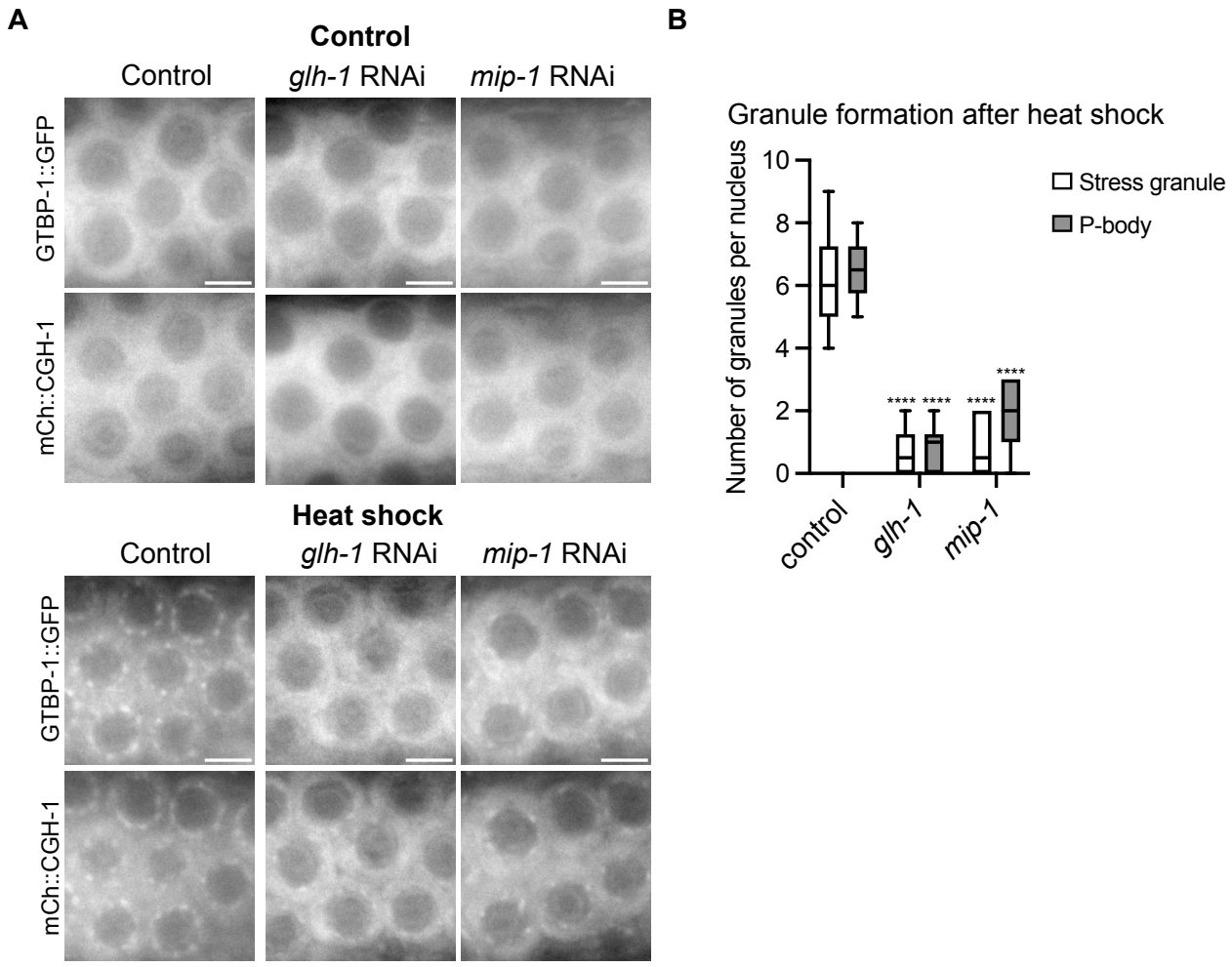

Figure 4.6: Germ granules promote heat stress induced stress granule and P-body perinuclear formation.

(**A**) Representative live-fluorescent images of young adult pachytene germ cells expressing both stress granule marker GTBP-1::GFP and P-body marker mCh::CGH-1 for control, *glh-1*, or *mip-1* RNAi conditions for control or exposure to heat shock conditions. Scale bars = 5 μm. (**B**) Boxplots showing the number of granules per germ cell nucleus for stress granule marker or P-body marker for animals exposed to heat shock. For the boxplots, the line indicates the median value, the box indicates the first and third quartiles, and the whiskers indicate the min and max values. Two-tailed p values were calculated using Mann-Whitney-Wilcoxon test. ****, $p<0.0001$.

results indicate germ granule assembly factors facilitate perinuclear stress granule and P-body assembly.

To further support these findings, we performed the same knockdowns in animals expressing a different set of P granule and stress granule markers in control and heat shock conditions. First in the control condition without heat stress, knockdown of *glh-1* resulted in reduced enrichment and number of WAGO-1 marked P granules compared to P granules in control knockdown animals (Figure 4.7, A-B). In the control condition without heat stress, knockdown of *mip-1* resulted in a reduced number of enlarged WAGO-1 marked P granules compared to P granules in control knockdown animals (Figure 4.7A-B). These results indicate successful knockdown of these factors and reflect the slightly different roles of GLH-1 and MIP-1 in germ granule assembly. In animals exposed to heat shock, we observed further reduction in number of WAGO-1 marked P-granules in control, *glh-1*, and *mip-1* knockdown animals (Figure 4.7A-B). For the stress granule marker, RNAi knockdown of *glh-1* and *mip-1* both resulted in decreased stress granule formation compared to control knockdown animals after heat shock (Figure 4.7A and C). Overall, these results suggest germ granule assembly factors promote stress granule and P-body assembly at the perinucleus of germ cells during stress.

Stress granules and P-bodies form independently at the perinucleus after stress

Based on our findings that stress granule and P-body assembly at the nuclear periphery depends on germ granule assembly factors, we next asked whether stress granule and P-body assembly occurs independently of each other. Based on evidence in other organisms, these granules are largely proposed to form independently (Stoecklin & Kedersha, 2013). However, one study in

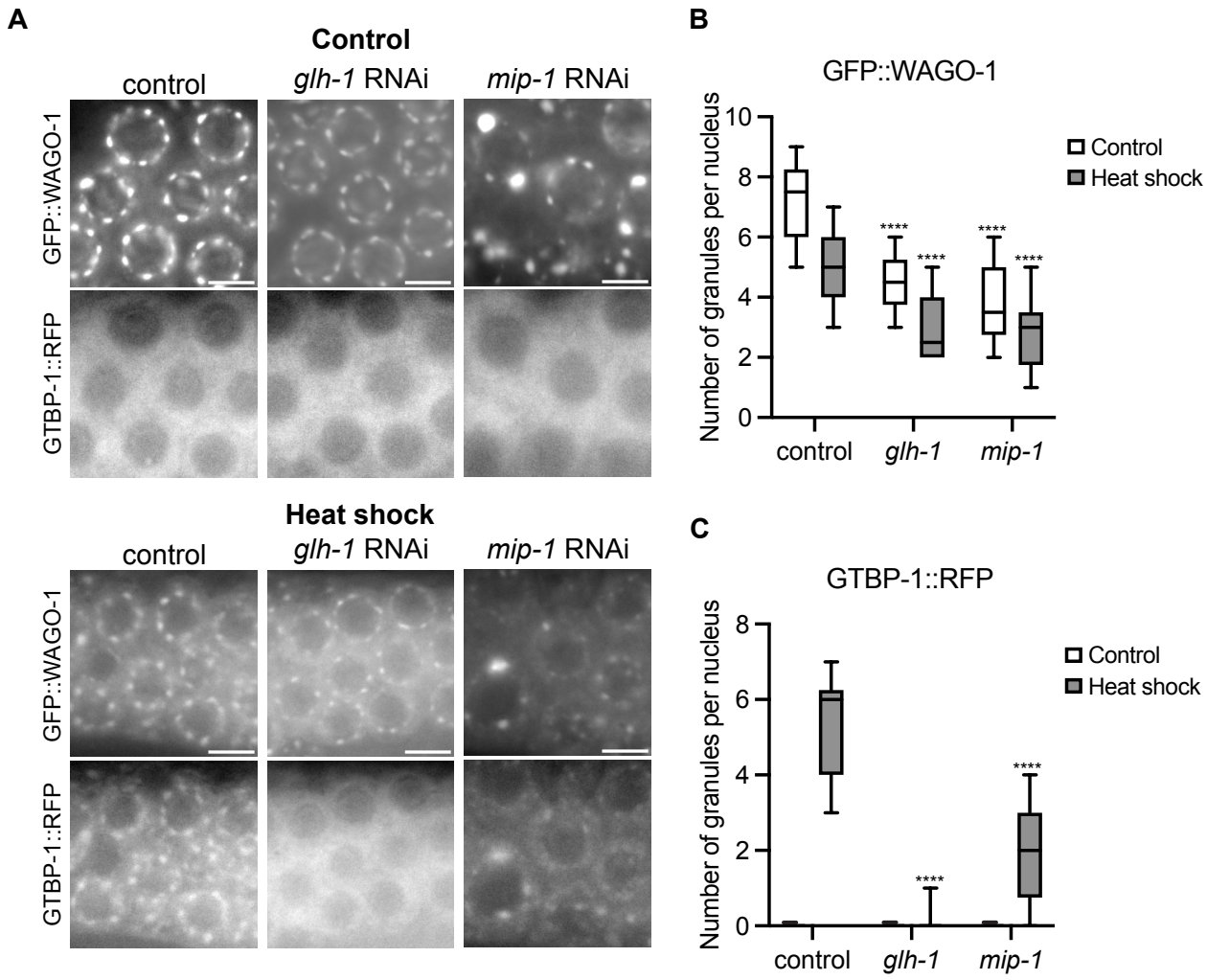

Figure 4.7: Germ granule assembly factors promote stress granule and P-body perinuclear formation after heat shock.

(**A**) Representative live-fluorescent images of young adult pachytene germ cells expressing both P granule marker GFP::WAGO-1 and stress granule marker GTBP-1::RFP for control, *glh-1*, or *mip-1* RNAi conditions for control or exposure to heat shock conditions. Scale bars = 5 µm. (**B**) Boxplots showing the number of granules per germ cell nucleus for P granule marker GFP::WAGO-1 for RNAi conditions and control or heat shock animals. (**C**) Boxplots showing the number of granules per germ cell nucleus for stress granule marker GTBP-1::RFP for RNAi conditions and control or heat shock animals. For all boxplots, the line indicates the median value, the box indicates the first and third quartiles, and the whiskers indicate the min and max values. Two-tailed p values were calculated using Mann-Whitney-Wilcoxon test. ****, $p<0.0001$.

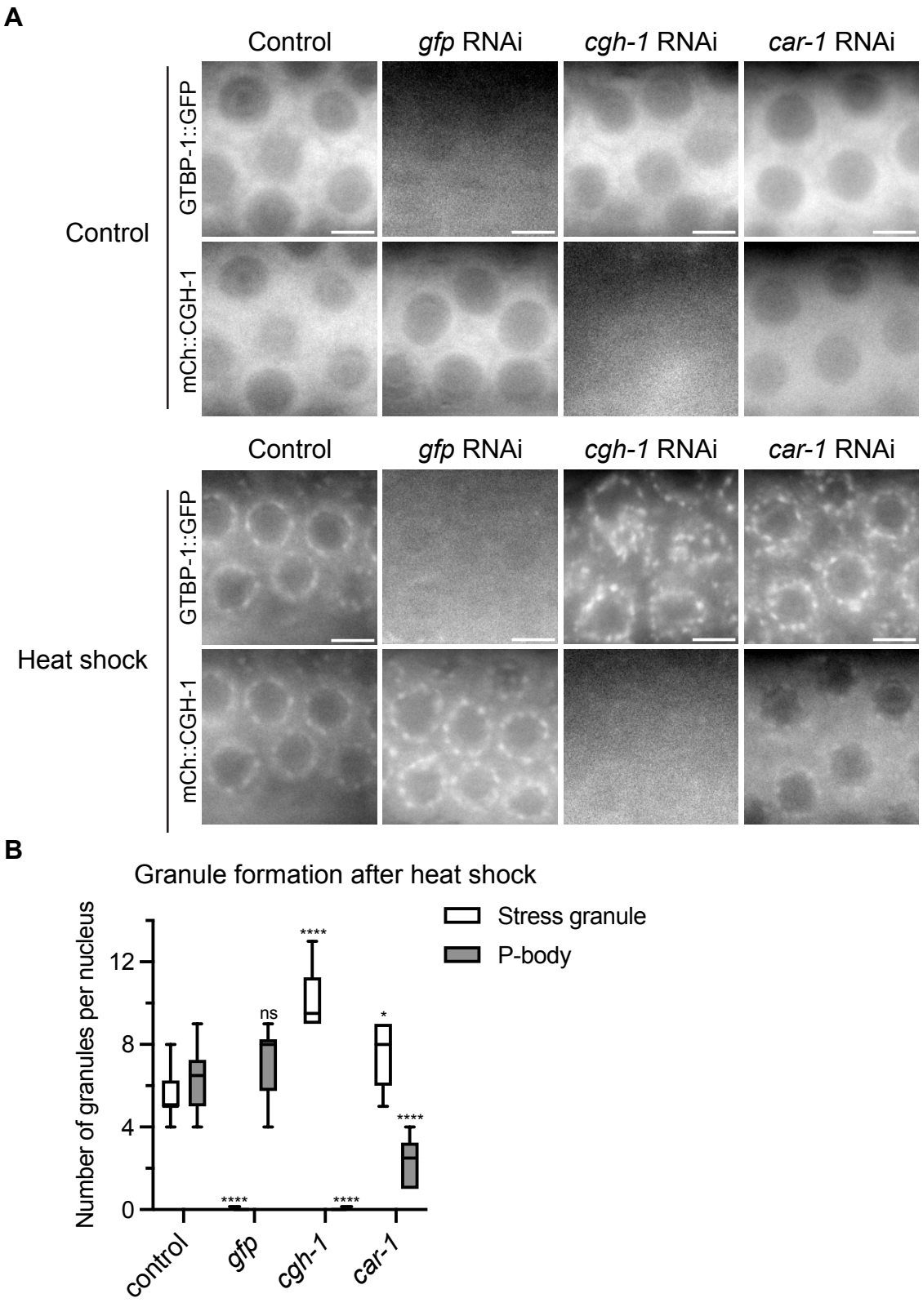

Figure 4.8: Heat stress induced perinuclear stress granules and P-bodies form independently.

Figure 4.8 continued
(**A**) Representative live-fluorescent images of young adult pachytene germ cells co-expressing stress granule marker GTBP-1::GFP and P-body marker mCh::CGH-1 for control, *gfp-1*, *cgh*-1, or *car-1* RNAi conditions for control or exposure to heat shock conditions. Scale bars = 5 μm. (**B**) Boxplots showing the number of granules per germ cell nucleus for stress granule marker or P-body marker for animals exposed to heat shock. For the boxplots, the line indicates the median value, the box indicates the first and third quartiles, and the whiskers indicate the min and max values. Two-tailed p values were calculated using Mann-Whitney-Wilcoxon test. *, $p<0.05$; ****, $p<0.0001$.

mammalian cells observed that P-body factor DDX6 (CGH-1) promoted the assembly of both P-bodies and stress granules in stress conditions, highlighting that stress granules do not always form independently (Majerciak et al., 2023). To test this, we performed RNAi knockdown of the stress granule core factor GTBP-1 and P-body assembly factors CGH-1 and CAR-1. We performed these knockdowns in animals expressing both stress granule and P-body markers in control and heat shock conditions. First, to knockdown GTBP-1, we utilized RNAi targeting *gfp* in animals expressing tagged *gtbp-1::gfp* at the endogenous gene locus. As a result, in both control and heat shock conditions, *gtbp-1::gfp* knockdown resulted in complete loss of GTBP-1::GFP signal (Figure 4.8A-B). In heat shock conditions, P-bodies still formed in *gtbp-1::gfp* knockdown animals (Figure 4.8A-B). This result suggests P-bodies form at the perinucleus independent of stress granule factor GTBP-1.

Next, we examined whether stress granule formation requires P-body assembly. In *cgh-1* and *car-1* knockdown, we observed reduced or complete loss of P-bodies marked by CGH-1 compared to control knockdown animals after exposure to heat shock (Figure 4.8A-B). In contrast, knockdown of *cgh-1* and *car-1* resulted in increased stress granule formation compared to control knockdown animals after heat shock (Figure 4.8A-B). These findings suggest stress granules assemble independent of P-bodies in germ cells after stress. These stress granules formed an increased number per nucleus in animals with reduced P-body function.

Germ granule assembly factors promote germ cell recovery from heat stress

Since we found germ granule assembly promoted stress granule and P-body formation at germ cell nuclei after heat shock, we wondered whether germ granules contribute to recovery after stress. The stress response, including stress granule and P-body induction, is critical for cellular

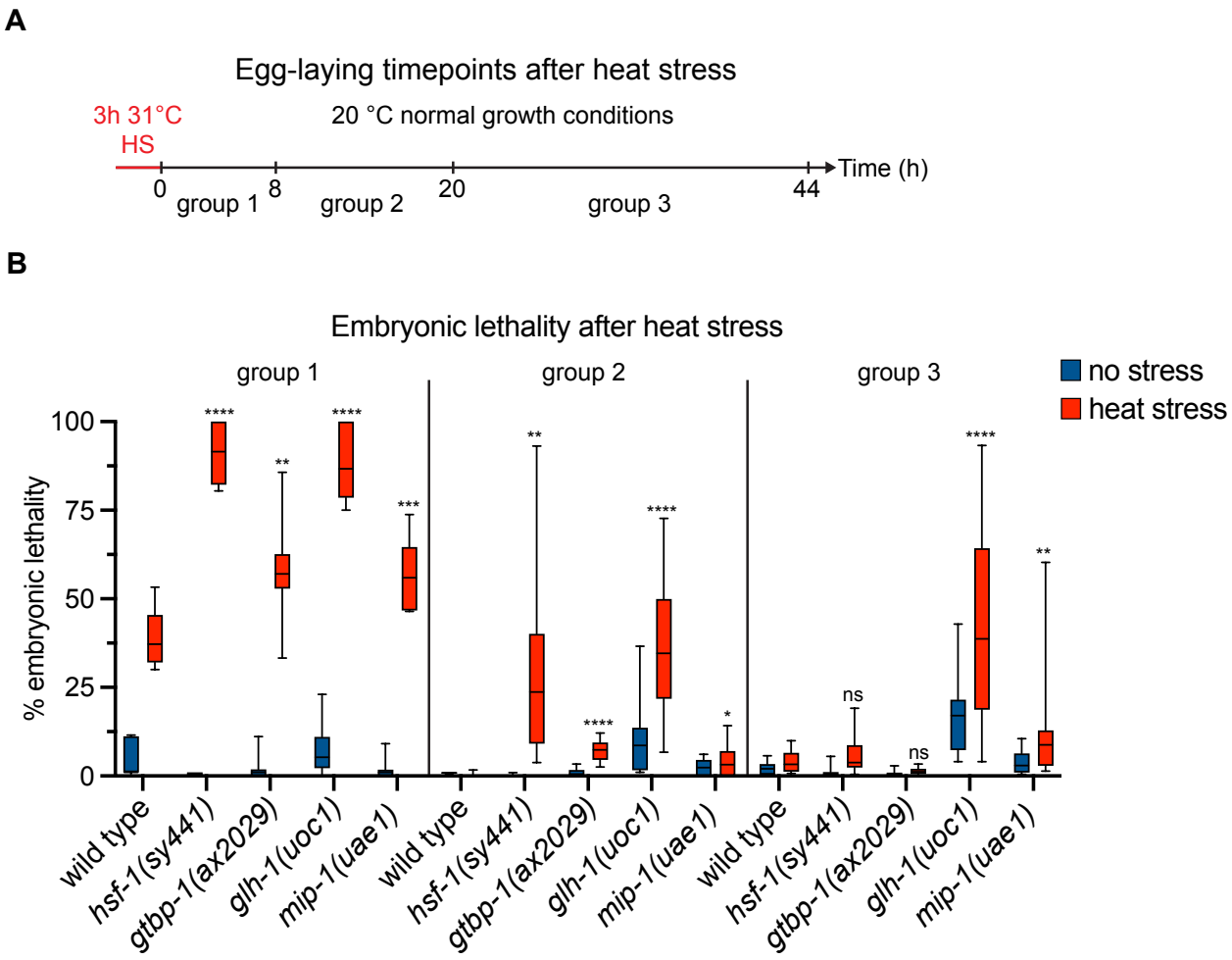

Figure 4.9: Germ granule assembly factors promote germ cell recovery after heat stress. (**A**) Experiment timeline outlining heat stress (HS) and transfer of animals to normal growth conditions. At normal growth conditions, animals were transferred at time points to separate eggs/ embryos laid. Groups indicate the timing of embryos laid after heat stress. (**B**) Boxplots showing the total number of unhatched embryos divided by the total number of embryos laid as a percentage, percentage of embryonic lethality. Strains and conditions indicated. Groups reflect quantification of embryos laid in time point groups shown in (**A**). For the boxplots, the line indicates the median value, the box indicates the first and third quartiles, and the whiskers indicate the min and max values. Two-tailed p values were calculated using Mann-Whitney-Wilcoxon test. *, $p<0.05$, **, $p<0.01$; ***, $p<0.001$; ****, $p<0.0001$; ns, no significance.

and organismal recovery from environmental stressors (Huelgas-Morales et al., 2016; Kuo et al., 2020). Based on our findings, we wondered if germ granule assembly factors contribute to germ cell recovery after stress. Germ cell viability is greatly reduced during exposure to heat stress (31 °C, 3 hours), but viability recovers when animals are shifted back to normal temperature conditions (Figure 4.9A-B). The recovery of germ cell viability, or reduced embryonic lethality, observed in wild-type animals requires the stress response (Pakos-Zebrucka et al., 2016; Servello & Apfeld, 2020). Animals with defects in the stress response, either Heat shock factor 1 ortholog *hsf-1(sy441)* hypomorph mutant or *gtbp-1(ax2029)* null mutant, showed increased embryonic lethality compared to wild type immediately following heat stress (group 1 in Figure 4.9A-B). These mutants also displayed delayed recovery of embryo viability compared to wild type (group 2 and 3 in Figure 4.9A-B).

Next, we tested the role of germ granule assembly factors GLH-1 and MIP-1 in germline recovery following heat stress. As a result, both *glh-1(uoc1)* null mutant and *mip-1(uae1)* null mutant animals showed increased embryonic lethality immediately following heat stress compared to wild type (group 1 in Figure 4.9A-B). Additionally, both *glh-1(uoc1)* and *mip-1(uae1)* mutant animals displayed delayed recovery of embryo viability compared to wild type (group 2 and 3 in Figure 4.9A-B). Germ granule assembly factors are also known to contribute to fertility in normal growth conditions. This may contribute to the lack of recovery in embryonic viability observed in *glh-1(uoc1)* and *mip-1(uae1)* mutants compared to wild-type animals (group 3) (Figure 4.9B). Together, our findings suggest germ granules promote germ cell recovery after heat stress, like well-known stress response factors.

4.4 Discussion

Animals experience various environmental stressors and must coordinate a stress response to protect normal cellular functions. In this study, we found a previously undescribed role for germ granules in stress granule and P-body formation at the nuclear periphery of germ cells (Figure 4.10). Specifically, we found their formation depended largely on germ granule assembly factors GLH-1 and MIP-1. Potentially linked to this role, we demonstrated that germ granule assembly factors, GLH-1 and MIP-1, were critical for germline recovery after environmental heat stress. Additionally, we found heat shock largely disrupted germ granule compartments, including factors critical for RNA interference and small RNA-based inheritance (Figure 4.10). This disruption to germ granule compartment organization may lead to the previously reported defects in small RNA-mediated gene silencing and inheritance after exposure to environmental stress (Houri-Zeevi et al., 2021).

Our lab previously identified an interaction between germ granules and P-bodies in adult germ cells under normal growth conditions. P-bodies were found to promote the compartmentalization of germ granules necessary for the robust inheritance of small RNA-based gene silencing (Du et al., 2023). This same work identified Z granule factor Argonaute WAGO-4 as the link to the transgenerational silencing defect observed in *cgh-1* mutants. After stress, we observed disrupted WAGO-4 Z granule localization, as well as complete dispersal of the Mutator foci. Components of these granules perform well-described roles in RNAi-triggered gene silencing and inheritance. Our findings suggest the specific disruption of these granules may contribute to the reported RNAi and transgenerational silencing defects observed after stress (Houri-Zeevi et al., 2021). In line with our observations, this published report found that animals exposed to stress showed drastically reduced *Mutator*-dependent small RNAs compared to

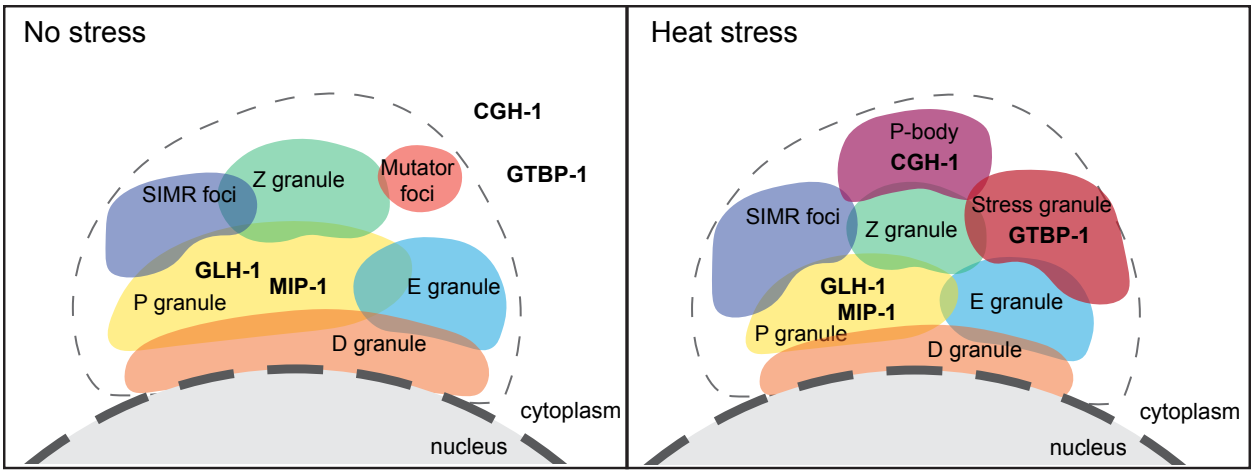

Figure 4.10: Model illustrating germ granule compartments in response to heat stress. Germ granule compartments are disrupted in response to heat stress. Heat stress induces stress granules and P-bodies formation at germ granules. Germ granule assembly factors GLH-1 and MIP-1 promote stress granule (GTBP-1) and P-body formation (CGH-1) at germ granules in response to heat stress. Stress granules (GTBP-1) and P-bodies form (CGH-1) at germ granules independent of each other although close in proximity.

control animals. In contrast, they found CSR-1-dependent small RNAs were upregulated following stress. In line with this, we observed CSR-1 small RNA biogenesis factors, CSR-1 and EGO-1, largely maintained granule localization after stress. Together, our findings highlight that environmental stress leads to specific changes in germ granule organization that correspond to changes in the small RNA populations and function.

Stress granules and P-bodies are clearly distinguishable RNA granules but also share many components and mRNAs. They often assembly in proximity to each other during stress, suggesting they may coordinate mRNA storage and degradation. Interestingly, previous studies identified that the mammalian ortholog of CGH-1, DDX6, promoted the formation of both P-bodies and stress granules in cells exposed to stress (Majerciak et al., 2023). This finding revealed that in certain conditions, stress granule assembly depends on P-bodies. In our findings, stress granule assembly was intact and perhaps even more robust in germ cells during knockdowns of core P-body assembly factors CGH-1 or CAR-1. Additionally, heat-induced P-body assembly continued during knockdown of stress granule factor GTBP-1. Although we also observed stress granules and P-bodies closely associated, we found their assembly occurs independently in *C. elegans* adult germ cells after stress. Taken together, our studies highlight the environment and cell context dependent interactions between distinct RNA granules.

Germ granules perform well-established roles in germ cell development and inheritance. Here, we uncover a crucial role for germ granules in protecting germ cells from heat stress. Our study identifies an interaction between germ granules, P-bodies, and stress granules after exposure to environmental stress. The assembly of stress granules and P-bodies depended on germ granule assembly factors GLH-1 and MIP-1. This suggested docking of the P-body and stress granule at the nuclear periphery required interactions with either germ granule RNAs or

specific protein components. Our findings suggest that germ granules may facilitate the stress response by promoting stress granule and P-body assembly at the nuclear periphery in germ cells. Notably, in somatic cells stress granules and P-bodies form dispersed in the cytoplasm (Banani et al., 2017). Whether their specific formation adjacent to germ granules is critical for their function in germ cells remains unclear. Germ granules may also contribute to stress recovery through broader roles in RNA regulation and small RNA processing. Overall, our work expands our understanding of how distinct types of RNA granules coordinate the recovery of germ cell function after environmental stress.

4.5 Methods

Caenorhabditis elegans strains and maintenance

Animals were grown on standard nematode growth media (NGM) plates seeded with the Escherichia coli OP50 strain at 20 °C.

Table 4.1: List of *C. elegans* strains used in this study.

Strain	Genotype	Gene(s)	Origin
N2	*C. elegans wild isolate (Bristol)*		CGC
JH3308	*gtbp-1(ax5000[gtbp-1::tagRFP]) IV*	*gtbp-1*	CGC
JH3199	*gtbp-1(ax2055[gtbp-1::GFP]) IV*	*gtbp-1*	CGC
USC744	*simr-1(cmp15[simr-1::mCherry::2xHA loxP Cbr-unc-119 loxP]) mut-16(cmp3[mut-16::gfp::3xFLAG + loxP]) I; unc-119(ed3) III*	*simr-1; mut-16*	CGC
YY968	*znfx-1(gg544[3xflag::gfp::znfx-1]) II; pgl-1(gg547[pgl-1::3xflag::tagRFP]) IV*	*znfx-1; pgl-1*	CGC
DG3922	*tiar-1(tn1545[tiar-1::s::tev::GFP]) II*	*tiar-1*	CGC
DZ419	*GFP::wago-4 II; mCherry::cgh-1 III*	*wago-4; cgh-1*	Z Du et al. 2023
JMC219	*tor113[GFP::3xFLAG::wago-1] I*	*wago-1*	CGC
GLW63	*pqn-59(utx51[mNG::3xFlag::pqn-59]) I*	*pqn-59*	CGC
SHG1936	*ego-1(ust356[mCherry::ego-1]) I*	*ego-1*	CGC

Table 4.1 continued

HCL390	*wago-1(tor113[GFP::3xFLAG::wago-1]) I; gtbp-1(ax5000[gtbp-1::tagRFP]) IV*	*wago-1; gtbp-1*	This study
SHG1941	*ustIS268[mex-5p::tagrfp::elli-1::tbb-2_3'UTR] I*	*elli-1*	X Chen et al. 2024
HCL391	*mCherry::cgh-1 III; gtbp-1(ax2055[gtbp-1::GFP]) IV*	*cgh-1; gtbp-1*	This study
HCL392	*tiar-1(tn1545[tiar-1::s::tev::GFP]) II; pgl-1(gg640[pgl-1::3xflag::mCardinal]) IV*	*tiar-1; pgl-1*	This study
SHG2207	*ddx-19(ust399[ddx-19::GFP::3xFlag]) II*	*ddx-19*	CGC
YY1492	*mut-16(cmp3[mut-16::gfp::flag + loxP] I; znfx-1(gg634[HA::tagRFP::znfx-1]) II; pgl-1(gg640[pgl-1::3xflag::mCardinal]) IV*	*mut-16; znfx-1; pgl-1*	CGC
HCL336	*pgl-1(gg640[pgl-1::3xflag::mCardinal]) IV*	*pgl-1*	This study
HCL376	*wago-1(tor113[GFP::3xFLAG::wago-1]) I; csr-1(gc029[degron::mCherry::3xflag::ha::csr-1]) IV*	*wago-1; csr-1*	This study
GKC1	*mip-1(uae1) III*	*mip-1*	CGC
HCL118	*glh-1(uoc1) I*	*glh-1*	W Chen et al. 2020
JH3176	*gtbp-1(ax2029) IV*	*gtbp-1*	CGC
PS3551	*hsf-1(sy4441) I*	*hsf-1*	CGC
MHE69	*ieSi64 [gld-1p::TIR1::mRuby::gld-1 3'UTR + Cbr-unc-119(+)] II; csr-1(gc029[degron::mCherry::3xflag::ha::csr-1]) IV*	*csr-1*	P Quarato et al. 2020

Heat shock assay

Day before heat shock fifty L4 stage worms were transferred to new plate. Next day fifteen worms per condition were transferred to 2% agarose pad on slide with M9 buffer [22 mM KH2PO4, 42 mM Na2HPO4, and 86 mM NaCl] with 10–50 mM levamisole. For controls, animals kept on slide at room temperature for 15 minutes. For heat shock group, slides were placed on aluminum block kept inside 37 °C incubator. Slides were imaged immediately after 15 minutes on a Zeiss compound microscope.

RNA interference

RNAi was performed by feeding animals with *E. coli* HT115 (DE3) strains expressing the appropriate dsRNA. RNAi bacterial strains were obtained from the Ahringer *C. elegans* RNAi Collection (Source BioScience). Bacterial cultures were grown in Luria broth supplemented with 100 μg/mL ampicillin and 50 μg/mL tetracycline overnight at 37°C. Cultures were seeded on NGM plates containing 100 μg/mL ampicillin, 50 μg/mL tetracycline, and 1 mM IPTG and incubated at room temperature for 24 hours. HT115 (DE3) expressing empty RNAi vector L4440 was used for control. RNAi conditions were seeded in duplicate and fifty L1 stage animals were transferred to each plate. After three days, young adult animals were used in the heat shock assay described above.

Confocal live imaging

Tagged fluorescent proteins were visualized in living nematodes by mounting young adult animals on 2% agarose pads with M9 buffer (22 mM KH_2PO4, 42 mM Na_2HPO4, and 86 mM

NaCl) with 30 mM levamisole. Fluorescent images used for localization studies were captured using a Zeiss LSM800 confocal microscope with a Plan-Apochromat 40×/1.4 Oil objective.

Image processing and analysis

Image processing and quantification of fluorescent puncta were performed using ImageJ. Single slice images of gonads were used for quantification. ROIs were selected, and areas of ROIs were measured. For quantitative co-localization analysis, all image manipulations were performed with ImageJ using the Coloc 2 plugin. Images of 7–10 gonads were collected and quantified. Data were compared by two-tailed p values were calculated using Mann-Whitney-Wilcoxon test.

Heat stress embryonic lethality assay

Day before heat stress assay fifty L4 stage worms were transferred to new plate. On the next day, twenty-five worms per genotype were transferred to new plate. Animals remaining on the original plate were used as control animals. For heat stress condition, these new plates were wrapped with parafilm to make airtight. Plates were submerged in temperature-controlled water bath held at 31 °C. After 3 hours, ten worms were transferred to single plates at 20 °C normal growth temperature. For controls, ten worms were transferred to single plates at 20 °C normal growth temperature from the original plate. After 8 hours, adult heat stress and control worms were transferred to new single plate. Embryos laid during 0 to 8 hours after heat stress or controls are group 1. Total embryos laid per plate was recorded for group 1. After 12 more hours, worms were transferred to new single plate. Embryos laid during 8 to 20 hours after heat stress or controls are group 2. Total embryos laid per plate was recorded for group 2. After 24 more hours, worms were transferred to new single plate. Embryos laid during 20 to 44 hours after heat

stress or controls are group 3. Total embryos laid per plate was recorded for group 3. For each group of embryos, 24 hours after parent worms were transferred off plates, hatched larvae were counted. Total number of lethal embryos were measured by subtracting number of hatched larvae from total embryos counted the day before. Unhatched embryos over total embryos laid are shown as percentage and labeled percentage of embryonic lethality. Complete experiment was performed twice.

CHAPTER 5

Discussion: conclusions and future directions

Since the discovery of small RNAs uncovered a new conserved mechanism of gene regulation, the types of small interfering RNAs and their physiological roles continue to expand. Perhaps most extensively studied are the small RNAs, including siRNAs and piRNAs, that guard the genetic integrity of germ cells. These small RNAs detect and robustly silence mutagenic viral and transposon RNAs. Intriguingly, recent studies have elucidated broader roles for these germline small RNAs in endogenous gene regulation, complicating our understanding of how small RNAs distinguish and regulate the proper mRNA targets during germ cell development.

In this dissertation, I investigated the regulation and sub-compartment germ granule organization of germline small RNA pathways. In Chapter 2, I identified RNA helicase RHA-1 as a key regulator of small RNA sorting and uncovered a fundamental mechanism by which germ cells distinguish "self" from "non-self" RNAs. My work in Chapter 3 explored how small RNA pathway competition regulates sex-dependent RNAi activity and inheritance. In Chapter 4, I demonstrated how germ granules adapt following environmental stress to protect germ cell fertility. In this chapter, I will discuss several outstanding questions and future directions prompted by my thesis work.

How are "self" mRNAs recognized?

As described throughout this dissertation, CSR-1 small RNAs target endogenous germline-expressed mRNAs or "self" RNAs, while WAGO small RNAs target "non-self" RNAs like transposons. Although these Argonautes target distinct sets of mRNAs, they bind molecularly indistinguishable secondary siRNAs termed 22G-RNAs. These 22G-RNAs are synthesized by

RNA-dependent RNA polymerases RRF-1 and EGO-1 directly from mRNA transcripts (W. Gu et al., 2009). The production of WAGO secondary siRNAs is triggered downstream of primary siRNAs, either siRNAs from RNAi or piRNAs. As a result, loss of these primary siRNA pathways results in loss of corresponding WAGO bound siRNAs (H. C. Lee et al., 2012). Following from this mechanism, primary siRNAs should similarly trigger CSR-1 small RNA production. However, currently there are no known signals upstream of CSR-1 small RNA production on "self" mRNAs. Therefore, how "self" RNAs are initially determined remains unclear.

My work in Chapter 2 identified RHA-1 as a pivotal factor in the specificity of small RNA sorting to CSR-1. Without RHA-1, small RNAs targeting "self" genes were mis-sorted to WAGO-1, disrupting both endogenous gene regulation and dsRNA-triggered gene silencing. Interestingly, small RNAs derived from the 3' ends of mRNAs were produced and correctly sorted to CSR-1, independent of RHA-1. Instead, RHA-1 activity promoted the amplification and sorting of CSR-1 small RNAs within the 5' regions of "self" mRNAs. This indicated RHA-1 activity likely functions downstream of initial CSR-1 small RNA synthesis and that an additional mechanism must establish CSR-1 small RNA production on "self" mRNAs. Notably, this initial CSR-1 small RNA production is restricted to the extreme 3' end of mRNAs largely outside of the protein coding-sequence, suggesting this synthesis may coincide with active mRNA translation. Several potential mechanisms could be utilized to distinguish "self" from "non-self" RNAs. CSR-1 could recognize target mRNAs through a signal that marks "self" mRNAs. Alternatively, a signal could mark "non-self" mRNAs, and by default all other mRNAs considered "self". This default model could explain how CSR-1 small RNAs target nearly all germline-expressed genes (Claycomb et al., 2009b). Lastly, a combination of "self" and "non-self" signals could exist.

One intriguing distinction between “self” and “non-self” RNAs comes from previous work by Dr. Jordan Brown in our lab. His work uncovered a negative correlation between the density of introns and WAGO small RNAs, suggesting mRNAs with low density of introns are more likely to be established as “non-self”. In line with his finding, another study found transgenes with higher intron density were more likely to evade “non-self” recognition and gene silencing (Aljohani et al., 2020). The position of the first intron was also predictive of transgene expression, where first introns closer to the translational start site promoted expression. Establishing introns, or the absence of introns, as a system of “self” and “non-self” gene recognition could be valuable considering retrotransposon copies are missing introns. Small RNAs are largely synthesized in the cytoplasm, so how would intron density be a factor in this recognition? Precursor mRNA transcripts with introns undergo splicing to excise introns and join the remaining exons, forming mature mRNAs (J. Han et al., 2011). During splicing, exon junction complexes (EJCs) are deposited on mRNAs upstream of exon-exon junctions (Schlautmann & Gehring, 2020). EJCs remain bound to mRNAs during its entire life in the nucleus and cytoplasm, regulating mRNA export, translation, and nonsense-mediated mRNA decay. The EJCs are only removed from mRNA during translation. Taken together, EJCs serve as promising candidates for establishing “self” signals on mRNAs. This enticing model has yet to be experimentally tested.

Following from this EJC model, loss of core EJC components would result in loss of CSR-1 small RNAs and/or gained WAGO small RNAs targeting “self” genes. This could be tested by RNAi knockdown of core EJC components like Y14/RNP-4 and MAGOH/MAG-1 followed by immunoprecipitation of WAGO/ CSR-1 and sequencing of the bound small RNAs (Kawano et al., 2004). We could then compare WAGO “non-self” and CSR-1 “self” mRNA

targets with and without EJCs. Additionally, we could use a reporter-based approach and monitor the expression of a "self" GFP transgene in control and EJC knockdown animals. Following our model, GFP expression would decrease or undergo silencing in EJC knockdown compared to controls. A potential pitfall of these experiments arises from the multi-step role of EJC complexes in mRNA splicing, export, and translation. Completely blocking these processes could result in loss of all "self" GFP gene expression. Moreover, disrupted mRNA export would prevent mRNAs from interacting with small RNA machinery. If so, potentially the use of an auxin-inducible degron system for EJC core components could provide more controlled and rapid degradation and experimentation (L. Zhang et al., 2015). Overall, this EJC model could work in combination with a translation model, where actively translating mRNAs could serve as templates for initial CSR-1 small RNA production at the 3' ends of "self" mRNAs.

How is Argonaute slicer activity regulated?

My work in Chapter 2 highlights the important function of Argonaute CSR-1 slicer activity in mRNA finetuning. Only a subset of CSR-1 target mRNAs are finetuned, while the majority are protected from piRNA-mediated gene silencing independent of CSR-1 slicer activity. Whether CSR-1 slicer activity is differentially regulated between these two sets of target mRNAs remains unknown. Additionally, where spatially within germ cells CSR-1 slices target mRNAs is unclear.

Only a handful of Argonaute proteins possess slicer activity and function as RNA-guided endonucleases (Tolia & Joshua-Tor, 2007). Argonaute slicer activity on target mRNAs can directly inactivate mRNAs or lead to their degradation by other exonucleases. Several known mechanisms regulate Argonaute slicer activity to ensure the precise control of gene expression. These mechanisms include the degree of complementarity between the small RNA and its

mRNA target, and interactions of Argonautes with other regulatory proteins (Sheu-Gruttadauria & MacRae, 2017). For the first case, Argonaute-miRNA complexes can cleave target mRNAs only if there is sufficient or near perfect complementarity. Without sufficient complementarity, Argonaute-miRNA complexes do not slice target mRNAs but rather repress their translation. Notably, CSR-1 small RNAs are synthesized directly from mRNA templates and therefore target mRNAs with perfect complementarity. This suggests either CSR-1 always slices target mRNAs, or a different mechanism regulates CSR-1 slicer activity, such as protein interactions or protein modifications.

Previous studies identified the specific role for CSR-1 slicer activity in the biogenesis of small RNAs targeting the 5' region of mRNAs, but not the 3' ends (Singh et al., 2021). These 5' targeting CSR-1 small RNAs are required for mRNA fine-tuning. This study found that the sequences of CSR-1 small RNAs possess a 3-nucleotide periodicity in phase with ribosomal protected fragments. These results suggested CSR-1 small RNA synthesis from the 5' ends of mRNAs occurred on mRNA templates engaged with translation. Further, they found the abundance of 5' CSR-1 small RNAs anticorrelated with the target mRNA translation efficiency. Taken together, this group proposed a model where CSR-1 slicer activity and 5' small RNA synthesis occurred in the cytoplasm on mRNAs engaged with translation.

Our work in Chapter 2 and another recent study have uncovered several factors that when mutated phenocopy CSR-1 slicer mutants. This includes two factors specifically required for the assembly of the E compartment of germ granules, and as I found, RHA-1 that is typically enriched within the E compartment (Chen et al., 2024). Notably, EGO-1, the RdRP that synthesizes CSR-1 small RNAs, also localizes to the E compartment of germ granules. Together, this suggested that the production of CSR-1 small RNAs from the 5' region of target mRNAs,

and potentially CSR-1 slicer activity, required the E compartment and function of factors enriched there. However, because CSR-1, EGO-1, and RHA-1 localize to germ granules and the cytoplasm, it has proved difficult to disentangle where CSR-1 small RNAs are produced, and where CSR-1 slicer activity occurs on target mRNAs. From our work in Chapter 2, we describe a hybrid model in which CSR-1 mRNA slicing occurs in the cytoplasm, followed by 22G-RNA synthesis and sorting to CSR-1 at the E compartment. This model explains how CSR-1 loading specificity is achieved and why both cytoplasmic translation and the E compartment contribute to CSR-1 small RNA synthesis at the 5' ends of target mRNAs.

One outstanding question remains as to how this process is coordinated between the cytoplasm and germ granule. Two potential models are as follows: (1) CSR-1 slices target mRNAs in the cytoplasm and 5' mRNA fragments are transported to the E granule for amplified small RNA production, or (2) CSR-1 bound to small RNAs shuttles from cytoplasm to germ granule for amplified small RNA production on newly exported target mRNAs (Figure 5.1). Similar questions were explored for human and fly Argonautes Ago2 that function in miRNA and RNAi pathways. Because Ago2 localizes to P-bodies and the cytoplasm, it was unclear where Ago2 slicer activity occurred on target mRNAs (Sen & Blau, 2005). Two models were originally proposed: (1) Ago2 slices target mRNAs in the cytoplasm and the cleaved mRNAs are then transported to the P-body, or (2) mRNAs first associate with P-bodies, where Ago2 samples targets for hybridization followed by cleavage of successful hybrids. Upon loss of P-body assembly, miRNA and RNAi function remained intact, suggesting P-bodies are not necessary for Ago2 slicer activity (Eulalio et al., 2007). This finding highlights how RNA granules are not always necessary for small RNA function.

Model 1

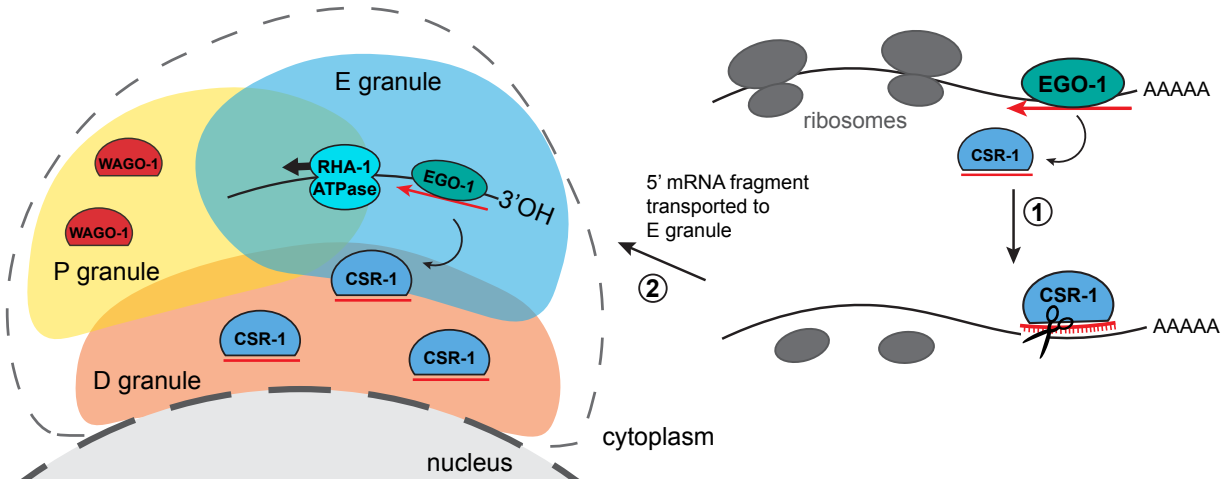

Model 2

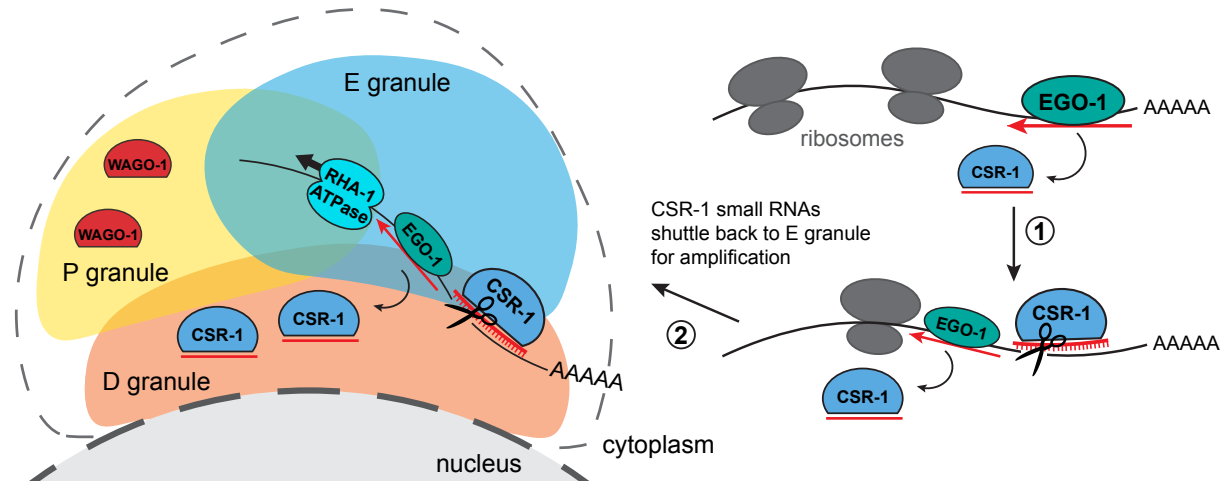

Figure 5.1: Two models for CSR-1 small RNA amplification on target mRNAs.
(**Model 1**) EGO-1 synthesizes CSR-1 small RNAs from the 3' ends of target mRNAs engaged with translation. Following CSR-1 slicing of target mRNAs, the 5' mRNA fragments are transported to the E granule for amplified small RNA production. (**Model 2**) Initial small RNA synthesis by EGO-1 occurs on transcripts with stalled ribosomes. CSR-1 small RNAs shuttle back to the germ granule to facilitate amplification of small RNA production at the E granule on newly exported target mRNAs. In this model, CSR-1 slicer activity occurs in the cytoplasm and germ granule. In both models, RHA-1 and the E compartment promote small RNA sorting to CSR-1 and inhibit WAGO-1 binding.

Overall, the dual roles of CSR-1 in mRNA-finetuning and mRNA protection suggests CSR-1 activity is regulated. Because CSR-1 and EGO-1 are essential genes, genetic screens to uncover direct regulators of their activity have not been possible. Potentially, suppressor screens in the background of the E compartment or RHA-1 mutants may uncover more regulators of the CSR-1 small RNA pathway. Positive hits would be those that suppress the temperature sensitive fertility defect observed in the E compartment or RHA-1 mutants. Additionally, single molecule RNA fluorescence in situ hybridization (smFISH) for different sets of CSR-1 mRNA targets, fine-tuned and protected, could be utilized to explore whether the subcellular localization of differentially regulated mRNAs correlates to their downstream regulation, either protected or fine-tuned. These smFISH experiments would be in combination with protein staining for CSR-1 and E compartment factors.

Does the site of small RNA targeting the mRNA length facilitate target recognition?

Germ cells employ an array of gene silencing pathways to detect and silence invasive mutagenic nucleic acids. These pathways detect "non-self" sequences by sensing copy-number, unpaired DNA, or aberrant RNA like dsRNA (Shirayama et al., 2012). These "non-self" sequences often have structural features that deviate from endogenous sequences. For two examples, viral RNAs lack mRNA modifications observed on endogenous mRNAs, and dsRNAs differ in structure from many endogenous mRNAs (Thompson et al., 2021). How are more disguised "non-self" sequences distinguished? An intriguing phenomenon was uncovered by exploring the expression of fusion genes that contained both "self" and "non-self" RNA sequences. Fusion genes that contained gfp insertions at the 5' ends were more often silenced compared to insertions at the 3' end (Shirayama et al., 2012). Why does the position of the "non-

self" sequence change the gene regulatory outcome? This observation suggested mechanisms exist to detect more subtle differences in "self" and "non-self" RNAs.

A recent investigation identified that conserved RNA helicase ZNFX-1 contributed to the fusion gene phenomenon. Loss of ZNFX-1 altered the stability of fusion gene expression and silencing observed in wild-type animals (Ishidate et al., 2018). They found ZNFX-1 impacted the site of small RNA production on target gene lengths, rather than the overall abundance of small RNA production. Specifically, loss of ZNFX-1 resulted in increased small RNA synthesis at the 5' ends of WAGO and CSR-1 target mRNAs. These changes in small RNA targeting position on mRNAs corresponded to defects in gene silencing of "non-self" sequences. This study suggested the site of small RNA targeting on the mRNA impacts the efficiency of downstream gene regulation. Similarly, my work in Chapter 2 uncovered a role for RHA-1 helicase activity in regulating the position of CSR-1 small RNA producton on target mRNAs. While CSR-1 small RNAs are enriched at the 3' ends of most mRNA targets, RHA-1 contributed to CSR-1 small RNA production and sorting from the 5' regions. We found RHA-1 activity promoted CSR-1 target mRNA fine-tuning but appeared dispensable for "self" mRNA protection from piRNA-mediated silencing. Our work in Chapter 2 added to evidence that the position of small RNA targeting on mRNA lengths sorted mRNAs for two different gene regulatory outcomes. Together, this work highlighted that the position or balance of small RNA production on RNA targets may facilitate "self" versus "non-self" distinction.

As explored in Chapter 3, RNAi is a highly conserved "non-self" gene silencing mechanism, triggered by exogenous dsRNAs, crucial for both plant and animal immunity. This pathway shares similarities with endogenous small RNA pathways in that endo-siRNAs are also produced from dsRNAs. In yeast, plants, and *C. elegans*, endo-siRNAs are derived from dsRNAs

generated by RNA-dependent RNA polymerases (RdRPs) that catalyze the replication of RNA from endogenous mRNA templates (Billi et al., 2014; Drinnenberg et al., 2009; Vaucheret & Voinnet, 2023). Although RdRP has not been identified in flies or mice, these animals generate endo-siRNAs from naturally occurring dsRNAs (Czech et al., 2008b; R. Song et al., 2011). In animals, these endo-siRNAs play a critical role in female and male germ cell development. Intriguingly, although endo-siRNAs are generated by slightly different processes in worms and mice, endo-siRNAs target the most extreme 5' and 3' ends of mRNAs in the male germ cells of both species (shown for worms in Figure 5.2A). Endo-siRNAs in murine germ cells were shown to induce target mRNA degradation in vitro and were proposed to have less well-described nuclear effects on chromatin modification (R. Song et al., 2011). Endo-siRNAs in worm male germ cells are capable of inducing both positive and negative forms of gene regulation (Conine et al., 2013a). How worm endo-siRNAs guide two distinct regulatory mechanisms remains mysterious.

In male germ cells, endo-siRNAs termed 26G-RNAs are bound by Argonautes ALG-3 and ALG-4. ALG-3/4 bound 26G-RNAs target endogenous genes expressed in the male germline during sperm development (Conine et al., 2013a). Previous studies described a correlation between ALG-3/4 small RNA 5' targeting with gene downregulation, and conversely, ALG-3/4 small RNA 3' targeting with positive gene regulation (Almeida et al., 2019). This study suggested the two regulatory modes of ALG-3/4 26G-RNA targeting could be determined by the balance of 5' and 3' targeting. These positional targeting events may lead to opposite gene regulatory outcomes by recruiting distinct downstream factors to target mRNAs. ALG-3/4 26G-RNAs are primary siRNAs capable of triggering secondary siRNA (22G-RNAs) production. In *alg-3/4* mutant animals, I found 22G- RNAs were only decreased from the most 5' end of target

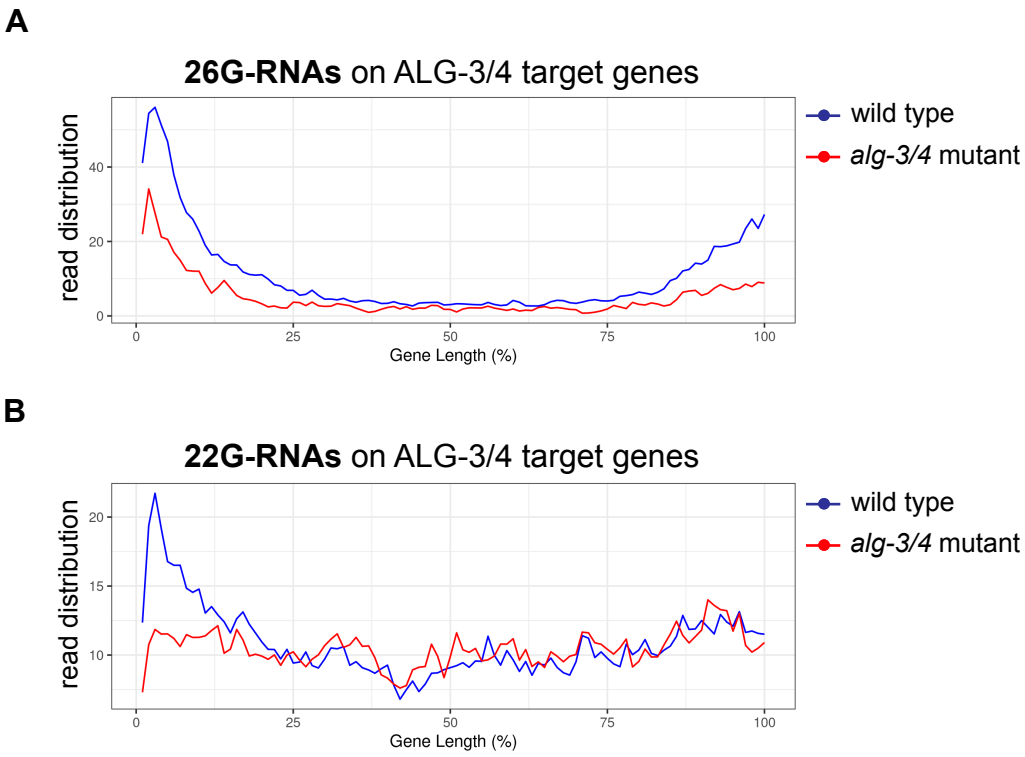

Figure 5.2: ALG-3/4 26G-RNAs promote secondary siRNA production at mRNA 5' ends. (**A** and **B**) Metagene traces show the distribution of normalized 26G-RNAs (**A**) or 22G-RNAs (**B**) in arbitrary units mapping to ALG-3/4 target genes (n=1142) by percentage of target gene length. Reads from wild type (blue) and *alg-3/4* mutants (red). 0% gene length corresponds to the 5' end of mRNAs. Small RNA-sequencing libraries were prepared from L4 stage animals undergoing spermatogenesis grown at normal growth temperature 20 °C.

mRNAs (Figure 5.2B). This suggests ALG-3/4 26G-RNAs trigger secondary siRNA production on the 5' ends of target mRNAs. These 22G-RNAs are likely bound by WAGOs because a separate study presented evidence that CSR-1 small RNAs are not produced downstream of ALG-3/4 26G-RNA targeting (Nguyen & Phillips, 2021). This work so far supports that two distinct regulatory modes arise from two distinct positions of small RNA targeting on mRNAs.

Whether the position of 26G-RNA targeting on mRNAs determines the differences in gene regulation remains to be experimentally tested. To this aim, the use of GFP reporters with a highly abundant 26G-RNA target sequence at either the 5' or 3' end of the reporter gene could serve as tool to examine the consequence of ALG-3/4 26G-RNA targeting site. Similar reporters have been utilized to investigate the role of other small RNA pathways, including piRNAs and female endo-siRNAs (J. S. Brown et al., 2023; Montgomery et al., 2012). These reporters also serve as tools to uncover factors that function within these small RNA pathways. Candidate screens in the reporter backgrounds could probe for factors that distinguish 5' and 3' endo-siRNA functions. Since endo-siRNAs perform critical roles in gene regulation during germ cell development across species, understanding their complex roles in gene regulation may be broadly applicable.

Do distinct RNA granules coordinate the stress response in germ cells?

In Chapter 4, we uncover an interaction between germ granules, stress granules, and P-bodies in germ cells following heat stress. Our observations mark only the start of this project with the larger goal of understanding how the function of these distinct RNA granules may be integrated during the stress response, and whether small RNAs contribute to stress recovery. When animals are exposed to elevated temperature, small RNA pathways and germ granules are already known

to play a protective role in germ cells (W. Gu et al., 2009; Phillips & Updike, 2022). Our work in Chapter 4 provides more evidence that germ granules, and likely small RNAs, contribute to germ cell stress resilience. Notably, Argonaute proteins have been found to be enriched within stress granules and P-bodies in mammalian cells (Leung et al., 2006; Pare et al., 2009). These identified Argonautes are part of the miRNA and RNAi-siRNA pathways. During stress, this redirection of Argonaute proteins to stress granules and P-bodies may change the normal small RNA function. These new small RNA functions may reflect priorities to respond to environmental stress and may contribute to the disruption of both piRNA-mediated silencing and RNAi inheritance (Houri-Zeevi et al., 2021). Because piRNAs and RNAi inheritance are important processes for germline genome integrity, it may seem disadvantageous for stress to disrupt the function of these pathways. However, this mechanism could enable animals to better cope with newly introduced environmental challenges. Resetting the inherited RNAi and piRNA response may allow for gene expression to adapt to the new environmental challenges, especially if these pathways were previously silencing genes useful for survival in particular environments. Alternatively, disruption to the function of RNAi and piRNA pathways may result from cells temporarily prioritizing germ cell recovery from stress, rather than genome integrity. In support of this, RNAi function is regained and piRNA silencing is re-established in the offspring of parents exposed to stress (Houri-Zeevi et al., 2021). Further work is needed to gain mechanistic insight into how small RNA pathways adapt during the stress response.

Two wider scale goals for future research exploring dynamics of the stress response include: (1) broader understanding of the protein components assembled within stress granule, P-bodies, and germ granules during different environmental stressors, and (2) the population of mRNAs regulated by each granule type. Toward the first aim, the use of TurboID proximity

labeling would allow us to determine the protein components recruited to RNA granules during stress (Doerr, 2018). This technique has previously been used to characterize the components within germ granules (Price et al., 2021). Probing each type of RNA granule, will enable us to evaluate how granule components change during various environmental stressors. Second, interrogating the mRNAs sequestered in each RNA granule will allow us to evaluate the mRNAs regulated during the stress response and recovery. Our lab is currently working on adapting the PIE-seq method for use in *C. elegans*. PIE-seq allows for the identification of RNA-binding protein target mRNAs (Ruan et al., 2023). By fusing your protein of interest with RNA deaminases, preparation of mRNA libraries allows subsequent computational analysis to identify target mRNAs associated with your protein of interest. This tool will not only be valuable for interrogating mRNAs regulated in distinct RNA granules during stress, but also for investigations into the mRNA binding targets of various small RNA pathway factors.

Overall, exploring the dynamics of the stress response in *C. elegans* allows us to understand tissue-dependent mechanisms, like those in germ cells and neurons, that studies in yeast and cell culture cannot probe.

Concluding remarks

In this dissertation, I investigated how germ granules facilitate specialized small RNA processing during normal growth and heat stress conditions. My work uncovered a fundamental mechanism by which germ cells distinguish “self” from “non-self” RNAs. My findings further support the emerging field where the compartmentalization of biological condensates contributes to the specificity of gene regulation. I also explored differences in how female and male germ cells respond to environmental dsRNA, highlighting that small RNA pathway competition regulates

the sex-differences in functional output of these pathways. More broadly, this dissertation expands our knowledge of how small RNAs coordinate the regulation of threatening RNAs and endogenous mRNAs to protect germ cells from varying environmental challenges for future generations.

Appendix

Mapping the interface between nuclear pores and germ granules

Germ granules play critical roles in specifying germ lineage, post-transcriptional gene regulation, and epigenetic inheritance (Pamula & Lehmann, 2024). Germ granules are enriched for protein components of RNA metabolism and small RNA gene regulatory pathways. In various animals including worms, flies, zebrafish, and mice, germ granules have been observed to associate closely with nuclear pore complexes (NPCs) on the cytoplasmic surface of the nuclear envelope (Pamula & Lehmann, 2024). Whether this close association between germ granules and NPCs is mediated by specific factor interactions, due to NPCs being RNA-rich sites, or a combination of both remains an active area of investigation. Additionally, whether germ granule association with NPCs is critical for small RNA pathway functions in post-transcriptional gene regulation and epigenetic inheritance remains a driving question in the field.

Previous work from our lab utilized candidate RNAi screens to identify factors that positively or negatively regulate piRNA-mediated gene silencing (J. S. Brown et al., 2023; Shi et al., 2025). Among both sets of genes were several different nucleoporins (NPPs). NPPs found to negatively regulate the piRNA pathway include NPP-14 and NPP-24. NPPs found to positively regaulte the piRNA pathway include NPP-6 and NPP-7. We wondered whether loss of these NPPs leads to defects in germ granule integrity. Germ granules in *C. elegans* are organized into spatially distinct sub-compartments that promote the fidelity of small RNA-mediated gene silencing (Huang et al., 2025; Phillips & Updike, 2022; Wan et al., 2018). Intriguingly, we observed that loss or knockdown of different NPPs results in distinct changes to germ granule organization. Loss of NPP-14 or NPP-24 both resulted in the loss of germ granule compartmentalization (Shi et al., 2025). In contrast, knockdown of *npp-6* or *npp-7* resulted in

robust disruption of the germ granule D compartment factor CSR-1, while P compartment factors were less impacted (Figure A.1, A and B) (J. S. Brown et al., 2023). Overall, our results suggested NPPs differentially impact both the organization of germ granules and small RNA pathway function.

Since our published work found NPPs differentially contribute to germ granule integrity, we next compared the impact of several NPP knockdowns on the D, P, and E compartments. As we described in Chapter 2, the E compartment factor RHA-1 promotes CSR-1 small RNA biogenesis. Like D compartment factor CSR-1, we found knockdown of *npp-6* and *npp-7* disrupts RHA-1 granule localization (Figure A.2, A and B). As previously observed, P compartment factor PGL-1 granule localization is largely maintained in *npp-6* and *npp-7* knockdown animals (Figure A.2A). To determine whether the granule integrity defects are specific to *npp-6* and *npp-7* knockdowns, we examined the impact of *npp-10* knockdown on E, D, and P compartment factors. We found *npp-10* knockdown disrupts the size and number of RHA-1, CSR-1, and PGL-1 granules, suggesting NPP-10 may more broadly function in germ granule-NPC interactions (Figure A.2, A and B). In our previous candidate screens, NPP-10 was not found to play a role piRNA-mediated gene silencing (J. S. Brown et al., 2023; Shi et al., 2025). However, whether NPP-10 regulates the output of other small RNA pathways remains untested.

Strikingly, RHA-1 nuclear enrichment was also disrupted by NPP knockdowns (Figure A.2, A and B). We wondered whether loss of RHA-1 nuclear enrichment during NPP knockdowns reflected broader changes to NPC composition and nuclear chromatin organization. To this aim, we examined the localization of nuclear basket factor NPP-7 and heterochromatin protein 1 (HPL-2) during NPP knockdowns (Bannister et al., 2001; Lachner et al., 2001). In

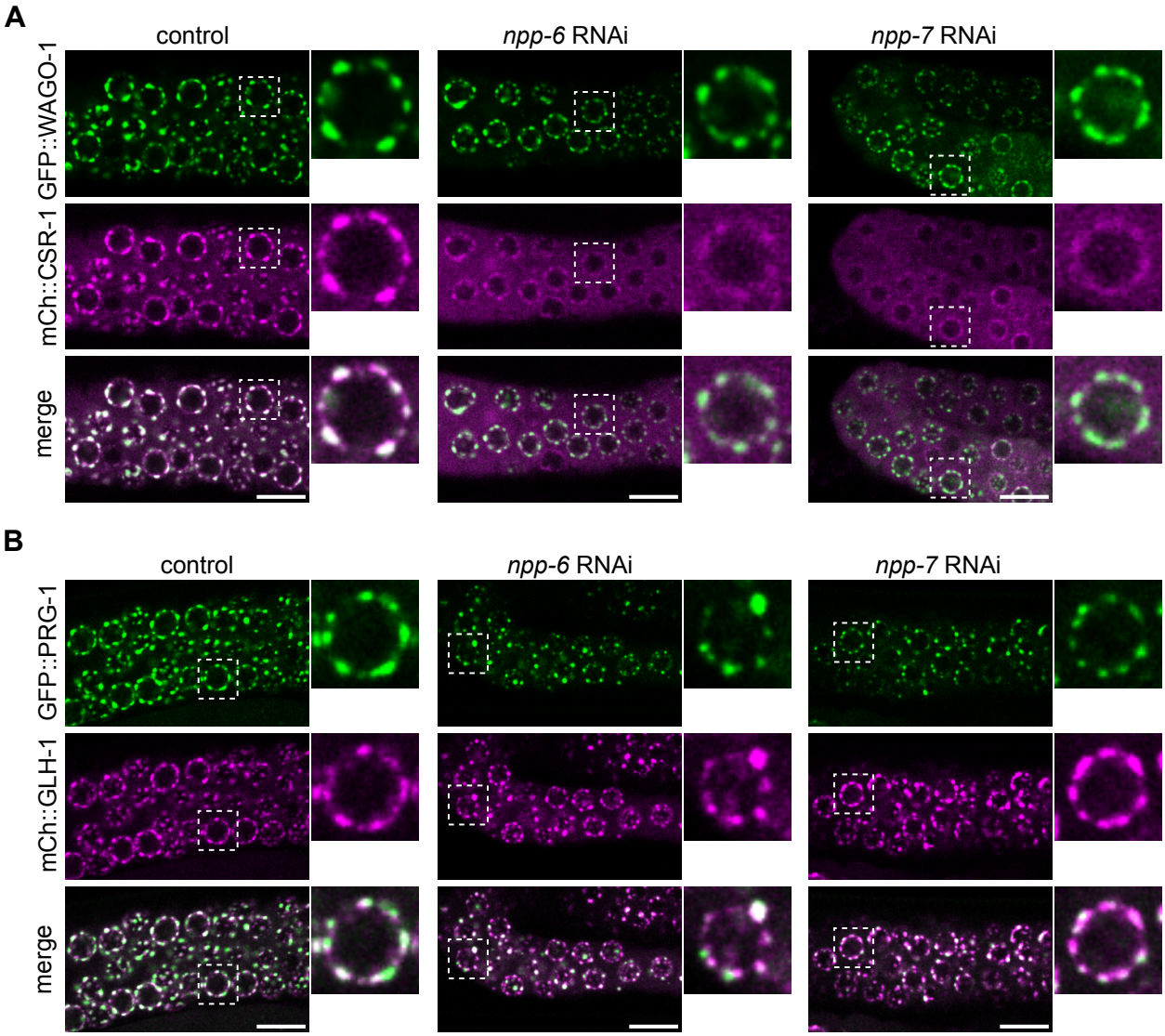

Figure A.1: Nucleoporins NPP-6/7 regulate CSR-1 localization.
(**A**) Representative live-fluorescent images of young adult germlines co-expressing P compartment factor GFP::WAGO-1 and D compartment factor mCh::CSR-1 in empty vector control, *npp-6*, or *npp-7* RNAi. (**B**) Representative live-fluorescent images of young adult germlines co-expressing P compartment factors GFP::PRG-1 and mCh::GLH-1 in empty vector control, *npp-6*, or *npp-7* RNAi. For all images scale bars = 10 μm. Dashed white boxes outline the individual germ cell shown in the enlarged images.

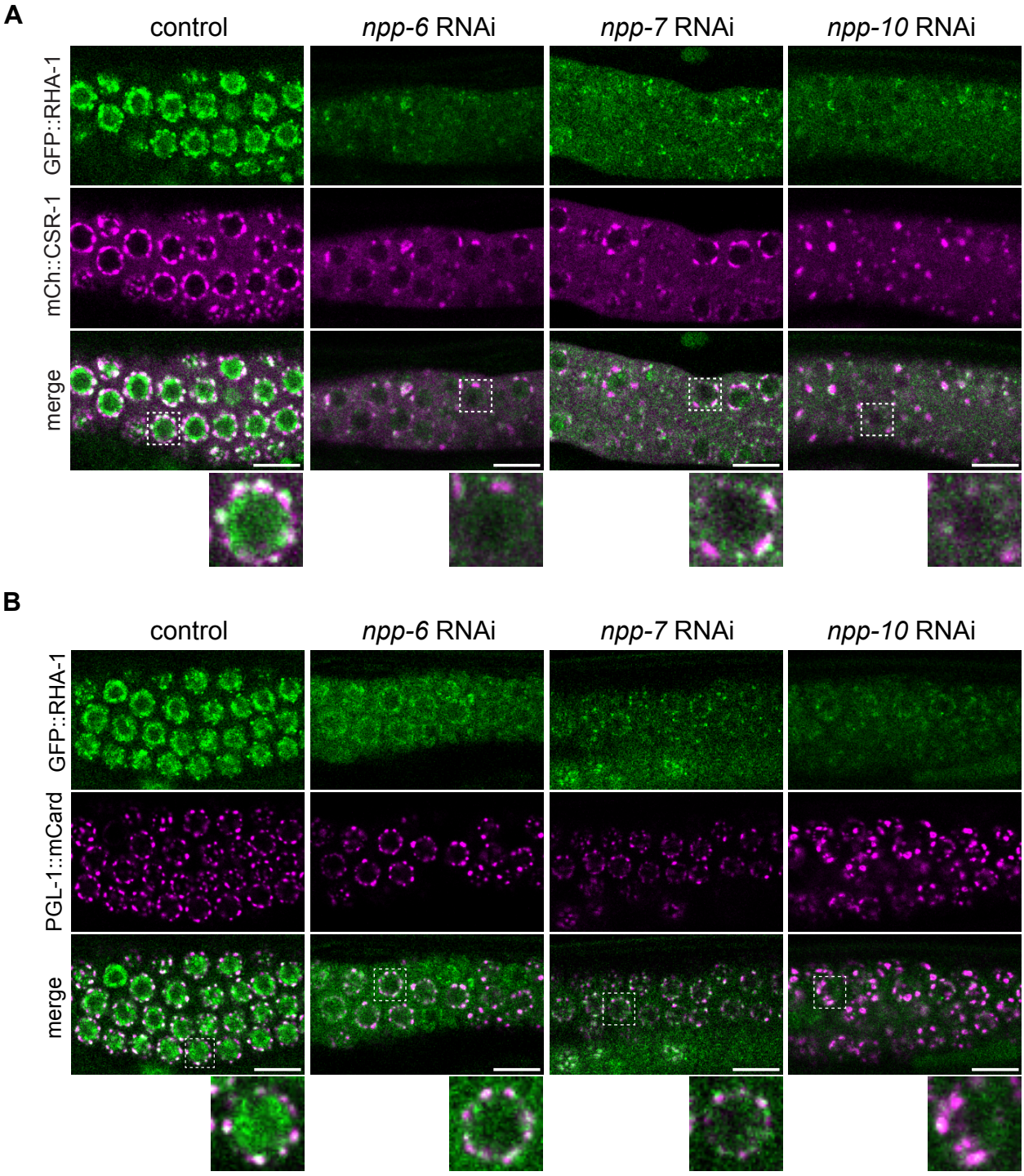

Figure A.2: Nucleoporins regulate multiple germ granule compartments.
(**A** and **B**) Representative live-fluorescent images of young adult germlines co-expressing E and D compartment factors GFP::RHA-1 and mCh::CSR-1, respectively (**A**) or E and P compartment factors GFP::RHA-1 and PGL-1::mCard , respectively (**B**) in the indicated RNAi conditions. For all images scale bars = 10 μm. Dashed white boxes outline the individual germ cell shown in the enlarged images.

control animals, NPP-7 localizes closely to the nuclear periphery of germ cells (Figure A.3A). In *npp-6* and *npp-10* knockdown animals, NPP-7 localized evenly throughout germ cell nuclei (Figure A.3A). In contrast, NPP-7 nuclear envelope localization was not impacted by knockdown of cytoplasmic filament *npp-9* (Figure A.3A). Our results suggest knockdown of certain NPPs impact the NPC composition. For heterochromatin protein HPL-2, in control animals HPL-2 and RHA-1 show similar regions of enrichment within nuclei (Figure A.3B). Knockdown of NPPs resulted in loss of enrichment of RHA-1 and HPL-2 to varying degrees. Knockdown of *npp-6* and *npp-10* resulted in the most robust disruption of HPL-2 localization, suggesting loss of normal heterochromatin organization (Figure A.3B). Our results reveal NPCs are important for regulation of chromatin state. Our NPP knockdowns included components from different regions within the NPC structure (Figure A.3C). Notably, NPPs that function on the nuclear side of NPCs (NPP-6/-7/-10) more greatly affected germ granule integrity, NPC composition, and chromatin state.

Although the NPC is best known for its primary function as a regulator of traffic between the cytoplasm and nucleus, a growing body of work suggests this structure facilitates a broad range of cellular functions on both sides of the nuclear envelope. For example, the NPC and their constituent nucleoporins have been shown to interact with the genome and perform important roles in gene regulation (Kuhn & Capelson, 2019). Our work highlights an important functional connection between NPCs, small RNA-mediated gene regulation, and germ granule organization. Work in this Appendix provides a starting point for future research integrating the role of NPCs in small RNA-mediated post-transcriptional and transcriptional gene regulation.

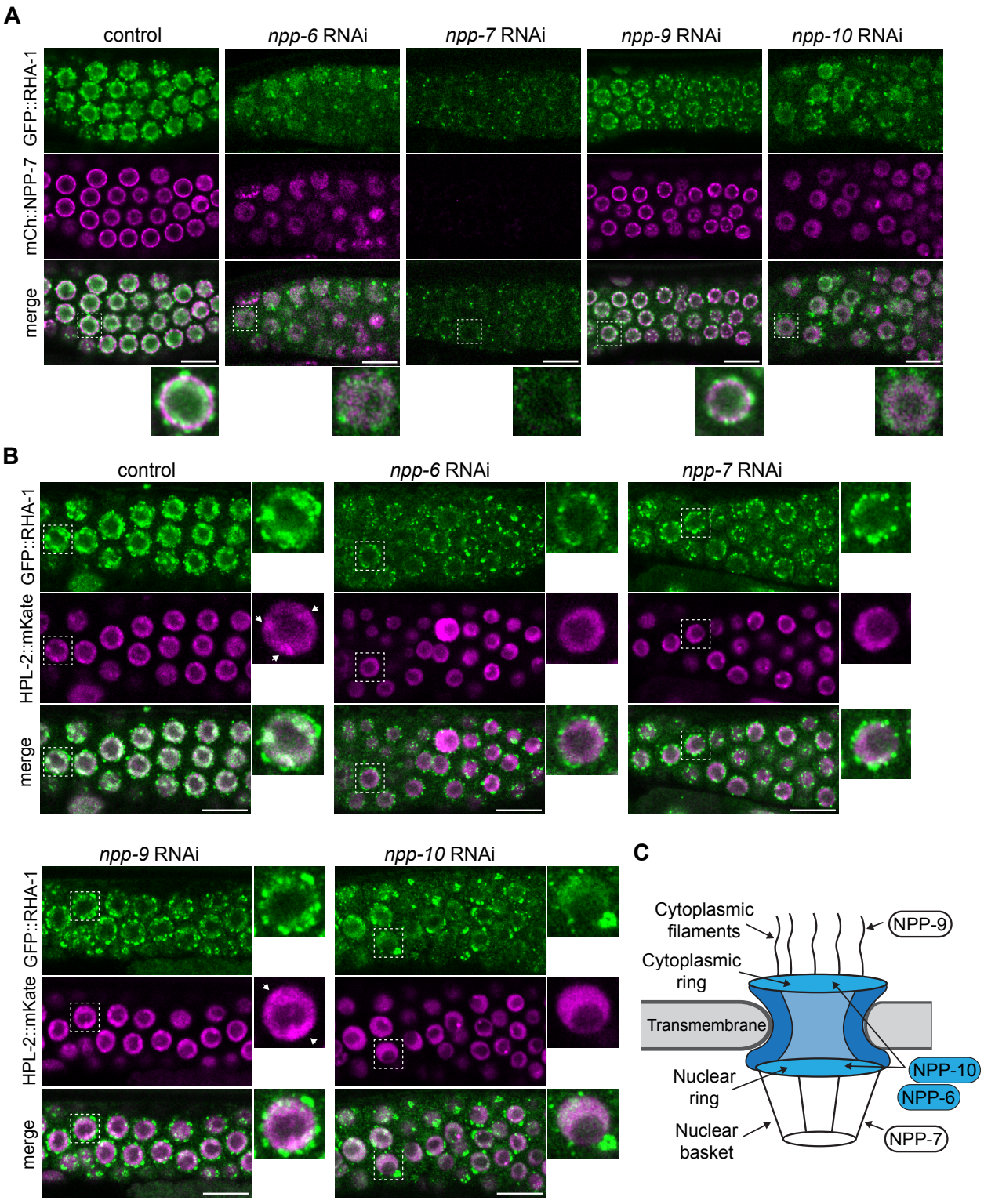

Figure A.3: Nucleoporins impact NPC assembly and nuclear heterochromatin foci.
(**A**) Representative live-fluorescent images of young adult germlines co-expressing E compartment factor GFP::RHA-1 and mCh::NPP-7 in indicated RNAi conditions (**B**) Representative live-fluorescent images of young adult germlines co-expressing E compartment

Figure A.3 continued
factor GFP::RHA-1 and heterochromatin protein 1 HPL-2::mKate in indicated RNAi conditions. White arrows point to regions of HPL-2 enrichment. For all images scale bars = 10 μm. Dashed white boxes outline the individual germ cell shown in the enlarged images. (**C**) A schematic illustrating the structure of the nuclear pore complex, highlighting cytoplasmic filament factor NPP-9, nuclear and cytoplasmic ring factors NPP-6 and NPP-10, and nuclear basket factor NPP-7.

Methods

Caenorhabditis elegans maintenance

Animals were grown on standard nematode growth media (NGM) plates seeded with the Escherichia coli OP50 strain at 20 °C.

Table A.1: List of C. elegans strains used in this study.

Strain	Genotype	Gene(s)	Origin
HCL125	*gfp::prg-1 flag::mCherry::glh-1 I*	*prg-1; glh-1*	Chen et al. 2020
HCL376	*wago-1(tor113[GFP::3xFLAG::wago-1]) I; csr-1(gc029[degron::mCherry::3xflag::ha::csr-1]) IV*	*wago-1; csr-1*	This study
OH14220	*hpl-2(ot860 [hpl-2::mKate2]) III*	*hpl-2*	CGC
HCL400	*rha-1(uoc39[gfp::rha-1]) II; hpl-2(ot860 [hpl-2::mKate2]) III*	*rha-1; hpl-2*	This study
HCL333	*npp-7(uoc21[mCherry::npp-7]) I; rha-1(uoc39[gfp::rha-1]) II*	*npp-7; rha-1*	This study
HCL334	*rha-1(uoc39[gfp::rha-1]) II; pgl-1(gg640[pgl-1::3xflag::mCardinal]) IV*	*rha-1; pgl-1*	This study
HCL335	*rha-1(uoc39[gfp::rha-1]) II; csr-1(gc029[degron::mCherry::3xflag::ha::csr-1]) IV*	*rha-1; csr-1*	This study

RNA interference

RNAi was performed by feeding animals with *E. coli* HT115 (DE3) strains expressing the appropriate dsRNA. RNAi bacterial strains were obtained from the Ahringer *C. elegans* RNAi Collection (Source BioScience). Bacterial cultures were grown in Luria broth supplemented with 100 μg/mL ampicillin and 50 μg/mL tetracycline overnight at 37°C. Cultures were seeded on NGM plates containing 100 μg/mL ampicillin, 50 μg/mL tetracycline, and 1 mM IPTG and incubated at room temperature for 24 hours. HT115 (DE3) expressing empty RNAi vector L4440 was used for control. RNAi conditions were seeded in duplicate and fifty L2-L3 stage animals were transferred to each plate. After three days, young adult animals were imaged (see below).

Confocal live imaging

Tagged fluorescent proteins were visualized in living nematodes by mounting young adult animals on 2% agarose pads with M9 buffer (22 mM KH_2PO4, 42 mM Na_2HPO4, and 86 mM NaCl) with 30 mM levamisole. Fluorescent images used for localization studies were captured using a Zeiss LSM800 confocal microscope with a Plan-Apochromat 40×/1.4 Oil objective.

REFERENCES

Abbatemarco, S., Bondaz, A., Schwager, F., Wang, J., Hammell, C. M., & Gotta, M. (2021). PQN-59 and GTBP-1 contribute to stress granule formation but are not essential for their assembly in C. elegans embryos. *Journal of Cell Science*, *134*(22). https://doi.org/10.1242/JCS.258834/272513/AM/PQN-59-AND-GTBP-1-CONTRIBUTE-TO-STRESS-GRANULE

Ahmed, S., & Hodgkin, J. (2000). MRT-2 checkpoint protein is required for germline immortality and telomere replication in C. elegans. *Nature*, *403*(6766), 159–164. https://doi.org/10.1038/35003120

Alam, U., & Kennedy, D. (2019). Rasputin a decade on and more promiscuous than ever? A review of G3BPs. *Biochimica et Biophysica Acta (BBA) - Molecular Cell Research*, *1866*(3), 360–370. https://doi.org/10.1016/J.BBAMCR.2018.09.001

Aljohani, M. D., El Mouridi, S., Priyadarshini, M., Vargas-Velazquez, A. M., & Frøkjær-Jensen, C. (2020). Engineering rules that minimize germline silencing of transgenes in simple extrachromosomal arrays in C. elegans. *Nature Communications*, *11*(1), 1–14. https://doi.org/10.1038/S41467-020-19898-0;TECHMETA=11,42,44,64;SUBJMETA=1513,1647,199,208,631;KWRD=GENE+EXPRESSION,GENETIC+TECHNIQUES

Almeida, M. V., de Jesus Domingues, A. M., & Ketting, R. F. (2019). Maternal and zygotic gene regulatory effects of endogenous RNAi pathways. *PLOS Genetics*, *15*(2), e1007784. https://doi.org/10.1371/journal.pgen.1007784

Almeida, M. V., Dietz, S., Redl, S., Karaulanov, E., Hildebrandt, A., Renz, C., Ulrich, H. D., König, J., Butter, F., & Ketting, R. F. (2018). GTSF -1 is required for formation of a functional RNA -dependent RNA Polymerase complex in Caenorhabditis elegans. *The EMBO Journal*, *37*(12). https://doi.org/10.15252/EMBJ.201899325/SUPPL_FILE/EMBJ201899325-SUP-0004-SDATAEV.ZIP

Ambros, V. (2000). Control of developmental timing in *Caenorhabditis elegans*. *Current Opinion in Genetics & Development*, *10*(4), 428–433. https://doi.org/10.1016/S0959-437X(00)00108-8

Andralojc, K. M., Campbell, A. C., Kelly, A. L., Terrey, M., Tanner, P. C., Gans, I. M., Senter-Zapata, M. J., Khokhar, E. S., & Updike, D. L. (2017). ELLI-1, a novel germline protein, modulates RNAi activity and P-granule accumulation in Caenorhabditis elegans. *PLOS Genetics*, *13*(2), e1006611. https://doi.org/10.1371/JOURNAL.PGEN.1006611

Aoki, S. T., Lynch, T. R., Crittenden, S. L., Bingman, C. A., Wickens, M., & Kimble, J. (2021). C. elegans germ granules require both assembly and localized regulators for mRNA repression. *Nature Communications*, *12*(1). https://doi.org/10.1038/S41467-021-21278-1

Aravin, A. A., Naumova, N. M., Tulin, A. V., Vagin, V. V., Rozovsky, Y. M., & Gvozdev, V. A. (2001). Double-stranded RNA-mediated silencing of genomic tandem repeats and transposable elements in the D. melanogaster germline. *Current Biology: CB*, *11*(13), 1017–1027. https://doi.org/10.1016/s0960-9822(01)00299-8

Aravin, A. A., Sachidanandam, R., Bourc'his, D., Schaefer, C., Pezic, D., Toth, K. F., Bestor, T., & Hannon, G. J. (2008). A piRNA Pathway Primed by Individual Transposons Is Linked to De Novo DNA Methylation in Mice. *Molecular Cell*, *31*(6), 785–799. https://doi.org/10.1016/j.molcel.2008.09.003

Aravin, A., Gaidatzis, D., Pfeffer, S., Lagos-Quintana, M., Landgraf, P., Iovino, N., Morris, P., Brownstein, M. J., Kuramochi-Miyagawa, S., Nakano, T., Chien, M., Russo, J. J., Ju, J., Sheridan, R., Sander, C., Zavolan, M., & Tuschl, T. (2006). A novel class of small RNAs bind to MILI protein in mouse testes. *Nature*, *442*(7099), 203–207. https://doi.org/10.1038/nature04916

Ashe, A., Sapetschnig, A., Weick, E. M., Mitchell, J., Bagijn, M. P., Cording, A. C., Doebley, A. L., Goldstein, L. D., Lehrbach, N. J., Le Pen, J., Pintacuda, G., Sakaguchi, A., Sarkies, P., Ahmed, S., & Miska, E. A. (2012). PiRNAs can trigger a multigenerational epigenetic memory in the germline of C. elegans. *Cell*, *150*(1), 88–99. https://doi.org/10.1016/j.cell.2012.06.018

Balendra, R., & Isaacs, A. M. (2018). C9orf72-mediated ALS and FTD: Multiple pathways to disease. *Nature Reviews. Neurology*, *14*(9), 544–558. https://doi.org/10.1038/s41582-018-0047-2

Banani, S. F., Lee, H. O., Hyman, A. A., & Rosen, M. K. (2017). Biomolecular condensates: Organizers of cellular biochemistry. *Nature Reviews Molecular Cell Biology 2017 18:5*, *18*(5), 285–298. https://doi.org/10.1038/nrm.2017.7

Banisch, T. U., Goudarzi, M., & Raz, E. (2012). Small RNAs in Germ Cell Development. *Current Topics in Developmental Biology*, *99*, 79–113. https://doi.org/10.1016/B978-0-12-387038-4.00004-5

Bannister, A. J., Zegerman, P., Partridge, J. F., Miska, E. A., Thomas, J. O., Allshire, R. C., & Kouzarides, T. (2001). Selective recognition of methylated lysine 9 on histone H3 by the HP1 chromo domain. *Nature*, *410*(6824), 120–124. https://doi.org/10.1038/35065138

Bashkirov, V. I., Scherthan, H., Solinger, J. A., Buerstedde, J. M., & Heyer, W. D. (1997). A mouse cytoplasmic exoribonuclease (mXRN1p) with preference for G4 tetraplex substrates. *The Journal of Cell Biology*, *136*(4), 761–773. https://doi.org/10.1083/jcb.136.4.761

Batista, P. J., Ruby, J. G., Claycomb, J. M., Chiang, R., Fahlgren, N., Kasschau, K. D., Chaves, D. A., Gu, W., Vasale, J. J., Duan, S., Conte, D., Luo, S., Schroth, G. P., Carrington, J. C., Bartel, D. P., & Mello, C. C. (2008). PRG-1 and 21U-RNAs interact to form the piRNA complex required for fertility in C. elegans. *Mol. Cell*, *31*(1), 67–78. https://doi.org/10.1016/j.molcel.2008.06.002

Bernstein, E., Caudy, A. A., Hammond, S. M., & Hannon, G. J. (2001a). Role for a bidentate ribonuclease in the initiation step of RNA interference. *Nature*, *409*(6818), 363–366. https://doi.org/10.1038/35053110;KWRD=SCIENCE

Bernstein, E., Caudy, A. A., Hammond, S. M., & Hannon, G. J. (2001b). Role for a bidentate ribonuclease in the initiation step of RNA interference. *Nature*, *409*(6818), 363–366. https://doi.org/10.1038/35053110

Bezler, A., Braukmann, F., West, S. M., Duplan, A., Conconi, R., Schütz, F., Gönczy, P., Piano, F., Gunsalus, K., Miska, E. A., & Keller, L. (2019). Tissue- and sex-specific small RNAomes reveal sex differences in response to the environment. *PLOS Genetics*, *15*(2), e1007905. https://doi.org/10.1371/JOURNAL.PGEN.1007905

Billi, A. C., Alessi, A. F., Khivansara, V., Han, T., Freeberg, M., Mitani, S., & Kim, J. K. (2012). The Caenorhabditis elegans HEN1 ortholog, HENN-1, methylates and stabilizes select subclasses of germline small RNAs. *PLoS Genetics*, *8*(4), e1002617. https://doi.org/10.1371/journal.pgen.1002617

Billi, A. C., Fischer, S. E. J., & Kim, J. K. (2014). Endogenous RNAi pathways in C. elegans. *WormBook : The Online Review of C. Elegans Biology*, 1–49. https://doi.org/10.1895/WORMBOOK.1.170.1

Billi, A. C., Freeberg, M. A., Day, A. M., Chun, S. Y., Khivansara, V., & Kim, J. K. (2013). A conserved upstream motif orchestrates autonomous, germline-enriched expression of Caenorhabditis elegans piRNAs. *PLoS Genetics*, *9*(3), e1003392. https://doi.org/10.1371/journal.pgen.1003392

Bohmert, K., Camus, I., Bellini, C., Bouchez, D., Caboche, M., & Benning, C. (1998). AGO1 defines a novel locus of Arabidopsis controlling leaf development. *The EMBO Journal*, *17*(1), 170–180. https://doi.org/10.1093/emboj/17.1.170

Brangwynne, C. P., Eckmann, C. R., Courson, D. S., Rybarska, A., Hoege, C., Gharakhani, J., Jülicher, F., & Hyman, A. A. (2009). Germline P granules are liquid droplets that localize by controlled dissolution/condensation. *Science (New York, N.Y.)*, *324*(5935), 1729–1732. https://doi.org/10.1126/science.1172046

Brennecke, J., Aravin, A. A., Stark, A., Dus, M., Kellis, M., Sachidanandam, R., & Hannon, G. J. (2007a). Discrete small RNA-generating loci as master regulators of transposon activity in Drosophila. *Cell*, *128*(6), 1089–1103. https://doi.org/10.1016/j.cell.2007.01.043

Brennecke, J., Aravin, A. A., Stark, A., Dus, M., Kellis, M., Sachidanandam, R., & Hannon, G. J. (2007b). Discrete Small RNA-Generating Loci as Master Regulators of Transposon Activity in Drosophila. *Cell*, *128*(6), 1089–1103. https://doi.org/10.1016/j.cell.2007.01.043

Brown, J. S., Zhang, D., Gaylord, O., Chen, W., & Lee, H. C. (2023). Sensitized piRNA reporter identifies multiple RNA processing factors involved in piRNA-mediated gene silencing. *Genetics*, *224*(4). https://doi.org/10.1093/GENETICS/IYAD095

Brown, K. C., Svendsen, J. M., Tucci, R. M., Montgomery, B. E., & Montgomery, T. A. (2017). ALG-5 is a miRNA-associated Argonaute required for proper developmental timing in the Caenorhabditis elegans germline. *Nucleic Acids Research*, *45*(15), 9093–9107. https://doi.org/10.1093/nar/gkx536

Buckley, B. A., Burkhart, K. B., Gu, S. G., Spracklin, G., Kershner, A., Fritz, H., Kimble, J., Fire, A., & Kennedy, S. (2012). A nuclear Argonaute promotes multigenerational epigenetic inheritance and germline immortality. *Nature*, *489*(7416), 447–451. https://doi.org/10.1038/nature11352

Bumcrot, D., Manoharan, M., Koteliansky, V., & Sah, D. W. Y. (2006). RNAi therapeutics: A potential new class of pharmaceutical drugs. *Nature Chemical Biology*, *2*(12), 711–719. https://doi.org/10.1038/nchembio839

Burton, N. O., Burkhart, K. B., & Kennedy, S. (2011). Nuclear RNAi maintains heritable gene silencing in Caenorhabditis elegans. *Proceedings of the National Academy of Sciences of the United States of America*, *108*(49), 19683–19688. https://doi.org/10.1073/PNAS.1113310108/-/DCSUPPLEMENTAL

Calixto, A., Chelur, D., Topalidou, I., Chen, X., & Chalfie, M. (2010). Enhanced neuronal RNAi in C. elegans using SID-1. *Nature Methods 2010 7:7*, *7*(7), 554–559. https://doi.org/10.1038/nmeth.1463

Campbell, A. C., & Updike, D. L. (2015). CSR-1 and P granules suppress sperm-specific transcription in the C. elegans germline. *Development*, *142*(10), 1745–1755. https://doi.org/10.1242/dev.121434

Carmell, M. A., Girard, A., van de Kant, H. J. G., Bourc'his, D., Bestor, T. H., de Rooij, D. G., & Hannon, G. J. (2007). MIWI2 Is Essential for Spermatogenesis and Repression of Transposons in the Mouse Male Germline. *Developmental Cell*, *12*(4), 503–514. https://doi.org/10.1016/j.devcel.2007.03.001

Carmell, M. A., Xuan, Z., Zhang, M. Q., & Hannon, G. J. (2002). The Argonaute family: Tentacles that reach into RNAi, developmental control, stem cell maintenance, and tumorigenesis. *Genes & Development*, *16*(21), 2733–2742. https://doi.org/10.1101/gad.1026102

Cecere, G., Hoersch, S., O'keeffe, S., Sachidanandam, R., & Grishok, A. (2014). Global effects of the CSR-1 RNA interference pathway on the transcriptional landscape. *Nature Structural & Molecular Biology 2014 21:4*, *21*(4), 358–365. https://doi.org/10.1038/nsmb.2801

Chalfie, M., Horvitz, H. R., & Sulston, J. E. (1981). Mutations that lead to reiterations in the cell lineages of C. elegans. *Cell*, *24*(1), 59–69. https://doi.org/10.1016/0092-8674(81)90501-8

Charlesworth, A. G., Seroussi, U., Lehrbach, N. J., Renaud, M. S., Sundby, A. E., Molnar, R. I., Lao, R. X., Willis, A. R., Woock, J. R., Aber, M. J., Diao, A. J., Reinke, A. W., Ruvkun, G., & Claycomb, J. M. (2021). Two isoforms of the essential C. elegans Argonaute CSR-1 differentially regulate sperm and oocyte fertility. *Nucleic Acids Research*, *49*(15), 8836–8865. https://doi.org/10.1093/nar/gkab619

Chen, S., & Phillips, C. M. (2024). HRDE-2 drives small RNA specificity for the nuclear Argonaute protein HRDE-1. *Nature Communications*, *15*(1), 957. https://doi.org/10.1038/s41467-024-45245-8

Chen, W., Brown, J. S., He, T., Wu, W. S., Tu, S., Weng, Z., Zhang, D., & Lee, H. C. (2022). GLH/VASA helicases promote germ granule formation to ensure the fidelity of piRNA-mediated transcriptome surveillance. *Nature Communications 2022 13:1*, *13*(1), 1–14. https://doi.org/10.1038/s41467-022-32880-2

Chen, W., Hu, Y., Lang, C. F., Brown, J. S., Schwabach, S., Song, X., Zhang, Y., Munro, E., Bennett, K., Zhang, D., & Lee, H. C. (2020). The Dynamics of P Granule Liquid Droplets Are Regulated by the Caenorhabditis elegans Germline RNA Helicase GLH-1 via Its ATP Hydrolysis Cycle. *Genetics*, *215*(2), 421. https://doi.org/10.1534/GENETICS.120.303052

Chen, X., Wang, K., Mufti, F. U. D., Xu, D., Zhu, C., Huang, X., Zeng, C., Jin, Q., Huang, X., Yan, Y. H., Dong, M. Q., Feng, X., Shi, Y., Kennedy, S., & Guang, S. (2024). Germ granule compartments coordinate specialized small RNA production. *Nature Communications*, *15*(1). https://doi.org/10.1038/S41467-024-50027-3

Cipriani, P. G., Bay, O., Zinno, J., Gutwein, M., Gan, H. H., Mayya, V. K., Chung, G., Chen, J. X., Fahs, H., Guan, Y., Duchaine, T. F., Selbach, M., Piano, F., & Gunsalus, K. C. (2021). Novel lotus-domain proteins are organizational hubs that recruit c. Elegans vasa to germ granules. *eLife*, *10*, 1–34. https://doi.org/10.7554/eLife.60833

Claycomb, J. M., Batista, P. J., Pang, K. M., Gu, W., Vasale, J. J., van Wolfswinkel, J. C., Chaves, D. A., Shirayama, M., Mitani, S., Ketting, R. F., Conte, D., & Mello, C. C. (2009a). The Argonaute CSR-1 and Its 22G-RNA Cofactors Are Required for Holocentric Chromosome Segregation. *Cell*, *139*(1), 123–134. https://doi.org/10.1016/J.CELL.2009.09.014

Claycomb, J. M., Batista, P. J., Pang, K. M., Gu, W., Vasale, J. J., van Wolfswinkel, J. C., Chaves, D. A., Shirayama, M., Mitani, S., Ketting, R. F., Conte, D., & Mello, C. C. (2009b). The Argonaute CSR-1 and Its 22G-RNA Cofactors Are Required for Holocentric Chromosome Segregation. *Cell*, *139*(1), 123–134. https://doi.org/10.1016/j.cell.2009.09.014

Collins, J., Saari, B., & Anderson, P. (1987). Activation of a transposable element in the germ line but not the soma of Caenorhabditis elegans. *Nature*, *328*(6132), 726–728. https://doi.org/10.1038/328726a0

Conine, C. C., Batista, P. J., Gu, W., Claycomb, J. M., Chaves, D. A., Shirayama, M., & Mello, C. C. (2010). Argonautes ALG-3 and ALG-4 are required for spermatogenesis-specific 26G-RNAs and thermotolerant sperm in Caenorhabditis elegans. *Proceedings of the National Academy of Sciences*, *107*(8), 3588–3593. https://doi.org/10.1073/pnas.0911685107

Conine, C. C., Moresco, J. J., Gu, W., Shirayama, M., Conte, D., Yates, J. R., & Mello, C. C. (2013a). Argonautes promote male fertility and provide a paternal memory of germline gene expression in C. Elegans. *Cell*, *155*(7), 1532–1544. https://doi.org/10.1016/j.cell.2013.11.032

Conine, C. C., Moresco, J. J., Gu, W., Shirayama, M., Conte, D., Yates, J. R., & Mello, C. C. (2013b). Argonautes Promote Male Fertility and Provide a Paternal Memory of Germline Gene Expression in C. elegans. *Cell*, *155*(7), 1532–1544. https://doi.org/10.1016/J.CELL.2013.11.032

Cornes, E., Bourdon, L., Singh, M., Mueller, F., Quarato, P., Wernersson, E., Bienko, M., Li, B., & Cecere, G. (2022). piRNAs initiate transcriptional silencing of spermatogenic genes during C. elegans germline development. *Developmental Cell*, *57*(2), 180-196.e7. https://doi.org/10.1016/J.DEVCEL.2021.11.025

Cugusi, S., Li, Y., Jin, P., & Lucchesi, J. C. (2016). The Drosophila Helicase MLE Targets Hairpin Structures in Genomic Transcripts. *PLoS Genetics*, *12*(1), 1–19. https://doi.org/10.1371/journal.pgen.1005761

Czech, B., Malone, C. D., Zhou, R., Stark, A., Schlingeheyde, C., Dus, M., Perrimon, N., Kellis, M., Wohlschlegel, J. A., Sachidanandam, R., Hannon, G. J., & Brennecke, J. (2008a). An endogenous small interfering RNA pathway in Drosophila. *Nature*, *453*(7196), 798–802. https://doi.org/10.1038/nature07007

Czech, B., Malone, C. D., Zhou, R., Stark, A., Schlingeheyde, C., Dus, M., Perrimon, N., Kellis, M., Wohlschlegel, J. A., Sachidanandam, R., Hannon, G. J., & Brennecke, J. (2008b). An endogenous small interfering RNA pathway in Drosophila. *Nature 2008 453:7196*, *453*(7196), 798–802. https://doi.org/10.1038/nature07007

Czech, B., Zhou, R., Erlich, Y., Brennecke, J., Binari, R., Villalta, C., Gordon, A., Perrimon, N., & Hannon, G. J. (2009). Hierarchical rules for Argonaute loading in Drosophila. *Molecular Cell*, *36*(3), 445–456. https://doi.org/10.1016/j.molcel.2009.09.028

Das, P. P., Bagijn, M. P., Goldstein, L. D., Woolford, J. R., Lehrbach, N. J., Sapetschnig, A., Buhecha, H. R., Gilchrist, M. J., Howe, K. L., Stark, R., Matthews, N., Berezikov, E., Ketting, R. F., Tavaré, S., & Miska, E. A. (2008). Piwi and piRNAs Act Upstream of an Endogenous siRNA Pathway to Suppress Tc3 Transposon Mobility in the Caenorhabditis elegans Germline. *Molecular Cell*, *31*(1), 79–90. https://doi.org/10.1016/J.MOLCEL.2008.06.003

Decker, C. J., & Parker, R. (2012). P-Bodies and Stress Granules: Possible Roles in the Control of Translation and mRNA Degradation. *Cold Spring Harbor Perspectives in Biology*, *4*(9), a012286. https://doi.org/10.1101/CSHPERSPECT.A012286

Dodson, A. E., & Kennedy, S. (2020). Phase Separation in Germ Cells and Development. *Developmental Cell*, *55*(1), 4–17. https://doi.org/10.1016/j.devcel.2020.09.004

Doerr, A. (2018). Proximity labeling with TurboID. *Nature Methods*, *15*(10), 764. https://doi.org/10.1038/S41592-018-0158-0;SUBJMETA=1647,2067,2230,338,475,631,92;KWRD=ISOLATION

Drinnenberg, I. A., Weinberg, D. E., Xie, K. T., Mower, J. P., Wolfe, K. H., Fink, G. R., & Bartel, D. P. (2009). RNAi in budding yeast. *Science (New York, N.Y.)*, *326*(5952), 544. https://doi.org/10.1126/SCIENCE.1176945

Du, Z., Shi, K., Brown, J. S., He, T., Wu, W. S., Zhang, Y., Lee, H. C., & Zhang, D. (2023). Condensate cooperativity underlies transgenerational gene silencing. *Cell Reports*, *42*(8), 112859. https://doi.org/10.1016/J.CELREP.2023.112859

Duchaine, T. F., Wohlschlegel, J. A., Kennedy, S., Bei, Y., Conte, D., Pang, K. M., Brownell, D. R., Harding, S., Mitani, S., Ruvkun, G., Yates, J. R., & Mello, C. C. (2006). Functional proteomics reveals the biochemical niche of C. elegans DCR-1 in multiple small-RNA-mediated pathways. *Cell*, *124*(2), 343–354. https://doi.org/10.1016/j.cell.2005.11.036

Eddy, E. M. (1976). Germ Plasm and the Differentiation of the Germ Cell Line. *International Review of Cytology*, *43*(C), 229–280. https://doi.org/10.1016/S0074-7696(08)60070-4

Ernst, C., Odom, D. T., & Kutter, C. (2017). The emergence of piRNAs against transposon invasion to preserve mammalian genome integrity. *Nature Communications*, *8*(1), 1411. https://doi.org/10.1038/s41467-017-01049-7

Eulalio, A., Behm-Ansmant, I., Schweizer, D., & Izaurralde, E. (2007). P-Body Formation Is a Consequence, Not the Cause, of RNA-Mediated Gene Silencing. *Molecular and Cellular Biology*, *27*(11), 3970–3981. https://doi.org/10.1128/MCB.00128-07

Fairman-Williams, M. E., Guenther, U. P., & Jankowsky, E. (2010). SF1 and SF2 helicases: Family matters. *Current Opinion in Structural Biology*, *20*(3), 313–324. https://doi.org/10.1016/J.SBI.2010.03.011

Ferguson, E. L., Sternberg, P. W., & Horvitz, H. R. (1987). A genetic pathway for the specification of the vulval cell lineages of Caenorhabditis elegans. *Nature*, *326*(6110), 259–267. https://doi.org/10.1038/326259a0

Fire, A., Albertson, D., Harrison, S. W., & Moerman, D. G. (1991). Production of antisense RNA leads to effective and specific inhibition of gene expression in C. elegans muscle. *Development*, *113*(2), 503–514. https://doi.org/10.1242/dev.113.2.503

Fire, A., Xu, S., Montgomery, M. K., Kostas, S. A., Driver, S. E., & Mello, C. C. (1998). Potent and specific genetic interference by double-stranded RNA in caenorhabditis elegans. *Nature*, *391*(6669), 806–811. https://doi.org/10.1038/35888

Fischer, S. E. J., Montgomery, T. A., Zhang, C., Fahlgren, N., Breen, P. C., Hwang, A., Sullivan, C. M., Carrington, J. C., & Ruvkun, G. (2011). The ERI-6/7 Helicase Acts at the First Stage of an siRNA Amplification Pathway That Targets Recent Gene Duplications. *PLoS Genetics*, *7*(11), e1002369. https://doi.org/10.1371/journal.pgen.1002369

Förstemann, K., Horwich, M. D., Wee, L., Tomari, Y., & Zamore, P. D. (2007). Drosophila microRNAs are sorted into functionally distinct argonaute complexes after production by dicer-1. *Cell*, *130*(2), 287–297. https://doi.org/10.1016/j.cell.2007.05.056

Frank, F., Sonenberg, N., & Nagar, B. (2010). Structural basis for 5'-nucleotide base-specific recognition of guide RNA by human AGO2. *Nature*, *465*(7299), 818–822. https://doi.org/10.1038/nature09039

Fraser, A. G., Kamath, R. S., Zipperlen, P., Martinez-Campos, M., Sohrmann, M., & Ahringer, J. (2000). Functional genomic analysis of C. elegans chromosome I by systematic RNA interference. *Nature*, *408*(6810), 325–330. https://doi.org/10.1038/35042517;KWRD=SCIENCE

Fu, Q., & Yuan, Y. A. (2013). Structural insights into RISC assembly facilitated by dsRNA-binding domains of human RNA helicase A (DHX9). *Nucleic Acids Research*, *41*(5), 3457–3470. https://doi.org/10.1093/NAR/GKT042

Gallo, C. M., Munro, E., Rasoloson, D., Merritt, C., & Seydoux, G. (2008). Processing bodies and germ granules are distinct RNA granules that interact in C. elegans embryos. *Developmental Biology*, *323*(1), 76–87. https://doi.org/10.1016/J.YDBIO.2008.07.008

Gaylord, O. J., Brown, J. S., Wu, W.-S., & Lee, H.-C. (2025). RNA Helicase A promotes small RNA biogenesis and sorting in germ cells. *bioRxiv*, 2025.05.11.653140. https://doi.org/10.1101/2025.05.11.653140

Gent, J. I., Schvarzstein, M., Villeneuve, A. M., Gu, S. G., Jantsch, V., Fire, A. Z., & Baudrimont, A. (2009). A Caenorhabditis elegans RNA-directed RNA polymerase in sperm development and endogenous RNA interference. *Genetics*, *183*(4), 1297–1314. https://doi.org/10.1534/genetics.109.109686

Gerson-Gurwitz, A., Wang, S., Sathe, S., Green, R., Yeo, G. W., Oegema, K., & Desai, A. (2016). A Small RNA-Catalytic Argonaute Pathway Tunes Germline Transcript Levels to Ensure Embryonic Divisions. *Cell*, *165*(2), 396–409. https://doi.org/10.1016/j.cell.2016.02.040

Ghanta, K. S., Ishidate, T., & Mello, C. C. (2021). Microinjection for precision genome editing in Caenorhabditis elegans. *STAR Protocols*, *2*(3). https://doi.org/10.1016/J.XPRO.2021.100748

Ghildiyal, M., & Zamore, P. D. (2009). Small silencing RNAs: An expanding universe. *Nature Reviews Genetics 2009 10:2*, *10*(2), 94–108. https://doi.org/10.1038/nrg2504

Grishok, A., Tabara, H., & Mello, C. C. (2000). Genetic requirements for inheritance of RNAi in C. elegans. *Science*, *287*(5462), 2494–2497. https://doi.org/10.1126/SCIENCE.287.5462.2494;REQUESTEDJOURNAL:JOURNAL:SCIENCE;CTYPE:STRING:JOURNAL

Gu, S. G., Pak, J., Guang, S., Maniar, J. M., Kennedy, S., & Fire, A. (2012). Amplification of siRNA in Caenorhabditis elegans generates a transgenerational sequence-targeted histone H3 lysine 9 methylation footprint. *Nature Genetics*, *44*(2), 157–164. https://doi.org/10.1038/ng.1039

Gu, W., Shirayama, M., Conte, D., Vasale, J., Batista, P. J., Claycomb, J. M., Moresco, J. J., Youngman, E. M., Keys, J., Stoltz, M. J., Chen, C. C. G., Chaves, D. A., Duan, S., Kasschau, K. D., Fahlgren, N., Yates, J. R., Mitani, S., Carrington, J. C., & Mello, C. C. (2009). Distinct Argonaute-Mediated 22G-RNA Pathways Direct Genome Surveillance in the C. elegans Germline. *Molecular Cell*, *36*(2), 231–244. https://doi.org/10.1016/j.molcel.2009.09.020

Gunawardane, L. S., Saito, K., Nishida, K. M., Miyoshi, K., Kawamura, Y., Nagami, T., Siomi, H., & Siomi, M. C. (2007). A slicer-mediated mechanism for repeat-associated siRNA 5' end formation in Drosophila. *Science (New York, N.Y.)*, *315*(5818), 1587–1590. https://doi.org/10.1126/science.1140494

Guo, S., & Kemphues, K. J. (1995). Par-1, a gene required for establishing polarity in C. elegans embryos, encodes a putative Ser/Thr kinase that is asymmetrically distributed. *Cell*, *81*(4), 611–620. https://doi.org/10.1016/0092-8674(95)90082-9

Hamilton, A. J., & Baulcombe, D. C. (1999). A Species of Small Antisense RNA in Posttranscriptional Gene Silencing in Plants. *Science*, *286*(5441), 950–952. https://doi.org/10.1126/science.286.5441.950

Hammond, S. M., Bernstein, E., Beach, D., & Hannon, G. J. (2000). An RNA-directed nuclease mediates post-transcriptional gene silencing in Drosophila cells. *Nature*, *404*(6775), 293–296. https://doi.org/10.1038/35005107

Han, J., Xiong, J., Wang, D., & Fu, X. D. (2011). Pre-mRNA splicing: Where and when in the nucleus. *Trends in Cell Biology*, *21*(6), 336. https://doi.org/10.1016/J.TCB.2011.03.003

Han, T., Manoharan, A. P., Harkins, T. T., Bouffard, P., Fitzpatrick, C., Chu, D. S., Thierry-Mieg, D., Thierry-Mieg, J., & Kim, J. K. (2009). 26G endo-siRNAs regulate spermatogenic and zygotic gene expression in Caenorhabditis elegans. *Proceedings of the National Academy of Sciences of the United States of America*, *106*(44), 18674–18679. https://doi.org/10.1073/pnas.0906378106

Horvitz, H. R., & Sulston, J. E. (1980). Isolation and genetic characterization of cell-lineage mutants of the nematode Caenorhabditis elegans. *Genetics*, *96*(2), 435–454. https://doi.org/10.1093/genetics/96.2.435

Houri-Ze'evi, L., Korem, Y., Sheftel, H., Faigenbloom, L., Toker, I. A., Dagan, Y., Awad, L., Degani, L., Alon, U., & Rechavi, O. (2016). A Tunable Mechanism Determines the Duration of the Transgenerational Small RNA Inheritance in C. elegans. *Cell*, *165*(1), 88–99. https://doi.org/10.1016/J.CELL.2016.02.057/ATTACHMENT/DBBEE8B6-40B5-47EA-B415-65379321A5E8/MMC7.PDF

Houri-Zeevi, L., Teichman, G., Gingold, H., & Rechavi, O. (2021). Stress resets ancestral heritable small RNA responses. *eLife*, *10*. https://doi.org/10.7554/ELIFE.65797

Hu, H. Y., Yan, Z., Xu, Y., Hu, H., Menzel, C., Zhou, Y. H., Chen, W., & Khaitovich, P. (2009). Sequence features associated with microRNA strand selection in humans and flies. *BMC Genomics*, *10*, 413. https://doi.org/10.1186/1471-2164-10-413

Huang, X., Feng, X., Yan, Y.-H., Xu, D., Wang, K., Zhu, C., Dong, M.-Q., Huang, X., Guang, S., & Chen, X. (2025). Compartmentalized localization of perinuclear proteins within germ granules in C. elegans. *Developmental Cell*, *60*(8), 1251-1270.e3. https://doi.org/10.1016/J.DEVCEL.2024.12.016

Hubstenberger, A., Courel, M., Bénard, M., Souquere, S., Ernoult-Lange, M., Chouaib, R., Yi, Z., Morlot, J.-B., Munier, A., Fradet, M., Daunesse, M., Bertrand, E., Pierron, G., Mozziconacci, J., Kress, M., & Weil, D. (2017). P-Body Purification Reveals the Condensation of Repressed mRNA Regulons. *Molecular Cell*, *68*(1), 144-157.e5. https://doi.org/10.1016/j.molcel.2017.09.003

Huelgas-Morales, G., Silva-García, C. G., Salinas, L. S., Greenstein, D., & Navarro, R. E. (2016). The Stress Granule RNA-Binding Protein TIAR-1 Protects Female Germ Cells from Heat Shock in Caenorhabditis elegans. *G3 (Bethesda, Md.)*, *6*(4), 1031–1047. https://doi.org/10.1534/G3.115.026815

Hutvagner, G., & Simard, M. J. (2008). Argonaute proteins: Key players in RNA silencing. *Nature Reviews Molecular Cell Biology 2008 9:1*, *9*(1), 22–32. https://doi.org/10.1038/nrm2321

Ikenishi, K., Tanaka, T. S., & Komiya, T. (1996). Spatio-temporal distribution of the protein of Xenopus vasa homologue (Xenopus vasa-like gene 1, XVLG1) in embryos. *Development, Growth & Differentiation*, *38*(5), 527–535. https://doi.org/10.1046/j.1440-169X.1996.t01-4-00009.x

Iki, T., Kawaguchi, S., & Kai, T. (2023). miRNA/siRNA-directed pathway to produce noncoding piRNAs from endogenous protein-coding regions ensures Drosophila spermatogenesis. *Science Advances*, *9*(29). https://doi.org/10.1126/SCIADV.ADH0397

Illmensee, K., & Mahowald, A. P. (1974). Transplantation of posterior polar plasm in Drosophila. Induction of germ cells at the anterior pole of the egg. *Proceedings of the National Academy of Sciences of the United States of America*, *71*(4), 1016–1020. https://doi.org/10.1073/pnas.71.4.1016

Ishidate, T., Ozturk, A. R., Durning, D. J., Sharma, R., Shen, E. zhi, Chen, H., Seth, M., Shirayama, M., & Mello, C. C. (2018). ZNFX-1 Functions within Perinuclear Nuage to Balance Epigenetic Signals. *Molecular Cell*, *70*(4), 639-649.e6. https://doi.org/10.1016/j.molcel.2018.04.009

Ivanov, P., Kedersha, N., & Anderson, P. (2019). Stress Granules and Processing Bodies in Translational Control. *Cold Spring Harbor Perspectives in Biology*, *11*(5). https://doi.org/10.1101/CSHPERSPECT.A032813

Izant, J. G., & Weintraub, H. (1985). Constitutive and conditional suppression of exogenous and endogenous genes by anti-sense RNA. *Science (New York, N.Y.)*, *229*(4711), 345–352. https://doi.org/10.1126/science.2990048

Jadhav, V., Vaishnaw, A., Fitzgerald, K., & Maier, M. A. (2024). RNA interference in the era of nucleic acid therapeutics. *Nature Biotechnology*, *42*(3), 394–405. https://doi.org/10.1038/s41587-023-02105-y

Johnston, M., & Hutvagner, G. (2011). Posttranslational modification of Argonautes and their role in small RNA-mediated gene regulation. *Silence*, *2*, 5. https://doi.org/10.1186/1758-907X-2-5

Kallweit, L., Hamlett, E. D., Saternos, H., Gilmore, A., Granholm, A.-C., & Horowitz, S. (2025). Chronic RNA G-quadruplex accumulation in aging and Alzheimer's disease. *eLife*, *14*, RP105446. https://doi.org/10.7554/eLife.105446

Kamath, R. S., Fraser, A. G., Dong, Y., Poulin, G., Durbin, R., Gotta, M., Kanapin, A., Le Bot, N., Moreno, S., Sohrmann, M., Welchman, D. P., Zipperien, P., & Ahringer, J. (2003). Systematic functional analysis of the Caenorhabditis elegans genome using RNAi. *Nature*, *421*(6920), 231–237. https://doi.org/10.1038/NATURE01278;KWRD=SCIENCE

Kamath, R. S., Martinez-Campos, M., Zipperlen, P., Fraser, A. G., & Ahringer, J. (2000). Effectiveness of specific RNA-mediated interference through ingested double-stranded RNA in Caenorhabditis elegans. *Genome Biology*, *2*(1), research0002.1. https://doi.org/10.1186/GB-2000-2-1-RESEARCH0002

Kawano, T., Kataoka, N., Dreyfuss, G., & Sakamoto, H. (2004). Ce-Y14 and MAG-1, components of the exon–exon junction complex, are required for embryogenesis and germline sexual switching in Caenorhabditis elegans. *Mechanisms of Development*, *121*(1), 27–35. https://doi.org/10.1016/J.MOD.2003.11.003

Kawasaki, I., Amiri, A., Fan, Y., Meyer, N., Dunkelbarger, S., Motohashi, T., Karashima, T., Bossinger, O., & Strome, S. (2004). The PGL family proteins associate with germ granules and function redundantly in Caenorhabditis elegans germline development. *Genetics*, *167*(2), 645–661. https://doi.org/10.1534/genetics.103.023093

Kedersha, N. L., Gupta, M., Li, W., Miller, I., & Anderson, P. (1999). RNA-binding proteins TIA-1 and TIAR link the phosphorylation of eIF-2 alpha to the assembly of mammalian stress granules. *The Journal of Cell Biology*, *147*(7), 1431–1442. https://doi.org/10.1083/jcb.147.7.1431

Kemph, A., & Lynch, J. A. (2022). Evolution of germ plasm assembly and function among the insects. *Current Opinion in Insect Science*, *50*. https://doi.org/10.1016/j.cois.2022.100883

Ketting, R. F., Fischer, S. E. J., Bernstein, E., Sijen, T., Hannon, G. J., & Plasterk, R. H. A. (2001). Dicer functions in RNA interference and in synthesis of small RNA involved in developmental timing in C. elegans. *Genes & Development*, *15*(20), 2654–2659. https://doi.org/10.1101/GAD.927801

Knaut, H., Pelegri, F., Bohmann, K., Schwarz, H., & Nüsslein-Volhard, C. (2000). Zebrafish vasa RNA but Not Its Protein Is a Component of the Germ Plasm and Segregates Asymmetrically before Germline Specification. *Journal of Cell Biology*, *149*(4), 875–888. https://doi.org/10.1083/jcb.149.4.875

Kobayashi, S., Yamada, M., Asaoka, M., & Kitamura, T. (1996). Essential role of the posterior morphogen nanos for germline development in Drosophila. *Nature*, *380*(6576), 708–711. https://doi.org/10.1038/380708a0

Kuhn, T. M., & Capelson, M. (2019). Nuclear Pore Proteins in Regulation of Chromatin State. *Cells*, *8*(11), 1414. https://doi.org/10.3390/CELLS8111414

Kuo, C. T., You, G. T., Jian, Y. J., Chen, T. S., Siao, Y. C., Hsu, A. L., & Ching, T. T. (2020). AMPK-mediated formation of stress granules is required for dietary restriction-induced longevity in Caenorhabditis elegans. *Aging Cell*, *19*(6), e13157. https://doi.org/10.1111/ACEL.13157

Lachner, M., O'Carroll, D., Rea, S., Mechtler, K., & Jenuwein, T. (2001). Methylation of histone H3 lysine 9 creates a binding site for HP1 proteins. *Nature*, *410*(6824), 116–120. https://doi.org/10.1038/35065132

Langmead, B., & Salzberg, S. L. (2012). Fast gapped-read alignment with Bowtie 2. *Nature Methods 2012 9:4*, *9*(4), 357–359. https://doi.org/10.1038/nmeth.1923

Lau, N. C., Lim, L. P., Weinstein, E. G., & Bartel, D. P. (2001). An abundant class of tiny RNAs with probable regulatory roles in Caenorhabditis elegans. *Science (New York, N.Y.)*, *294*(5543), 858–862. https://doi.org/10.1126/science.1065062

Lee, C. G., Da Costa Soares, V., Newberger, C., Manova, K., Lacy, E., & Hurwitz, J. (1998). RNA helicase A is essential for normal gastrulation. *Proceedings of the National Academy of Sciences of the United States of America*, *95*(23), 13709–13713. https://doi.org/10.1073/PNAS.95.23.13709

Lee, C.-Y. S., Putnam, A., Lu, T., He, S., Ouyang, J. P. T., & Seydoux, G. (2020). Recruitment of mRNAs to P granules by condensation with intrinsically-disordered proteins. *eLife*, *9*, e52896. https://doi.org/10.7554/eLife.52896

Lee, H. C., Gu, W., Shirayama, M., Youngman, E., Conte, D., & Mello, C. C. (2012). C. elegans piRNAs mediate the genome-wide surveillance of germline transcripts. *Cell*, *150*(1), 78–87. https://doi.org/10.1016/j.cell.2012.06.016

Lee, R. C., Feinbaum, R. L., & Ambros, V. (1993). The C. elegans heterochronic gene lin-4 encodes small RNAs with antisense complementarity to lin-14. *Cell*, *75*(5), 843–854. https://doi.org/10.1016/0092-8674(93)90529-y

Lee, R. C., Hammell, C. M., & Ambros, V. (2006). Interacting endogenous and exogenous RNAi pathways in Caenorhabditis elegans. *RNA*, *12*(4), 589–597. https://doi.org/10.1261/RNA.2231506

Lee, Y., Ahn, C., Han, J., Choi, H., Kim, J., Yim, J., Lee, J., Provost, P., Rådmark, O., Kim, S., & Kim, V. N. (2003). The nuclear RNase III Drosha initiates microRNA processing. *Nature*, *425*(6956), 415–419. https://doi.org/10.1038/nature01957

Lee, Y., Jeon, K., Lee, J.-T., Kim, S., & Kim, V. N. (2002). MicroRNA maturation: Stepwise processing and subcellular localization. *The EMBO Journal*, *21*(17), 4663–4670. https://doi.org/10.1093/emboj/cdf476

Leung, A. K. L., Calabrese, J. M., & Sharp, P. A. (2006). Quantitative analysis of Argonaute protein reveals microRNA-dependent localization to stress granules. *Proceedings of the National Academy of Sciences of the United States of America*, *103*(48), 18125–18130. https://doi.org/10.1073/PNAS.0608845103

Lev, I., Toker, I. A., Mor, Y., Nitzan, A., Weintraub, G., Antonova, O., Bhonkar, O., Ben Shushan, I., Seroussi, U., Claycomb, J. M., Anava, S., Gingold, H., Zaidel-Bar, R., & Rechavi, O. (2019). Germ Granules Govern Small RNA Inheritance. *Current Biology : CB*, *29*(17), 2880-2891.e4. https://doi.org/10.1016/J.CUB.2019.07.054

Lewis, B. P., Shih, I. -hung, Jones-Rhoades, M. W., Bartel, D. P., & Burge, C. B. (2003). Prediction of mammalian microRNA targets. *Cell*, *115*(7), 787–798. https://doi.org/10.1016/s0092-8674(03)01018-3

Liu, Z. C., & Ambros, V. (1989). Heterochronic genes control the stage-specific initiation and expression of the dauer larva developmental program in Caenorhabditis elegans. *Genes & Development*, *3*(12B), 2039–2049. https://doi.org/10.1101/gad.3.12b.2039

Love, M. I., Huber, W., & Anders, S. (2014). Moderated estimation of fold change and dispersion for RNA-seq data with DESeq2. *Genome Biology*, *15*(12), 1–21. https://doi.org/10.1186/S13059-014-0550-8/FIGURES/9

Lu, P., Deng, B., Li, X., Niu, X., Qiu, Y., Liang, Y., Liang, Y., Tang, G., Yuan, Z., Luo, G., Kennedy, S., & Wan, G. (2025). A nuclear pore-anchored condensate enables germ granule organization and transgenerational epigenetic inheritance. *Nature Structural & Molecular Biology*. https://doi.org/10.1038/s41594-025-01515-7

Mahowald, A. P. (1971). Polar granules of Drosophila. III. The continuity of polar granules during the life cycle of Drosophila. *Journal of Experimental Zoology*, *176*(3), 329–343. https://doi.org/10.1002/jez.1401760308

Majerciak, V., Zhou, T., Kruhlak, M. J., & Zheng, Z. M. (2023). RNA helicase DDX6 and scaffold protein GW182 in P-bodies promote biogenesis of stress granules. *Nucleic Acids Research*, *51*(17), 9337–9355. https://doi.org/10.1093/NAR/GKAD585

Malone, C. D., Brennecke, J., Dus, M., Stark, A., McCombie, W. R., Sachidanandam, R., & Hannon, G. J. (2009). Specialized piRNA Pathways Act in Germline and Somatic Tissues of the Drosophila Ovary. *Cell*, *137*(3), 522–535. https://doi.org/10.1016/j.cell.2009.03.040

Manage, K. I., Rogers, A. K., Wallis, D. C., Uebel, C. J., Anderson, D. C., Nguyen, D. A. H., Arca, K., Brown, K. C., Cordeiro Rodrigues, R. J., de Albuquerque, B. F., Ketting, R. F., Montgomery, T. A., & Phillips, C. M. (2020). A tudor domain protein, SIMR-1, promotes siRNA production at piRNA-targeted mRNAs in C. elegans. *eLife*, *9*, e56731. https://doi.org/10.7554/eLife.56731

Maniar, J. M., & Fire, A. Z. (2011). EGO-1, a C. elegans RdRP, modulates gene expression via production of mRNA-templated short antisense RNAs. *Current Biology*, *21*(6), 449–459. https://doi.org/10.1016/J.CUB.2011.02.019/ATTACHMENT/20981CDF-D625-4BA1-A2B6-49FBA7CFFF6C/MMC2.XLS

Marnik, E. A., Fuqua, J. H., Sharp, C. S., Rochester, J. D., Xu, E. L., Holbrook, S. E., & Updike, D. L. (2019). Germline maintenance through the multifaceted activities of GLH/Vasa in caenorhabditis elegans P Granules. *Genetics*, *213*(3), 923–939. https://doi.org/10.1534/genetics.119.302670

Marré, J., Traver, E. C., & Jose, A. M. (2016). Extracellular RNA is transported from one generation to the next in Caenorhabditis elegans. *Proceedings of the National Academy of Sciences of the United States of America*, *113*(44), 12496–12501. https://doi.org/10.1073/PNAS.1608959113/SUPPL_FILE/PNAS.1608959113.SM09.AVI

Martin, M. (2011). Cutadapt removes adapter sequences from high-throughput sequencing reads. *EMBnet.Journal*, *17*(1), 10–12. https://doi.org/10.14806/EJ.17.1.200

Meikar, O., Vagin, V. V., Chalmel, F., Sõstar, K., Lardenois, A., Hammell, M., Jin, Y., Da Ros, M., Wasik, K. A., Toppari, J., Hannon, G. J., & Kotaja, N. (2014). An atlas of chromatoid body components. *RNA*, *20*(4), 483–495. https://doi.org/10.1261/RNA.043729.113

Mi, S., Cai, T., Hu, Y., Chen, Y., Hodges, E., Ni, F., Wu, L., Li, S., Zhou, H., Long, C., Chen, S., Hannon, G. J., & Qi, Y. (2008). Sorting of small RNAs into Arabidopsis argonaute complexes is directed by the 5' terminal nucleotide. *Cell*, *133*(1), 116–127. https://doi.org/10.1016/j.cell.2008.02.034

Montgomery, T. A., Rim, Y.-S., Zhang, C., Dowen, R. H., Phillips, C. M., Fischer, S. E. J., & Ruvkun, G. (2012). PIWI Associated siRNAs and piRNAs Specifically Require the Caenorhabditis elegans HEN1 Ortholog henn-1. *PLoS Genetics*, *8*(4), e1002616. https://doi.org/10.1371/journal.pgen.1002616

Mugler, C. F., Hondele, M., Heinrich, S., Sachdev, R., Vallotton, P., Koek, A. Y., Chan, L. Y., & Weis, K. (2016). ATPase activity of the DEAD-box protein Dhh1 controls processing body formation. *eLife*, *5*, e18746. https://doi.org/10.7554/ELIFE.18746

Napoli, C. (1990). Introduction of a Chimeric Chalcone Synthase Gene into Petunia Results in Reversible Co-Suppression of Homologous Genes in trans. *The Plant Cell Online*, *2*(4), 279–289. https://doi.org/10.1105/tpc.2.4.279

Navarro, R. E., Shim, E. Y., Kohara, Y., Singson, A., & Blackwell, T. K. (2001). Cgh-1, a conserved predicted RNA helicase required for gametogenesis and protection from physiological germline apoptosis in C. elegans. *Development*, *128*(17), 3221–3232. https://doi.org/10.1242/DEV.128.17.3221

Nguyen, D. A. H., & Phillips, C. M. (2021). Arginine methylation promotes siRNA-binding specificity for a spermatogenesis-specific isoform of the Argonaute protein CSR-1. *Nature Communications 2021 12:1*, *12*(1), 1–15. https://doi.org/10.1038/s41467-021-24526-6

Ni, J. Z., Kalinava, N., Chen, E., Huang, A., Trinh, T., & Gu, S. G. (2016). A transgenerational role of the germline nuclear RNAi pathway in repressing heat stress-induced transcriptional activation in C. elegans. *Epigenetics and Chromatin*, *9*(1), 1–15. https://doi.org/10.1186/S13072-016-0052-X/FIGURES/5

Nover, L., Scharf, K. D., & Neumann, D. (1983). Formation of cytoplasmic heat shock granules in tomato cell cultures and leaves. *Molecular and Cellular Biology*, *3*(9), 1648–1655. https://doi.org/10.1128/mcb.3.9.1648-1655.1983

Okada, M., Kleinman, I. A., & Schneiderman, H. A. (1974). Restoration of fertility in sterilized Drosophila eggs by transplantation of polar cytoplasm. *Developmental Biology*, *37*(1), 43–54. https://doi.org/10.1016/0012-1606(74)90168-7

Okamura, K., & Lai, E. C. (2008). Endogenous small interfering RNAs in animals. *Nature Reviews Molecular Cell Biology 2008 9:9*, *9*(9), 673–678. https://doi.org/10.1038/nrm2479

Ouyang, J. P. T., Folkmann, A., Bernard, L., Lee, C. Y., Seroussi, U., Charlesworth, A. G., Claycomb, J. M., & Seydoux, G. (2019). P Granules Protect RNA Interference Genes from Silencing by piRNAs. *Developmental Cell*, *50*(6), 716-728.e6. https://doi.org/10.1016/J.DEVCEL.2019.07.026

Ouyang, J. P. T., Zhang, W. L., & Seydoux, G. (2022). The conserved helicase ZNFX-1 memorializes silenced RNAs in perinuclear condensates. *Nature Cell Biology*, *24*(7), 1129–1140. https://doi.org/10.1038/s41556-022-00940-w

Özata, D. M., Yu, T., Mou, H., Gainetdinov, I., Colpan, C., Cecchini, K., Kaymaz, Y., Wu, P.-H., Fan, K., Kucukural, A., Weng, Z., & Zamore, P. D. (2020). Evolutionarily conserved pachytene piRNA loci are highly divergent among modern humans. *Nature Ecology & Evolution*, *4*(1), 156–168. https://doi.org/10.1038/s41559-019-1065-1

Pak, J., & Fire, A. (2007). Distinct populations of primary and secondary effectors during RNAi in C. elegans. *Science*, *315*(5809), 241–244. https://doi.org/10.1126/SCIENCE.1132839/SUPPL_FILE/PAK.SOM.PDF

Pakos-Zebrucka, K., Koryga, I., Mnich, K., Ljujic, M., Samali, A., & Gorman, A. M. (2016). The integrated stress response. *EMBO Reports*, *17*(10), 1374–1395. https://doi.org/10.15252/EMBR.201642195/ASSET/0DAEE82D-AE0E-426E-AEB3-E480374DFBD2/ASSETS/GRAPHIC/EMBR201642195-FIG-0004-M.PNG

Pamula, M. C., & Lehmann, R. (2024). How germ granules promote germ cell fate. *Nature Reviews Genetics* |, *25*, 803–821. https://doi.org/10.1038/s41576-024-00744-8

Pare, J. M., Tahbaz, N., López-Orozco, J., LaPointe, P., Lasko, P., & Hobman, T. C. (2009). Hsp90 regulates the function of argonaute 2 and its recruitment to stress granules and P-bodies. *Molecular Biology of the Cell*, *20*(14), 3273–3284. https://doi.org/10.1091/MBC.E09-01-0082,

Parker, D. M., Winkenbach, L. P., Boyson, S., Saxton, M. N., Daidone, C., Al-Mazaydeh, Z. A., Nishimura, M. T., Mueller, F., & Osborne Nishimura, E. (2020). mRNA localization is linked to translation regulation in the Caenorhabditis elegans germ lineage. *Development (Cambridge, England)*, *147*(13), dev186817. https://doi.org/10.1242/dev.186817

Pasquinelli, A. E., Reinhart, B. J., Slack, F., Martindale, M. Q., Kuroda, M. I., Maller, B., Hayward, D. C., Ball, E. E., Degnan, B., Müller, P., Spring, J., Srinivasan, A., Fishman, M., Finnerty, J., Corbo, J., Levine, M., Leahy, P., Davidson, E., & Ruvkun, G. (2000). Conservation of the sequence and temporal expression of let-7 heterochronic regulatory RNA. *Nature*, *408*(6808), 86–89. https://doi.org/10.1038/35040556

Phillips, C. M., Montgomery, B. E., Breen, P. C., Roovers, E. F., Rim, Y. S., Ohsumi, T. K., Newman, M. A., Van Wolfswinkel, J. C., Ketting, R. F., Ruvkun, G., & Montgomery, T. A. (2014). MUT-14 and SMUT-1 DEAD box RNA helicases have overlapping roles in germline RNAi and endogenous siRNA formation. *Current Biology*, *24*(8), 839–844. https://doi.org/10.1016/j.cub.2014.02.060

Phillips, C. M., Montgomery, T. A., Breen, P. C., & Ruvkun, G. (2012). MUT-16 promotes formation of perinuclear Mutator foci required for RNA silencing in the C. elegans germline. *Genes and Development*, *26*(13), 1433–1444. https://doi.org/10.1101/GAD.193904.112,

Phillips, C. M., & Updike, D. L. (2022). Germ granules and gene regulation in the Caenorhabditis elegans germline. *Genetics*, *220*(3). https://doi.org/10.1093/GENETICS/IYAB195

Pitt, J. N., Schisa, J. A., & Priess, J. R. (2000). P granules in the germ cells of Caenorhabditis elegans adults are associated with clusters of nuclear pores and contain RNA. *Developmental Biology*, *219*(2), 315–333. https://doi.org/10.1006/dbio.2000.9607

Prabu, J. R., Müller, M., Thomae, A. W., Schüssler, S., Bonneau, F., Becker, P. B., & Conti, E. (2015). Structure of the RNA Helicase MLE Reveals the Molecular Mechanisms for Uridine Specificity and RNA-ATP Coupling. *Molecular Cell*, *60*(3), 487–499. https://doi.org/10.1016/J.MOLCEL.2015.10.011

Price, I. F., Hertz, H. L., Pastore, B., Wagner, J., & Tang, W. (2021). Proximity labeling identifies lotus domain proteins that promote the formation of perinuclear germ granules in c. Elegans. *eLife*, *10*. https://doi.org/10.7554/ELIFE.72276

Quarato, P., Singh, M., Cornes, E., Li, B., Bourdon, L., Mueller, F., Didier, C., & Cecere, G. (2021). Germline inherited small RNAs facilitate the clearance of untranslated maternal mRNAs in C. elegans embryos. *Nature Communications 2021 12:1*, *12*(1), 1–14. https://doi.org/10.1038/s41467-021-21691-6

Quinlan, A. R., & Hall, I. M. (2010). BEDTools: A flexible suite of utilities for comparing genomic features. *Bioinformatics*, *26*(6), 841–842. https://doi.org/10.1093/BIOINFORMATICS/BTQ033

Raguseo, F., Wang, Y., Li, J., Petrić Howe, M., Balendra, R., Huyghebaert, A., Vadukul, D. M., Tanase, D. A., Maher, T. E., Malouf, L., Rubio-Sánchez, R., Aprile, F. A., Elani, Y., Patani, R., Di Michele, L., & Di Antonio, M. (2023). The ALS/FTD-related C9orf72 hexanucleotide repeat expansion forms RNA condensates through multimolecular G-quadruplexes. *Nature Communications*, *14*(1), 8272. https://doi.org/10.1038/s41467-023-43872-1

Reinhart, B. J., Slack, F. J., Basson, M., Pasquinelli, A. E., Bettinger, J. C., Rougvie, A. E., Horvitz, H. R., & Ruvkun, G. (2000). The 21-nucleotide let-7 RNA regulates developmental timing in Caenorhabditis elegans. *Nature*, *403*(6772), 901–906. https://doi.org/10.1038/35002607

Riggs, C. L., Kedersha, N., Ivanov, P., & Anderson, P. (2020). Mammalian stress granules and P bodies at a glance. *Journal of Cell Science*, *133*(16). https://doi.org/10.1242/JCS.242487/225735

Robb, G. B., & Rana, T. M. (2007). RNA helicase A interacts with RISC in human cells and functions in RISC loading. *Molecular Cell*, *26*(4), 523–537. https://doi.org/10.1016/J.MOLCEL.2007.04.016

Rogers, A. K., & Phillips, C. M. (2020). RNAi pathways repress reprogramming of C. elegans germ cells during heat stress. *Nucleic Acids Research*, *48*(8), 4256–4273. https://doi.org/10.1093/nar/gkaa174

Ruan, X., Hu, K., & Zhang, X. (2023). PIE-seq: Identifying RNA-binding protein targets by dual RNA-deaminase editing and sequencing. *Nature Communications 2023 14:1*, *14*(1), 1–16. https://doi.org/10.1038/s41467-023-39054-8

Ruby, J. G., Jan, C., Player, C., Axtell, M. J., Lee, W., Nusbaum, C., Ge, H., & Bartel, D. P. (2006). Large-scale sequencing reveals 21U-RNAs and additional microRNAs and endogenous siRNAs in C. elegans. *Cell*, *127*(6), 1193–1207. https://doi.org/10.1016/j.cell.2006.10.040

Ruvkun, G., & Giusto, J. (1989). The Caenorhabditis elegans heterochronic gene lin-14 encodes a nuclear protein that forms a temporal developmental switch. *Nature*, *338*(6213), 313–319. https://doi.org/10.1038/338313a0

Saito, K., Ishizuka, A., Siomi, H., & Siomi, M. C. (2005). Processing of pre-microRNAs by the Dicer-1-Loquacious complex in Drosophila cells. *PLoS Biology*, *3*(7), e235. https://doi.org/10.1371/journal.pbio.0030235

Schlautmann, L. P., & Gehring, N. H. (2020). A Day in the Life of the Exon Junction Complex. *Biomolecules*, *10*(6), 866. https://doi.org/10.3390/BIOM10060866

Sen, G. L., & Blau, H. M. (2005). Argonaute 2/RISC resides in sites of mammalian mRNA decay known as cytoplasmic bodies. *Nature Cell Biology*, *7*(6), 633–636. https://doi.org/10.1038/ncb1265

Seroussi, U., Lugowski, A., Wadi, L., Lao, R. X., Willis, A. R., Zhao, W., Sundby, A. E., Charlesworth, A. G., Reinke, A. W., & Claycomb, J. M. (2023). A comprehensive survey of c. Elegans argonaute proteins reveals organismwide gene regulatory networks and functions. *eLife*, *12*. https://doi.org/10.7554/ELIFE.83853

Servello, F. A., & Apfeld, J. (2020). The heat shock transcription factor HSF-1 protects Caenorhabditis elegans from peroxide stress. *Translational Medicine of Aging*, *4*, 88–92. https://doi.org/10.1016/J.TMA.2020.07.002

Seth, M., Shirayama, M., Gu, W., Ishidate, T., Conte, D., & Mello, C. C. (2013). The C. elegans CSR-1 Argonaute Pathway Counteracts Epigenetic Silencing to Promote Germline Gene Expression. *Developmental Cell*, *27*(6), 656–663. https://doi.org/10.1016/J.DEVCEL.2013.11.014

Shakes, D. C., & Ward, S. (1989). Initiation of spermiogenesis in C. elegans: A pharmacological and genetic analysis. *Developmental Biology*, *134*(1), 189–200. https://doi.org/10.1016/0012-1606(89)90088-2

Shen, E.-Z., Chen, H., Ozturk, A. R., Tu, S., Shirayama, M., Tang, W., Ding, Y.-H., Dai, S.-Y., Weng, Z., & Mello, C. C. (2018). Identification of piRNA Binding Sites Reveals the Argonaute Regulatory Landscape of the C. elegans Germline. *Cell*, *172*(5), 937-951.e18. https://doi.org/10.1016/j.cell.2018.02.002

Sheth, U., Pitt, J., Dennis, S., & Priess, J. R. (2010). Perinuclear P granules are the principal sites of mRNA export in adult C. elegans germ cells. *Development (Cambridge, England)*, *137*(8), 1305–1314. https://doi.org/10.1242/dev.044255

Sheu-Gruttadauria, J., & MacRae, I. J. (2017). Structural Foundations of RNA Silencing by Argonaute. *Journal of Molecular Biology*, *429*(17), 2619–2639. https://doi.org/10.1016/j.jmb.2017.07.018

Shi, K., Zhang, Y., Du, Z., Liu, S. C., Leon, I., Fan, X., Lee, H. C., & Zhang, D. (2025). Nucleoporins shape germ granule architecture and balance small RNA silencing pathways. *Nature Communications*, *16*(1). https://doi.org/10.1038/S41467-025-59526-3,

Shirayama, M., Seth, M., Lee, H. C., Gu, W., Ishidate, T., Conte, D., & Mello, C. C. (2012). piRNAs initiate an epigenetic memory of non-self RNA in the C. elegans germline. *Cell*, *150*(1), 65. https://doi.org/10.1016/J.CELL.2012.06.015

Shukla, A., Perales, R., & Kennedy, S. (2021). piRNAs coordinate poly(UG) tailing to prevent aberrant and perpetual gene silencing. *Current Biology*, *31*(20), 4473-4485.e3. https://doi.org/10.1016/J.CUB.2021.07.076

Sijen, T., Fleenor, J., Simmer, F., Thijssen, K. L., Parrish, S., Timmons, L., Plasterk, R. H. A., & Fire, A. (2001). On the role of RNA amplification in dsRNA-triggered gene silencing. *Cell*, *107*(4), 465–476. https://doi.org/10.1016/S0092-8674(01)00576-1

Simmer, F., Tijsterman, M., Parrish, S., Koushika, S. P., Nonet, M. L., Fire, A., Ahringer, J., & Plasterk, R. H. A. (2002). Loss of the putative RNA-directed RNA polymerase RRF-3 makes C. Elegans hypersensitive to RNAi. *Current Biology*, *12*(15), 1317–1319. https://doi.org/10.1016/S0960-9822(02)01041-2

Simon, M., Sarkies, P., Ikegami, K., Doebley, A.-L., Goldstein, L. D., Mitchell, J., Sakaguchi, A., Miska, E. A., & Ahmed, S. (2014). Reduced insulin/IGF-1 signaling restores germ cell immortality to Caenorhabditis elegans Piwi mutants. *Cell Reports*, *7*(3), 762–773. https://doi.org/10.1016/j.celrep.2014.03.056

Singh, M., Cornes, E., Li, B., Quarato, P., Bourdon, L., Dingli, F., Loew, D., Proccacia, S., & Cecere, G. (2021). Translation and codon usage regulate Argonaute slicer activity to trigger small RNA biogenesis. *Nature Communications 2021 12:1*, *12*(1), 1–18. https://doi.org/10.1038/s41467-021-23615-w

Smardon, A., Spoerke, J. M., Stacey, S. C., Klein, M. E., MacKin, N., & Maine, E. M. (2000). EGO-1 is related to RNA-directed RNA polymerase and functions in germ-line development and RNA interference in C. elegans. *Current Biology*, *10*(4), 169–178. https://doi.org/10.1016/S0960-9822(00)00323-7

Smith, C. J. S., Watson, C. F., Ray, J., Bird, C. R., Morris, P. C., Schuch, W., & Grierson, D. (1988). Antisense RNA inhibition of polygalacturonase gene expression in transgenic tomatoes. *Nature*, *334*(6184), 724–726. https://doi.org/10.1038/334724a0

Smith, H. A., Swaney, S. L., Parks, T. D., Wernsman, E. A., & Dougherty, W. G. (1994). Transgenic plant virus resistance mediated by untranslatable sense RNAs: Expression, regulation, and fate of nonessential RNAs. *The Plant Cell*, *6*(10), 1441–1453. https://doi.org/10.1105/tpc.6.10.1441

Song, J.-J., Liu, J., Tolia, N. H., Schneiderman, J., Smith, S. K., Martienssen, R. A., Hannon, G. J., & Joshua-Tor, L. (2003). The crystal structure of the Argonaute2 PAZ domain reveals an RNA binding motif in RNAi effector complexes. *Nature Structural Biology*, *10*(12), 1026–1032. https://doi.org/10.1038/nsb1016

Song, R., Hennig, G. W., Wu, Q., Jose, C., Zheng, H., & Yan, W. (2011). Male germ cells express abundant endogenous sirnas. *Proceedings of the National Academy of Sciences of the United States of America*, *108*(32), 13159–13164. https://doi.org/10.1073/PNAS.1108567108/SUPPL_FILE/SAPP.PDF

Spike, C., Meyer, N., Racen, E., Orsborn, A., Kirchner, J., Kuznicki, K., Yee, C., Bennett, K., & Strome, S. (2008). Genetic Analysis of the Caenorhabditis elegans GLH Family of P-Granule Proteins. *Genetics*, *178*(4), 1973. https://doi.org/10.1534/GENETICS.107.083469

Spracklin, G., Fields, B., Wan, G., Becker, D., Wallig, A., Shukla, A., & Kennedy, S. (2017). The RNAi inheritance machinery of caenorhabditis elegans. *Genetics*, *206*(3), 1403–1416. https://doi.org/10.1534/genetics.116.198812

Steiner, F. A., Hoogstrate, S. W., Okihara, K. L., Thijssen, K. L., Ketting, R. F., Plasterk, R. H. A., & Sijen, T. (2007). Structural features of small RNA precursors determine Argonaute loading in Caenorhabditis elegans. *Nature Structural & Molecular Biology*, *14*(10), 927–933. https://doi.org/10.1038/nsmb1308

Stoecklin, G., & Kedersha, N. (2013). Relationship of GW/P-Bodies with Stress Granules. *Advances in Experimental Medicine and Biology*, *768*, 197. https://doi.org/10.1007/978-1-4614-5107-5_12

Strome, S., & Wood, W. B. (1982). Immunofluorescence visualization of germ-line-specific cytoplasmic granules in embryos, larvae, and adults of Caenorhabditis elegans. *Proceedings of the National Academy of Sciences of the United States of America*, *79*(5), 1558–1562. https://doi.org/10.1073/PNAS.79.5.1558

Subramaniam, K., & Seydoux, G. (1999). Nos-1 and nos-2, two genes related to Drosophila nanos, regulate primordial germ cell development and survival in Caenorhabditis elegans. *Development (Cambridge, England)*, *126*(21), 4861–4871. https://doi.org/10.1242/dev.126.21.4861

Tabara, H., Sarkissian, M., Kelly, W. G., Fleenor, J., Grishok, A., Timmons, L., Fire, A., & Mello, C. C. (1999a). The rde-1 Gene, RNA Interference, and Transposon Silencing in C. elegans. *Cell*, *99*(2), 123–132. https://doi.org/10.1016/S0092-8674(00)81644-X

Tabara, H., Sarkissian, M., Kelly, W. G., Fleenor, J., Grishok, A., Timmons, L., Fire, A., & Mello, C. C. (1999b). The rde-1 gene, RNA interference, and transposon silencing in C. elegans. *Cell*, *99*(2), 123–132. https://doi.org/10.1016/S0092-8674(00)81644-X

Tam, O. H., Aravin, A. A., Stein, P., Girard, A., Murchison, E. P., Cheloufi, S., Hodges, E., Anger, M., Sachidanandam, R., Schultz, R. M., & Hannon, G. J. (2008). Pseudogene-derived small interfering RNAs regulate gene expression in mouse oocytes. *Nature*, *453*(7194), 534–538. https://doi.org/10.1038/nature06904

Thompson, M. G., Sacco, M. T., & Horner, S. M. (2021). How RNA modifications regulate the antiviral response. *Immunological Reviews*, *304*(1), 169. https://doi.org/10.1111/IMR.13020

Timmons, L., Court, D. L., & Fire, A. (2001). Ingestion of bacterially expressed dsRNAs can produce specific and potent genetic interference in Caenorhabditis elegans. *Gene*, *263*(1–2), 103–112. https://doi.org/10.1016/S0378-1119(00)00579-5

Tolia, N. H., & Joshua-Tor, L. (2007). Slicer and the Argonautes. *Nature Chemical Biology*, *3*(1), 36–43. https://doi.org/10.1038/nchembio848

Tops, B. B. J., Plasterk, R. H. A., & Ketting, R. F. (2006). The Caenorhabditis elegans Argonautes ALG-1 and ALG-2: Almost identical yet different. *Cold Spring Harbor Symposia on Quantitative Biology*, *71*, 189–194. https://doi.org/10.1101/sqb.2006.71.035

Trcek, T., & Lehmann, R. (2019). Germ granules in Drosophila. *Traffic*, *20*(9), 650–660. https://doi.org/10.1111/TRA.12674,

Uebel, C. J., Anderson, D. C., Mandarino, L. M., Manage, K. I., Aynaszyan, S., & Phillips, C. M. (2018). Distinct regions of the intrinsically disordered protein MUT-16 mediate assembly of a small RNA amplification complex and promote phase separation of Mutator foci. *PLOS Genetics*, *14*(7), e1007542. https://doi.org/10.1371/JOURNAL.PGEN.1007542

Uebel, C. J., Rajeev, S., & Phillips, C. M. (2023). Caenorhabditis elegans germ granules are present in distinct configurations and assemble in a hierarchical manner. *Development (Cambridge)*, *150*(24). https://doi.org/10.1242/DEV.202284/335702/AM/CAENORHABDITIS-ELEGANS-GERM-GRANULES-ARE-PRESENT

Updike, D., & Strome, S. (2010). P Granule Assembly and Function in Caenorhabditis elegans Germ Cells. *Journal of Andrology*, *31*(1), 53–60. https://doi.org/10.2164/JANDROL.109.008292

Van Blokland, R., Van der Geest, N., Mol, J. n. m., & Kooter, J. m. (1994). Transgene-mediated suppression of chalcone synthase expression in Petunia hybrida results from an increase in RNA turnover. *The Plant Journal*, *6*(6), 861–877. https://doi.org/10.1046/j.1365-313X.1994.6060861.x

van der Krol, A. R., Lenting, P. E., Veenstra, J., van der Meer, I. M., Koes, R. E., Gerats, A. G. M., Mol, J. N. M., & Stuitje, A. R. (1988). An anti-sense chalcone synthase gene in transgenic plants inhibits flower pigmentation. *Nature*, *333*(6176), 866–869. https://doi.org/10.1038/333866a0

van Wolfswinkel, J. C., Claycomb, J. M., Batista, P. J., Mello, C. C., Berezikov, E., & Ketting, R. F. (2009). CDE-1 Affects Chromosome Segregation through Uridylation of CSR-1-Bound siRNAs. *Cell*, *139*(1), 135–148. https://doi.org/10.1016/j.cell.2009.09.012

Vaucheret, H., Vazquez, F., Crété, P., & Bartel, D. P. (2004). The action of ARGONAUTE1 in the miRNA pathway and its regulation by the miRNA pathway are crucial for plant development. *Genes & Development*, *18*(10), 1187–1197. https://doi.org/10.1101/gad.1201404

Vaucheret, H., & Voinnet, O. (2023). The plant siRNA landscape. *The Plant Cell*, *36*(2), 246. https://doi.org/10.1093/PLCELL/KOAD253

Walstrom, K. M., Murphy, D., Bean, C. J., & Kelly, W. G. (2014). Corrigendum to 'RNA helicase A is important for germline transcriptional control, proliferation, and meiosis in C. elegans' [Mechanisms of Development 122 (2005) 707–720]. *Mechanisms of Development*, *132*(1), 93. https://doi.org/10.1016/J.MOD.2014.01.002

Walstrom, K. M., Schmidt, D., Bean, C. J., & Kelly, W. G. (2005). RNA helicase A is important for germline transcriptional control, proliferation, and meiosis in C. elegans. *Mechanisms of Development*, *122*(5), 707–720. https://doi.org/10.1016/j.mod.2004.12.002

Wan, G., Fields, B. D., Spracklin, G., Shukla, A., Phillips, C. M., & Kennedy, S. (2018). Spatiotemporal regulation of liquid-like condensates in epigenetic inheritance. *Nature*, *557*(7707), 679–683. https://doi.org/10.1038/S41586-018-0132-0

Wang, G., & Reinke, V. (2008). A C. elegans Piwi, PRG-1, Regulates 21U-RNAs during Spermatogenesis. *Current Biology*, *18*(12), 861–867. https://doi.org/10.1016/j.cub.2008.05.009

Wang, T., Birsoy, K., Hughes, N. W., Krupczak, K. M., Post, Y., Wei, J. J., Lander, E. S., & Sabatini, D. M. (2015). Identification and characterization of essential genes in the human genome. *Science*, *350*(6264), 1096–1101. https://doi.org/10.1126/SCIENCE.AAC7041/SUPPL_FILE/WANG-SM.PDF

Waterhouse, P. M., Graham, M. W., & Wang, M.-B. (1998). Virus resistance and gene silencing in plants can be induced by simultaneous expression of sense and antisense RNA. *Proceedings of the National Academy of Sciences of the United States of America*, *95*(23), 13959–13964. https://doi.org/10.1073/pnas.95.23.13959

Watkins, B., & Schisa, J. A. (2021). Phase separation dynamics of the C. elegans PGL-1 P granule protein in oocytes are sensitive to heat stress. *microPublication Biology*, *2021*. https://doi.org/10.17912/MICROPUB.BIOLOGY.000476

Wedeles, C. J., Wu, M. Z., & Claycomb, J. M. (2013). Protection of Germline Gene Expression by the C. elegans Argonaute CSR-1. *Developmental Cell*, *27*(6), 664–671. https://doi.org/10.1016/J.DEVCEL.2013.11.016

Wickham, H. (2007). Reshaping Data with the reshape Package. *Journal of Statistical Software*, *21*(12), 1–20. https://doi.org/10.18637/JSS.V021.I12

Wightman, B., Ha, I., & Ruvkun, G. (1993). Posttranscriptional regulation of the heterochronic gene lin-14 by lin-4 mediates temporal pattern formation in C. elegans. *Cell*, *75*(5), 855–862. https://doi.org/10.1016/0092-8674(93)90530-4

Wu, P. H., Fu, Y., Cecchini, K., Özata, D. M., Arif, A., Yu, T., Colpan, C., Gainetdinov, I., Weng, Z., & Zamore, P. D. (2020). The evolutionarily conserved piRNA-producing locus pi6 is required for male mouse fertility. *Nature Genetics 2020 52:7*, *52*(7), 728–739. https://doi.org/10.1038/s41588-020-0657-7

Wu, W. S., Brown, J. S., Shiue, S. C., Chung, C. J., Lee, D. E., Zhang, D., & Lee, H. C. (2023). Transcriptome-wide analyses of piRNA binding sites suggest distinct mechanisms regulate piRNA binding and silencing in C. elegans. *RNA (New York, N.Y.)*, *29*(5), 557–569. https://doi.org/10.1261/RNA.079441.122

Xie, Z., Kasschau, K. D., & Carrington, J. C. (2003). Negative feedback regulation of Dicer-Like1 in Arabidopsis by microRNA-guided mRNA degradation. *Current Biology: CB*, *13*(9), 784–789. https://doi.org/10.1016/s0960-9822(03)00281-1

Xu, F., Feng, X., Chen, X., Weng, C., Yan, Q., Xu, T., Hong, M., & Guang, S. (2018). A Cytoplasmic Argonaute Protein Promotes the Inheritance of RNAi. *Cell Reports*, *23*(8), 2482–2494. https://doi.org/10.1016/j.celrep.2018.04.072

Yang, X., Shen, Y., Garre, E., Hao, X., Krumlinde, D., Cvijović, M., Arens, C., Nyström, T., Liu, B., & Sunnerhagen, P. (2014). Stress granule-defective mutants deregulate stress responsive transcripts. *PLoS Genetics*, *10*(11), e1004763. https://doi.org/10.1371/journal.pgen.1004763

Yigit, E., Batista, P. J., Bei, Y., Pang, K. M., Chen, C. C. G., Tolia, N. H., Joshua-Tor, L., Mitani, S., Simard, M. J., & Mello, C. C. (2006). Analysis of the C. elegans Argonaute Family Reveals that Distinct Argonautes Act Sequentially during RNAi. *Cell*, *127*(4), 747–757. https://doi.org/10.1016/j.cell.2006.09.033

Zamore, P. D., Tuschl, T., Sharp, P. A., & Bartel, D. P. (2000). RNAi: Double-Stranded RNA Directs the ATP-Dependent Cleavage of mRNA at 21 to 23 Nucleotide Intervals. *Cell*, *101*(1), 25–33. https://doi.org/10.1016/S0092-8674(00)80620-0

Zhang, D., Tu, S., Stubna, M., Wu, W.-S., Huang, W.-C., Weng, Z., & Lee, H.-C. (2018). The piRNA targeting rules and the resistance to piRNA silencing in endogenous genes. *Science*, *359*(6375), 587–592. https://doi.org/10.1126/science.aao2840

Zhang, L., Ward, J. D., Cheng, Z., & Dernburg, A. F. (2015). The auxin-inducible degradation (AID) system enables versatile conditional protein depletion in C. elegans. *Development (Cambridge)*, *142*(24), 4374–4384. https://doi.org/10.1242/DEV.129635/-/DC1

Zhou, R., Czech, B., Brennecke, J., Sachidanandam, R., Wohlschlegel, J. A., Perrimon, N., & Hannon, G. J. (2009). Processing of Drosophila endo-siRNAs depends on a specific Loquacious isoform. *RNA*, *15*(10), 1886–1895. https://doi.org/10.1261/rna.1611309

Zhuang, J. J., & Hunter, C. P. (2011). Tissue Specificity of Caenorhabditis elegans Enhanced RNA Interference Mutants. *Genetics*, *188*(1), 235–237. https://doi.org/10.1534/genetics.111.127209

Zhuang, J. J., & Hunter, C. P. (2012). The Influence of Competition Among C. elegans Small RNA Pathways on Development. *Genes 2012, Vol. 3, Pages 671-685*, *3*(4), 671–685. https://doi.org/10.3390/GENES3040671